Universidade do Minho
Escola de Engenharia

Rui André Martins da Silva

Repair of Earth Constructions by Means of Grout Injection

Repair of Earth Constructions by Means of Grout Injection
Rui André Martins da Silva
UMinho | 2013

Novembro de 2013

Universidade do Minho
Escola de Engenharia

Rui André Martins da Silva

Repair of Earth Constructions by Means of Grout Injection

Tese de Doutoramento
Estruturas / Engenharia Civil

Trabalho efectuado sob a orientação do
Professor Doutor Daniel Vitorino de Castro Oliveira

Co-Orientador:
Professor Doutor Koen Van Balen

Novembro de 2013

DECLARAÇÃO

Rui André Martins da Silva

Endereço electrónico: ruisilva@civil.uminho.pt

Telefone: 253510200 Número do Bilhete de Identidade: 12312857

Título da tese:

Repair of Earth Constructions by Means of Grout Injection

Ano de conclusão: 2013

Orientador:

Professor Doutor Daniel Vitorino de Castro Oliveira

Co-Orientador:

Professor Doutor Koen van Balen

Designação do Doutoramento:

Engenharia Civil

Escola de Engenharia

Departamento de Engenharia Civil

É AUTORIZADA A REPRODUÇÃO INTEGRAL DESTA TESE APENAS PARA EFEITOS DE INVESTIGAÇÃO, MEDIANTE DECLARAÇÃO ESCRITA DO INTERESSADO, QUE A TAL SE COMPROMETE.

Guimarães, ___/___/_____

Assinatura: _____

Acknowledgments

The present PhD research was developed at the Departments of Civil Engineering of the Catholic University of Leuven (Belgium) and University of Minho (Portugal). During this time, several persons and institutions contributed to make possible the conclusion of this thesis, and to whom I want to express my gratitude:

- To my supervisors, Professors Daniel Oliveira, Luc Schueremans and Koen Van Balen, for their full, support encouragement, interesting discussions and careful reading;
- To the Professors Dionys Van Gemert, Julio Vargas and Tiago Miranda for their interest and valuable advices and suggestions;
- To all technical and administrative staff from the Catholic University of Leuven for their support in the execution of the experimental program: Kristine, Gerda, Iris, Frank, Stephan, Danielle, Danny and Freddy;
- To all my colleagues during my stay at the Department of Civil Engineering of the Catholic University of Leuven for their valuable friendship and interest: Els, Prigiarto, Ugur, Nicho, Roel, Karel, Bjorn, Özlem, Anna, María del Mar, Wine, Holger, Salman and Iveta;
- To all technical staff from the laboratory of Civil Engineering of the University of Minho for their friendship, knowledge and help in the execution of the experimental program: Marco Jorge, José Gonçalves, António Matos, Carlos Jesus, Carlos Palha, Hélder Torres, Fernando Pokee and Rui Oliveira;
- To all my colleagues in the Department of Civil Engineering of the University of Minho, for their friendship, support and interest: Nuno Mendes, José Cunha, Elisa Poletti, João Martins, Ana Araújo, Eduarda Luso, Ricardo Barros, Ana Carlota, Catarina Silva, João Pereira, João Leite, Leonardo Avila and Susana Moreira;
- To all Master students who contributed hardly for the execution of the experimental work: Karolien Dekoning, Tine Gysels, Catarina Martins and Júlio Machado;
- To Francisco Seixas, António Amador, Maria Fernandes, Raul Almeida and Deolinda Tavares for sharing their knowledge on rammed earth construction;
- To Lorenzo Miccoli, Urs Müller and Chiara Perrone (on the behalf of BAM-ZRS) for providing the experimental results used in the numerical analysis;
- To the company Wienerberger for providing the kaolin powder RR40;

- To the companies David & Loução-Construções Civis Lda and Monumenta (in the name of Luís Mateus) for providing the soil used in the rammed earth specimens;
- To the Portuguese Science and Technology Foundation (FCT) for the granted scholarship with reference SFRH/BD/39145/2007 and for the funding provided through project FCOMP-01-0124-FEDER-028864 (FCT-PTDC/ECM-EST/2396/2012);
- And finally, but not least, to my family and friends for the patient, encouragement and support.

Abstract

Nowadays, one fourth of the World's population lives in a house made from earth. Consequently, there is a large built stock widely distributed around the World going much beyond simple dwellings. An important part of the earth built stock is found often affected by cracking, whose repair is fundamental for the reestablishment of the structural integrity. However, the successful cracking repair of earthen walls requires employing adequate intervention techniques. With this respect, the injection of mud grouts is being put forward in the recent years and has been showing good results in the few reported cases.

This thesis aims at contributing to the development of the limited knowledge on the injection technique applied to earth constructions. The broad extension of this topic led to selecting the injection of unmodified mud grouts (without mineral binders) in rammed earth constructions as case study. This thesis also intends contributing for the characterization of the rammed earth construction from southern Portugal and for the numerical simulation of its behaviour.

An experimental program was defined and included the execution of a composition study about the behaviour of unmodified mud grouts, involving several variables of their composition and the characterization of important properties governing the injection technique. The design of a mud grout has shown to require accounting for both the limitation of the clay content and the effect of the addition of a deflocculant.

The experimental program continued with the suitability assessment of four soils from Alentejo (Portugal) for unstabilised rammed earth construction, and the selection of a representative soil used to manufacture medium- and large-scale rammed earth specimens. These specimens were used to assess the repair effectiveness of three different unmodified mud grouts. The results indicated that the injection of mud grouts is capable of attaining adequate repair effectiveness, providing that the same soil used in the construction is incorporated in the grout composition.

Finally, the shear behaviour of rammed earth wallets tested under diagonal-compression was modelled resorting to the finite element method, where both the macro- and micro-modelling approaches were used. Both cases provided an adequate simulation of the non-linear shear behaviour, being highlighted the enhanced shear ductility of rammed earth.

Resumo

Atualmente estima-se que um quarto da população mundial viva numa casa construída em terra. Consequentemente, existe um extenso património construído espalhado pelo mundo e que vai muito além de simples habitações. Uma parte importante deste património é frequentemente afetado por fendilhação, cuja reparação é fundamental para restabelecer a integridade estrutural. Contudo, a reparação bem sucedida da fendilhação requer o emprego de soluções de intervenção adequadas. A este respeito, a injeção de caldas de terra tem-se evidenciado nos últimos anos e tem demonstrado bons resultados nos poucos casos documentados.

A presente tese tem como objetivo contribuir para o desenvolvimento do conhecimento limitado sobre injeção de caldas em construções de terra. A grande diversidade deste tema levou a que fosse selecionada a injeção de caldas de terra não modificadas (sem adição de ligantes minerais) em taipa como caso de estudo. A presente tese também pretende contribuir para a caraterização da construção em taipa do Sul de Portugal e para a simulação numérica do seu comportamento.

Definiu-se um programa experimental que incluiu a realização de um estudo de composição sobre o comportamento de caldas de terra não modificadas, envolvendo várias variáveis da sua composição e a caraterização de propriedades relevantes para a técnica da injeção. Mostrou-se que o dimensionamento de uma calda de terra requer considerar uma percentagem de argila limitada e o efeito da adição de um desfloculante.

O programa experimental continuou com a avaliação da adequabilidade de quatro solos do Alentejo (Portugal) para a construção em taipa não estabilizada, e com a seleção de um solo representativo utilizado na construção de provetes de taipa de média e grande escala. Estes provetes foram utilizados na avaliação da eficiência da capacidade de reparação de três caldas de terra não modificadas. Os resultados indicaram que a injeção de caldas de terra é capaz de proporcionar uma eficiência de reparação adequada, caso o mesmo solo utilizado na construção seja incorporado na calda.

Finalmente, simulou-se comportamento ao corte de paredes de taipa ensaiadas à compressão diagonal com recurso ao método dos elementos finitos, utilizando-se tanto a abordagem da macro- como da micro-modelação. Ambos os casos proporcionaram uma simulação adequada do comportamento não linear ao corte, tendo sido evidenciada uma ductilidade relativamente elevada da taipa ao corte.

Contents

Acknowledgments iii

Abstract v

Resumo vii

Contents ix

Index of Figures xiii

Index of Tables xxi

Chapter 1

Introduction 1

1.1 General Framework and Motivation 1
1.2 Objectives 2
1.3 Outline of the Thesis 3

Chapter 2

Earth Construction: Concept, Damage and Rehabilitation Solutions 5

2.1 Introduction 5
2.2 Earth construction techniques 5
2.2.1 Adobe masonry 7
2.2.2 Rammed earth 8
2.2.3 Wattle-and-daub 11
2.2.4 Compressed earth blocks (CEB) masonry 11
2.3 Soil testing, selection and stabilisation 12
2.3.1 Expeditious tests 14
2.3.2 Laboratory tests 16
2.3.3 Stabilisation 19
2.4 Vulnerabilities of earth constructions 19
2.5 Structural intervention techniques 22
2.6 Conclusions 27

Chapter 3

Grouting Technology in Historical Constructions: Short Overview 29

3.1 Introduction 29
3.2 Grout injection of ancient masonry 29
3.2.1 Grout properties 31
3.2.2 Grouting materials 32
3.2.3 Grout design 37
3.2.4 Application procedure 39

3.2.5 Strengthening of three-leaf stone masonry 41
3.3 Grout injection of earth constructions 45
3.3.1 State of art 45
3.3.2 Approach for mud grout design 49
3.4 Colloid behaviour of clay suspensions 52
3.4.1 Clay mineralogy 52
3.4.2 Clay particles surfaces 56
3.4.3 Flocculation of clay particles 58
3.4.4 Flow behaviour of clay suspensions 63
3.5 Conclusions 66

Chapter 4

Behaviour of Unmodified Mud Grouts 69
4.1 Introduction 69
4.2 Experimental program at KULeuven 69
4.2.1 Materials 70
4.2.2 Mixtures and mixing procedure 71
4.2.3 Experimental procedures 72
4.3 Experimental program at UMinho 76
4.3.1 Materials 77
4.3.2 Mixtures and mixing procedure 78
4.3.3 Experimental procedures 78
4.4 Results and discussion 80
4.4.1 Rheology 80
4.4.2 Time-dependent rheological behaviour 92
4.4.3 Strength 93
4.4.4 Shrinkage 94
4.4.5 Adhesion 96
4.4.6 Stability 99
4.5 Conclusions 99

Chapter 5

Assessment of Soils for Unstabilised Rammed Earth Construction 103
5.1 Introduction 103
5.2 Methodology 104
5.3 Soil assessment 104
5.3.1 Visual inspection 105
5.3.2 Sedimentation test 106
5.3.3 Ribbon test 107
5.3.4 Drop test 108
5.3.5 Dry strength test 108
5.3.6 PSD analysis 109
5.3.7 Atterberg limits 110
5.3.8 Standard Proctor 111
5.4 Rammed earth performance assessment 112
5.4.1 Compression behaviour 113
5.4.2 Durability (Geelong test) 118
5.5 Characterization of the selected soil 119
5.5.1 Sedimentation test 120
5.5.2 Ribbon test 120

5.5.3 Drop test 121
5.5.4 Dry strength test 121
5.5.5 PSD analysis 121
5.5.6 Atterberg limits 122
5.5.7 Standard Proctor 123
5.5.8 Suitability for rammed earth construction 123
5.6 PSD correction of the selected soil 124
5.7 Performance of the corrected soil 125
5.7.1 Compression behaviour 127
5.7.2 Durability (Geelong test) 129
5.8 Conclusions 129

Chapter 6

Repair of Rammed Earth by Means of Mud Grouts Injection 133

6.1 Introduction 133
6.2 Adhesion tests on medium-scale specimens 133
6.2.1 Manufacture of the specimens 134
6.2.2 Testing procedure 136
6.2.3 Repair procedure 136
6.2.4 Results and discussion 140
6.3 Adhesion tests on large-scale specimens 145
6.3.1 Manufacture of the specimens 145
6.3.2 Testing procedure 147
6.3.3 Repair procedure 147
6.3.4 Results and discussion 151
6.4 Repair effectiveness assessment by means of UPV 161
6.4.1 Testing procedure 161
6.4.2 Results and discussion 162
6.5 Conclusions 165

Chapter 7

Shear Behaviour Modelling of Rammed Earth 167

7.1 Introduction 167
7.2 Experimental data 168
7.2.1 Compression tests 169
7.2.2 Diagonal-compression tests 170
7.3 Modelling of the tests carried out by BAM-ZRS 171
7.3.1 Geometry, boundary conditions and loading 172
7.3.2 Constitutive laws 173
7.3.3 Calibration of the models and results 175
7.4 Sensitivity analysis 181
7.4.1 Young modulus 182
7.4.2 Poisson ratio 183
7.4.3 Compressive strength 183
7.4.4 Tensile strength 184
7.4.5 Tensile fracture energy 185
7.4.6 Shear retention factor 185
7.4.7 Cohesion 186
7.4.8 Friction angle 188
7.4.9 Interface tensile strength 189

7.4.10 Layer thickness 191
7.4.11 Discussion 192
7.5 Modelling of the tests carried out at UMinho 194
7.6 Conclusions 197

Chapter 8
Conclusions and Future Work 199
8.1 Main conclusions 199
8.2 Recommendations for the injection of rammed earth walls 201
8.3 Future work 204

References 205

Annex A
Mud Grouts Behaviour 217

Annex B
Soil Assessment 235

Annex C
Repair Effectiveness 239

Index of Figures

Figure 2.1 – World's Geographical distribution of earth construction (source: CRATerre-ENSAG). 6
Figure 2.2 – Earth construction techniques according to Houben and Guillaud (2008).....7
Figure 2.3 – Production of adobes in Aveiro, Portugal: (a) preparation of the earth mix; (b) filling of the moulds; (c) drying. 8
Figure 2.4 – Examples of adobe construction from Aveiro (Oliveira *et al.* 2007).....8
Figure 2.5 – Construction of a new rammed earth house in Colos (Odemira), Portugal.....9
Figure 2.6 – Rammed earth formworks: (a) Crawling and externally supported formwork (Cointeraux 1791); elements of a traditional crawling formwork (Cabral 2006).....9
Figure 2.7 – Rammers used to compact rammed earth (Minke, 2006). 10
Figure 2.8 – Wattle-and-daub ("*tabique*") exterior wall of a house in Douro North Valley Region, Portugal (Pinto *et al.* 2010). 11
Figure 2.9 – Compressed earth blocks manufactured by means of a manual press (Gomes 2008).....12
Figure 2.10 – Assessment of the soil suitability for earth construction.....14
Figure 2.11 – Expeditious tests: (a) sedimentation test, (b) ribbon test, (c) drop test and (d) dry strength test (Minke 2006). 15
Figure 2.12 – Laboratory tests for soil characterization: (a) PSD, (b) Atterberg's limits, (c) Proctor test (Houben and Guillaud 2008). 17
Figure 2.13 – World's Geographical distribution of regions with moderate to very high seismic hazard (after De Sensi 2003). 22
Figure 2.14 – Repair of the basal erosion of Paderne's Castle by compacting new rammed earth material in place (Costa *et al.* 2008).....23
Figure 2.15 – Repair of the basal erosion of Paderne's Castle by projecting earth at high speed (Costa *et al.* 2008). 24
Figure 2.16 – Repair of cracks by stitching (Keefe 2005).....25
Figure 2.17 – Strengthening of a rammed earth construction by introduction of buttress in Vila Alva, Alentejo (Gomes 2008). 25
Figure 2.18 – Strengthening of opposing walls tie bars (Jaquin 2008). 26
Figure 2.19 – Strengthening by fixation of: (a) timber elements and (Lacouture *et al.* 2007); (b) metallic meshes (Pérez *et al.* 2007).....26
Figure 3.1 – Examples of the application of the grout injection technique: injection of cracks in a masonry chimney; (b) injection of the inner leaf of a masonry wall (Cóias 2006); (c) injection of the joints of a stone fountain. 30
Figure 3.2 – Injection by gravity (Ashurst and Ashurst 1988). 40
Figure 3.3 – Injection points distribution in a closest pattern (Van Rickstal 2000). 40

Figure 3.4 – Approach for the design of a mud grout. 49
Figure 3.5 – Building elements of clay minerals (De Wit 1995): (a) tetrahedral sheet (T); (b) octahedral sheet (O). 53
Figure 3.6 – Unit cells of 1:1 and 2:1 layer minerals (Encyclopaedia Brittannica 2013). 54
Figure 3.7 – Association modes of clay particles in suspension (Luckham and Rossi 1999): (a) dispersed; (b) Face-to-Face (FF); (c) Edge-toFace (EF); Edge-to Edge (EE). 58
Figure 3.8 – Net potential energy of interaction between particles in a colloidal suspension (Williamson 2008); the electrolyte concentration decreases from 1 to 7. 59
Figure 3.9 – Schematic representation of the dominant and hidden electric double layers forming around the montmorillonite lamellae under different solution conditions of electrolyte concentration and pH (Tombácz and Szekeres 2004). 60
Figure 3.10 – Schematic representation of the dominant and hidden electric double layers forming around the kaolinite particles under different solution conditions of electrolyte concentration and pH (Tombácz and Szekeres 2006). 61
Figure 3.11 – Association of clay particles in suspension as a function of the asymmetry, electrolyte concentration and pH. 62
Figure 3.12 – Possible flow curves of a fluid (Luckham and Rossi 1999). 64
Figure 3.13 – Typical flow curves for concentrated thixotropic clay suspensions (Luckham and Rossi 1999). (1) initial flow curve; (2) flow curve after shearing; (3) thixotropic loop. 65
Figure 4.1 – PSD curves of the kaolin RR40 and limestone powder Calcitec 2001 S (ASTM D 422 - ASTM 1998). 71
Figure 4.2 – Matrix of the mixtures tested at KULeuven. 72
Figure 4.3 – Apparatus used in the characterization of the rheological behaviour: (a) Marsh funnel (dimensions in mm) and (b) Viskomat PC rheometer. 73
Figure 4.4 – Configuration of the Viskomat PC testing cup and paddle (Hendrickx 2009). 73
Figure 4.5 – Viskomat PC flow profiles for (a) KH mixtures and (b) KLH mixtures. 73
Figure 4.6 – Water content of the beam-specimens: (a) time evolution of the weight of KLH specimens with [HMP]=5g/kg and K/L=0.05; and (b) equilibrium water content of all KLH specimens. 75
Figure 4.7 – Preparation of the earthen beams for (a) the adhesion tests and (b) injection of the earthen beams after testing. 76
Figure 4.8 – Particles size distribution curves of the kaolin Mibal-A and limestone powder Micro 200-OU (ASTM D 422 - ASTM 1998). 78
Figure 4.9 – Matrix of the mixtures tested at UMinho. 78
Figure 4.10 – Marsh cone used in the flow time tests carried out at UMinho (dimensions in mm). 79
Figure 4.11 – Equilibrium water content of the KLH mixtures specimens tested at UMinho. 79
Figure 4.12 – Flow time measurements of the K mixtures carried out at (a) KULeuven and (b) UMinho. 81
Figure 4.13 – Flow time measurements of the KH mixtures carried out at (a) KULeuven and (b) UMinho. 82

Figure 4.14 – Flow curves of KH mixtures with ϕ_v= 15% (Bingham's model fitted to the descending branch). 83
Figure 4.15 – Bingham's parameters of the KH mixtures with ϕ_i= 21%. 84
Figure 4.16 – Influence of the shear stress in the flowing capacity of the KH mixtures through the marsh funnel. 85
Figure 4.17 – Flow time measurements of the KL mixtures carried out at KULeuven. 86
Figure 4.18 – Flow time measurements of the KLH mixtures with ϕ_i=55%: (a) KULeuven (b) UMinho. 87
Figure 4.19 – Flow time measurements of the LH mixtures tested at KULeuven. 88
Figure 4.20 – Flow curves of the KLH mixtures with ϕ_i=55% and *K/L*=0.05 (with Bingham's model fitted to the descending branch). 88
Figure 4.21 – Bingham's parameters of KLH mixtures with ϕ_i=55%. 89
Figure 4.22 – Influence of the shear stress in the flowing capacity of the KLH mixtures through the marsh funnel. 89
Figure 4.23 – Plastic viscosity of the KLH mixtures with [HMP]= 20g/kg presented as a function of ϕ_v. 90
Figure 4.24 – Comparison between the measured flow time and the predicted flow time using (a) Equation (4.8) and (b) Equation (4.9). 91
Figure 4.25 – Plastic viscosity of the KLH mixtures tested at UMinho estimated resorting to Equation (4.8). 92
Figure 4.26 – Time-dependent rheological behaviour of the mud grouts tested at KULeuven. 92
Figure 4.27 – Strength of the KLH mixtures with *K/L*=0.15 tested at KULeuven: (a) flexural strength and (b) compressive strength. 93
Figure 4.28 – Strength of the KLH mixtures with ϕ_i=58% tested at KULeuven: (a) flexural strength; (b) compressive strength. 94
Figure 4.29 – Strength of the KLH mixtures tested at UMinho: (a) flexural strength; (b) compressive strength. 94
Figure 4.30 – Volumetric shrinkage of the KLH mixtures: (a) as a function of ϕ_i (mixtures with *K/L*= 0.15); (b) as a function of [HMP] (mixtures with ϕ_i=58%). 95
Figure 4.31 – Volumetric shrinkage of the KLH mixtures tested at KULeuven with ϕ_i=58% as a function of the dry density. 95
Figure 4.32 – Volumetric shrinkage of the KLH mixtures tested at UMinho. 96
Figure 4.33 – Adhesion capacity of the tested mud grouts and respective repair effectiveness: (a) KULeuven; (b) UMinho. 97
Figure 4.34 – Drying shrinkage evolution of a mud grout used to repair a crack. 98
Figure 4.35 – Failure modes of the adhesion specimens tested at KULeuven: (a) failure by the grout and (b) failure by the interface grout-beam. 98
Figure 4.36 – Failure modes of the adhesion specimens tested at UMinho: (a) by the earthen material; (b) by the interface grout-earthen material and (c) by the grout. 98
Figure 4.37 – Bleeding test of the grout I55MG15 after 24 hours of mixing. 99
Figure 5.1 - Visual inspection of the assessed soils (fraction sizes defined according ASTM D 2488 (ASTM 2000a)). 106

Figure 5.2 – Sedimentation test of the soils (S1 to S4 from left to right). 106
Figure 5.3 – Results from the sedimentation test. 107
Figure 5.4 – Sequential execution of the ribbon test. 107
Figure 5.5 – Possible states of the ball after impact on the ground: (a) completely crumbled, (b) partially crumbled with minor cracks; (c) flattened. 108
Figure 5.6 – Execution of the dry strength test. 109
Figure 5.7 – Comparison between the PSD curves of the soils and the envelopes for rammed earth construction recommended by: (a) Houben and Guillaud (2008); (b) MOPT (1992) and; Portuguese National Laboratory of Civil Engineering (LNEC 1953). 110
Figure 5.8 – Comparison of the consistency parameters of the soils against the envelope of recommended values by Houben and Guillaud (2008) for unstabilised rammed earth. 111
Figure 5.9 – Compaction curves of the soils. 112
Figure 5.10 – Preparation of the rammed earth cylindrical specimens: (a) compaction with electrical hammer; (b) scraping of the surface of the first layer for improving the adhesion with the second layer; (c) disaggregation of one of the specimens prepared with lower water content. 113
Figure 5.11 – Compression test: (a) test setup; (b) LVDTs configuration. 114
Figure 5.12 – Stress-strain curves of the rammed earth cylindrical specimens: (a) soil S1; (b) soil S2; (c) soil S3; (d) soil S4. 115
Figure 5.13 – Relation between dry density and compressive strength. 115
Figure 5.14 – Relation between dry density, compressive strength and Young modulus: (a) soil S1; (b) soil S2; (c) soil S3; (d) soil S4. 116
Figure 5.15 – Failure mode of the rammed earth cylindrical specimens: (a) material crushing and consequent disaggregation of the specimen; (b) main vertical/diagonal crack formation with spalling of the specimen surface. 118
Figure 5.16 – Preparation of the specimens for the Geelong test: (a) compaction with manual rammer; (b) trimming of the last layer; (c) specimens after drying. 118
Figure 5.17 – Geelong test: (a) test setup; (b) pitting depth measurement; (c) depth of moisture penetration measurement. 119
Figure 5.18 – Result of the sedimentation test showing that the fraction layers are hardly identified. 120
Figure 5.19 – Mixing of the soil with water: clay sticking to the hands and formation of agglomerates. 120
Figure 5.20 – Comparison between the PSD curves of the soils S5 and S4, and the envelopes for rammed earth construction recommended by: (a) Houben and Guillaud (2008); (b) MOPT (1992) and; Portuguese National Laboratory of Civil Engineering (LNEC 1953). 121
Figure 5.21 – Comparison of the consistency parameters of soils S5 and S4 against the envelope of recommended values by Houben and Guillaud (2008) for unstabilised rammed earth. 122
Figure 5.22 – Compaction curve of soil S5. 123
Figure 5.23 – Materials used in the PSD correction of soil S5: (a) river sand; (b) Gravel obtained from crushed granite. 124

Figure 5.24 – Correction of the soils S5: (a) PSD of the gravel and river sand; (b) correction with 50% of soil S5, 28% of sand and 22% of gravel (soil S6)..... 125
Figure 5.25 – Comparison of the consistency parameters of soil S6 against the envelope of recommended values by Houben and Guillaud (2008) for unstabilised rammed earth. 126
Figure 5.26 – Compaction curves of soils S5 and S6 126
Figure 5.27 – Stress-strain curves of the rammed earth cylindrical specimens manufactured with soil S6. 127
Figure 5.28 – Failure mode of the rammed earth cylindrical specimens: (a) formation of a diagonal crack; (b) main vertical/diagonal crack formation with spalling of the specimen surface..... 129
Figure 6.1 – Comparison between the oven and microwave oven heating methods for determination of the water content in the manufacture of the medium-scale specimens. 135
Figure 6.2 – Preparation of the mixture to compact the specimens: (a) component materials of soil S6; (b) dry mixing; (c) addition of the water with a watering can; (d) wet mixing and (e) compaction of a specimen..... 135
Figure 6.3 – Test setup of the bending test carried out on the rammed earth medium-scale specimens: (a) specimen before injection; (b) specimen after injection..... 136
Figure 6.4 – Preparation of the beam-specimens for injection: (a) water spraying; (b) line of silicone sealant being applied at the bottom face; (c) line of silicone sealant being applied at a side face. 137
Figure 6.5 – PSD curves of the materials composing the mud grouts..... 138
Figure 6.6 – PSD curves of the mud grouts II55MG25 and IINMG40-60..... 139
Figure 6.7 – Injection of the rammed earth beam-specimens: (a) injection with a 100 ml syringe from one of the sides; (b) rising of the mud grout at the opposite side of the injection; (c) crack completely filled..... 140
Figure 6.8 – Load–deflection curves of the medium-scale specimens: (a) grout II55MG25 and d_{cr} = 2 mm; (b) grout II55MG25 and d_{cr} = 8 mm; (c) grout II55NMG40-60 and d_{cr} = 2 mm; (d) grout II55NMG40-60 and d_{cr} = 8 mm..... 142
Figure 6.9 – Comparison between the oven and microwave oven heating methods for determination of the water content in the manufacture of the large-scale specimens. 146
Figure 6.10 – Manufacture of the wallet-specimens: (a) plywood formwork; (b) compaction by electric rammer; (c) demoulding..... 146
Figure 6.11 – Test setup of the diagonal compression tests carried out on the rammed earth large-scale specimens..... 147
Figure 6.12 – Remounting of the specimens: (a) simple remounting by application of mortar at the cracks near the surface and introduction of injection tubes; (b) tying by two opposite boards; (c) sealing of the cracks with earth mortar. 148
Figure 6.13 – PSD curves of the mud grouts IINMG40-60 and IINMG50-50..... 149
Figure 6.14 – Repair of the wallets by grout injection: (a) mud grout mixing; (b) injection of water; (c) injection of the mud grout..... 149

Figure 6.15 – Shear stress–shear strain curves of the wallets: (a) set repaired with grout II55NMG40-60 before injection; (b) set repaired with grout II55NMG40-60 after injection; (c) set repaired with grout II55NMG50-50 before injection; (d) set repaired with grout II55NMG50-50 before injection. 154
Figure 6.16 – Failure crack patterns of the wallets repaired with grout II55NMG40-60, before and after injection. 155
Figure 6.17 – Failure crack patterns of the wallets repaired with grout II55NMG50-50, before and after injection. 156
Figure 6.18 – UPV measurements: (a) equipment used; (b) test setup (dimensions in mm). 162
Figure 6.19 – UPV measurements on the medium-scale specimens. 162
Figure 6.20 – Ultrasonic pulse transmission time (UPTT) of the medium-scale specimens (before the first test) as a function of distance between probes: (a) set of specimens repaired with grout II55MG25 and d_{cr} = 2 mm; (b) set of specimens repaired with grout II55MG25 and d_{cr} = 8 mm; (c) set of specimens repaired with grout II55NMG40-60 and d_{cr} = 2 mm; (d) set of specimens repaired with grout II55NMG40-60 and d_{cr} = 8 mm. 163
Figure 6.21 – Initial flexural strength as a function of the average UPV of the medium-scale specimens. 164
Figure 6.22 – Average UPV variation (the standard deviation is represented as error bars) as a function of the flexural strength recovery rate. 164
Figure 7.1 – Manufacture of the rammed earth wallets tested by BAM-ZRS. 168
Figure 7.2 – Compression tests carried out by BAM-ZRS: (a) test setup; (b) compression stress – axial strain curves and respective envelope. 169
Figure 7.3 – Diagonal-compression tests carried out by BAM-ZRS: (a) test setup; (b) shear stress – shear strain curves and respective envelope. 170
Figure 7.4 – Crack pattern of one of the rammed earth wallets tested by BAM-ZRS under diagonal-compression. 171
Figure 7.5 – FEM models used to simulate the compression tests carried out by BAM-ZRS: (a) macro-model; (b) micro-model. 172
Figure 7.6 – FEM models used to simulate the diagonal-compression tests carried out by BAM-ZRS: (a) macro-model; (b) micro-model. 173
Figure 7.7 – Stress-strain relationships adopted in the TSFCM: (a) compression; (b) tension; (c) shear. 174
Figure 7.8 – Coulomb friction model used in the modelling of the interfaces between rammed earth layers. 175
Figure 7.9 – Influence of the stiffness of the interface elements on the deformability of the micro-model of the compression tests. 176
Figure 7.10 – Multi-linear relationship in compression adopted in the FEM models. 177
Figure 7.11 – Compression stress – axial strain curves of the macro- and micro-models using the multi-linear relationship in compression and the reference parameters. 177
Figure 7.12 – Behaviour of the macro- and micro-model of the diagonal-compression tests with reference parameters. 178

Figure 7.13 – Effect of the mode-I tensile fracture energy (G_f^I) on the behaviour of the models of the diagonal-compression tests: (a) macro-model; (b) micro-model. 178
Figure 7.14 – Behaviour of macro- and micro-model of the diagonal compression tests after adjustment of G_f^I (x10) and β (=5%). 179
Figure 7.15 – Principal tensile strains of the macro-model for an imposed vertical displacement (Δu) of: (a) 0.40 mm; (b) 1.00 mm. 180
Figure 7.16 – Principal tensile strains of the micro-model for an imposed vertical displacement (Δu) of: (a) 0.40 mm; (b) 1.00 mm. 181
Figure 7.17 – Shear stress – shear strain curves after varying the Young's modulus: (a) macro-model; (b) micro-model. 182
Figure 7.18 – Shear stress – shear strain curves after varying the Poisson ratio: (a) macro-model; (b) micro-model. 183
Figure 7.19 – Shear stress – shear strain curves after varying the compressive strength : (a) macro-model; (b) micro-model. 184
Figure 7.20 – Shear stress – shear strain curves after varying the tensile strength: (a) macro-model; (b) micro-model. 184
Figure 7.21 – Shear stress – shear strain curves after varying the tensile fracture energy: (a) macro-model; (b) micro-model. 185
Figure 7.22 – Shear stress – shear strain curves after varying the shear retention factor: (a) macro-model; (b) micro-model. 186
Figure 7.23 – Shear stress – shear strain curves after varying the cohesion of the interfaces. 186
Figure 7.24 – Principal tensile strains of the micro-model for a vertical displacement Δu = 0.60 mm and after varying the cohesion: (a) $0.5c_{ref}$; (b) $2c_{ref}$. 187
Figure 7.25 – Principal tensile strains of the reference micro-model for a vertical displacement Δu = 0.60 mm. 188
Figure 7.26 – Shear stress – shear strain curves after varying the friction angle of the interfaces. 188
Figure 7.27 – Principal tensile strains of the micro-model for a vertical displacement Δu = 0.60 mm and after varying the friction angle: (a) $\tan(\phi_{low})$; (b) $\tan(\phi_{upp})$. 189
Figure 7.28 – Shear stress – shear strain curves after varying the tensile strength of the interfaces. 190
Figure 7.29 – Principal tensile strains of the micro-model for a vertical displacement Δu = 0.60 mm and after varying the tensile strength of the interface elements: (a) $0.5\, f_{t,ref}^i$; (b) $2\, f_{t,ref}^i$ 190
Figure 7.30 – Shear stress – shear strain curves after varying the thickness of the rammed earth layers. 191
Figure 7.31 – Principal tensile strains of the micro-model for a vertical displacement Δu = 0.60 mm and after varying the thickness of the rammed earth layers: (a) $0.5t_{lay,ref}$; (b) $1.5t_{lay,ref}$. 192
Figure 7.32 – Non-dimensional relationship between the maximum shear stress and the parameters assessed (x) for the macro-model in sensitivity analysis. 193

Figure 7.33 – Non-dimensional relationship between the maximum shear stress and the parameters assessed (x) for the micro-model in sensitivity analysis: (a) layer parameters; (b) interface parameters. 194
Figure 7.34 – Multilinear relationship adopted for the modelling of the diagonal-compression tests carried out at UMinho. 195
Figure 7.35 – Shear stress – shear strain curves of the macro- and micro-model after calibration. 196
Figure 7.36 – Principal tensile strains for an imposed vertical displacement of 3.0 mm: (a) macro-model; (b) micro-model. 196

Index of Tables

Table 2.1 – List of some of the most important documents regulating earth construction. 13
Table 2.2 – Interpretation of the ribbon test according to Standards Australia (2002). 15
Table 2.3 – Interpretation of the dry strength test according to Houben and Guillaud (2002). 16
Table 3.1 – Effects of admixtures incorporated in cementicious mixtures (Luso 2012). 37
Table 3.2 – Requirements of grouts regarding the structural behaviour of the injected construction, as depicted by (Toumbakari 2002) 38
Table 3.3 – Requirements of grouts regarding the durability of the injected construction, as depicted by (Toumbakari 2002). 38
Table 3.4 – Mixing porportions and compressive strength of the grouts tested by Vintezileou and Tassios (1995) 42
Table 3.5 – Composition and mechanical strength of the grouts tested by Toumbakari (2002). 42
Table 3.6 – Consistency requirements for mud grouts defined by Roselund (1990). 46
Table 3.7 – Results of the diagonal-compression tests carried out by Vargas *et al.* (2008). 47
Table 3.8 – Requirements of mud grouts for injection of earth constructions. 52
Table 4.1 – Properties of the materials composing the solid fraction of the mixtures (Kaolin RR40 and limestone powder Calcitec 2001 S). 70
Table 4.2 – Mineralogical analysis of the kaolin RR40 (provided by Wienerberger) 70
Table 4.3 – Chemical composition of the kaolin RR40 (provided by Wienerberger). 71
Table 4.4 – Composition of the mud grouts selected for assessing the time-dependent rheological behaviour and the adhesion capacity. 74
Table 4.5 – Properties of the soils used in the adhesion tests after sieving (KULeuven). 75
Table 4.6 – Mineralogical analysis of the kaolin Mibal-A (provided by Mibal – Minas de Barqueiros S.A.) 77
Table 4.7 – Chemical composition of the kaolin Mibal-A (provided by Mibal – Minas de Barqueiros S.A) 77
Table 4.8 – Properties of the materials composing the solid fraction of the mixtures (Kaolin Mibal-A and limestone powder Micro 200-OU). 77
Table 4.9 – Composition of the KLH mixtures used to test the adhesion capacity. 80
Table 4.10 – Properties of the soils used in the adhesion tests after sieving (UMinho). 80
Table 4.11 – Rheological and mechanical properties of the grouts used in the adhesion tests carried out at KULeuven (coefficient of variation between brackets). 96
Table 4.12 – Rheological and mechanical properties of the mud grouts used in the adhesion tests carried out at UMinho(coefficient of variation between brackets). 97
Table 5.1 – Expeditious and laboratory tests used to characterize the soils under analysis. 105

Table 5.2 – Results from the visual inspection. 105
Table 5.3 – Results of the ribbon tests and respective interpretation. 108
Table 5.4 – Compaction water content obtained from the drop test. 108
Table 5.5 – Particles size fractions of the assessed soils (according to the size fractions usually adopted in earth construction). 109
Table 5.6 – Atterberg's limits of the soils and respective USCS classification. 111
Table 5.7 – Compaction properties of the soils. 112
Table 5.8 – Minimum compressive strength for rammed earth according to standards/recommendations for earth construction. 117
Table 5.9 – Results of the Geelong test. 119
Table 5.10 – Particles size fractions of the soils S5 and S4 (according to the size fractions usually adopted in earth construction). 122
Table 5.11 – Atterberg's limits of the soils S5 and S4 and respective USCS classification. 122
Table 5.12 – Compaction properties of the soils S5 and S4. 123
Table 5.13 – Particles size-fractions of soil S6 and respective components, namely soil S5, river sand and gravel (according to the size fractions usually adopted in earth construction). 125
Table 5.14 – Atterberg's limits of the soils S5 and S6 and respective USCS classification. 125
Table 5.15 – Compaction properties of the soils S5 and S6. 126
Table 5.16 – Results of the rammed earth cylindrical specimens tested under compression. 127
Table 6.1 – Size-fractions percentages of the materials used to compose the mud grouts and respective particles specific gravity. 138
Table 6.2 – Size-fractions percentages of the grouts II55MG25 and IINMG40-60. 138
Table 6.3 – Composition of the mud grouts injected in the medium-scale specimens. 139
Table 6.4 – Properties of the mud grouts injected in the medium-scale specimens. 139
Table 6.5 – Injection conditions of the medium-scale specimens. 140
Table 6.6 – Results of the tests carried out on the medium-scale specimens. 141
Table 6.7 – Failure surfaces of the medium-scale specimens repaired with grout II55MG25 and d_{cr} = 2 mm (the tensile zone is highlighted). 143
Table 6.8 – Failure surfaces of the medium-scale specimens repaired with grout II55MG25 and d_{cr} = 8 mm (the tensile zone is highlighted). 143
Table 6.9 – Failure surfaces of the medium-scale specimens repaired with grout II55NMG40-60 and d_{cr} = 2 mm (the tensile zone is highlighted). 144
Table 6.10 – Failure surfaces of the medium-scale specimens repaired with grout II55NMG40-60 and d_{cr} = 8 mm (the tensile zone is highlighted). 144
Table 6.11 – Composition of the "natural" mud grouts used to repair the large-scale specimens. 149
Table 6.12 – Size-fractions percentages of the mud grouts IINMG40-60 and IINMG50-50. 149
Table 6.13 – Properties of the mud grouts used to repair the large-scale specimens. 150
Table 6.14 – Injection conditions of the wallets. 151
Table 6.15 – Results of the diagonal-compression tests carried out on the wallets repaired with grout II55NMG40-60. 152

Table 6.16 – Results of the diagonal-compression tests carried out on the wallets repaired with grout II55NMG50-50.....152
Table 6.17 – First crack initiation of the wallets repaired with grout II55NMG40-60 before and after injection. 157
Table 6.18 – First crack initiation of the wallets repaired with grout II55NMG50-50 before and after injection. 157
Table 6.19 – Failure surfaces of the wallets repaired with grout II55NMG40-60. 158
Table 6.20 – Failure surfaces of the wallets repaired with grout II55NMG50-500. 159
Table 7.1 – Results of the compression tests carried out by BAM-ZRS. 169
Table 7.2 – Results of the diagonal-compression tests carried out by BAM-ZRS. 170
Table 7.3 – Initial parameters assumed for the TSFCM used to simulate the rammed earth material. 174
Table 7.4 – Initial parameters assumed for the Coulomb friction model used to simulate the interfaces. 175
Table 7.5 – Parameters considered in the sensitivity analysis. 182
Table 7.6 – Maximum shear stresses obtained from the sensitivity analysis of the macro-model. 193
Table 7.7 – Maximum shear stresses obtained from the sensitivity analysis of the micro-model. 193
Table 7.8 – Calibrated parameters assumed for the TSFCM used to simulate the rammed earth material of the tests carried out at UMinho. 195
Table 7.9 – Calibrated parameters of the Coulomb friction model used to simulate the interfaces used in the micro-model of the tests carried out at UMinho. 195

Chapter 1

Introduction

1.1 General Framework and Motivation

The earth building techniques are several and are frequently associated to vernacular architecture. Despite that, the most common and widespread are the adobe masonry and the rammed earth (Houben and Guillaud 2008, Minke 2006). Adobes are moulded blocks of moistened earth that are sundried, while rammed earth consists in compacting layers of moistened earth between formwork, whereby walls are erected. Earthen materials are considered as non-industrial ones (Bui *et al.* 2009) and usually show great vulnerability against several damaging agents, such as earthquakes and floods (Houben and Guillaud 2008, Warren 1999). It is a fact that the seismic performance of earth constructions is poor, due to several factors (Lacouture *et al.* 2007), although the very low tensile strength of earthen materials is probably the first to be evidenced.

Nowadays, building with earth is still considered one of the most popular solutions for shelter and housing, but its use has been continuously decreasing. In 1982, the World's population living in a house built with raw earth was of about one third (Houben and Guillaud 2008), whereas nowadays is estimated to be of about one fourth, as argued by Jaquin (2013). In general, earth constructions have great presence in developing countries, where economical and technical limitations often make this type of construction the only feasible alternative. On the other hand, in developed countries the practice of building with raw earth has fallen into disuse over the past century, because of the technological development and extensive use of modern building materials (mainly concrete and steel). Despite that, there is a large housing stock built from earth, widely distributed around the world comprising many sites, monuments and buildings

of acknowledged historic, cultural and architectural value (Delgado and Guerrero 2007, Jaquin *et al.* 2008). In developing countries, the importance of the earth built stock goes much beyond cultural and architectonic aspects, since it also assumes a higher economic and social relevance. However, an important part of the earth built stock is found abandoned and/or in bad condition, due to the lack of proper conservation. The walls of these constructions are often found affected by cracking and by basal erosion, which reduce their bearing capacity and may cause structural failure. The presence of this kind of damage also promotes the progression of other damage forms, such as rainfall infiltrations, which increase the decay rate and lead to the short-term loss of these constructions. This problem is further enhanced by the fact that these debilitated constructions are rather common in zones of moderate to significant seismic hazard (Blondet *et al.* 2003), which compromises their further existence and puts at risk the life of millions of people.

The aforementioned importance of the earth built heritage justifies an urgent need for its adequate conservation. However, the successful repair and strengthening of earth constructions require employing adequate intervention solutions and materials (Warren 1999, Keefe 2005, Jaquin 2008). With this respect, the use of earthen materials for repair is fundamental to fulfil compatibility requirements.

The presence of structural cracks in load-bearing walls, besides constituting a path for further propagation of damage, greatly decreases the overall strength and stiffness of the construction, whereby they must be repaired in order to re-establish the original structural performance (Tolles *et al.* 1996). Cracks are usually repaired by filling with mortar, stitching and by partial rebuilding the zone around the crack. However, these techniques fail often at establishing continuity (bond), are excessively intrusive or are of difficult execution (Warren 1999, Keefe 2005, Silva *et al.* 2010). The injection of grouts is a solution often used for repairing cracks in ancient masonry, with good results (Mazzon 2010). With this respect, the grout injection seems to constitute a feasible, efficient and economic repair solution for earth constructions. Nevertheless, grouts compatible with earthen materials must be employed, which is not the case of those used for consolidating ancient masonry (fired brick or stone), including the recently proposed binary and ternary grouts (Toumbakari 2002). The obvious trend is to adopt grouts incorporating earth (Getty 2007), named as mud grouts (Warren 1999). However, the knowledge on these grouts is very limited, meaning that this is a topic requiring deep research. Furthermore, the success of this technique applied to earth constructions demands the development of a design methodology that takes into account the specificities of earth constructions and mud grouts.

1.2 Objectives

The present thesis deals with the development of the existing knowledge on the grout injection technique applied to earth constructions. Given the broad extension of this

topic, the research is limited to the case of the unmodified mud grouts (without addition of mineral binders) applied to rammed earth walls. Selecting the case of the rammed earth technique intended also to contribute for the experimental characterization and numerical analysis of this type of material. Thus, the objectives of the thesis are summarised as follows:

- Proposal of a design methodology for mud grouts;
- Comprehension of the influence of the composition of an unmodified mud grout on the properties that govern the injection, namely the rheological behaviour, bond capacity, strength, fresh-state stability;
- Assessment of the suitability of the soils from Alentejo (Portugal) for unstabilised rammed earth construction;
- Assessment of the mechanical properties of rammed earth;
- Evaluation of the effectiveness of the injection of unmodified mud grouts on the repair of cracks in rammed earth;
- Evaluation of the ultrasound pulse method as a non-destructive test for assessment of the grout injection quality and effectiveness in rammed earth walls;
- Development of recommendations for the injection of earth constructions;
- Modelling of the non-linear shear behaviour of rammed earth.

1.3 Outline of the Thesis

In order to fulfil the aforementioned objectives, the present thesis is organised in eight Chapters, as follows.

Chapter 1 introduces the framework and motivation of the thesis, presents its objectives and describes its structure.

Chapter 2 presents an overview on the state of art regarding the topic of earth construction, with focus on the concept, vulnerabilities and structural intervention solutions for this type of construction.

Chapter 3 presents an overview on the grouting technology applied to ancient masonry constructions, which includes the description of the main properties characterising a grout, of its composition materials, design methodology, application procedure and strengthening capacity. Moreover, the short state of art on grout injection of earth constructions is revised and a design approach for mud grouts is proposed. This Chapter ends with a brief insight on the colloid behaviour of clay suspensions.

Chapter 4 presents a composition study addressing the behaviour of mud grouts. This study is divided into two complementary phases, where the first was carried out at the Catholic University of Leuven and the second at the University of Minho. The

properties addressed are the rheological behaviour, strength, shrinkage, adhesion capacity and fresh-state stability.

Chapter 5 deals with the assessment of the suitability of four soils from Alentejo (Portugal) for unstabilised rammed earth construction. An experimental program addressing the characterization of the soils, resorting to expeditious and laboratorial tests, is presented. The characterization of the compression behaviour and water resistance capacity of the respective manufactured rammed earth is also addressed. The Chapter ends with the selection and study of a soil used in the manufacture of medium- and large-scale specimens tested in Chapter 6.

Chapter 6 presents an experimental program, where the adhesion capacity of unmodified mud grouts was assessed by means of tests carried out on medium- and large-scale rammed earth specimens. The medium-scale specimens consisted in beams tested under three-point bending, while the large-scale specimens consisted in wallets tested under diagonal compression. These specimens were first tested and then were repaired resorting to three unmodified mud grouts, namely an "artificial" mud grout composed by kaolin and limestone powder and two "natural" mud grouts composed by sieved soil and limestone powder. The adhesion capacity was then assessed by testing again the repaired specimens. Furthermore, the experimental program also allowed characterizing the behaviour of rammed earth in bending and shear. The Chapter ends with the evaluation of the capacity of the ultrasound pulse velocity (UPV) technique in assessing the repair effectiveness of the injection of mud grouts.

Chapter 7 presents the FEM modelling of diagonal-compression tests carried out on rammed earth wallets. The macro- and micro-modelling approaches were used for this purpose. Furthermore, a sensitivity analysis of the models is presented in order to include the variability of the most important rammed earth properties.

Finally, Chapter 8 presents the main conclusions of the thesis and a proposal for future work. Furthermore, recommendations for the injection of earth constructions are presented with basis on the experimental work performed.

Chapter 2

Earth Construction: Concept, Damage and Rehabilitation Solutions

2.1 Introduction

The current chapter aims at presenting an overview on the topic of earth construction, focusing the concept, the vulnerabilities and intervention solutions for this type of construction. This helps to clarify the importance of earth construction in the World and the necessity in developing solutions that promote the conservation and preservation of the earth built heritage.

2.2 Earth construction techniques

Raw earth is used as building material since ancient times, as is confirmed by archaeological evidences from millenarian cities that were built entirely with earth, such as Jericho (Israel), Çatal Huyuk (Turkey), Harappa (Pakistan), Akhlet-Aton (Egypt), Chan-Chan (Peru), Babylonia (Iraq) and Duheros (Spain) (Lacouture *et al.* 2007).

Nowadays, there is a large housing stock built from earth widely distributed around the world (Figure 2.1). This heritage resulted from the intensive use of this material as low cost housing solution in developing countries, but also as building material resource in developed countries during crisis periods, such as the German reconstruction after WWII.

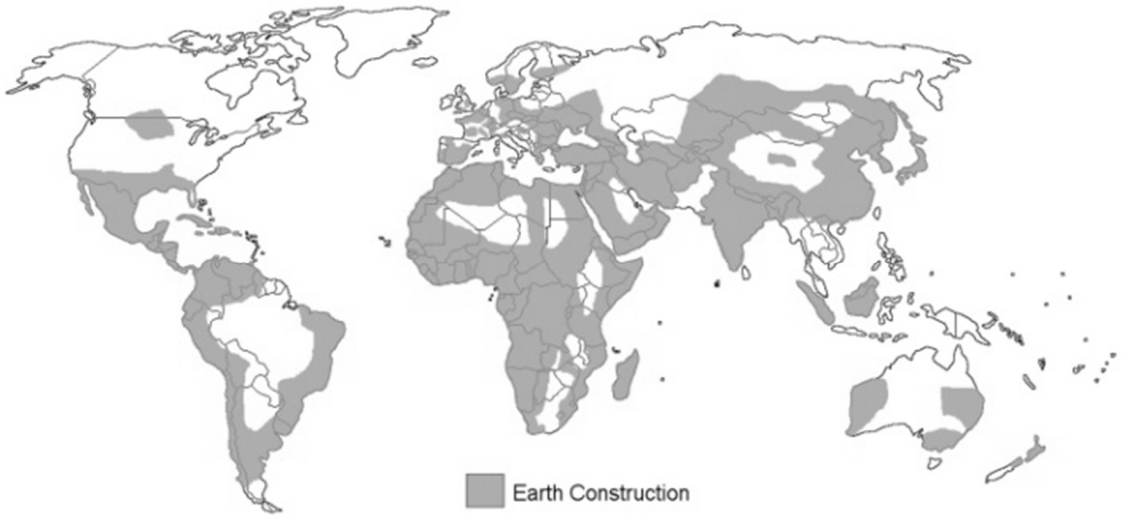

Figure 2.1 – World's Geographical distribution of earth construction (source: CRATerre-ENSAG).

The concept of traditional earth construction implies using the available local soil, which in general associates this type of construction to vernacular architecture. In fact, there are diverse earth construction techniques in the World, which in addition present numerous variations. This is a consequence of remarked differences in the properties of soils from region to region, and of other factors, such as the climate, existence of other available building materials and the culture of the population and respective economical resources.

The vernacular character of earth construction techniques makes very difficult their identification or systematization, but according to Houben and Guillaud (2008) this can be simplified into 18 techniques, as illustrated in Figure 2.2. This figure also shows that the raw earth material may assume three functions according to the technique used: as monolithic bearing structure, as bearing masonry and as infill material of another material structure (e.g.: timber).

However, the most popular traditional earth construction techniques are summarised into adobe masonry, rammed earth and wattle-and-daub, while the compressed earth block (CEB) technique assumes the position of the most popular modern earth construction technique. These four techniques are described with more detail in the following sections.

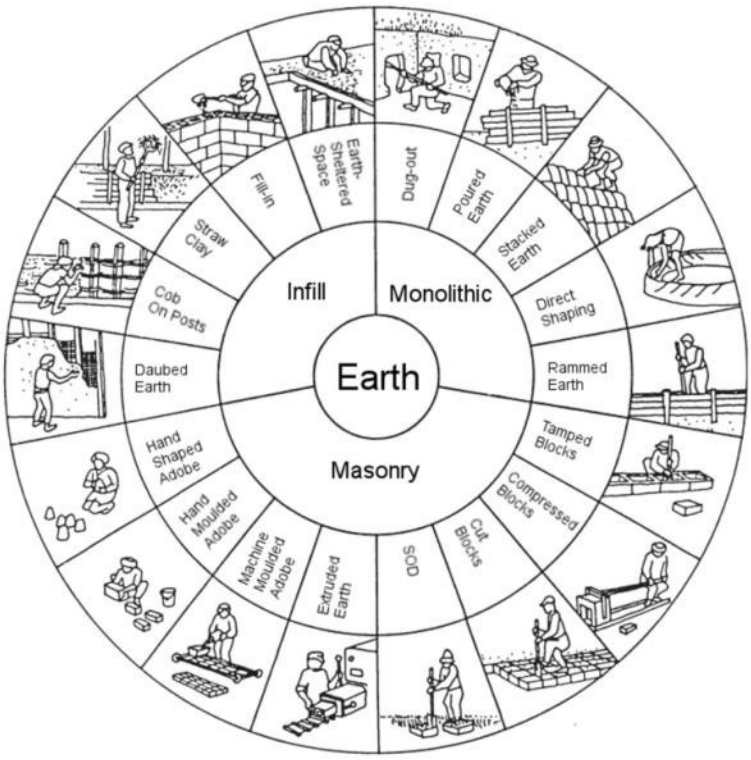

Figure 2.2 – Earth construction techniques according to Houben and Guillaud (2008).

2.2.1 Adobe masonry

Adobes are sundried bricks or blocks prepared from a pasty mix of earth and water, which may also include the addition of straw, lime or dung. Typically, the adobes are moulded in timber bottomless moulds, by simply filling them or by throwing lumps of an earth mix. Then the surface is smoothed either by using the hand, a timber piece, a trowel or a wire and the adobes are immediately unmolded and put to dry (Minke 2006). The drying of the adobes is a critical phase of their production due to the inevitable shrinkage resulting from the evaporation of the water, which has a harmful impact on the mechanical properties. In dry climates, measures to mitigate the shrinkage should be adopted, such as frequent turning over of the adobes or covering them with straw. In the case where stabilizers are used is also necessary to provide the moisture required for the curing. The dimensions of the adobes are very variable from region to region. For example, the dimensions in Spain are usually 150x150x300 mm^3 and in Portugal 400x150x300 mm^3 (Gomes 2008). The adobe production is illustrated in Figure 2.3.

Upon drying, the adobes are ready to be used as masonry units to perform walls, arches, vaults or domes. The mortar used in the masonry is in general earth based, and is prepared with the same soil used in the production of the adobes.

This technique is present in all inhabited continents. In Africa there are several heritage places built with adobe, such as Ksar of Ait-Ben-Haddou (Morocco). The same happens in the Middle-East (Bam Citadel), America (Chan Chan Archaeological Zone), Asia and Oceania. In Europe it appears in Mediterranean countries and in Portugal constitutes

great part of the historical centre of the city of Aveiro, through the architectonical style of Art Nouveau (see Figure 2.4).

(a) (b) (c)

Figure 2.3 – Production of adobes in Aveiro, Portugal: (a) preparation of the earth mix; (b) filling of the moulds; (c) drying.

Figure 2.4 – Examples of adobe construction from Aveiro (Oliveira *et al.* 2007).

2.2.2 Rammed earth

Rammed earth, also known as "*taipa*", "*taipa de pilão*" "*tapial*", "*pise de terre*", "*pisé*" or "*stampflehm*", consists in compacting moist earth by layers inside a removable formwork to build monolithic walls (Figure 2.5). In fact, the formwork constitutes a key feature, which differentiates this technique from the other. The conception and design of the formwork have been an evolving process, which resulted in several configurations. In order to grant the quality of the rammed earth wall, this element must present adequate strength and stability to support the dynamic loads of the compaction process, and adequate stiffness to mitigate the consequent deformations (Minke 2006). Another important feature to be controlled is the weight of the formwork, which must be sufficiently low in order to make it easily handled by the workers (in the assembling and disassembling operations). Typically, the formwork is supported directly on the wall and is dislocated as the rammed earth blocks are built, and whereby this is called crawling formwork (Jaquin 2008). The construction of a wall is carried out by courses (like masonry), where the formwork runs horizontally along the perimeter of the construction and then is moved vertically to build the next course. In alternative, it can be used a formwork externally supported, implying thus the assembly of a scaffolding structure (see Figure 2.6a). In Spain, some pre-Muslim rammed earth sites where this type of formwork was used are reported in literature, which is identified by absence of

putlog holes (result from the removal or deterioration these timber elements used to support a crawling formwork, which get embedded in the wall when the block is compacted) (Jaquin 2008).

Figure 2.5 – Construction of a new rammed earth house in Colos (Odemira), Portugal.

The elements of traditional formworks are made of timber (see Figure 2.6b), but not exclusively, as ropes and tying needles, for example, can be used for holding the shutters in place. Nowadays, the trend is to use the same metallic shutters used in concrete technology to constitute the formwork; a crawling formwork is constituted by two metallic shutters or a self-supporting formwork is constituted by assembling the shutters in such a way that they cover the entire wall.

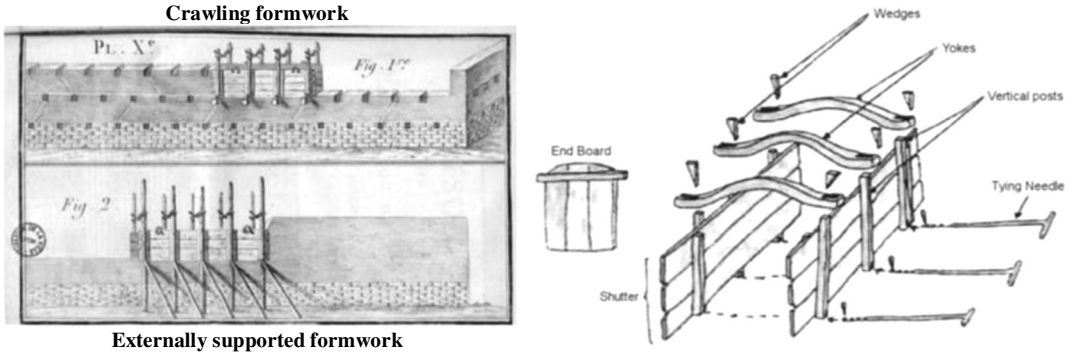

(a) (b)

Figure 2.6 – Rammed earth formworks: (a) Crawling and externally supported formwork (Cointeraux 1791); elements of a traditional crawling formwork (Cabral 2006).

The compaction of rammed earth blocks is traditionally carried out manually, resorting to rammers that in general are made of timber. Nowadays, the compaction process has been simplified by the introduction of mechanical apparatus such as pneumatic and vibratory rammers (Figure 2.7), which reduce substantially the labour and time consumed in the construction.

The dimensions of the rammed earth blocks are very variable from country to country, from region to region or even within the region; for example in Alentejo (Portugal) the length of rammed earth blocks from typical dwellings may vary from 1.40 to 2.50m, the height from 0.4 to 0.55m and the thickness from 0.4 to 0.57m (Correia 2007).

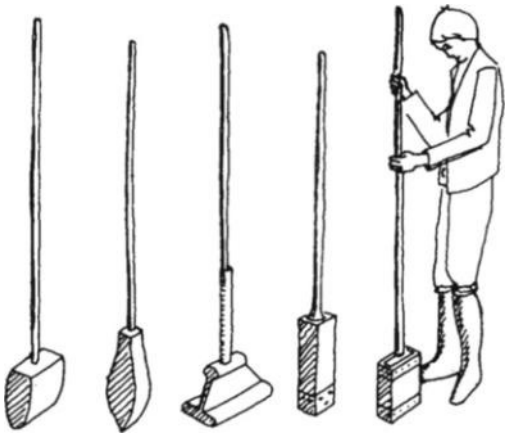

Manual rammers

Pneumatic rammers

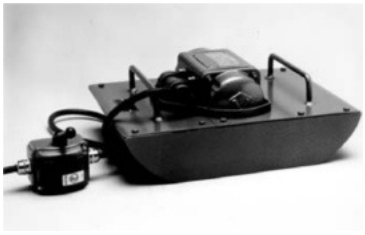

Vibratory rammer

Figure 2.7 – Rammers used to compact rammed earth (Minke, 2006).

From the history of all earth construction techniques, rammed earth is relatively recent (Fernandes 2008) and its origin is not consensual. According to Houben and Guillaud (2008) this technique was first developed in its "true" form in China during the Three Kingdoms period (221-581 AD). On the other hand, Jaquin et al. (2008) argued that the technique had two independent origin focuses: in China and around the Mediterranean. Despite that, the rammed earth technique remarks its presence around the World in resemblance to the adobe technique.

In the 16th century AD, the rammed earth technique was rather used in South America by the Portuguese and Spanish settlers, and later on (18th and 19th centuries) in North America and Oceania by the European colonisation. The publication of construction manuals of François Cointeraux in 1791 (Cointeraux 1791) marked and stimulated rammed earth construction in Europe, which was re-introduced as a fireproof solution alternative to the typical timber constructions of that period. This technique was extensively used in Germany to solve the housing problem generated after the end of WWII (Fernandes 2008). Nowadays, the rammed earth technique is commonly used in Australia and New Zealand, where there was developed solid recommendations and standards to regulate earth construction.

In Portugal, the rammed earth built stock is mainly concentrated in the southern region, namely in Alentejo, Algarve and Ribatejo. However, this type of constructions appears more often in southern Alentejo, where there is less rain and other building materials such as stone and timber (Rocha 2005). In general, the Portuguese rammed earth built stock is classified according to its use, as civil and military. The fist group includes most of the built stock and is associated to the construction of dwellings, windmills, silos and religious constructions. The second group is mainly constituted by fortifications built during the Islamic presence in the Iberian Peninsula, namely between the 8th and 13th centuries (Correia 2004).

2.2.3 Wattle-and-daub

In a general manner, the wattle-and-daub technique consists on a grid structure of timber elements (Figure 2.8), which is filled and covered by earth, and it serves to build walls, arches, vaults and domes. The timber grid is responsible for the bearing capacity and it can be constituted by wooden poles nailed together, by wickerwork or by a plaited straw support (Houben and Guillaud 2008). The earth infill serves as protection of the bearing structure and has no structural function. In general, the earth mix is very clayey and includes very often the addition of natural fibres (e.g.: straw). Thus, this technique is characterized for including high percentage of organic materials, which are prone to exhibit durability problems related to the presence of rodents or termites (Houben and Guillaud 2008).

The walls built using the wattle-and-daub technique are very thin, when compared to those of adobe or rammed earth, and thus they are also very lightweight. This combined with the flexibility of the timber elements results in a technique with interesting seismic performance when compared with the previous ones (Camilloni 2003, Houben and Guillaud 2008). Currently, this technique is very common in countries from South America (known locally as "*quincha*" or "*bahareque*") where the seismic hazard is important, such as in Peru or Equator. In Europe, this technique is frequently found in constructions used to support rural activities (Houben and Guillaud 2008), and in Portugal it is frequently found in historical centres of northern cities as a technique locally termed "*tabique*" (Pinto *et al.* 2010).

Figure 2.8 – Wattle-and-daub ("*tabique*") exterior wall of a house in Douro North Valley Region, Portugal (Pinto *et al.* 2010).

2.2.4 Compressed earth blocks (CEB) masonry

The CEB masonry technique is very recent in comparison with the traditional earth construction techniques presented previously. The CEBs can be seen as an upgrade of the adobes, which had their properties (mainly the mechanical) improved by increasing the density of the material. Despite compacting earthen materials being a traditional

stabilisation technique, the CEB technique introduced a novelty in earth construction, which consists in the usage of specific presses (Figure 2.9). This brought a certain degree of industrialization to the production of earthen materials; the blocks produced by CEB are more standard building materials, since it is promoted higher strength and quality (regularization of the dimensions and shape and decrease of the variability of the material). The Columbian researcher G. Ramires developed in the fifties one of the first CEB manual presses, which became worldwide known as CINVA-RAM (Barbosa and Mattone 2002). Nowadays, the compaction of CEBs can also be carried out resorting to hydraulic presses (Doat *et al.* 1991) that apply substantially higher pressure than those manual, which results in higher strength of blocks (Gomes 2008).

Figure 2.9 – Compressed earth blocks manufactured by means of a manual press (Gomes 2008).

The CEBs require employing soils having particles with size bellow 20 mm (Gomes 2008), which are very frequently stabilised by addition of lime or Portland cement to further improve the strength and durability. After being compacted, CEBs are put to dry under the sun or in ovens (depending on the industrialization level of the process), if they are not stabilised. If CEBs are stabilised, adequate moisture, temperature and time should be provided to cure the blocks.

Despite the young age of this technique, it can be easily found in several countries, such as Brazil, Zimbabwe, Australia, Germany and France, where it has been used as a sustainable and economical solution for housing.

2.3 Soil testing, selection and stabilisation

In most of the countries, raw earth is considered to be a non-standard material in the building industry. On the other hand, there are few countries that already developed or are developing documents to regulate earth construction. These documents are in general dedicated to three main building techniques: adobe, rammed earth and CEB. According to Delgado and Guerrero (2007), the documents can be divided into three

groups: (i) standards and regulations; (ii) normative documents such as rules and guidelines; (iii) general bibliography on technical aspects of earth construction.

A list of some the most important worldwide documents supporting earth construction is presented in Table 2.1. The design methodologies included in the documents are, in general, very simple, and are based on codes for unreinforced masonry. However, they consider larger safety factors that account for the uncertainties of earthen materials. This is a consequence of the lack of material testing and of studies to understand and to develop knowledge on these materials (Jaquin 2008).

Table 2.1 – List of some of the most important documents regulating earth construction.

Document type	Country	Document	Technique
Standard and regulation	USA	NMAC (2006): 14.7.4	A, RE, CEB
	France	AFNOR (2001): XP P13-901	CEB
	New Zealand	NZS (1998a): 4297	A, RE, CEB
		NZS (1998b): 4298	A, RE, CEB
		NZS (1998c): 4299	A, RE, CEB
	Peru	SENCICO (2000): NTE E 080	A
	Zimbabwe	SAZS (2001): 724	RE
Normative	Germany	Lehmbau Regeln (2000)	A, RE, CEB
	Australia	Standards Australia (2002): HB 195	A, RE, CEB
	Spain	MOPT (1992)	A, RE, CEB
	Portugal	LNEC (1953)	A, RE
Technical		Houben and Guillaud (2008)	A, RE, CEB
		OIA (1970)	A, RE, CEB
		Minke (2006)	A, RE, CEB

A: Adobe / RE: Rammed Earth / CEB: Compressed Earth Blocks

The evaluation of soil suitability for earth construction takes an important part in these documents, which also consider the possibility of improving the soils that cannot be used in their natural state by stabilisation with addition of binders. The evaluation of soil suitability depends on the building technique and is carried out according to two approaches (Figure 2.10): based on the evaluation of the properties of the soil or based on the properties of the final earthen material. The first approach is more usual, where properties such as texture, plasticity, organic content, binding force and compactability are assessed. In general, the second approach consists in the assessment of the compressive strength (mechanic) and the resistance to erosion against water (durability). The soil properties are assessed through testing, where expeditious tests and laboratory tests can be carried out for this purpose. On the other hand, charactering the properties of the earthen materials requires performing laboratory tests.

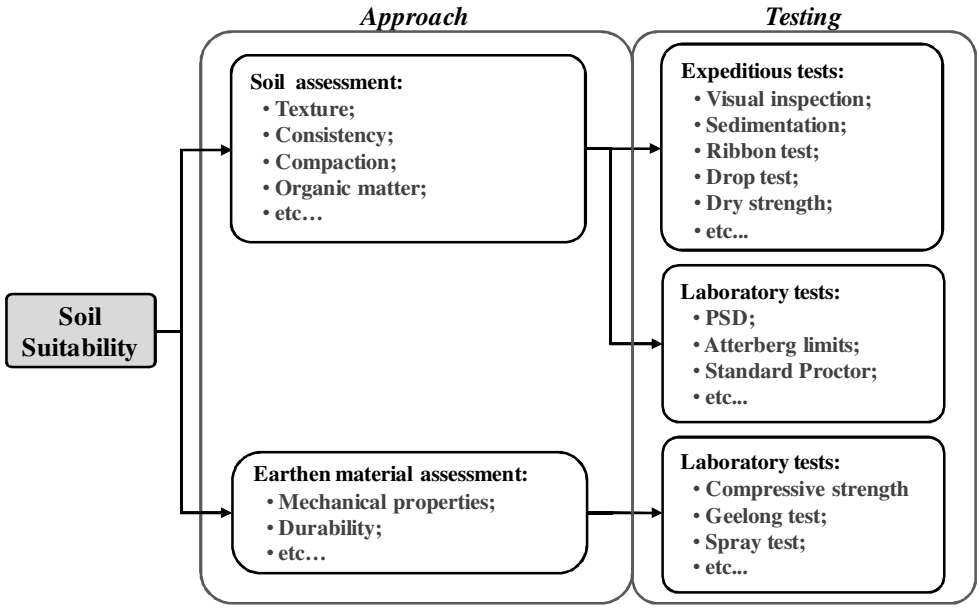

Figure 2.10 – Assessment of the soil suitability for earth construction.

2.3.1 Expeditious tests

Expeditious tests (Figure 2.11) are of easy execution and resort to simple tools, thus they are especially prone to be carried out on site. The results provide qualitative information on the soil, but are obtained very quickly. In general, the documents regulating earth construction give special importance to these tests, inclusively they provide information on the procedure and on how to interpret the results. In general, the texture of the soil is the main property being addressed by these tests, namely in what concerns the behaviour of the fine fraction.

The visual inspection of the soil gives instantaneous and useful information, and thus it should be the first step in the soil suitability assessment for earth construction. One should look at the colour and smell to determine the presence of organic matter. Looking at the texture and particles shape allows having insight on particles fractions composing the soil and on genesis of the soil (transported or residual).

The sedimentation test, also known as jar test, allows estimating the proportions between the particles fractions composing the soil (clay, silt, sand and gravel). The test requires a transparent flask that is partially filled with soil up to 1/4 of its height and then is filled with water in the remaining 3/4. The flask is slightly shaken and is left to rest for one hour to soak the soil sample. Then the flask is vigorously shaken and left to rest on a flat surface After 45 min to 60 min, the fine gravel, sand and silt layers are visible at the bottom of the flask and after a further 24 hours the clay particles should also have settled out of suspension (Standards Australia 2002). The proportion of each fraction is determined by measuring the height of the respective layer, which is converted into a percentage of the total height. This test may provide misleading conclusions if the results are not interpreted carefully; it should be paid attention to the

swelling behaviour of the clay fraction and to the flocculation of clay particles, which increase substantially the volume occupied by this fraction.

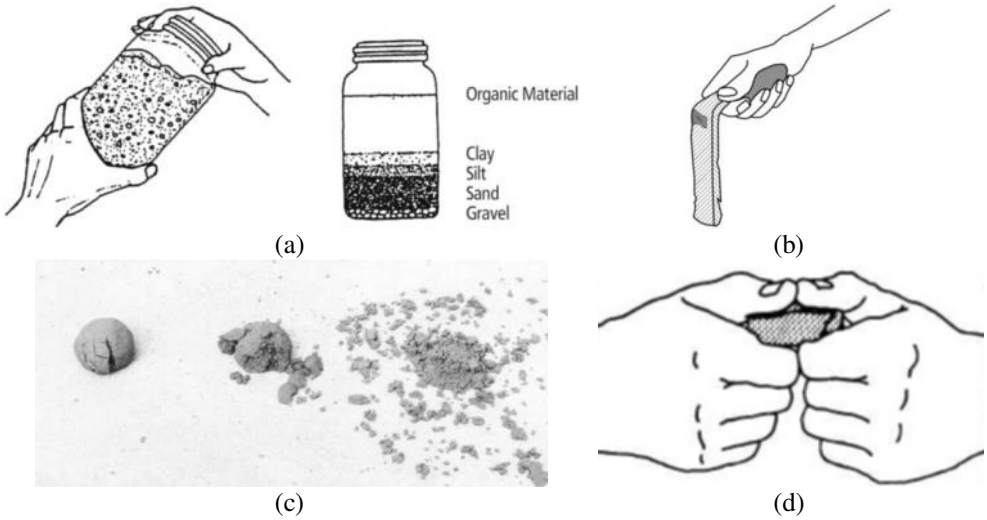

Figure 2.11 – Expeditious tests: (a) sedimentation test, (b) ribbon test, (c) drop test and (d) dry strength test (Minke 2006).

The ribbon test is used to determine if the proportions of the particles fractions of the soil are suitability for earth construction. This test is carried out by shaping, from moistened soil, a "sausage" with approximately 150 mm long and 20 mm thick. Whilst in the palm of one hand, the soil "sausage" is flattened between thumb and forefingers to produce a ribbon 4-6 mm thick, which is continuously fed forward out of the hand. The length of ribbon attained before breaking allows concluding on the proportions between particles fractions, as suggested in Table 2.2.

Table 2.2 – Interpretation of the ribbon test according to Standards Australia (2002).

Ribbon length (mm)	Interpretation
< 40 mm	Soil contains insufficient clay for mud brick and stabilised pressed block, but may be suitable, for rammed earth
40 mm – 80 mm	Soil contains low to moderate amount of clay. The longer the ribbon the greater clay content; suitable for stabilised pressed block and rammed earth
60 mm – 120 mm	Range suitable for mud brick and poured earth
> 150 mm	Generally unsuitable for earth building

The drop test is performed by firmly squeezing a handful of moist soil into a ball, which is then dropped from shoulder height at arm's length (or from 1.5 m height, depending on the regulating document) onto firm ground. From the ball impact on the ground three possible results can be obtained: (i) the ball breaks into many pieces or totally disintegrates; (ii) the ball does not break, but it gets flatten; (iii) the ball breaks into a few roughly even sized pieces. In general, this test is used to determine the optimum moisture content of the soil for starting to compact rammed earth or CEBs; the moisture content of the soil is adjusted such that the third situation described previously is observed. Minke (2006) gives an alternative interpretation of this test, which is addressed to the proportions between particles fractions.

The dry strength test is performed to evaluate the binding capacity of the fine fraction of the soil (particles bellow 0.425 mm), giving indication on clay, silt and sand proportions. This test is carried out on dry pats (40 mm diameter and 10 mm thick) prepared with the fine fraction of the soil, which is previously moistened to make it plastic and allow moulding it. The test operator evaluates qualitatively the effort required to break the pat into two pieces and effort required to crush it between the thumb and forefinger (see Table 2.3).

Table 2.3 – Interpretation of the dry strength test according to Houben and Guillaud (2002).

Observation	Interpretation
High dry strength	The pat is very difficult to break, and when it does, it breaks with a snap. The pat cannot be crushed, it can merely be crumbled though without reducing it to dust: almost pure clay
Moderate dry strength	The pat is not too difficult to break. It can be crushed to powder after little effort: silty or sandy clay
Low dry strength	The pat can be easily broken and it can be reduced to powder without any difficulty at all: silt or fine sand, low clay content

The expeditious tests described above are the most commonly used and thus they were described with more detail, but there other tests that can referred, such as: nibble test, hand wash test, water retention test and shrinkage test.

2.3.2 Laboratory tests

Laboratory tests are more complex and rigorous than expeditious tests, since in general they provide quantitative results that are not so dependent of the evaluation of the test operator. Laboratory tests have this designation because their execution requires apparatus that are easily found in laboratories, but it does not mean that they cannot be carried on site. The laboratory tests that address the characterization of the soil for earth construction are common to those carried out in geotechnical works (Figure 2.12).

Determining the particle size distribution (PSD) of the soil is essential to quantify accurately the proportions of the particles fractions composing it. The test is performed by making a soil sample go through a set of sieves, whose retained material is then weighted. The individual proportions of clay and silt cannot be determined by this method, since at this scale the particles form agglomerates that should not be considered as real particles. Thus, it is required to carry out a sedimentation test, where the individual clay and silt particles are dispersed in an aqueous solution. The principle of this test is based on the different settling rate of the individual particles, which is larger for the coarser particles. The proportions between particles are determined by resorting to Stoke's law, which requires measuring the density of the suspension along time. Then the PSD curve of the soil can be defined and compared to recommendations of regulating documents, which include from limits for the particles fractions to PSD envelopes. Nevertheless, the clay fraction is in general in evidence, due to its

importance in the strength of the earthen material and due to the fact that its presence is responsible for shrinkage of the material upon drying.

The liquid limit (LL) and plastic limit (PL) are two of the Atterberg's limits remarkably present in regulating documents, whereas the shrinkage limit (SL) is not found so frequently. Their determination gives indication on the sensibility of the soil fine fraction (particles bellow 0.425 mm) against water, which strongly depends on its clay content and respective mineralogy. This allows detecting soils that have possibly very low clay content or that the respective clay fraction contains swelling clay minerals. In fact, the moisture content of a soil defines its possible consistency states as solid, semi-solid, plastic or liquid, where the transitions are established by SL, PL and LL.

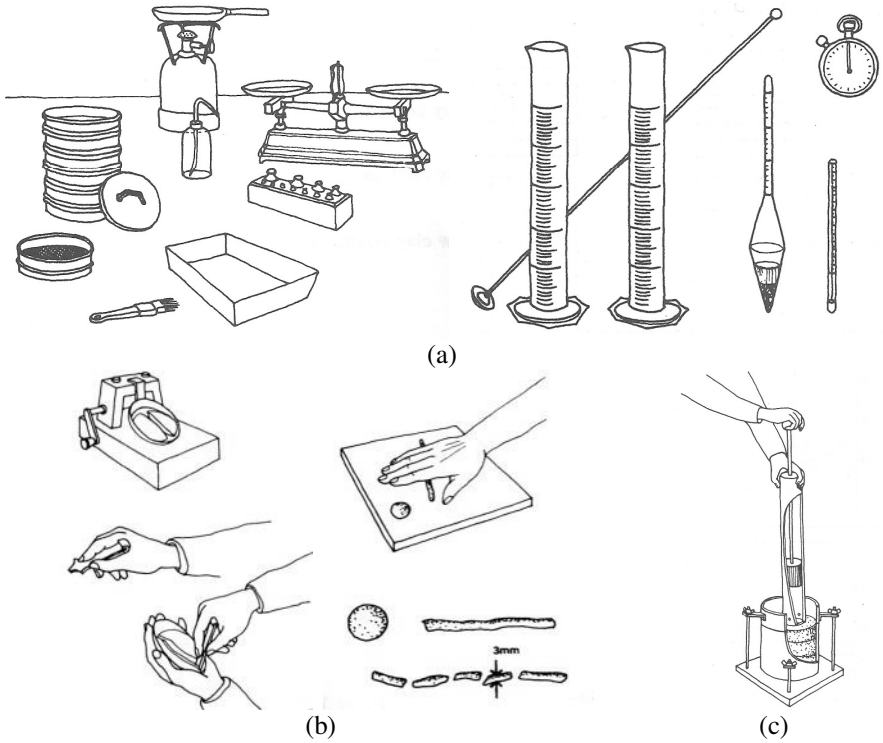

(a) (b) (c)

Figure 2.12 – Laboratory tests for soil characterization: (a) PSD, (b) Atterberg's limits, (c) Proctor test (Houben and Guillaud 2008).

The LL defines the transition between the liquid and plastic states, and is determined by using the Casagrande's apparatus. The PL defines the transition between the plastic and semi-solid states, and corresponds to the moisture content required to roll a thread of soil 5-6 cm long, which breaks into sections with 1-2 cm long when the thread diameter is reduced to 3 mm. The SL defines the transition between the semi-solid and solid states, and corresponds to a moisture content below which the soil exhibits no shrinkage. This limit can be determined by means of the mercury method or the wax method, where the objective is to measure the volume of the a soil pat after drying and shrinking from an initial known volume. The PL of a soil gives indication of its clay content, i.e., the higher the PL the higher is the clay content. The plasticity index (PI) is the difference between LL and PL, and gives indication on the presence of swelling clay minerals. Soils with high PI are more prone to have presence of swelling clay minerals.

Building in rammed earth or producing CEBs requires compacting soil, whereby the compressible behaviour of the soil is important to be known. The standard Proctor test is usually carried out for this purpose. In alternative, the modified Proctor test can also be carried out, but the energy spent in manual compaction is in general more similar to that of the standard one. The test consists in compacting soil samples with different moisture contents. The samples are compacted in a mould with standard capacity and with a specified standard compaction energy. The maximum dry density and the respective optimum water content are determined from the plotting of the dry density and water content for each sample. The maximum dry density gives indication on the strength of the earthen material; the higher the maximum dry density the higher is the expected strength. The rammed earth or CEBs should be compacted with a water content close to the optimum water content.

Knowing the soil properties gives an idea on the properties and behaviour of earthen materials manufactured with that soil. However, the properties are not really known until they are tested. Regarding the structural performance of earth constructions, the main property considered in regulating documents is the compressive strength of the earthen material. However, the dispersion between these documents, in terms of testing procedures and specimens configuration, is great (Delgado and Guerrero 2007). Thus, a comparison between limiting values for compressive strength is difficult to be made, but Houben and Guillaud (2008) states that a value between 2 and 2.5 N/mm^2 satisfies the requirements of most standards.

The durability of the earthen material is another important feature, which is typically addressed to its resistance to water erosion. In this context, the tests performed for other building materials are not adequate for earthen materials, as they are extremely severe and produce results that do not represent the observed reality (Houben and Guillaud 2008). There are tests developed/adapted specifically for earthen materials, namely the Geelong test and the spay test (Standards Australia 2002 and NZS 1998b). The Geelong test consists in exposing the surface of the earthen material, during a determined period, to water drops that fall from a specific height at a specific rate. Then the effect of the impact is measured through the pit depth and water penetration within the specimen. Despite being generally accepted, this test is much less severe than the spray test and Standards Australia (2002) putts even its reliability in cause. The spray test is an accelerated erosion test and consists in exposing the surface of the earthen material to a horizontal water spray. The spray is provided with a specific pressure and the nozzle of the apparatus is designed such the spray has a determined geometry. Like the Geelong test, the durability is defined in terms of pit depth and water penetration within the material.

2.3.3 Stabilisation

If a locally available soil is not adequate for earth construction, there are two possible solutions: transporting a suitable soil from another location or improving the properties of the available soil by stabilisation. The second option is in general the most popular, since the first can result in logistic problems, such as long transportation distances, that can make the construction more expensive. On the other hand, the stabilisation of the soil is not always feasible or economical.

There are several methods for improving a soil, which include increasing the density by compaction, reinforcing with fibres or chemical stabilisation by addition of bitumen, lime, cement or other binders. Chemical stabilisation by addition of binders is nowadays a recurrent solution used in earth construction, even though that in many situations this is not a real necessity. The stabilisation by addition of bitumen aims at improving mainly the durability of the earthen material, namely in what concerns to the resistance against water (erosion and swelling behaviour). The bitumen is added in aqueous emulsion and then is mixed with earth. Upon drying, the bitumen forms a thin strong film that holds together the particles of the soil, which also improves the cohesion of the material and thus its strength. This stabilisation technique is particularly indicated for sandy or sandy-gravel soils (Houben and Guillaud 2008).

Lime stabilisation is historically related to rammed earth construction as a successful case, since the millenary fortresses currently existing in the Iberian Peninsula are evidence of the durability and mechanical strength promoted by this stabilisation technique. The cementitious compounds resulting from pozzolanic reactions between the lime and the clay fraction in the soil are the main responsible for this improvement. Thus, this technique is indicated for clayey soils.

The addition of cement is currently the preferred stabilisation technique for new earth constructions, since it improves significantly the strength of almost all soil types. The stabilisation effect is provided by the formation of a cementious matrix that binds the particles of the soil, which results from hydration reactions and from pozzolanic reactions with the clay fraction. The addition of cement grants higher strength at short-term than the addition of lime, since hydration reactions are much faster than the pozzolanic ones.

Finally, it should be noted that chemical stabilisation is not common in heritage earth constructions (except in military earth constructions), as in general, binders were excessively expensive and inaccessible to the majority of the population.

2.4 Vulnerabilities of earth constructions

Earthen materials are subjected to several types of degradation, likely to other building materials, but the degradation rate is faster, especially if compared to modern materials (Warren 1999). In general, the decay of earth constructions may be attributed to:

(i) material deficiencies; (ii) foundation problems; (iii) structural defects; (iv) thermal movements; (v) water; (vi) biological activity; (vii) natural disasters; (viii) wind.

Material deficiencies are normally related to the texture of the soil used in the construction or to the composition of the earth mixture. If the soil has low clay content and presents excessive content of stones and gravel, it may result in an earthen material with low compressive strength and water resistance. On the other hand, if the clay content of the soil is excessive, it may result into excessive cracking due to shrinkage (Warren 1999). The addition of natural materials to the earth mixture, such as straw and manure, is a traditional procedure in earth construction. Straw has beneficial effects in terms of tensile strength, but at long-term and if adverse conditions are observed, it will decompose, leaving undesired voids that have negative impact on the mechanical properties.

Commonly to other type of structures, foundation problems may result in terrible consequences to the structural integrity, such as severe cracking or even collapse. These problems are related to the capacity of the foundation soil to bear the loads transmitted by the construction. Moreover, the low tensile strength of earthen materials does not allow them to absorb differential settlements caused by seasonal variations of the water table or by the presence of soils with different behaviour in the foundations.

Structural defects caused by incorrect or inexistent design or due to construction errors can also result into severe damage to rammed earth constructions. For example, timber A-frame trusses are often used as support structure of the roof of rammed earth constructions, but if incorrectly designed they may transmit horizontal thrusts that cannot be absorbed by the walls, resulting into cracking and leaning (Keefe 2005).

Thermal movements are often ignored as a decay agent, since it is assumed that the inherent softness and pliability of earthen structures may render them immune to such problems, but in general this is not true (Warren 1999). These movements normally result in vertical cracks, found through the walls length (spaced in regular intervals) and at walls junctions, which debilitate their monolithic behaviour and stiffness.

The action of water is considered one of the worst enemies of earth constructions. Problems with water start immediately after the construction, due to the inherent drying shrinkage, which may result in cracking to the material, reducing its strength and exposing it to other decay agents. The shrinkage behaviour of earth is function of the water content of the earth mixture, i.e. the higher the water content the higher is the shrinkage of the earthen material. Although, the volume decrease only occurs until the moisture content reaches the shrinkage limit of the soil (Minke 2006 and Warren 1999).

The strength of earthen materials is strongly affected by its moisture content; the higher the moisture content the lower is the strength. Thereby the walls of earth constructions must be protected against moisture intake after being built. The direct impact of rain on the surface of earthen walls has other prejudicial effects at long-term, such as the occurrence of basal erosion that reduces its bearing section. These problems are usually

mitigated by protecting walls with roof overhangs, external renderings and masonry plinths (Keefe 2005). This last element serves also to avoid the direct contact of earthen walls with the ground to prevent the occurrence of rising damp. It should be noted that renderings with low water vapour permeability (e.g.: cement based mortar) are harmful for earth constructions, since the interior moisture may accumulate inside the walls. In fact, this is judged to be the underlying cause of some recent earth constructions collapses (Keefe 2005).

The high moisture content in an earth construction, may also lead to the growth of plants. The development and penetration of plant roots results in cracking, due to the tensile stress caused by their expansion. The tunnels provided by dead plant roots attract animals searching for food or shelter, extending the damage even more, by drilling new tunnels and feed from the incorporated organic matter (e.g.: straw) (Warren 1999). Small animals, like insects, are more damaging than the larger ones (e.g.: rodents), since huge colonies may develop extending the damage into larger areas.

Natural disasters, such as earthquakes and floods, can inflict severe damage and even lead earth constructions to collapse. In particular, earthquakes are the natural disasters with the highest catastrophic effect. This is both a consequence of the fact that earth constructions are usually built on places with moderate to high seismic hazard (Figure 2.13) and that these constructions present high seismic vulnerability. In fact, the seismic performance of earth constructions is very deficient when compared with contemporary structures, due to their low strength and high deadweight. The deficient constructive dispositions also greatly contribute for the poor seismic behaviour of earth constructions. Such deficiencies are typically related with the lack of connection between structural elements (walls, arches, domes, vaults, roof frames, etc.) composing the earth construction. Therefore, a strong earthquake may lead them to collapse or may inflict severe structural damage, by originating harsh cracks and reducing the overall structural stiffness (Tolles *et al.* 2002).

Wind has mainly an erosive action over earth constructions. However, it can also affect other decay agents, like shrinkage or rain.

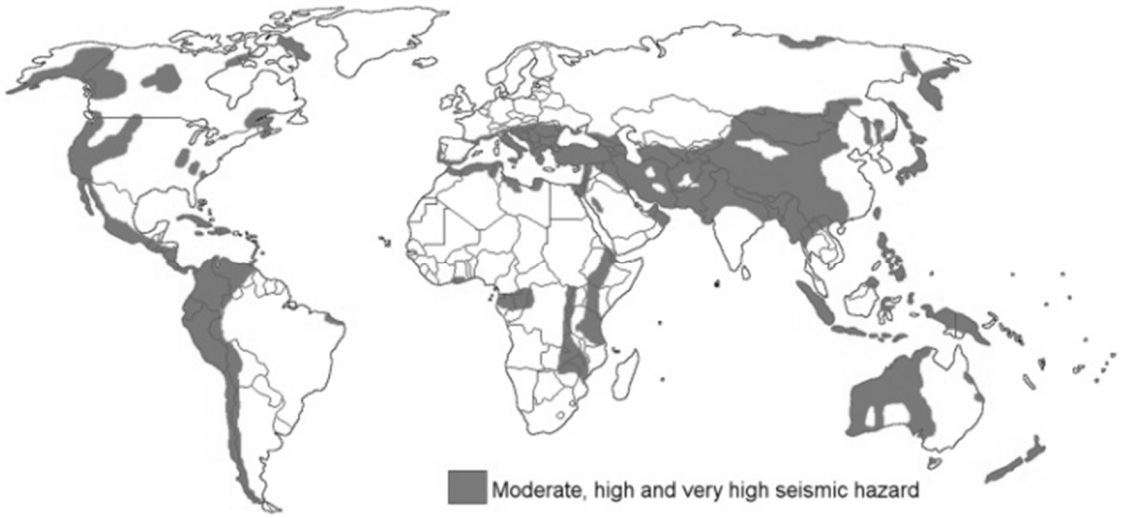

Figure 2.13 – World's Geographical distribution of regions with moderate to very high seismic hazard (after De Sensi 2003).

2.5 Structural intervention techniques

The conservation of the earthen built stock requires the adoption of intervention measures that must follow specific principles. However, this is a topic almost absent from technical documents on conservation of historical buildings. It is generally accepted that intervention measures on these constructions must allow the structure to function in a soft mode, and that excessive stiffening of a structure can lead to further damage. It is also recognized that guidelines for the clear identification of structural and seismic cracks are necessary and that improved methods for the repair of such cracks are required (Jaquin 2008).

The purpose of a structural intervention on an earth construction is at repairing or/and at strengthening its structural capacity. In the first case, it is intended to recover the original structural behaviour partially or totally, which is in agreement with the principles referred previously. The second case intends to improve the structural behaviour significantly, and thus such interventions are not so prone to follow the conservation principles.

Repair interventions on earth constructions have two main goals: to replace lost volumes of material and to reconnect cracks. The absence of great volumes of material is a common pathology found in earth constructions, which can be attributed to several factors such as: partial collapse caused by an earthquake or another external factor, presence of biological activity, basal erosion caused by rising damp and erosion caused by rain impact. In the case of adobe constructions, the obvious repair solution for this problem is rebuilding the damaged zone with similar adobe masonry. In the case of monolithic earth constructions, the obvious solution is replacing the missing material with new material, where some techniques exist to serve this purpose.

A common technique used to repair basal erosion of rammed earth walls consists in using a mixture of soil (previously studied) similar to that of the original construction, which is compacted in place (Figure 2.14). First, the missing section is regularized and the loose material is removed. Then, a single-sided formwork is assembled covering the damaged section partially and the earth mixture is compacted from the uncovered zone into horizontal layers. One of the main problems of this technique lies on the difficulty of compacting adequately the last layers due to the limited vertical free space within the formwork. This situation is normally overcome by leaning the last layers, which allows compacting them from outside the wall surface. Another problem comes from the shrinkage of the new rammed earth material upon drying, which is responsible for difficulties in bonding the repair material to the original rammed earth. Thereby, steel reinforcements and plastics meshes are often included. An alternative to this procedure, which also mitigates the shrinkage problem, consists in prefabricating earth blocks that are put in place and then bonded with earth mortar. There are also reported cases where bricks, adobes and even concrete were used as replacing materials (Warren 1999 and Mileto *et al.* 2011).

Figure 2.14 – Repair of the basal erosion of Paderne's Castle by compacting new rammed earth material in place (Costa *et al.* 2008).

Projected earth is a recent intervention technique for repairing basal erosion (Figure 2.15), which was applied successfully in the conservation of Paderne's Castle in Portugal (Cóias and Costa 2006) and of the Alhambra in Spain (García 2010). This technique consists in projecting a mixture of moist earth at high speed against the damaged area, where the impact energy is supposed to grant a compaction similar to that of the original rammed earth. This technique has some aesthetical limitations, since the rammed earth layers are not recreated, where a surface texture much more homogeneous is obtained. The shrinkage is another problem of this technique, since the projection of the earth is only possible by the wet method (García 2010), which requires high moisture content of the earth mixture in order to provide adequate flowability through the projection apparatus. It should be noted that this technique is recent and further investigation must be carried out on the optimization of earth mixtures.

The presence of structural cracks is a common pathology of earth constructions, whose cause is often attributed to settlements of the foundations, to concentrated loads, to horizontal thrusts applied by the roofs or to earthquakes. Repairing such cracks is essential to recover the original structural behaviour (at least partially). Moreover, cracks are weak points for water infiltration, which are prone to cause even further decay to the construction.

Figure 2.15 – Repair of the basal erosion of Paderne's Castle by projecting earth at high speed (Costa *et al.* 2008).

The most basic technique for repairing cracks consists in simply filling them with earth mortar. The mortar, with composition similar to that of the original earthen material, is introduced from the faces. When the crack is particularly thinner, the wall is cut back to enlarge the crack and allow its filling. This method is inefficient in terms of restabilising the lost continuity due to the crack, but it may solve the problem of water infiltration. The efficiency of this technique can be increased by adopting a mortar with fluid consistency, such as a grout, which may grant the complete filling of the crack.

Stitching the crack is another solution to this problem, and consists in creating a mechanical connection between the sides of the crack ("stapling" the crack), Figure 2.16. According to Keefe (2005), this is carried out by cutting horizontal chases in the wall with a determined spacing along the crack, which are then filled with mud bricks and earth mortar prepared with a soil similar to that of the original rammed earth.

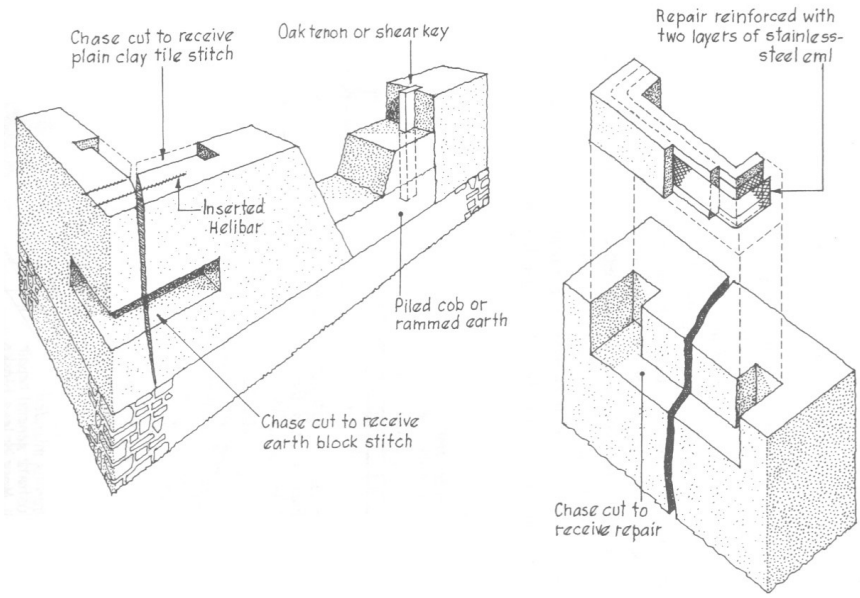

Figure 2.16 – Repair of cracks by stitching (Keefe 2005).

Regarding the strengthening of earthen walls, the introduction of stone masonry buttresses (Figure 2.17) is probably one of the most basic and ancient solutions for out-of-plane behaviour strengthening. This solution serves both as amendment to the seismic performance and as solution to solve a problem of leaning walls caused by horizontal thrusts transmitted by traditional timber roofs. The introduction of steel tie bars to connect opposed facades is another method to improve the out-of-plane behaviour of rammed earth walls (Figure 2.18). The placement of external beams tied by wires on opposed walls is an alternative to the previous technique. This constitutes a more global strengthening, as the forces from the beams are transmitted along the walls. On the other hand, the forces in the tie bars are transmitted to the walls in localized points by anchorage plates, whose dimensions are recommended to be 1 m^2 in order to avoid punching failure (Ashurst and Ashurst 1988).

Figure 2.17 – Strengthening of a rammed earth construction by introduction of buttress in Vila Alva, Alentejo (Parreira 2007).

The connection between perpendicular earthen walls is in general weak, since cracks are very often observed at their junctions, which debilitate the structural behaviour, specially the seismic performance. The placement of grouted anchors connecting perpendicular walls is a technique used to face this problem. However, Pearson (1997) argues that their use in earth walls is limited because of the low shear strength of earthen materials, whereby they should not be relied upon to stitch major structural cracks.

As it is generally accepted, the tensile strength of earthen materials is very low and constitutes a key factor contributing to the high seismic vulnerability of earth constructions. Improving the tensile strength of earthen walls is possible through the fixation of timber elements on the facades of the building, which are then rendered with a compatible earth mortar. An alternative to timber elements is the use of metallic meshes or geo-meshes, constituting a reinforced plaster (Figure 2.19). From an aesthetical point of view, this solution should not be used where important wall coverings are present.

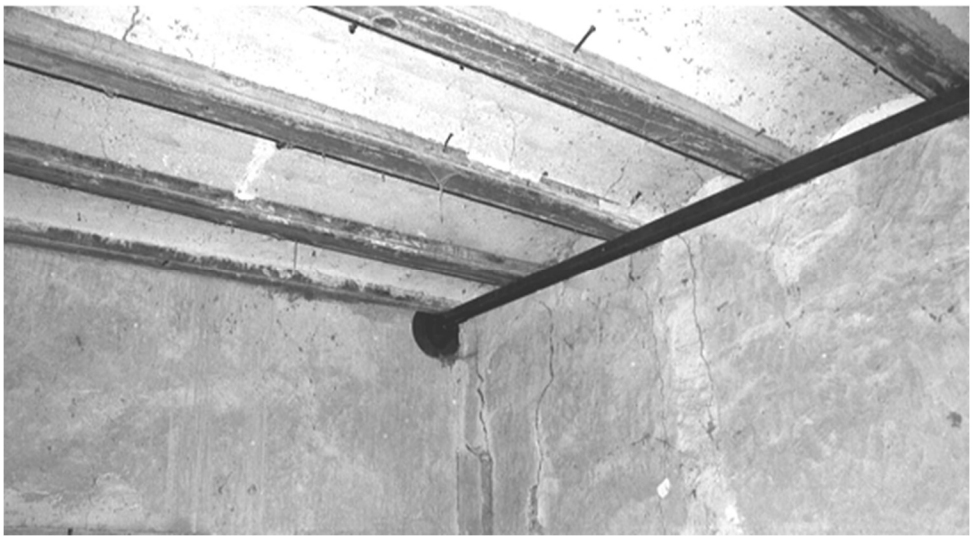

Figure 2.18 – Strengthening of opposing walls tie bars (Jaquin 2008).

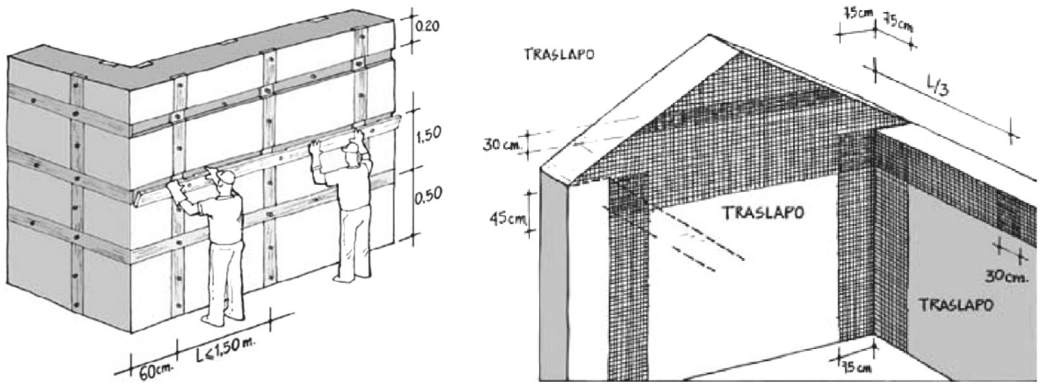

(a) (b)

Figure 2.19 – Strengthening by fixation of: (a) timber elements and (Lacouture *et al.* 2007); (b) metallic meshes (Pérez *et al.* 2007).

2.6 Conclusions

The concept of earth construction is closely related to the concept of vernacular architecture, which explains the enormous diversity of earth building techniques and their successful use around the World. Nevertheless, the most popular traditional earth construction techniques can be summarised into adobe masonry, rammed earth and wattle-and-daub, while CEB masonry assumes the position of the most popular modern technique.

In most countries, raw earth is considered as a non-standard material in the building industry, but few countries have already developed documents to regulate earth construction. The design methodologies included in these documents are, in general, very simple and are based on codes for unreinforced masonry. The suitability of soils occupies another important part of these documents, where it is carried out according to two approaches: based on the evaluation of the properties of the soil or based on the properties of the final earthen material. The texture, plasticity, organic content, binding force and compactability of the soil are the properties mainly addressed in the first approach, whose assessment is carried out through expeditious and laboratory tests. The strength and durability are the main properties addressed in the second approach.

The decay of earth constructions may be attributed to several factors, which include material deficiencies, foundation problems, structural defects, thermal movements, water action, biological activity, wind action and natural disasters (earthquakes and floods). Typically, the damage found is summarised into lost volumes of material and cracking. There are several techniques that can be used to repair this kind of damage, which include rebuilding, projecting earth at high speed, filling and stitching. Nevertheless, the employed materials should look at respecting the compatibility with the earth construction to be repaired.

There are several techniques proposed for strengthening existing earth constructions, which were described in section 2.5 and include buttressing, introduction of steel tie bars, placement of grouted anchors and fixation of timber elements and meshes on the walls.

Chapter 3

Grouting Technology in Historical Constructions: Short Overview

3.1 Introduction

The current Chapter starts by presenting an overview on the grouting technology applied to ancient masonry constructions. This includes the description of the main properties characterizing a grout, of the materials used in their composition, their design methodology and application procedure. Then, the strengthening capacity of grout injection applied to three-leaf masonry is discussed. The short state of art on grout injection of earth constructions is also reviewed, where the trend was shown to be the adoption of earth based grouts (mud grouts) due to their enhanced compatibility.

Gathering this information allowed proposing a design approach for mud grouts, which served as basis for the elaboration of the experimental work developed in the thesis. This Chapter ends with a brief insight on the colloid behaviour of clay suspensions due to its expected importance on the behaviour of mud grouts.

3.2 Grout injection of ancient masonry

According to Toumbakari (2002), a grout can be defined as "a fluid binder employed for the filling, homogeneisation, imperviousness, consolidation and/or upgrading of the mechanical properties of systems presenting pores, voids, cracks, loss of cohesion or of cohesionless systems". However, this definition becomes more complete if the term mortar is used instead of binder, since a grout also may include aggregates with filler

purposes (such as limestone and quartz powders) and other admixtures, such as superplasticisers.

With respect to the injection of ancient masonry, grouts are used to fill cracks and voids, being those visible or not (Ignoul *et al.* 2005). In general, the injection of cracks allows repairing the bond disrupted and promotes the consolidation of the masonry (Figure 3.1a). The injection of voids includes the filling of gaps between leaves and units, and of voids existing in inner leaves made from rubble masonry (Figure 3.1b). This allows consolidating the masonry, and in the last case, it may promote a strengthening effect, by improving the mechanical properties and the monolithic behaviour of the masonry. Another function of the grout within the masonry is to serve as a barrier against water penetration and flow. For example, Figure 3.1c illustrates a case where the injection was used to seal the joints of a stone fountain in Guimarães (Portugal). The grout injection technique is also frequently used to complement other consolidation/strengthening solutions. The application of anchoring systems is an example of these solutions (Oliveira *et al.* 2012). In this case, the grout is responsible for the stress transmission between the masonry and the reinforcing element (eg.: steel or FRP rods).

(a) (b) (c)

Figure 3.1 – Examples of the application of the grout injection technique: injection of cracks in a masonry chimney; (b) injection of the inner leaf of a masonry wall (Cóias 2006); (c) injection of the joints of a stone fountain.

The great advantage of grout injection towards other masonry strengthening solutions is the low aesthetical impact (Roque 2002). This means that this technique can be used in masonry walls presenting coatings with artistic and cultural value, such as frescoes and ceramic tile-works (eg.: *"azulejos"*), providing that adequate grouts are used. However, the grout injection is a technique with very limited reversibility. In the case of the injection of three-leaf masonry, this means that the grout will be integrated as a permanent material. The grout, as a strange body, must exist and work in harmony within the masonry. This brings up the concept of compatibility (chemical, physical and mechanical), which is further discuss in Section 3.2.2 by taking into account the several possible materials that may compose a grout. Therefore, the decision of applying this

intervention technique should be preceded of a thorough survey of the structure, which is not a topic of discussion in this thesis; see Binda *et al.* (2000) and Binda *et al.* (2006) for further information.

3.2.1 Grout properties

The injection of a grout requires knowing in advance its properties, since the effectiveness and feasibility of this type of intervention depends on them. Therefore, the most important properties featured by a grout in both fresh- and hardened-state are here depicted, namely the fluidity, penetrability, static bleeding, segregation, water retention, setting time, mechanical strength, volume variation and adhesion.

The fluidity of a grout consists in its capacity of remaining fluid during sufficient time for allowing its flow into the voids within the masonry (Valluzzi 2000). This property depends on the particle size distribution (PSD) of the solid phase, as well as on its nature, shape and specific surface. The percentage of the mixing water and the mixing method also take their important role in the definition of the fluidity (Vintzilou 2006). It should be noted that the fluidity of a grout is deeply related with its rheological behaviour. The fluidity can be measured by means of the flow time through a Marsh cone (eg: ASTM C 939 (ASTM 1994)).

The penetrability of a grout consists in its capacity of penetrating through voids, gaps, cracks and porous substrata. This capacity depends on inherent properties of the grout and on the properties of the substrata. The maximum particle size of the solid phase of the grout dictates the minimum injectable void size. According to Miltiadou (1990) the maximum particle size of the grout should be, at least, three times lesser than the minimum void size to be injected. The water sorption of the substrata is another factor affecting the penetrability. High sorption rates may hinder the penetration of the grout due to clogging caused by its drying at the contact surface. The penetrability can be assessed by means of sand column tests (eg: NF P 18-891 (AFNOR 1992)).

The static bleeding (or just bleeding) consists on the formation of water layer at the surface due to its migration from the grout. This phenomenon is mainly related with excessive percentages of mixing water and with the PSD of the solid phase (deficiency of ultrafine particles). This property can be assessed by means of bleeding tests (eg: ASTM C 940 (ASTM 2003)).

The segregation is interlinked with the bleeding and consists on the stratification of solid phase by sizes of the particles. This phenomenon is related with sedimentation of the coarse particles, caused by excessive mixing water and/or deficit of ultrafine particles in the grout. The segregation can be assessed qualitatively by visual inspection. A standard test for quantitative assessment does not exist, but Van Rickstal (2000) proposed a procedure based on the measurement of the density of the grout through time.

The water retention property of a grout consists in its capacity of holding the mixing water required to maintain the injectability properties of the grout during the injection. It should be noted that the injectability of a grout is defined by its fluidity, penetrability, stability and water retention capacity. The water retention capacity is not directly measurable, but it is known that incorporating materials such as lime improves it. Moreover, the water sorption by the substrata can be mitigated by wetting it previously to the injection.

The setting time is an important property of a grout, since it must be sufficiently long to allow the injection of the grout without compromising its fluidity. This property is affected by several factors, such as the mixing temperature, the injection temperature, the volume of the prepared grout and the shape of the mixing container (Luso 2012). The setting time can be determined by resorting to a Vicat apparatus (eg: ASTM C 953 (ASTM 2010)).

The mechanical strength of a grout defines the final strength of the element where is applied. In order to avoid a substantial disproportion between injected and non-injected elements in a structure, the strength of the grout should be comparable to that of the element. Otherwise, it may disturb substantially the stress distribution within the structure, which may cause damage (Luso 2012). The strength of the grout can be assessed by means of three-point bending and compression tests (eg: EN 1015-11 (CEN 1999)).

The volume change of a grout includes both shrinkage and expansion. The shrinkage can have drying, chemical, autogeneous, and thermal origins; see Neto *et al.* (2002) for more details. The expansion of the grout is associated to the formation of expansive compounds from the hydration of the binder, such as ettringite and portlandite.

The adhesion capacity of a grout to the substrata is possibly one of the most important properties regarding the effectiveness of a grouting intervention. A grout with good adhesion is capable of granting the continuity between materials disconnected by cracks, gaps and voids.

Being depicted the main properties of a grout, the next Section presents and discusses the possible raw materials that may compose a grout. The influence of these materials on the aforementioned properties is also addressed.

3.2.2 Grouting materials

Several materials can be used to compose the binder of a grout, but in general they can be distinguished into two main categories: organic and inorganic (also known as mineral binders).

The binders included in the organic category consist on polymeric systems, which can be applied in pure form, pigmented or complemented with filling materials Toumbakari (2002). These polymeric systems include materials such as epoxy,

polyurethane, methacrylic and unsaturated polyester resins (Brás 2011). These resins may feature a wide range of viscosity and yield stress values, which make them very desirable materials for injection. Resins also do not require solid particles in suspension to be applied, meaning that they do not suffer from thickening due to loss of the liquid phase when injected in a porous substratum. Therefore, resins with very low viscosity are very suitable for injection works where the penetrability is an issue, namely in the injection of thin cracks (Perret 2002). However, the high penetrability of the resins can also be a problem in the case of the injection of brick masonry. Resins can be absorbed by the masonry unit in about 5-6 mm depth, emptying cracks that would be expected to be filled. Moreover, this also has implications on the masonry unit, by changing its colour, porosity and mechanical properties (Toumbakari 2002). The porosity of masonry impregnated with resins decreases dramatically, and this has consequences on the natural water and vapour transmission within the masonry. The "natural breathing" of masonry can be impeded by the presence of resins and can be source of durability problems, namely freeze-thaw and cryptoflurescence degradation.

In terms of hardened-state properties, resins are characterized by their relative high mechanical properties (Young's modulus, and compressive and tensile strength) and adhesion capacity to dry substrata. However, their mechanical properties can be very different from those of ancient masonry. The thermal behaviour of the resins also differs from that of ancient masonry, which makes them to be physically and mechanically incompatible. These differences may result in stress concentrations caused by changes in the loading and temperature conditions, which may damage the masonry. Damage also may occur from the setting of these binders, because of its important exothermicity. Another major limitation of the use of resins is their decrease in bond strength when the substratum presents wet surfaces (Van Rickstal 2000 and Vintzileou 2006), which is the general case of ancient masonry (Toumbakari 2002). In general, the injection of ancient masonry with organic binders should be avoided, since these are expensive materials and present several incompatibilities with masonry.

On the other hand, the inorganic category includes the use of binders such as hydrated lime, hydraulic lime and cement. Pozzolanic materials can be used in combination with these binders, but are specially required when hydrated lime is used in order to provide hydraulicity to the hardening. This is necessary to overcome the slow kinetics of the hydrated lime air-hardening, which is an effective impediment to the contribution of the grout to the repair and strengthening of the masonry. In fact, the air-hardening rate of hydrated lime is so slow that there are known cases of historical mortars in thick walls where this process is incomplete, even after several centuries (Ferretti and Bažant 2006). Restoration mortars prepared with hydraulic lime present great compatibility with ancient masonry, since these are softer or more permeable than the masonry units and are no harder or more impermeable than the historic mortar (Sepulcre-Aguilar and Hernández-Olivares 2010). Nevertheless, it should be again emphasized that the slow hardening of hydrated lime constitutes a huge impediment to

its use as single binder of a grout. The hydraulicity problem can be solved if hydraulic lime is used instead. The hardening of this binder is much faster than that of hydrated lime, but is also slower than that of cement. In fact, the slow strength gain may compromise the use of this binder if an important short-term strength is required. On the other hand, hydraulic lime is also expected to have good compatibility with ancient masonry. However, the use of hydraulic lime based grouts as single binder is still quite recent (Vintzileou 2006 and Brás 2011) and little studied in terms of durability. In terms of applicability, Vintzileou and Miltiadou-Fenzas (2008) showed that these grouts satisfy sufficient injectability properties for injection of fine cracks and voids in three-leaf masonry. The strength levels achieved were also satisfactory, but the required minimum compressive strength (6 N/mm^2) was attained just after six months of age.

Ordinary Portland cement (OPC) is probably the most common type of cement used for preparation of cement based grouts (grouts where the main binder is cement), but other modern cements are also used. With this respect, ultrafine and microfine cements have particular interest in grout injection. One of the major advantages of these cements is the enhancement of the grout injectability properties. According to Perret *et al.* (2003) and Ignoul *et al.* (2005), the injectability properties of these grouts may be comparable to those of resins, allowing the injection of cracks with width inferior to 0.3 mm. Other advantage of microfine cements is the enhancement of the bonding properties (Luso 2012). During the hardening, small CSH (calcium silicate hydrate) crystals are formed around the aggregate, constituting dense and homogeneous layers of CSH gel, which promote the adhesion between both materials (Perret 2002).

However, the use of cement based grouts in the injection of ancient masonry is controversial. Since the eighties that several problems related with the application of these grouts have been pointed out, mostly related with durability features. Several chemical incompatibilities between the materials of ancient masonry and cement based repair materials have been reported, despite their similar chemical composition. The formation of expansive compounds, such as ettringite, constitutes one of these incompatibilities. Ettringite formation can occur from within the hardened cement grout due to sulphate attack, damaging the grout and the masonry (Collepardi 1999). The presence of sulphates in historical masonry is common and may have as source the surrounding ambient and even the masonry itself (Van Hees *et al.* 2004). According to Van Rickstal (2001), this problem can be reduced if slag cement is used. Furthermore, when a cement grout is injected it introduces soluble alkali salts in the masonry, which can be source of efflorescence and cryptoflurescence damage. With this respect, white cement has lower alkali content, but its use makes the grout more vulnerable to sulphate attack (Jeffs 2001).

The mechanical properties of cement based grouts are also higher than those of ancient masonry, which make them mechanically incompatible. For example, Miltiadou (1990) reports values of compressive strength varying between 10-30 N/mm^2 for grouts constituted by 50-75% (wt.) of cement. On the other hand, the compressive strength of

masonry may vary between 1-10 N/mm^2. This large difference in strength means also a large difference in stiffness, which may result in damage to masonry due to the occurrence of stress concentrations, originated in a similar way to that referred for the grouts based on organic binders. This breaks the idea that stronger grouts are synonymous of higher strengthening effectiveness. Cement based grouts also cannot be said to be physically compatible with ancient masonry. In general, the open porosity of these grouts is much lesser than that of ancient masonry, which may constitute a problem for the water and vapour transmission within the masonry. Given the many drawbacks of the use of cement based grouts, their injection should be only considered if the durability of the masonry is not compromised or if emergency consolidation is required.

The last decade brought to the scene the injection of binary and ternary grouts in the consolidation of three-leaf masonry. The binder of a binary grout combines two materials in its constitution, but in general it consists in mixing cement or hydraulic lime with hydrated lime or pozzolanas. The binder of a ternary is constituted by combining more than two materials, namely cement, hydrated lime, hydraulic lime and pozzolanas. According to Toumbakari (2002), these grouts should include cement in their composition, whose percentage may vary between 10% and 30%. A minimum percentage is required in order provide to the grout short-term strength. On the other hand, this percentage should be kept low in order to avoid the compatibility problems aforementioned for the cement based grouts. In this way, it is possible to combine the advantages of both lime and cement based grouts. Ternary grouts also include the incorporation of pozzolanas, which bring advantages to the grout, such as: decrease in hydration heat, decrease in bleeding and segregation, improvement of the permeability, improvement of the fluidity and improvement of the durability against sulphate attack (Luso 2012).

Pozzolanas are siliceous materials with prone reactivity with hydrated lime at ambient temperature, and can have natural or synthetic origin. Natural pozzolanas consist in ashes and pumices of volcanic origin, which use was intensive during the Roman Empire in the manufacture of mortars. Pumice from Pozzuoli, Santorin earth and Rheinisch trass are examples of such pozzolanas (Toumbakari 2002).

The synthetic pozzolanas are in general industrial by-products where the original raw materials were subjected to a thermal treatment. In general, the properties of synthetic pozzolanas are more consistent and homogeneous than that of natural pozzolanas. The synthetic pozzolanas are usually preferred for incorporation in grouts, since the properties of the final product are more easily controlled. This group of pozzolanas includes materials such as fly ash, silica fume, blast furnace slag and metakaolin.

The incorporation of fly ash has the main advantage of improving the fluidity of the grout (Sybertz and Reick 1991), by promoting a decrease in plastic viscosity and yield stress (Brás 2011). Other advantages of the incorporation of fly ash include: reduction

of the hydration heat and enhancement of the durability, adhesion and strength (Luso 2012).

Silica fume is a pozzolana with high reactivity (Velosa 2006) due to its high fineness. Its incorporation in grouts allows enhancing the stability (bleeding and segregation), adhesion to the substrata (Toumbakari 2002), strength and durability (Luso 2012). However, their colloid size jeopardizes the injectability properties, by increasing substantially the plastic viscosity and yield stress (Toumbakari 2002).

The incorporation of blast furnace slag has as main advantage the enhancement in durability (especially against sulphate attack), but may endanger the rheological and mechanical properties (Toumbakari 2002).

Metakaolin is produced by calcination of kaolin at a temperature between 600ºC and 700ºC (Pinto 2004). The final amorphous product is provided of high fineness and percentage of aluminum-silicates, which confer high reactivity with hydrated lime. The incorporation of this pozzolana in concrete (as cement substitute) has been growing, due to enhancement of its durability and reduction of its environmental impact, related with the lower energy required for the production of metakaolin. The incorporation of this pozzolana in grouts provides adequate strength and enhances its durability. However, limited percentages of metakaolin should be considered (no more than 50% in wt.), since there are reported cases of strength decay due to phase change of the hydration compounds (Cizer 2009 and Oliveira *et al.* 2012). The incorporation of metakaolin has also implications on the rheological behaviour of a grout, due to irregular shape and small size of its particles.

Fillers constitute another category of admixtures that can be incorporated in a grout. These materials include fine sand and powders of quartz, limestone, marble, schist and crushed brick. The main purpose of these materials is to reduce the percentage of binder in the grout. This allows decreasing the cost of the grout and aids in the mitigation of the shrinkage. The incorporation of limestone powder also benefits the rheological properties, by decreasing the plastic viscosity and yield stress (Svermova *et al.* 2003).

Chemical admixtures are also often used in the design of grouts, in order to manipulate their fresh- and hardened-state properties. Table 3.1 lists out the effects that different admixtures can have on the properties of a cementicious mixture. A detailed review of these admixtures can be found in Paillère *et al.* (1992). From the list presented in Table 3.1, the most important type of admixture is probably the plasticizers and superplasticisers group. According to Van Rickstal *et al.* (2003), adequate superplasticisers are essential to obtain a fluid grout with adequate mixing water. Otherwise, the fluidity requirement of the grout would require high percentage of mixing water, which would result in stability, strength, shrinkage and adhesion problems (Luso 2012).

In this Section, the raw materials that can be incorporated in the composition of a grout were depicted and their limitations regarding the injection of ancient masonry were

discussed. These limitations should be taken into account when designing the grout. Therefore, the success of a grouting intervention is only granted if a design methodology is followed. The next Section serves to present an adequate design approach for grouts to be injected in ancient masonry.

Table 3.1 – Effects of admixtures incorporated in cementicious mixtures (Luso 2012).

Admixture type	Main effect	Secondary effect
Water reducers	Increase the fluidity and strength, and decrease the mixing water	Setting retarder and decrease the bleeding
Plasticizers and superplasticisers	Greatly increase the fluidity and decrease the mixing water	Higher setting time, decrease the bleeding and increase the strength
Water retainer	Retain the mixing water and decrease the bleeding	Setting retarder and increase the stability
Setting retarders	Increase the setting time	Reduce the strength at short-term but increase at long-term; Higher shrinkage
Setting accelerators	Decrease the setting time	Increase the strength at short-term
Hardening accelerators	Develop the maximum strength in a shorter period	Reduce the bleeding, mixing water; Increase the shrinkage and change the setting time
Air-entrainers	Increase the durability by improving the resistance against freeze-thaw	Improve the stability and decrease the fluidity
Expansive agents	Reduce the shrinkage	Unknown

3.2.3 Grout design

The design of a grout to be injected in ancient masonry should take into account a series of concerns (ICCROM 1982) already discussed in the previous Sections. Toumbakari (2002) systematizes these concerns as follows: (i) Mechanical strength development; (ii) formation of dangerous by-products; (iii) behaviour with respect to water (both liquid and vapor); (iv) expansion due to heat or water; (v) modifications due to weathering; (vi) application (which should be as simple and reliable as possible); (vii) limits of reversibility; (viii) aesthetic factors (for renderings, fillings and stuccoes); (ix) marking of materials added during conservation work (in the materials themselves or by documentation). These concerns are fully centred on the construction to be rehabilitated and address both requirements regarding the structural efficiency and durability. This means that the grouting intervention should promote the adequate improvement of the structural behaviour and durability of the construction, while being no harmful at short- and long-term.

Fulfilling the structural efficiency requirements demands designing a grout with good injectability and bonding properties, in order to allow the filling of small cracks and voids, and promoting the homogeneity and continuity to the masonry. The definition of the grout mechanical properties depends on the structural level of damage and on the structural improvement requirements. Moreover, the definition of the grout binder also should take into account the time span in which the required mechanical properties must

be attained. In practical terms, relying the hardening of a grout on slow hydration or air hardening binders makes impossible achieving adequate levels of strength within a reasonable short time, dictated by structural necessities. With this respect, Toumbakari (2002) has advanced with a synthetic approach on grout design, by defining the properties that a grout should feature in order to obtain adequate injectability, bonding capacity and strength. These properties are depicted in Table 3.2.

Table 3.2 – Requirements of grouts regarding the structural behaviour of the injected construction, as depicted by (Toumbakari 2002).

Requirement	Description
Injectability	- low yield value and viscosity
	- penetrability: in voids with diameter smaller than 0.3 mm
	- stability: no substantial density gradients along the height of the stored grout
	- low bleeding: lower than 5% after 120 min of resting
Bonding with existing materials	- relative low shrinkage (although autogeneous shrinkage is unavoidable)
	- minimal heat of hydration
	- setting and hardening in dry as well as in wet environment
Sufficient mechanical properties within a defined span	- development of the required mechanical properties in 90 days
	- compressive and flexural strength dictated from the structural analysis

On the other hand, the durability requirements demand that the grout develops a microstructure as close as possible to that of the existing materials. This can be achieved partly with the use of raw materials similar to the existing ones. However, the expected mechanical properties may be insufficient. Thus, a compromise is possible within the use of a limited Portland cement content. The bonding is also a key factor for the durability requirements, since it limits the intrusion of detrimental agents and the subsequent undesirable chemical reactions. Table 3.3 summarises the properties that a grout should feature in order promote adequate durability within the injected masonry.

Table 3.3 – Requirements of grouts regarding the durability of the injected construction, as depicted by (Toumbakari 2002).

Requirement	Description
Compatible microstructure	- compatible porosity and pore size distribution: they depend on the porosity of the existing materials as well as on the required strength of the new materials
	- type of the hydration products: similar (though not necessarily identical) to the existing
Bonding with the existing materials	- limitation of diffusion of SO2, chlorides, etc.
	- resistance against deterioration due to environmental factors
Properties of the raw materials	- minimal content in gypsum and soluble salts (especially in releasable alkali)

3.2.4 Application procedure

After designing the grout, the next step is to inject it in the masonry. The application procedure is, like the designing of the grout, of extreme importance for the effectiveness of the intervention. Therefore, it is recommended to be executed by specialized workers.

The injection can be processed according to three methods, namely by gravity, pressure and vacuum. Gravity injection is indicated for severely damaged masonry, but it constitutes a slow process. The grout is introduced, without causing excessive pressure within the masonry, from an elevated pan or directly from a recipient moulded at the surface of the wall (see Figure 3.2). The injection by pressure can also be used in severely damage masonry, providing that very low-pressure values are used. Grout pumps and pressure pots can be used for this purpose (see Figure 3.1b). The vacuum injection consists in introducing the grout from the lower injection points by introducing a suction pressure at the top points. This method is specially indicated for injection of highly fluid resins in small elements (Valluzzi 2000). The several steps of the injection by the pressure method are following depicted, since this is probably the most used method in practice, nowadays.

Before proceeding to the injection of the masonry itself, a series of preparatory works are required. First, the coatings should be removed (except if they have cultural and historical importance) and the wall washed out to remove debris and soluble salts. In general, during this operation the mortar of the joints is also partially removed manually. Then, the cracks are sealed and the removed mortar joints are repointed using a compatible mortar. During or after this process, the injection tubes are installed at the injection points, which should be distributed according to a closest pattern (Van Rickstal 2000), as illustrated in Figure 3.3. It should be noted that the density of the injection points depends on the characteristics of the masonry and on the injectability of the grout. Standards on the definition of the density that grants the homogeneous filling of the voids are not known, meaning that this decision depends on the experience of the designer or technical staff. Nevertheless, Roque (2002) recommends a distance between injection points of about 0.25 m, meaning a density of about nine injection points per square meter.

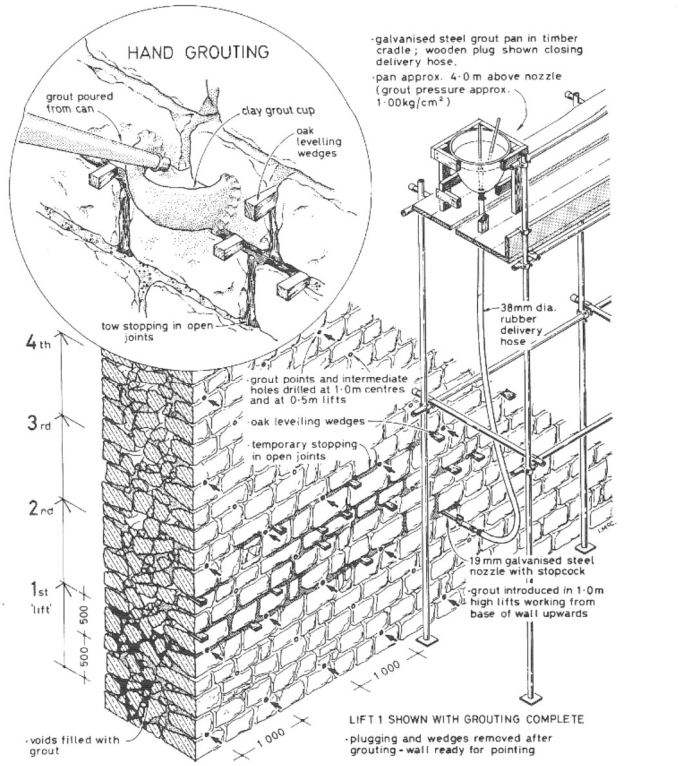

Figure 3.2 – Injection by gravity (Ashurst and Ashurst 1988).

The holes used to introduce the injection tubes are preferentially executed at the joints and should have a depth of about 2/3 of the wall thickness. Moreover, they should be drilled with a slightly downward inclination in order to facilitate the air evacuation during the injection. Then, the holes are sprayed to remove remaining debris and the tubes are installed and fixed with a sealing mortar. The diameter of the tubes is variable from case to case, but in average is of about 15-20 mm (Roque 2002). Normally, the injection tubes are only installed at the outer face of the walls. However, in thick walls (more than 0.7-0.8 m) they also should be installed at the inner face, if accessible. In this phase non-destructive tests (NDT) can be carried out in order to later assess the effectiveness and quality of the injection, by repeating these tests weeks after the injection (see Section 6.4 for more detail).

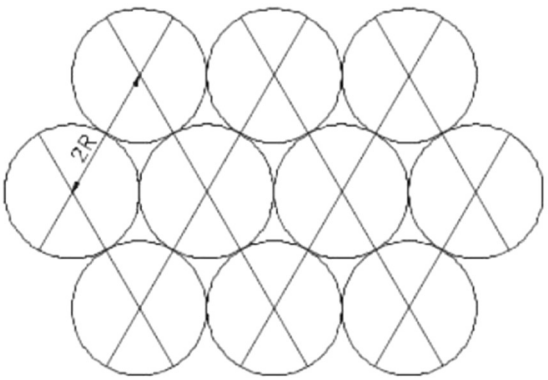

Figure 3.3 – Injection points distribution in a closest pattern (Van Rickstal 2000).

In the day before the injection of the grout, water should be introduced in the injection tubes in order to wash out debris, lubricate the masonry and reduce its water sorption. In general, this aims at enhancing the injectability.

Then, the injection of the grout starts from the lowest level of injection tubes and proceeds up to the top level, sequentially. This aims at promoting the evacuation of the air from the voids and at avoiding letting them unfilled. The injection pressure should be kept constant at a value that may vary between 0.05 N/mm^2 and 0.30 N/mm^2, depending on the strength and level of damage of the masonry. It should be noted that adopting an injection pressure excessively low might lead to the non-build up of sufficient pressure at the voids to allow their complete filling (Van Rickstal 2000). On the other hand, excessive pressure may produce unbearable tension stresses within the masonry, which are expected to cause damage and eventually failure of the sealing mortars. While the grout injection takes pace, small leakages are likely to occur, which should be promptly sealed (eg: using fast setting cement). Another important measure to be taken in this phase is the control of the properties of the grout.

After being presented the procedure for execution of a grouting intervention, the next Section discusses the structural effect of this technique applied to three-leaf masonry.

3.2.5 Strengthening of three-leaf stone masonry

The consolidation and strengthening of three-leaf masonry is often fulfilled by resorting to the grout injection of its inner leaf. However, the strengthening improvement of this intervention technique depends on the network of voids of the wall inner leaf, which must allow the grout to penetrate through it in order to promote its complete filling. Therefore, injecting walls with low percentage of voids (less than 4%) is very difficult and is likely to be ineffective in terms of structural performance improvement (Binda *et al.* 2006). The injection of the inner leaf is expected to contribute for improving the structural performance of the wall by promoting the homogeneisation and increase of the mechanical properties of this leaf. Moreover, the bond between the leaves is also expected to be improved, which enhances the monolithic behaviour of the wall and grants a stress distribution much more uniform (Vintzileou and Miltiadou-Fenzas 2008). The injection of highly fluid grouts can also improve the strength of the external leaves, by being able to penetrate and fill in cracks lying on them.

During the last few years, some experimental research has been carried out on the strengthening effectiveness of the grout injection technique applied to three-leaf stone masonry walls. Different grouts were tested within these researches, which included cement based, hydraulic lime based and ternary grouts. The results of the main researches regarding the structural performance of injected three-leaf stone masonry walls are following depicted and discussed.

Vintezileou and Tassios (1995) tested eight three-leaf wallets under compression and other two under diagonal-compression. The wallets were built using masonry performed

with limestone and lime/cement mortar. Two ordinary Portland cement (OPC) based grouts with addition of silica fume (SF) and lime (LH) were used to inject the walls, namely grout A and B (see Table 3.4).

Table 3.4 – Mixing proportions and compressive strength of the grouts tested by Vintezileou and Tassios (1995).

Grout	OPC (kg)	SF (kg)	LH (kg)	Superplasticiser (kg)	W (l)	f_c (N/mm^2)
A	75	25	0	1.33	90	30
B	60	22.5	27.5	1.66	100	13

Five of the injected wallets tested under compression were first tested and then retested after repair/strengthening. Two other injected walls were tested only after injection, without prior damage. This last procedure was the same adopted for the two injected walls tested under diagonal-compression.

Regarding the results of the experimental program, the authors provided the following main remarks:

- The unstrengthened wallets tested under compression experienced early separation of the external leaves, which rapidly lead to the disintegration of the wallet due to second-order effects;
- The compressive strength of the wallets after being repaired was improved in about 91% in the case of grout A and 200% with the case of grout B;
- The compressive stiffness after repairing increased in most wallets (24% in average);
- The homogeneisation effect introduced by the grout injection allowed the three-leaf wallets to behave almost as single-leaf;
- The grout injection seemed to improve the tensile behaviour by promoting enhanced tensile strength and post-peak deformability.

Toumbakari (2002) tested four three-leaf walls under compression and other three under diagonal-compression. The walls were built with limestone masonry with joints of lime/cement mortar. Two ternary grouts, obtained from different blends of lime, Rheinisch trass (RT), silica fume and OPC, and a OPC based grout (reference grout) were used to inject the specimens after a prior test (see Table 3.5). The ternary grouts presented low strength, while the OPC based grout presented high strength.

Table 3.5 – Composition and mechanical strength of the grouts tested by Toumbakari (2002).

Grout	LH (wt.%)	SF (wt.%)	RT (wt.%)	OPC (wt.%)	Superplasticiser (wt.%)	W/S (-)	f_c (90days) (N/mm^2)	f_b (90days) (N/mm^2)
Cb-0	20	0	0	80	N/A	N/A	19.5	4.5
13b-0	17.5	52.5	0	30	1.2	0.85	7.3	1.7
13b-10	17.5	10	42.5	30	5	1.1	9.0	1.1

The results of the tests allowed Toumbakari (2002) to draw the following conclusions:

- The collapse mechanism of the unstrengthened walls tested under compression was consequence of the separation of the external leaves from the inner leaf;
- The compressive strength of the walls clearly increased after being injected. The grout Cb-0 provided an increase of about 62% followed by the grout 13b-10 with about 60% increase and then the grout 13b-0 with 21% increase.
- The stiffness only seemed to have an important increase in the walls repaired with grout Cb-0 and 13b-10 (37% and 125%, respectively);
- The tensile strength of walls increased substantially with the injection (6-110%);
- The failure mode of the injected walls was similar to that before injection, however the transversal deformations (out-of-plane) were drastically reduced;
- The mechanical properties of the selected grouts seemed to have no influence on the effectiveness of the injection in terms of strength increase.

Valluzzi at al. (2004) tested under compression sixteen three-leaf walls of limestone masonry. The walls were tested unstrengthened or strengthened resorting to injection of two hydraulic lime based grouts, transversal tying, repointing or combination of these techniques. After testing, some of the unstrengthened walls were also repaired by resorting to these techniques, and subsequently retested. Both grouts used to inject the walls had low compressive strength, whose values at 28 days of age were of about 5.1 N/mm^2 and 3.2 N/mm^2. The execution of the repointing used hydraulic lime mortar with compressive strength at 28 days of age of about 1.72 N/mm^2. The transversal tying technique was applied by resorting to stainless steel rebars or threaded bars (four bars per square meter of wall) that were anchored by bending the rods from outside into a previously excavated mortar joint or through a system of washers and nuts, respectively.

The main relevant remarks derived from this research were:

- The failure of unstrengthened walls was consequence of the high transversal deformation of the external leaves, which caused their out-of-plane collapse;
- The injection was shown to be the most efficient technique, since it promoted the improvement of the compressive strength in about 40% (average) and of the stiffness in about 30% (average), as well it promoted the bond between leaves that resulted on a less brittle failure mode;
- The other techniques revealed their effectiveness mostly in terms of reduction of deformations;
- The best strengthening performance was achieved by combined techniques, especially when injection was involved.

More recently, Mazzon (2010) preformed shaking table tests on two experimental models built with limstone masonry similar to that tested by Valluzzi at al. (2004). This

experimental program allowed assessing the influence of the injection technique on the dynamic behaviour of stone masonry dwellings in unstrengthened, repaired and strengthened conditions. The models consisted in two identical two-stories dwellings with wooden floors and were built at reduced scale of 2:3. The first model was tested unstrengthened and then was repaired using a natural hydraulic lime based grout developed in Valluzzi *et al.* (2003). The compressive and flexural strength of the grout was of about 12.8 N/mm^2 and 3.8 N/mm^2, respectively. No further details on the grouts were addressed. The second model was tested only in the strengthened condition, which again consisted in the injection of the aforementioned grout.

The main outcomes of this research were:

- The injection technique can significantly reduce the detachment of the external leaves and out-of-plane collapse;
- Both injected models could resist a higher peak ground acceleration than the unreinforced model, with an increment of 30 and 50 % for repairing and strengthening interventions, respectively;
- The injection technique reduces the crack pattern at failure and does not practically modify the dynamic characteristics (initial frequencies and modal deformations) of original structure in both cases.

Finally, Oliveira *et al.* (2012) tested under compression ten three-leaf walls of granite masonry. Four walls were tested unstrengthened, while the remaining were tested strengthened, namely with transversal tying technique (three walls), grout injection (two walls) and combination of these techniques (one wall). It should be noted that the tying GFRP rebars used in the traversal tying technique were anchored to the walls by means of a localized grout injection. The injected grout of all strengthening solution was a commercial material, with designation Mape-Antique I. The grout presented high compressive strength, namely of about 17.6 N/mm^2 at 43 day of age. In terms of tensile strength (direct tension), it obtained a value of about 0.3 N/mm^2 at 60 days of age.

The results of the tests allowed to drawn the following main conclusions:

- The failure of unstrengthened walls was consequence of the out-of-plane rotation of the external leaves, caused by their buckling and detachment from the inner leaf;
- All strengthening technique increased the compressive strength of the walls, but those walls that involved complete injection were the best performing, namely of about 90% in the case of the combination between injection and transversal tying and of about 80% in the case of single injection;
- The injection slightly increased the stiffness of the walls, by increasing the Young's modulus in about 16%;

- The injection of the inner leaf promoted the homogeneisation of the masonry walls, by improving the mechanical properties of the inner leaf and the bond between leaves. This allowed the walls to behave as single leaf ones.

The differences between the aforementioned researches are substantial, since they study different materials, geometries, masonry fabrics, strengthening solutions and materials adjusted to the respective local ancient masonry features. Furthermore, the lack of specific standards and the different available testing conditions led to the adoption of different testing procedures. This compromises any attempt in comparing directly the results of these researches. Nevertheless, all authors agreed on the failure mode of unstrengthened three-leaf walls of stone masonry and on the repair and improvement capacity provided by the injection technique. Moreover, it was shown that low strength grouts originate similar structural performance efficiency to that of high strength grouts. This encourages the use of less the strong but highly compatible ternary and binary grouts, in the conservation of three-leaf masonry constructions. In general, the grout injection was shown to be a feasible and reliable technique for repair and strengthening of ancient masonry.

3.3 Grout injection of earth constructions

Currently, the research on the consolidation of ancient stone masonry by means of grouting is still lacking, but is much more developed than the research on this technique applied to earth constructions. In fact, cases where grout injection is studied or applied to earth constructions exist reported in a very limited number (Oliver 2008), meaning that the knowledge on adequate compatible grouts and effectiveness of the technique is also very limited. By having this in mind, the short state of art on the injection of earth constructions is following depicted and discussed and then a design approach is introduced.

3.3.1 State of art

Roselund (1990) describes a grouting solution applied to the restoration and strengthening of the Pio Pico mansion in Whittier, California, which was built in adobe. The damage to this mansion was mainly in the form of cracks in the adobe walls, as a consequence of the 1987 California earthquake. The cracks were repaired by injecting a modified mud grout (mud grout whose hardening relies not only on clay but also on another binder), whose composition consisted in the mixture of 60% of earth, 20% of silica sand (20 grit), 18% of fly ash and 2% of hydrated lime. Unfortunately, the properties of the grout were not provided. The design was mainly focused on obtaining a grout with adequate consistency, acceptable shrinkage, and with hardness, strength and abrasion resistance similar to those of the original adobes. Nevertheless, none of these requirements, with exception of the consistency, was measured quantitatively during the preliminary composition study that preceded the formulation of the injected

grout. This means that these properties were assessed qualitatively by means of visual inspection. On the other hand, the consistency requirements were defined as a function of the width of the cracks to be injected. Table 3.6 presents the set limits in terms of flow diameter. This test consisted in filling a mould (with dimensions 50 mm diameter and 100 mm height) with grout, which is then poured onto a smooth plastic surface from a height of about 150 mm. Then the spreading diameter is measured in two orthogonal directions and the average value is taken.

Table 3.6 – Consistency requirements for mud grouts defined by Roselund (1990).

Crack width	Flow diameter
< 13 mm	146 mm
1.3 mm – 25.4 mm	133 mm
> 25.4 mm	Should present mortar consistency

The results of the preliminary study of the intervention project also showed that the tested unmodified mud grouts (without addition of binders) presented excessive shrinkage, while the modified ones presented low shrinkage, justifying the preference for this later type of grout.

Later on, in 1994, the Pio Pico mansion was struck by the Northridge earthquake. The resulting damage was minor to moderate when compared to the damage to other buildings in a similar condition. This showed that the grout injection in combination with other consolidation/strengthening measures were effective in preventing serious additional damage. The aforementioned measures included strengthening of wall intersections with GFRP tie rods cored and grouted into the walls, introduction of vertical anchors cored and grouted into the tops of gable-end walls and anchoring of the north wall to the south wall (Tolles *et al.* 1996).

Jäger and Fuchs (2008) also used grout injection for consolidating the remaining adobe walls of the Sistani House at Bam Citadel in Iran, severely damaged during the 2003 earthquake. A modified mud grout composed by clay powder, lime and wallpaper paste was employed for this purpose. Unfortunately, no detailed information was given on the full composition neither on the final properties of the grout. The decision on the grout composition was preceded by a composition study that included testing the addition of other materials such as cement and water glass. The shrinkage and the mechanical properties, namely the compressive, flexural and splitting tensile strengths, were the properties that were controlled. Nevertheless, the required properties were not clearly defined or discussed.

On the other hand, Vargas *et al.* (2008) defends the employment of unmodified mud grouts rather than modified ones. This point of view is supported by an extended set of splitting tests carried out on specimens consisting of adobe sandwiches bonded by a layer of mortar. Several compositions were tested, namely two unstabilised earth mortars and nine stabilised earth mortars. One of the unstabilised mortars was

composed by raw soil and the other by soil sieved to remove the particles larger than 2 mm. The stabilised earth mortars were prepared with the sieved soil and included the addition of cement (5%, 7% and 10% in wt.), lime (5%, 7% and 10% in wt.) or gypsum (5%, 10% and 20% in wt.). The results showed that, in general, the unstabilised earth mortars have better adhesion capacity than those modified. The exception was the case of the specimens bonded with the earth mortar stabilised with 20% of gypsum. These results seemed to indicate that unmodified mud grouts would also present good adhesion capacity. Vargas *et al.* (2008) tried to confirm this assumption by carrying out a set of diagonal-compression on fifteen adobe masonry wallets, which were repaired by grout injection, after a first test, and then were retested. Four mud grouts were used, namely an unmodified mud grout and three modified mud grouts with addition of gypsum (10%, 20% and 30%). The same soil used to produce the wallets was used to blend the grouts, but the soil was previously sieved to remove the particles larger than 2 mm. The W/S ratio used in the grouts varied between 0.3 and 0.4, which corresponded to the minimum required ratio that allowed their injection into cracks of the specimens. No further details were offered on this criterion, neither on the properties of the grouts.

Table 3.7 presents the results obtained from the diagonal-compression tests (Vargas *et al.* 2008). From the wallets repaired with the unmodified mud grout (0% of gypsum) only two failed at recovering completely the initial strength. Vargas *et al.* (2008) highlights that this situation occurred due to deficiencies in the repair of these wallets. This confirmed the good adhesion capacity of the unmodified mud grouts, assumed with basis on the tests carried out on the sandwich specimens bonded with unstabilised earth mortar.

Table 3.7 – Results of the diagonal-compression tests carried out by Vargas *et al.* (2008).

Wallet	Mud grout (% gypsum)	Maximum force (kN)		Repair rate
		Initial	Repaired	
MDNR-1	0	7.4	8.43	114%
MDNR-2	0	6.2	4.44	72%
MDNR-3	0	8.93	9.63	108%
MDNR-4	0	8.44	3.65	43%
MDNR-5	0	6.83	9.17	134%
MDNR-6	10	7.62	6.59	86%
MDNR-7	10	9.11	10.25	113%
MDNR-8	10	7.4	3.59	49%
MDNR-9	10	7.37	5.96	81%
MDNR-10	20	9.46	12.79	135%
MDNR-11	20	5.55	11.21	202%
MDNR-12	20	10.44	6.37	61%
MDNR-13	30	5.43	9.27	171%
MDNR-14	30	8.32	8.63	104%
MDNR-15	30	13.22	15.14	115%

Regarding the results of the wallets repaired with the modified mud grouts, it was shown that a percentage of gypsum between 20% and 30% was required for, at least recovering completely the initial strength of the wallets. However, Vargas *et al.* (2008) highlights that the injection of the modified mud grout was more difficult than that of the unmodified mud grout. This was a consequence of the faster hardening of the modified mud grouts and possibly is also due to their inferior fluidity. For these reason, Vargas *et al.* (2008) states that the use of gypsum modified mud grouts is questionable, especially because the unmodified mud grout would attain similar level of repair, providing that the injection is executed with good quality.

The issue of the low fluidity of modified mud grouts is also pointed out by On Yee (2009), which carried out a composition study where this type of grouts was characterized. The composition study included the assessment of properties, such as the fluidity, segregation, bleeding, electrical resistivity, porosity, capillary absorption, shrinkage, mechanical strength, Young's modulus and flow behaviour. The grouts tested by On Yee (2009) were obtained from the blend of different proportions of cement, hydraulic lime, artificial soil (composed by kaolin and sand) and superplasticiser. Firstly, a preliminary experimental program was carried out based on the fluidity of the mixtures. This has shown that the grouts with the lowest fluidity were those composed by higher percentage of artificial soil, namely 75%. For this reason, this percentage was discarded from the phase of the composition study, being only considered percentages of 50% and 60%. A criticism should be made, since such low percentages of soil make these grouts more similar to those used in ancient masonry, rather than those studied by Roselund (1990) and Vargas *et al.* (2008). Consequently, the Young's modulus of the modified mud grouts varied between 4.6 GPa and 22.0 GPa. This corresponds to a value of stiffness that can be one to two orders of magnitude higher than that of earthen materials (being those stabilised or not). This fact deem these grouts to be mechanically incompatible with the majority of the earthen materials, whose typical Young's modulus is of about a few hundred kilopascal; for example see Silva (2008) and De Jongh and Van Wijnendaele (2009).

By taking into account the review of the state of art on the injection technique applied to earth constructions, it is notorious that the trend is to adopt earth based grouts, or in other words mud grouts. This option aims at promoting the compatibility between grout and the original earthen materials. Another interesting conclusion draw from this review is that the use of modified mud grouts with high percentage (higher than 30%) of mineral binders should be avoided due to mechanical incompatibilities, namely with respect to the stiffness. On the other hand, the grouts with low percentage of binder addition are likely to present low fluidity. Eventually, the solution to improve this drawback requires the development of specific superplasticisers, which is not a topic addressed in this thesis.

The use of unmodified mud grouts seems to be preferred, as they were show to promote the complete repair of adobe masonry, regardless of their higher shrinkage. This helps to explain why the unmodified mud grouts were the main focus of the thesis.

3.3.2 Approach for mud grout design

The design of a mud grout is a complex process. In the first instance it must consider the demands of the construction, namely recovering structural behaviour and granting durability, in a similar approach to that used in the conservation of ancient masonry (Toumbakari 2002). Then, the composition is defined such that the fresh- and hardened-state properties of the mud grout meet the demands. The fresh-state properties include the rheological behaviour and stability, while the hardened-state properties include the bond capacity, mechanical properties, chemical stability and microstructure. All the aforementioned properties have their particular role in the success of the grouting intervention. However, the complexity of the design of a mud grout resides in the interdependence between these properties, which is specially exhibited when the composition is adjusted. Therefore, it is essential to understand how the composition of a mud grout affects its properties in order to design it effectively. This approach is illustrated in the scheme of Figure 3.4.

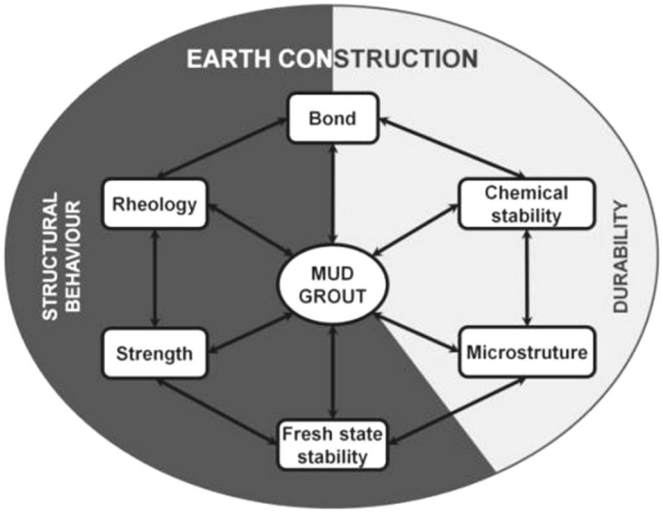

Figure 3.4 – Approach for the design of a mud grout.

The rheological behaviour of a fresh mud grout has great importance on its injectability and, consequently, on its applicability and on the quality of the grouting intervention. The grout must feature adequate fluidity and penetrability in order to, in a first instance, allow it to be injected (applicability), and in a second instance, allow it to completely fill a crack and assure the continuity of the repaired earthen material (efficiency). Therefore, the mud grout should present viscosity and yield stress values as low as possible. For this purpose, the main factors influencing the rheology must be carefully accounted for during the design of the mud grout, which include the texture (particles size, distribution and shape), the interaction between particles (dispersion or

flocculation), the water/solids ratio, the mixing procedure, the injection process and pressure, and the action of superplasticisers or dispersants. It should be noted that the interaction between clay particles is of great importance to the rheological behaviour during the fresh-state. In normal conditions, clay particles tend to flocculate and to form a gel that opposes to the flow, which does not allow the injection of the mud grout without incorporating an exaggerated percentage of water in their composition. Moreover, the capacity of the dry earthen materials of absorbing quickly high amounts of water requires that the mud grout presents a great water retention capacity during its injection. This is essential in order to maintain its fluidity and penetrability during all the injection process.

Another important property of a mud grout is its strength. However, the idea that strong mud grouts provide better repair efficiency is misleading. Instead, the strength developed by the mud grout must be adjusted to the strength of the original earthen. Moreover, stiff grouts can cause problems of mechanical incompatibility, since the hardened grout hardly follows the displacements occurring in the earth construction, resulting into damage to the intervention or construction. Like was aforementioned, the addition of mineral benders (such as cement or lime) in modified mud grouts has to be carefully accounted for, since they may increase greatly the stiffness.

Another objective of the grout injection is to grant the continuity of the earthen structure, both because of structural and durability reasons. The hardened grout is supposed to establish the bridge between the parts of a wall divided by a crack. Thus, both the strength developed by the hardened mud grout and the bond established between the original earthen materials and the hardened mud grout must be sufficient to grant the connection. Only in this way, it can be expected to achieve a structural state similar to that existing before damage. On the other hand, re-establishing the continuity broken by a crack hinders the propagation of damage in an earthen wall. For example, repairing cracks in walls is crucial to prevent rain water infiltrations through them, which can lead to a dramatic decrease of the wall strength. The bond established is highly dependent on the shrinkage of mud grout. The shrinkage of the mud grout during its drying can lead to cracking and consequently the required bond cannot be established, which is a problem common to other reparation works using earthen materials (Keefe 2005). Necessarily, the shrinkage of mud grouts cannot be fully avoided, but it can be minimized. Incorporating selected clays with low shrinkage ratio (such as kaolinite clays) helps to mitigate the shrinkage of the grout. The texture of the mud grout is another property that can be modified to mitigate the shrinkage, by decreasing the clay content of the mud grout and by adjusting the particles size distribution with addition of “unshrinkable” fine materials (fly ash, silica fume, calcium carbonate powder, quartz powder and etc.). Another possibility consists in decreasing the water content. However, this has direct consequences in the rheology, which can only be overcome by adding dispersants. Using stabilisers is also an alternative to solve

the shrinkage problem, but other problems may arise from this decision, as previously mentioned.

A mud grout also needs to present chemical stability over time. Its salt content has to be limited in order to avoid efflorescence and cryptoflorescence damage. Moreover, the grout must present resistance to aggressive compounds that may exist in the original earthen materials. For example if a possible mud grout contains Portland cement, there is a possibility of formation of expansive products since the presence of sulphates is very common in earthen materials.

A mud grout must present stability during the fresh-state, meaning that limited bleeding, segregation and adequate water retention are required. These are essential to assure fluidity and penetrability during the injection, and that the grout remains homogeneous while hardening. Therefore, using an earth with large particles in the composition of the mud grout for overcoming shrinkage issues may constitute a major drawback, since these particles will tend to settle.

Obtaining a hardened mud grout with a microstructure compatible to that of the original earthen materials is another essential condition for fulfilling durability requirements. The water vapour penetrating in the earthen materials has to be able to do it freely. If a grout with low porosity is injected, it may constitute a "barrier" where the water vapour is prone to condensate. This is harmful for the intervention or for the construction, depending on the size of the intervention. The condensed water can leech the material around the grout disturbing the bond created, and therefore, damaging the intervention. In the case where a large grout barrier is created, the condensed water can lead to the weakening of the earthen materials that at long-term can be responsible for an eventual collapse. Therefore, the incorporation of materials such as cement has to be carefully evaluated, since it reduces the porosity of the mud grout. The thermal properties of the hardened grout must also be closer to the ones of the original earth materials. This is even more important in monolithic earth constructions (for example rammed earth), where the grout has to be able to follow the thermal displacements of the earthen materials.

Finally, Table 3.8 summarises the requirements of mud grouts for injection of earth constructions. Unfortunately, the lack of knowledge on these grouts and on their interaction with earth constructions does not allow a quantitative definition of these requirements. The development of this knowledge is thus one of the objectives of the thesis, which is addressed through the following Chapters.

Table 3.8 – Requirements of mud grouts for injection of earth constructions.

Requirement	Description
Rheological behaviour	- adequate fluidity - adequate penetrability - low viscosity and yield stress - adequate water retention capacity
Mechanical strength	- strength compatible with that of the original earthen materials - stiffness compatible with that of the original earthen materials
Bond capacity	- adequate tensile strength - good adhesion with the original earthen materials - relative low shrinkage (the minimum possible)
Chemical Stability	- low soluble salt content - resistance against aggressive compound in the original earthen materials (normally granted if no cement is incorporated in the grout)
Stability	- limited bleeding (normally is granted by the clay fraction of the mud grout) - absence of segregation (normally is granted by the clay fraction, except if excessively large particles are incorporated in the grout)
Microstructure	- compatible water vapour penetration (normally granted if low percentage of mineral binders are incorporated in the grout) - thermal behaviour compatible with that of the original earthen materials (normally granted if their composition is similar)

3.4 Colloid behaviour of clay suspensions

The clay fraction of a mud grout is expected to have great importance in the development of its strength and adhesion. Furthermore, the presence of this fraction also has implications on the rheological behaviour. The size of this fraction is inferior 2 μm, meaning that a part of these particles has colloid-size (inferior to 1 μm). Therefore, it is important to understand the influence of the colloid behaviour of clay particles in properties of a mud grout, in order to design it properly. This Section serves to discuss briefly this topic by addressing the clay mineralogy, clay surface properties, clay flocculation and flow behaviour of clay suspensions.

3.4.1 Clay mineralogy

The clay minerals belong to the group of the phyllosilicates minerals (Van Olphen 1977), and they are basically built by two principal building elements, consisting of two-dimensional arrays of silicon-oxygen tetrahedral (T) and two-dimensional arrays of aluminium- or magnesium-oxygen-hydroxyl octahedral (O), as illustrated in Figure 3.5.

In the silicon-oxygen sheets formed by SiO4 tetrahedral (also called of tetrahedral sheets or silica sheets), the silicon atoms are coordinated with four equidistant oxygen atoms, being three of them shared with neighbouring tetrahedral. This confers a hexagonal symmetry to this type of sheet.

In the aluminium or magnesium sheets (also called of octahedral sheets, or alumina or magnesia sheets), the aluminium or magnesium atoms are coordinated with six oxygen atoms or hydroxyl groups which are located around the aluminium or magnesium atom with their centres on the six corners of a regular octahedron. The oxygen atoms and hydroxyl groups lie in two parallel planes with the aluminium or magnesium atoms between these planes. The oxygen atoms are also shared between neighbouring octahedral to form the octahedral sheet.

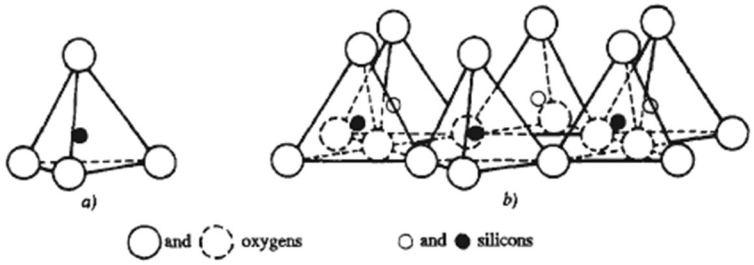

(a)

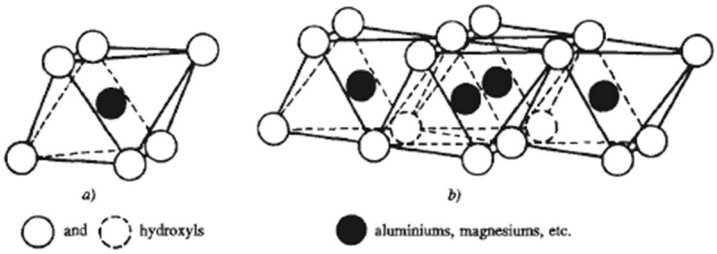

(b)

Figure 3.5 – Building elements of clay minerals (De Wit 1995): (a) tetrahedral sheet (T); (b) octahedral sheet (O).

The analogous symmetry and the almost identical dimensions of both types of sheets make possible the sharing of oxygen atoms between them. The fourth remaining oxygen atom of the tetrahedral sheet can be shared with an octahedral sheet. If this sharing occurs between one of each sheets, it constitutes a 1:1 layer mineral (TO). On the other hand, if one octahedral sheet shares oxygen atoms with two tetrahedral sheets, one on each side (TOT), it constitutes a 2:1 layer mineral. The clay minerals are constituted by stacking of these layers (Van Olphen 1977), which confers commonly a plate-like shape to the clay particles.

A structural layer can be constituted by repeating laterally an electro-neutral basic unit, which is called unit cell. This unit cell is defined from a certain plane in one layer to the corresponding plane in another following parallel layer of the crystal (Van Olphen 1977), as is illustrated in Figure 3.6. The unit cell of 2:1 layer clay minerals has three available positions for cations on the octahedral sheet that may be or not fully occupied. If all the positions are occupied, the arrangement of the structure is designated of trioctahedral, which is the case of talc mineral, where these positions are occupied by three divalent magnesium cations. If only two of the positions are occupied, the arrangement is called of dioctahedral, which is the case of the mineral

pyrophyllite, where two o these positions are occupied by two trivalent aluminium cations. The structures of these two minerals are considered to be prototypes of the structure of the 2:1 clay minerals, which are derived by introducing more or less random atom substitution in the prototypes crystal structure.

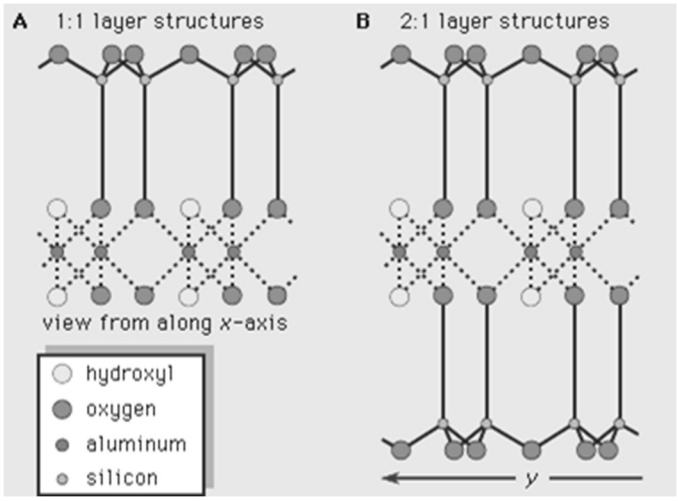

Figure 3.6 – Unit cells of 1:1 and 2:1 layer minerals (Encyclopaedia Brittannica 2013).

Smectites, illites and kaolinites are the most common groups of the phyllosilicates minerals present in soils. Therefore, they are further discussed with more detail.

The clay minerals in the smectite group present a 2:1 layer structure (TOT) and is derived from the pyrophyllite and talc minerals (prototypes) by substitution of certain cations for other. The tetravalent silicon cations are often partly replaced by trivalent aluminium cations. The trivalent aluminium cations may also be replaced by divalent magnesium cations without complete filling of the third vacant octahedral position. Cations of atoms such as iron, chromium, zinc or lithium can also be involved in this type of substitution (Van Olphen 1977). This process of replacement is called isomorphous substitution and it is promoted by the smaller size of the replacement cations. The isomourphous substitution of many clay minerals leads to the replacement of one cation of higher valence by other of lower valence. This results in an excess of negative charge in the layer, which is compensated by the adsorption of cations on the layer surfaces. These cations are unable to get in the crystalline structure since they are too large. In the presence of water, the compensation cations can be easily exchanged by other cations available in solution, thus they are called exchangeable cations. The exchange capacity can be determined analytically and by experimental means, and if expressed in milliequivalent per 100 g of dry clay it is called of cation exchange capacity (CEC) of the clay. The CEC can be used as a way to measure the degree of isomorphous substitution. The CEC of smectites is usually a high value (around 70-100 meq per 100 g).

The smectites are also known for their high swelling behaviour when in contact with water or water vapour. In this situation the water molecules are able to penetrate in between the stacked layers, promoting the so called interlayer swelling. The interlayer

swelling increases the c-spacing from the typical 9.6 Å of dry smectite clays to values of the of about 12.5-20 Å, depending on the type of clay and the type of the exchange cation. Thus, interlayer swelling can lead, at most, to a doubling of the volume of the dry clay (Van Olphen 1977).

The clay minerals of the illite group present, similarly to the smectite clays, a 2:1 layer structure (TOT). However, this group is primarily differentiated from smectite clays by the absence of interlayer swelling. In the case of illites, the isomorphous substitution occurs predominantly in the tetrahedral sheets, and the cations compensating the net negative layer charge are usually potassium ions. These cations are fixed and cannot be exchanged, since the layers do not part upon the addition of water. The CEC of illites is low but non zero (20-40 meq per 100 g), because the potassium ions lying on the external surfaces of the clay particles are able to be exchanged and the degree of isomorphous substitution is even higher than that of the majority of the clays of the smectite group (Van Olphen, 1977).

The specific electrostatic linking effect of the potassium cations is responsible for the non-swelling behaviour of illite clays. These cations have the right size to establish a favourable 12-coordination with opposite hexagonal oxygen rings of the adjoining layers (Van Olphen 1977). Despite of the c-spacing of the illite clays being slightly higher than that of smectite clays (10 Å), the higher degree of isomorphous substitutions allows the development of more links between the layers and potassium cations by unit of area, which increases the attractive forces between layers.

The clays of the kaolinite group present an almost perfect 1:1 layer mineral structure (TO). The main difference between the species of clay of this group is related with the layer stacking geometry. For example, this difference can be reflected in different level of hydrogen bonds established between the hydroxyl groups of one layer and the oxygen atoms of the adjoining layer. As example of clays from the kaolinite group, it can be referred the kaolinite, dickite, nacrite or halloysite (Van Olphen 1977).

The kaolinite clays, with the exception of the halloysite, are not expandable with water. This results from the strong cohesive attraction force between layers. This is primarily electrostatic, and then is augmented by van der Waals attraction forces. In addition, a certain level of hydrogen bonding between layers also contributes for the stacking cohesion of the layers. The small c-spacing (around 7 Å), in part, helps to understand the absence of exchangeable cations in the interlayer spaces of kaolinite clays, since the cations are too large to fit such small interlayer spaces. The exchangeable cations to compensate the small degree of isomorphous substitution are located on the external surface layers of the clay particles. This is verified by a low CEC of kaolinite clays (1-10 meq per 100 g) that, nevertheless, does not depend, exclusively, on the isomorphous substitution in the crystalline structure, as it is discussed later.

3.4.2 Clay particles surfaces

In the previous Sections it was remarkably stressed the process of isomorphous substitution typically experienced by the layers of clay minerals. Moreover, it was stated that this process results in a net negative charge of the crystalline structure, which is balanced by the exchange cations located on the layer surfaces.

In the presence of water, these cations have a tendency to diffuse way from the negatively charged external layer surfaces of the faces of clay particles, since their concentration is smaller in the bulk solution. Thus, an atmospheric distribution of the cations (electrical diffuse layer) is created on the face surfaces of the clay particles, since the cations are still attracted electrostatically towards the external layer surfaces due to the net negative charge that needs to be balanced. This system constitutes what is called of electrical double layer. The compensating cations in the diffuse layer act as the counter-ions of the double layer, and, like all counter-ions, they are exchangeable for other cations. The diffuse layer does not consist exclusively of an excess of cations in the neighbourhood of the layer surfaces. Anions (co-ions) are also present, nevertheless, they are electrostatically repelled way, which makes their concentration in the neighbourhood of the layer surfaces lower than in the bulk solution.

The model presented previously to describe the double layer of the flat layer surfaces of clay particles (also called of face surfaces or basal planes) is called Gouy's model (Gouy 1910 and Gouy 1917), and despite some of its unrealistic elements and limitations, it still constitutes a satisfactory approach to explain many colloid chemical phenomena. However, Stern (1924) refined the Gouy's model to overcome some of its limitations. The resulting model is called Stern-Gouy's model (Van Olphen 1977). Besides the electrical diffuse layer and the charged surface, it considers a layer of counter-ions in contact with the surface (Stern layer) that splits it from the diffuse layer. The charged surface together with the plane of the centres of the counter-ions of the Stern layer form what is called of a molecular condenser, where the electric potential drops linearly with the distance. The Stern-Gouy's model represents better the double layer of clay particles than the Gouy's model, since there are indications that, in many types of clay, specific adsorption forces between the surface layers and the counter-ions exist (Van Olphen 1977). However, the explanation of the interaction between clay particles will be further explained with basis on Gouy's model, due to its simplicity.

The plate-like shaped clay particles also have an edge surface, which is provided of different surface properties from those of the face surfaces. The tetrahedral and the octahedral sheets are disrupted at the edge surface of clay particle and primary bonds are broken, since the crystalline structure cannot be perpetually extended laterally due to the development of stresses in the crystalline structure (Van Olphen 1977). Consequently, the aluminol (Al–OH) and the silanol (Si–OH) groups of the octahedral and tetrahedral sheets, respectively, are exposed. These polar sites have an amphoteric behaviour. This means that the edge surface is conditionally charged positively or

negatively depending on the pH of the solution Tombácz and Szekeres 2004 and Tombácz and Szekeres 2006). Accordingly, protonation reactions of the aluminol groups in acid aqueous solution may lead to the development of positively charged edge surfaces (Equation (3.1)). On the other hand, deprotonation reactions of the aluminol and silanol groups in alkaline aqueous solution may lead to negatively charged edge surfaces (Equation (3.2) and (3.3)).

$$Al-OH+H^{+} \Leftrightarrow Al-OH_2^{+} \quad \text{(protonation)} \tag{3.1}$$

$$Al-OH+OH^{-} \Leftrightarrow Al-O^{-}+H_2O \quad \text{(deprotonation)} \tag{3.2}$$

$$Si-OH+OH^{-} \Leftrightarrow Si-O^{-}+H_2O \quad \text{(deprotonation)} \tag{3.3}$$

Therefore, the edge surfaces of clay particles have variable charge, depending on the pH of the aqueous solution, which is compensated by a cloud of counter-ions available in solution (Tombácz and Szekeres 2004 and Tombácz and Szekeres 2006). The pH at zero charge in this surface is called point of zero charge of the edge ($pH_{pzc,edge}$).

On the other hand, the face surfaces are expected to have a permanent negative charge, whose value depends only on the degree of isomorphous substitution of the surface layers. However, the described permanent charge character of the face surfaces of clay particles is not entirely correct for the case of kaolinite clays, like was formerly stated by many researchers (Schofield and Samson 1953, Flegmann *et al.* 1969, Rand and Melton 1977, Van Olphen 1977, and Williams and Williams 1978). In addition to the hydroxyl-terminated groups of the edges, these groups can also be found exposed at the face surfaces of the kaolinite particles, thus featuring an amphoteric behaviour.

Ma and Eggleton (1999a) investigated the external layer surfaces of kaolinite clays, using high-resolution transmission electron microscopy (HRTEM), which allowed defining three possible types of face surfaces. The type 1 surface has the expected 7 Å TO surface layer as terminations (i.e., the layer sequence is TO TO...TO TO). The type 2 has one pyrophylite-like layer (TOT) as termination of one of the faces (i.e., the layer sequence is TO TO...TO TOT), where the c-spacing between the TOT and the adjacent TO layer is not expandable. Finally, the type 3 surfaces have one or several TOT collapsed smectite-like layers at one or both sides of a stack, forming a special kind of kaolite-smectite interstratifications (i.e., the layer sequence can be for example TOT TO...TO TOT), which has only been recognized in some poorly-ordered kaolinites. The same authors in another paper (Ma and Eggleton 1999b) showed that the exchangeable cations of kaolinite clays occur mostly on the edges and on face surfaces with exposed hydroxyl groups. This was supported by comparing experimentally determined CEC of several kaolinite clays with theoretical calculations, which also showed that the CEC of

kaolinite clays strongly depends on the particle size (thickness and diameter in the basal plane) and pH value, rather than on the low degree of isomorphous substitution. Moreover, it was stated that the magnitude of the changes of CEC with pH could only be explained by the ionization of face surfaces with exposed hydroxyl groups, like has been defended by Zhou and Gunter (1992).

Therefore, in well-crystallised kaolinite clays with the expected type 1 external layer surfaces, one of the face surfaces has an exposed octahedral sheet (O face) that is provided of the discussed hydroxyl amphoteric sites. Thus, the value of the variable surface charge of the O face surfaces depends mostly on the pH of the aqueous solution, rather than on the low degree of isomorphous substitution that may happen in that surface layer. However, the O face hydroxyl groups are probably less reactive than edge aluminols and silanols, since the hydroxyl groups in these last ones are bound to undercoordinated metal atoms, while in the O face, the metallic atoms have complete environment coordination (Tombácz and Szekeres 2006). On the other hand, the tetrahedral sheet face surface (T face) has a low permanent negative charge resulting from minor isomorphous substitution.

3.4.3 Flocculation of clay particles

When two clay particles approach each other in aqueous medium due to Brownian motion or due motion caused by an external force, the interaction between them is dictated by electrostatic forces and by van der Waals forces. Consequently, two states can be originated: the particles remain deflocculated in the suspension or become flocculated. This is a typical problem that is, even nowadays, object of study of the DLVO theory (Derjaguin and Landau, Verwey and Overbeek).

The flocculation of plate-like shaped clay particles is possible according to three different association modes (Figure 3.7): face-to-face (FF), edge-to-face (EF) and edge-to-edge (EE). The electrical interaction energy for the three modes is governed by different combinations of the double layers emerging from the surfaces of the clay particles. Moreover, the van der Waals interaction energy is different for the three types of association, since different geometries must be considered in the summation of the attraction between all the atom pairs of the approaching particles. Consequently, the three association modes will not necessarily occur simultaneously or with same frequency (Van Olphen 1977).

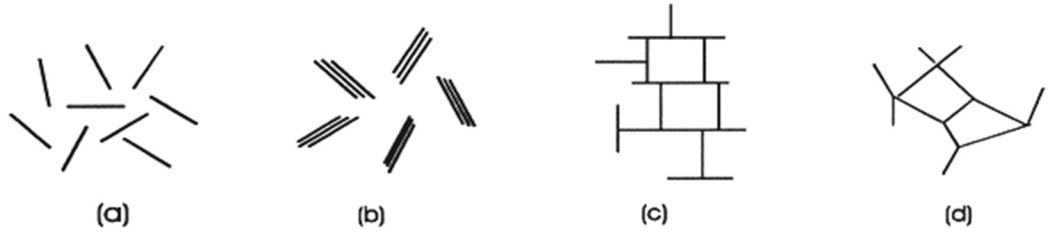

Figure 3.7 – Association modes of clay particles in suspension (Luckham and Rossi 1999): (a) dispersed; (b) Face-to-Face (FF); (c) Edge-to-Face (EF); Edge-to-Edge (EE).

The attractive van der Waals force between a pair of atoms has small magnitude and its decay is very rapid with distance (short range forces). However, the total van der Waals attraction between two particles results from the summation of all the attractive forces between every atom of one particle and every atom of the other particle. This originates a larger force and a less rapid decay with distance. The van der Waals attractive force between two atoms is estimated to be inversely proportional to the seventh power of the distance, while that of two large particles is estimated to be inversely proportional to the third power of the distance between the surfaces (Van Olphen 1977).

While two clay particles approach in aqueous suspension, their double layers start to interfere, changing the distribution of the counter-ions in both diffuse layers. In the case of double layers with like charge, this change involves an increase of the free energy of the system that results on a repulsive force between the particles (De Wit 1995). The presence of indifferent electrolytes has particular effect on the diffuse layers of the surfaces of clay particles. Increasing their concentration (c_{el}) makes the diffuse layer proportionally contract toward the surface, i. e., the higher is the concentration of ions of like charge to that of the counter-ions, lesser is the Debye length of the double layer (or in other words, the thickness of the double layer). According to the Schulze-Hardy rule, the valence of the indifferent electrolytes is another factor contributing for contraction of the diffuse layer. The contraction level is higher for indifferent electrolytes of higher valence for a same concentration in suspension. Contracting the diffuse layer results in the reduction of the range of the repulsive force, which can then be overcome by the attractive van der Waals forces, making the clay particles to flocculate. It should be noted that the van der Waals attractive forces are little dependent on the concentration of indifferent electrolytes (Van Olphen 1977). The influence of c_{el} on the interaction of colloid particles is illustrated in Figure 3.8, in terms of net potential energy of interaction.

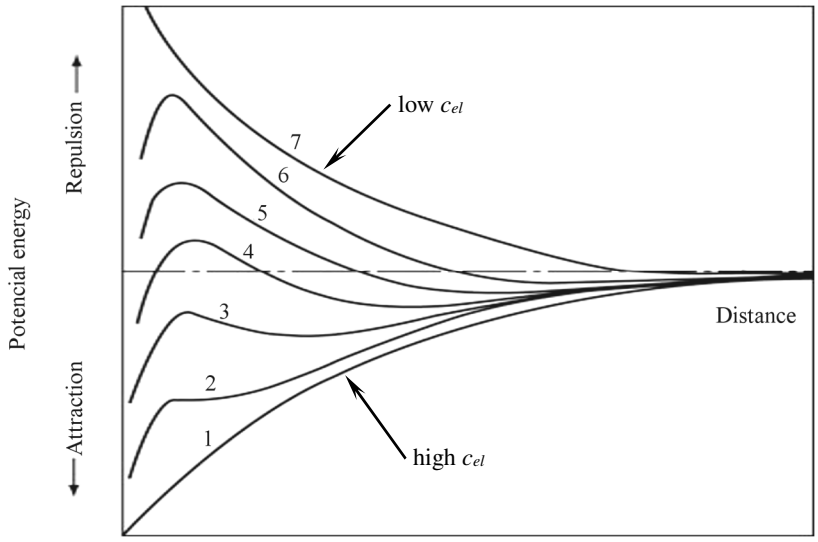

Figure 3.8 – Net potential energy of interaction between particles in a colloidal suspension (Williamson 2008); the electrolyte concentration decreases from 1 to 7.

The surface charge heterogeneity of clay particles and the effect of indifferent electrolytes are two topics that cannot be evaluated separately in the analysis of the flocculation of clay suspensions, especially in the case of hetero-coagulation (EF association mode). It is reasonable to think that oppositely charged surfaces of two clay particles generate an electrical attractive force between them that promotes their flocculation. But in fact, this is not so simple if the aspect ratio of the clay particles (particle geometry and asymmetry) and the influence of adjoining dominant double layers are included (Tombácz and Szekeres 2004 and Tombácz and Szekeres 2006). Figure 3.9 presents schematically the relation between the pH and the electrolyte concentration (c_{el}) in the definition of the double layers of motmorillonite clay particles. In the case of very low values of c_{el}, the negative double layers at the faces over spill the double layer at the edge surface. This is promoted by the extreme asymmetry of montmorillonite clay particles (diameter/thickness around 500) and by a Debye length (e.g. LD~3 nm for a solution of NaCl at concentration 10 mM) that is larger than the thickness of the montmorillonite clays thin lamellas (t_c~1 nm) (Tombácz and Szekeres 2006). Even if the pH of the medium is bellow the $pH_{pzc,edge}$ (~6.5) the formed positive double layer is hidden by the dominant negative double layer, which hinders hetero-coagulation. The double layer at the edges can only emerge above a threshold concentration of indifferent electrolytes (c_{et}). In this case, hetero-coagulation can only happen if the pH of the medium is bellow the $pH_{pzc,edge}$ (Tombácz and Szekeres 2006).

The asymmetry of kaolinite clay particles (diameter/thickness between 2 and 10) is not as extreme as that of montmorillonite clays. This attributes a higher importance to the edges in the surface charge properties of kaolinite clays, which is further emphasized by the lower permanent charge of the faces of the kaolinite clays. Therefore, the surface charge heterogeneity of kaolinite clays is expected to have greater importance on the flocculation process than it has for montemorillonite clays (Tombácz and Szekeres 2006).

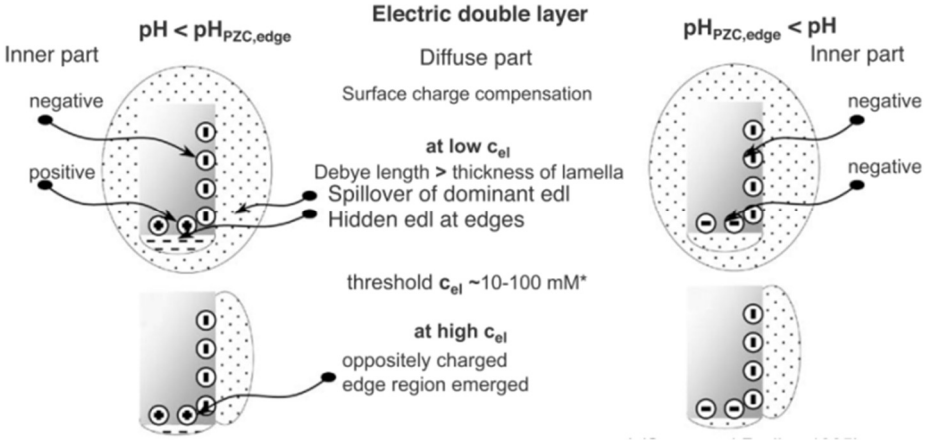

Figure 3.9 – Schematic representation of the dominant and hidden electric double layers forming around the montmorillonite lamellae under different solution conditions of electrolyte concentration and pH (Tombácz and Szekeres 2004).

The termination of the crystalline structure of kaolinite clays is another factor that needs to be accounted for. Kaolinite clays with face terminations of type 2 or 3 are expected to behave similarly to the montemorillonite clays. This may slightly change if the crystalline termination of the kaolinite clay is of type 1 (see Figure 3.10). However, the surface charge heterogeneity of kaolinite clays is only developed bellow the point of zero charge (PZC) of the amphoteric sites (mainly edges), which may range between a pH of 5 and 9 (Tombácz and Szekeres 2006). For a pH value inferior to PZC and very low c_{el}, the Debye length of the faces double layer (e.g. LD~3 nm for a solution of NaCl at concentration 10 mM) might be or not comparable to the thickness of the kaolinite clay particles (t_c), which can range between 10 nm and 120 nm (Brady *et al.* 1996). Thus, the double layer at the edges can be or not completely hidden. If the double layer at the edges is not completely hidden by the faces double layer, this results in the hetero-coagulation of the kaolinite clay particles. On the other hand, if the double layer at the edge is hidden, flocculation may not occur, except in the case of kaolin clay particles with type 1 termination. In this case, FF associations are more likely to occur due to the electrical attraction force between oppositely charged faces. However, if c_{el} is increased above c_{et}, the double layers at the edges emerge, resulting in hetero-coagulation (Tombácz and Szekeres 2006).

Figure 3.11 summarises, generically, the association of clay particles in solution as a function of the asymmetry, electrolyte concentration and pH. Here four regions are highlighted.

In region A both pH and electrolyte concentration are high (above $pH_{pzc,edge}$ and c_{et}, respectively), meaning that all three association modes (FF, EE and EF) can occur, independently of the asymmetry of the particles. The association frequency of each mode depends on the competition between the respective generated van der Waals forces.

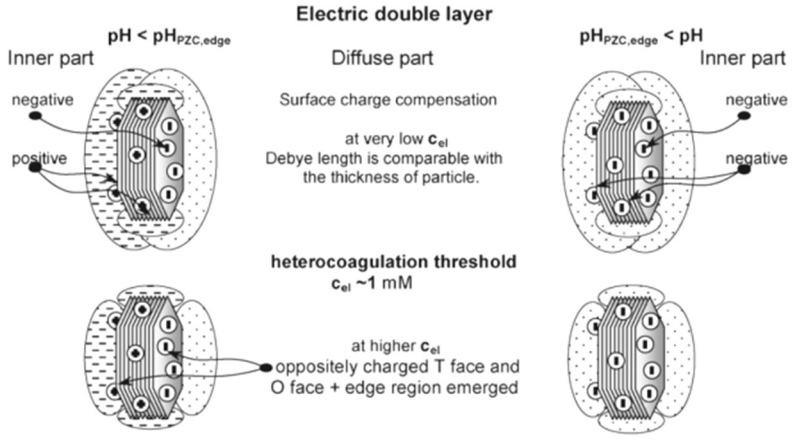

Figure 3.10 – Schematic representation of the dominant and hidden electric double layers forming around the kaolinite particles under different solution conditions of electrolyte concentration and pH (Tombácz and Szekeres 2006).

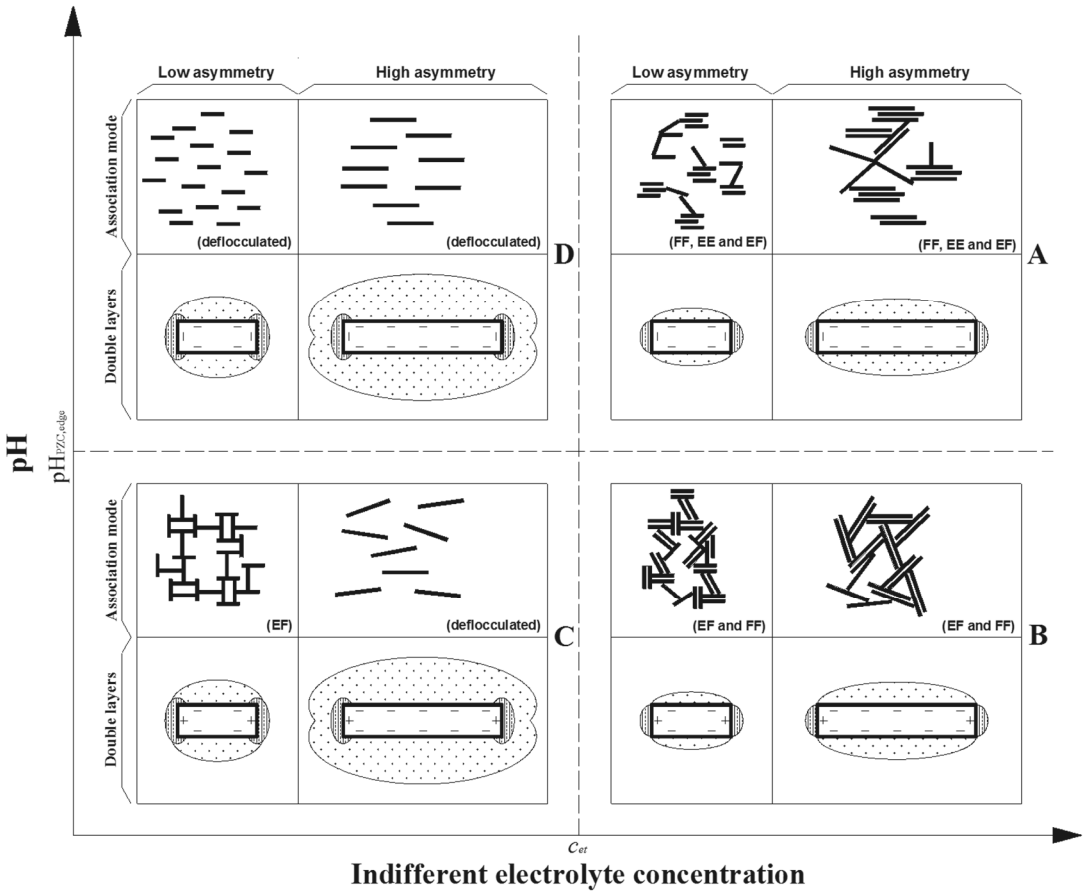

Figure 3.11 – Association of clay particles in suspension as a function of the asymmetry, electrolyte concentration and pH.

In region B, c_{el} is higher that c_{et} and the pH is lower than $pH_{pzc,edge}$. Consequently, hetero-coagulation and FF association dominate the interaction between clay particles in both cases of asymmetry. Van der Waals attractive forces are responsible for FF associations, while the electrostatic attractive forces between the oppositely charged faces and edges are responsible for EF associations. The EE association is unlikely to happen, since EF association is preferred due to its lower level of interaction energy. In region C both c_{el} and pH are inferior to c_{et} and $pH_{pzc,edge}$, respectively. In the case of highly asymmetric clay particles, they remain deflocculated, since the repulsive forces between the double layers of the faces overcome any attractive forces. In the case of little asymmetric clay particles, the positive double layers of the edges are exposed. The negatively charged faces attract these surfaces, which promotes EF associations. Additionally, the well developed negative double layers on the faces are responsible by an almost perpendicular orientation between hetero-coagulated particles. In the case of kaolinite clay particles with type 1 termination, FF association may also occur between T and O faces. In region D, c_{el} is inferior to c_{et} and the pH is higher than $pH_{pzc,edge}$. This situation promotes the supremacy of the repulsive forces, and thus the clay particles remain deflocculated.

Regarding the occurrence of flocculation in a mud grout, the most probable situation is that of region A. The pH of the raw soil used in earth construction is higher than the

$pH_{pzc,edge}$ of most clay minerals and the electrolyte concentration is also high. Therefore, flocculation according to the three association modes is likely to occur in a mud grout, especially because it corresponds to a highly concentrated suspension. In this situation, the clay particles are more prone to interact, since the inter-particles distance is short.

3.4.4 Flow behaviour of clay suspensions

The flow behaviour of any system is described in terms of the relationship between the shear stress (τ) and the shear rate ($\dot{\gamma}$). The shear rate is defined as the change of shear strain per unit time, and the shear stress as the tangential force applied per unit area. The ratio between shear stress and shear rate is called viscosity (η), and is a measure of the resistance to flow of the fluid (Equation (3.4)).

$$\mu = \frac{\tau}{\dot{\gamma}} \tag{3.4}$$

The flow curve of a material is built by plotting the shear stress against the shear rate. In general, four different types of flow curves may be distinguished, namely Newtonian, pseudoplastic, Bingham plastic and dilatant (see Figure 3.12). When the shear stress is directly proportional to the shear rate, the fluid is Newtonian and exhibits a constant viscosity. In the other types of flow behaviour, the viscosity varies with the shear rate and these are called non-Newtonian fluids (Luckham and Rossi 1999).

According to Luckham and Rossi (1999), clay suspensions with relatively high concentration have been described traditionally by the Bingham theory of plastic flow. The Bingham model postulates that a finite stress must be applied to initiate flow and at greater stresses the flow will be Newtonian. The resistance of the suspension to flow can therefore be considered as consisting of two parts: a Newtonian part in which the shear stress is proportional to the shear rate and a non-Newtonian part in which the shear stress is constant irrespective of the shear rate. The equation for the Bingham model is:

$$\tau = \tau_0 + \mu_p \dot{\gamma} \tag{3.5}$$

where μ_p is the plastic viscosity, defined as the slope of the curve, and τ_0 is the Bingham yield stress normally taken as the intercept of the flow curve at high shear rates.

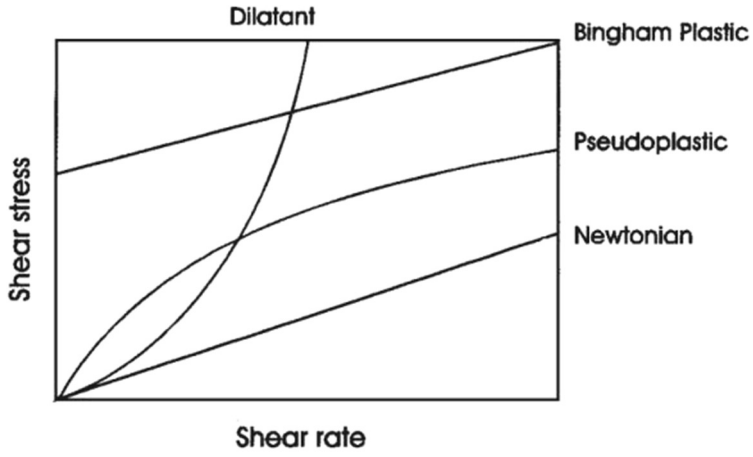

Figure 3.12 – Possible flow curves of a fluid (Luckham and Rossi 1999).

Very dilute clay suspensions or drilling fluids that contain polymers behave as pseudoplastic fluids, which may be described by the power-law of the following equation:

$$\tau = K\dot{\gamma}^n \tag{3.6}$$

where K is a measure of the consistency of the fluid; and n the flow-behaviour index, which is a measure of the decrease of effective viscosity with shear rate.

Other models have been considered in describing the rheological behaviour of clay suspensions, such as the Casson equation:

$$\tau^{1/2} = k_0 + k_1\dot{\gamma}^{1/2} \tag{3.7}$$

and the Herschel-Bulkey equation:

$$\tau = \tau_y + K\dot{\gamma}^n \tag{3.8}$$

Both Equations (3.7) and (3.8) have been used to describe the flow curves of drilling fluids, with the Herschel-Bulkley equation being the most suitable. In both cases, the suspension has an initial yield stress at low shear rates, and afterwards presents pseudoplastic behaviour at higher shear rates (Barnes *et al.* 1989).

Clay suspensions frequently show time-dependent flow behaviour, known as thixotropy. After mixing the suspension, the yield stress and plastic viscosity decrease but will recover with time if left standing (Figure 3.13). Curve 1 represents the initial flow behaviour, and after shearing the suspension displays a flow behaviour represented by curve 2. After a period of rest, the initial Curve 1 is again obtained. Concentrated clay suspensions are very sensitive to shear and their rheological properties vary during the determination of the flow curve. If the shear rate is ramped-up and then immediately ramped-down, the stresses recorded for each rate of shear will be lower and a hysteresis

loop is obtained (curve 3). This occurs because the fragments of the clay particles network are broken under shear and need time to be linked again to a three-dimensional network. In addition, when the clay system is subjected to a constant rate of shear, the viscosity decreases with time as the gel structure is broken down, until an equilibrium viscosity is reached. In view of their shear and time dependency, the clay suspensions require the same preparation, handling and measurement conditions if comparisons are to be made between the rheological properties of different samples.

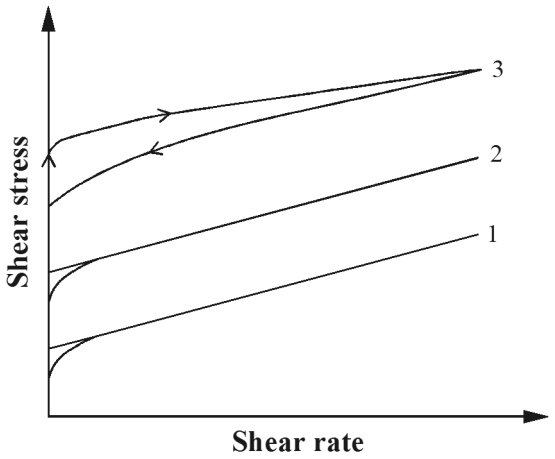

Figure 3.13 – Typical flow curves for concentrated thixotropic clay suspensions (Luckham and Rossi 1999). (1) initial flow curve; (2) flow curve after shearing; (3) thixotropic loop.

Various factors may affect the flow behaviour of clay suspensions. Naturally, the clay concentration will bring about an increase of all rheological properties. Due to the negative particle charge and double-layer structure, the yield stress and viscosity change with variations of the pH of the suspension and electrolyte concentration. Also, differences in the rheological properties are observed depending on the type of electrolyte in solution and on the nature of the exchangeable ions. A rise of the temperature increases the interparticle attractive forces, which in turn, leads to enhanced particle-particle interactions affecting the yield stress and suspension viscosity (Luckham and Rossi 1999).

However, the interaction between clay particles can be manipulated in order to improve the rheological behaviour. For this purpose, several types of deflocculants and dispersants compounds can be added to clay suspensions in small percentages. The main clay deflocculants can be categorised as organic and inorganic. Those organic include humic acids, alkaline lignosulfonates, tannin compounds, polyacrylates, polycarbonates, sodium citrate and gum Arabic. The inorganic deflocculants include sodium (or potassium) carbonates, sodium (or potassium) hydroxides, sodium silicates, phosphates, polyphosphates and sodium (or ammonium) oxalates. These compounds act on the clay suspensions by promoting one or several of the following mechanisms (Rodriges Neto *et al.* 2002):

- Shifting of the pH towards more alkaline values;

- Substitution of flocculant cations in the suspension by less flocculant prone alkaline cations;
- Increasing of the negative charge of the clay surfaces by adsorption of anions;
- Formation of a protective polymeric coating at clay surfaces that promotes steric hindrance.

Deflocculants presenting more than one of these mechanisms are normally more efficient in terms of reduction of the flow resistance. However, the effectiveness of these compounds varies from clay to clay. This means that the selection and optimization of the deflocculant addition requires prior testing for each case (Van Olphen 1977).

3.5 Conclusions

This Chapter presents an overview on the state of art of grout injection applied to ancient masonry and earth constructions. The analysis of the state of art on the injection of ancient masonry revealed that this technique is a feasible, reliable and efficient solution for its repair and strengthening. However, the success of the intervention requires following a design methodology, in which the structural performance and durability of the construction must be accounted for. This process demands the fulfilment of requirements set for the properties of the grout, namely in terms of injectability, bonding capacity, strength and compatibility.

The possible raw materials for composing grouts used in the consolidation of ancient masonry were also reviewed. However, the fulfilment of compatibility requirements (physical, chemical and mechanical) concentrated the attention on hydraulic lime based grouts, and on the binary and ternary grouts. These grouts were shown to present enhanced compatibility and adequate repair/strengthening effectiveness, despite of their relative low strength.

The state of art on the injection of earth constructions was revealed to be short when compared with that on ancient masonry. However, the demand for compatible grouts has been led to the adoption of earth based grouts, namely mud grouts. With this respect, two types of mud grouts are referred in the literature, namely those modified (with addition of mineral binders) and those unmodified (without addition of mineral binders). The modified mud grouts have been preferred due to their lower shrinkage. However, some issues have been reported regarding their lower fluidity and excessive stiffness (Vargas *et al.* 2008 and On Yee 2009). On the other hand, and more recently, the unmodified mud grouts have been shown to promote adequate effectiveness in the repair of cracks of adobe masonry, while presenting adequate fluidity (Vargas *et al.* 2008).

A consistent design methodology for mud grouts is absent from the bibliography, which is explained by the lack of knowledge on this type of grouts and on their interaction

with earthen materials. Therefore, an approach for the design of mud grouts based on the methodology used for ancient masonry was proposed as starting point. Like the predecessor, the proposed methodology takes into account the structural performance and durability of the earth construction to be injected. The required properties of the mud grout were then qualitatively set, in terms of the rheological behaviour, mechanical strength, bond capacity, chemical and fresh-state stability, and microstructure compatibility.

A review on the colloid behaviour of clay suspensions was also presented. This allowed obtaining an insight on the influence of the clay fraction in mud grout. The specific characteristics of the surfaces of clay particles were shown to have great influence on the rheological behaviour of mud grouts due to flocculation phenomena.

Finally, and taking into account the good performance of the unmodified mud reported by Vargas *et al.* (2008), it was decided to give exclusive focus to this type of grouts in the thesis.

Chapter 4

Behaviour of Unmodified Mud Grouts

4.1 Introduction

This Chapter presents an experimental program aiming at comprehending the influence of the composition of an unmodified mud grout on the properties that govern the injection intervention. It should be noted that the experimental work has been carried out in two phases. In the first phase, the experimental work was developed at the Catholic University of Leuven (KULeuven) and resulted in important conclusions regarding the behaviour of mud grouts, namely the rheological behaviour, strength, shrinkage, adhesion and stability. The second phase was carried out at University of Minho (UMinho) and served to confirm, validate and generalise the main findings of the first phase, using other locally available materials.

Thus, the experimental programs are first outlined in the Chapter and then, the obtained results are given and discussed.

4.2 Experimental program at KULeuven

The experimental program carried out at KULeuven addressed both the fresh-state and hardened-state state of mud grouts. It consisted of a composition study, where the properties of several mixtures composed by kaolin and limestone powders (provided by local companies), and by a desflocculant/dispersant for clays (sodium hexametaphosphate) were tested. The tested properties included the fresh-state rheological behaviour (and respective time-dependent behaviour), the strength, the

shrinkage, the adhesion and stability. The importance of these properties is discussed in Section 3.3.2.

4.2.1 Materials

In order to obtain reproducible results along the experimental program it was preferred to use commercial materials with controlled production quality, which in some extent, granted homogeneity and low dispersion of properties. These commercial materials were used to compose the solid phase of several mixtures, instead of using sieved soil. To constitute the clay fraction, kaolin powder was used (provided by Wienerberger with commercial designation of Kaolin RR40), while limestone powder (provided by Carmeuse with commercial designation of Calcitec 2001 S) was used to constitute the silt fraction of the mixtures. Table 4.1 provides the properties of both materials, in terms of particle size distribution (PSD), specific gravity (G_s), liquid limit (LL), plastic limit (PL) and plasticity index (PI). The high values obtained for LL and PI evidence the very high plasticity of the kaolin powder.

Table 4.1 – Properties of the materials composing the solid fraction of the mixtures (Kaolin RR40 and limestone powder Calcitec 2001 S).

Material	% Clay	% Silt	% Sand	G_s (-)	PL (%)	LL (%)	PI (%)
Kaolin RR40	81	10	9	2.65	31	108	77
Calcitec 2001 S	6	65	29	2.71	-	-	-

Clay: <0.002 mm / silt: ≥0.002 mm and <0.060 mm / sand: ≥0.060 mm and <2.0 mm

The kaolin RR40 powder mainly contains clay-sized particles (see Figure 4.1 for PSD curve), which are essentially kaolinite clay minerals (Table 4.2 and Table 4.3). The calcitec 2001 S is mainly constituted by silt-sized particles of calcium carbonate ($CaCO_3$> 98%), which resulted from grinding very pure natural limestone.

Table 4.2 – Mineralogical analysis of the kaolin RR40 (provided by Wienerberger).

Mineral	Kaolinite	Quartz	Other
% mass	87	8	5

Sodium hexametaphosphate (HMP) was also used in the composition study as a deflocculant for clays. This compound is a hexamer with molecular formula $(NaPO_3)_6$, and is produced by melting monosodium orthophosphate, followed by rapid cooling. Typically, the HMP is used as additive in food industry, as a component of cleaning/hygienic products and as a dispersant in clay ceramic industry. This diversity of applications is integrated in strong and established industries, which makes the HMP to be readily available on the worldwide market. Tap water was used for constituting the liquid phase of the mixtures.

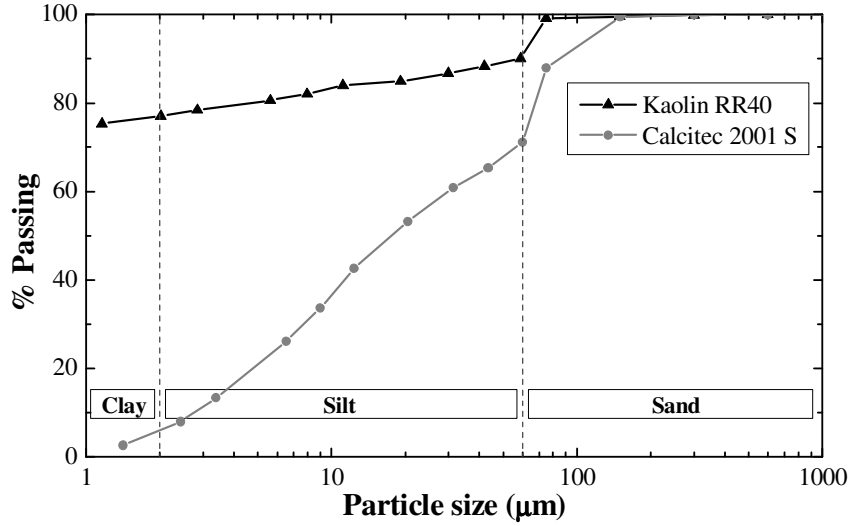

Figure 4.1 – PSD curves of the kaolin RR40 and limestone powder Calcitec 2001 S (ASTM D 422 - ASTM 1998).

Table 4.3 – Chemical composition of the kaolin RR40 (provided by Wienerberger).

Composition	SiO_2	Al_2O_3	Fe_2O_3	TiO_2	CaO	MgO	Na_2O	K_2O	L.O.I
% mass	48	34.5	1.9	1.9	0.44	0.18	0.04	0.04	13

4.2.2 Mixtures and mixing procedure

The composition study included the testing of 98 mixtures, which were composed by different proportions of the aforementioned materials. In order to simplify the comprehension of the composition study, the mixtures were grouped into the following types: (i) kaolin (K); (ii) kaolin and HMP (KH); (iii) kaolin and limestone powder (KL); (iv) and kaolin, limestone powder and HMP (KLH).

The variables of the study were then: (i) the volumetric solid fraction (ϕ_v); (ii) the amount of HMP added as function of the kaolin content ([HMP]); (iii) and the ratio between the weight of kaolin and limestone powder (*K/L*).

The volumetric solid fraction, ϕ_v, is given by equation (4.1):

$$\phi_v = \frac{V_s}{V_T} \times 100 \quad (\%) \tag{4.1}$$

where V_s is the volume of the solid phase and V_T is the total volume of the mixture.

The matrix of the tested mixtures is given in Figure 4.2, where the aforementioned variables are combined. Changing ϕ_v of each mixture type allows investigating the dependency of the rheological behaviour of the mixtures on the solid content. By changing the [HMP] it was expected to gather information on the capacity of this compound (or similar) in improving the fluidity of mud grouts. The clay content of the KL and KLH mixtures is reflected on the *K/L* ratio, whose variation aims at

investigating the influence of the clay content in the rheological behaviour and strength of a mud grout.

The mixing procedure was similar for all mixtures. First, the solid phase materials were manually dry-mixed and then tap water was progressively added and hand mixed until obtaining homogeneity (when HMP was added, it was previously dissolved in the composition water). Afterwards, the mixtures were mixed in three steps by a Hobart N50 planetary mixer with a wire whip paddle: first for 5 min at speed 1, then for 5 min at speed 2 and finally for 5 min at speed 1. In between each step, a resting time of 1 min was respected.

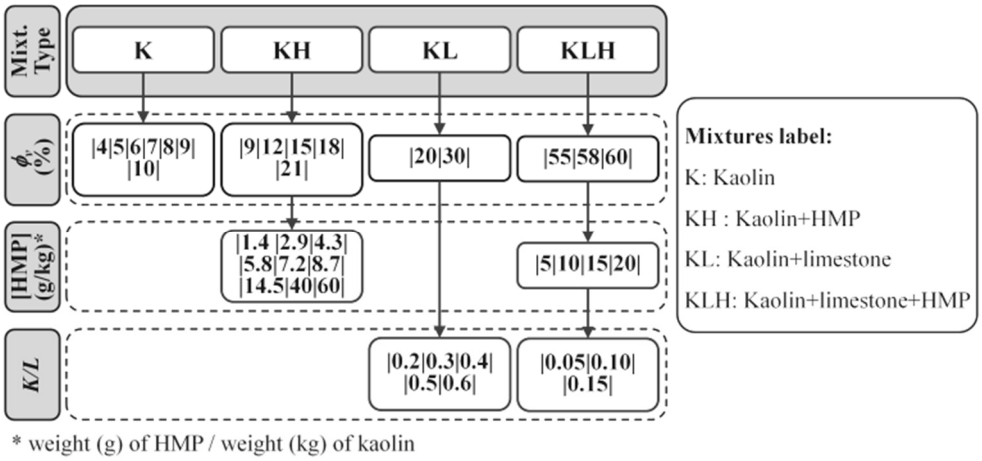

Figure 4.2 – Matrix of the mixtures tested at KULeuven.

4.2.3 Experimental procedures

Rheology

The flow time of each mixture was determined according the procedure of ASTM C 939 (ASTM 1994), but by testing a sample of 1 dm^3 using a Marsh cone different from that described in the standard. A Marsh funnel (see geometry in Figure 4.3a) with an average flow time of 34 s for 1 dm^3 of water at 18ºC was used. All the tests were initiated within 1 min after the mixer being stopped, in order to minimize the interference of possible time-dependent behaviour of the mixtures on the results.

The KH mixtures that were apparently less fluid or that showed great difficulty in flowing through the Marsh funnel (or did not flow at all) had, in addition, their flow curves determined by means of a Viskomat PC mixer-type rheometer (see Figure 4.3b) with a mortar paddle of 83 mm diameter (Hendrickx 2009). Figure 4.4 shows a detail of the configuration of the testing cup and paddle of the Viskomat PC rheometer. The paddle is specially designed to prevent sedimentation of solid particles and occurrence of localized shear, and thus it is indicated for the testing of suspensions. However, this apparatus has a main disadvantage, which resides in the difficulty of interpreting the outputs in terms of classic rheological parameters. The test is carried out by putting the

mixture sample in the rotating testing cup, which is then sheared by the paddle, while the torque (in the paddle) is measured.

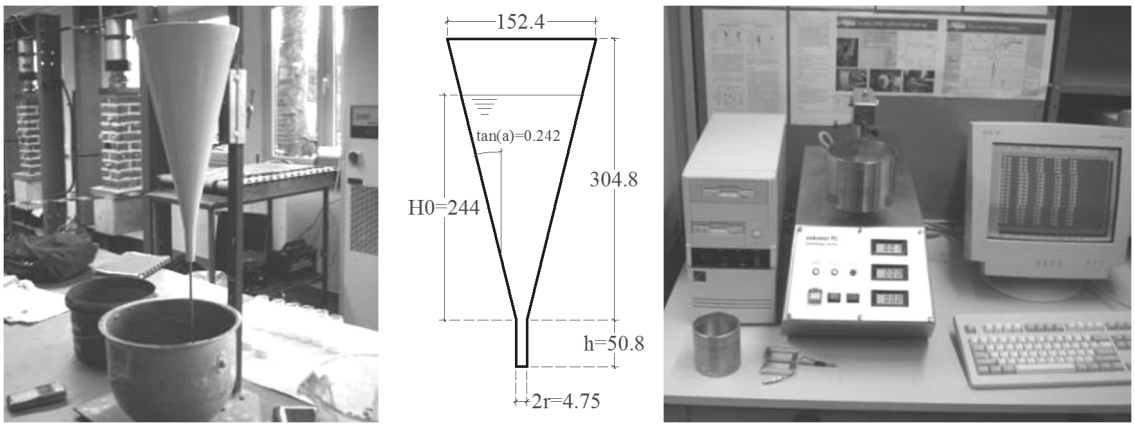

(a) (b)

Figure 4.3 – Apparatus used in the characterization of the rheological behaviour: (a) Marsh funnel (dimensions in mm) and (b) Viskomat PC rheometer.

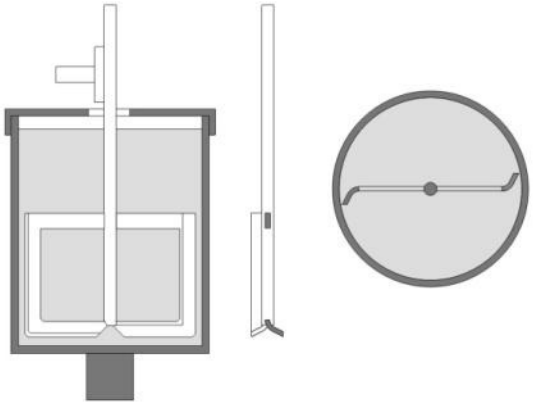

Figure 4.4 – Configuration of the Viskomat PC testing cup and paddle (Hendrickx 2009).

The flow profile applied on the KH mixtures had different configuration from that applied on the KLH mixtures. The maximum rotation speed was fixed at 120 rpm in the first case, and then was changed for 200 rpm in the second case (see Figure 4.5) in order to a obtain a broader extension of the flow curves.

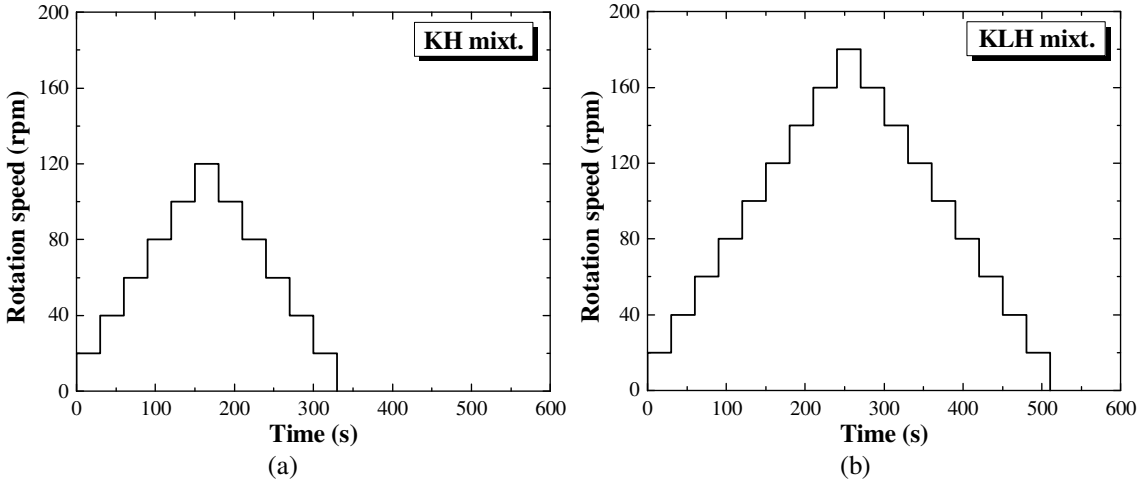

(a) (b)

Figure 4.5 – Viskomat PC flow profiles for (a) KH mixtures and (b) KLH mixtures.

Both profiles include an ascending stepwise (Δt=30s) branch followed by a descending stepwise (Δt=30s) branch in order to assign a similar reference state (in terms of shear history) to all mixtures. Moreover, this kind of flow profile allows also at investigating the time-dependent behaviour. The rheological parameters were only computed for the descending branch, where a similar reference state was assumed for all mixtures.

Time-dependent rheological behaviour

The time-dependent effect on the rheological behaviour of the fresh-state KLH mixtures was assessed for only three mixtures, which correspond to the three mud grouts selected to test the adhesion capacity. Table 4.4 presents the composition of the grouts, as well as the size-fractions composing them. The test consisted in applying the Viskomat PC profile of the KLH mixtures at different periods after mixing, namely at 0, 30, 60 and 90 min. The tested samples were the same for all periods, and were let to rest undisturbed in between tests.

Table 4.4 – Composition of the mud grouts selected for assessing the time-dependent rheological behaviour and the adhesion capacity.

Mud Grout	[HMP] (g/kg)	*K/L*	ϕ_v (%)	W/S (wt.)	% Clay	% Silt	% Sand
I55MG15	20	0.15	55	0.30	16	58	26
I58MG15	20	0.15	58	0.27	16	58	26
I60MG15	20	0.15	60	0.25	16	58	26

Strength

The flexural and compressive strengths were tested for each KLH mixture on three beam-specimens with dimensions 40×40×160 mm^3, according to the EN 1015-11 (CEN 1999) procedure. However, the testing age was defined in such a way that granted the establishment of the equilibrium water content of the specimens (ratio between weight of water and weight of dry solid particles) before testing, since the mechanical properties of earthen materials greatly depend on this parameter (Jaquin 2008). Therefore, the specimens were stored and dried in a controlled ambient room temperature (T= 20ºC) and humidity (RH= 65%), and the evolution of their weight was monitored after demoulding (at age of about 4-7 days). As it can be observed from Figure 4.6a, the demoulded specimens achieve a constant weight in a short-time (3-5 days) which corresponds to the establishment of the equilibrium water content. Thus, the specimens were tested at ages ranging from 29 to 31 days, and the equilibrium water content was measured after testing (see Figure 4.6b). For all mixtures, the equilibrium water content is very low and it seems to depend mainly on the kaolin content, as stated in Johansen and Dunning (1957); the higher the kaolin content, the higher is the equilibrium water content.

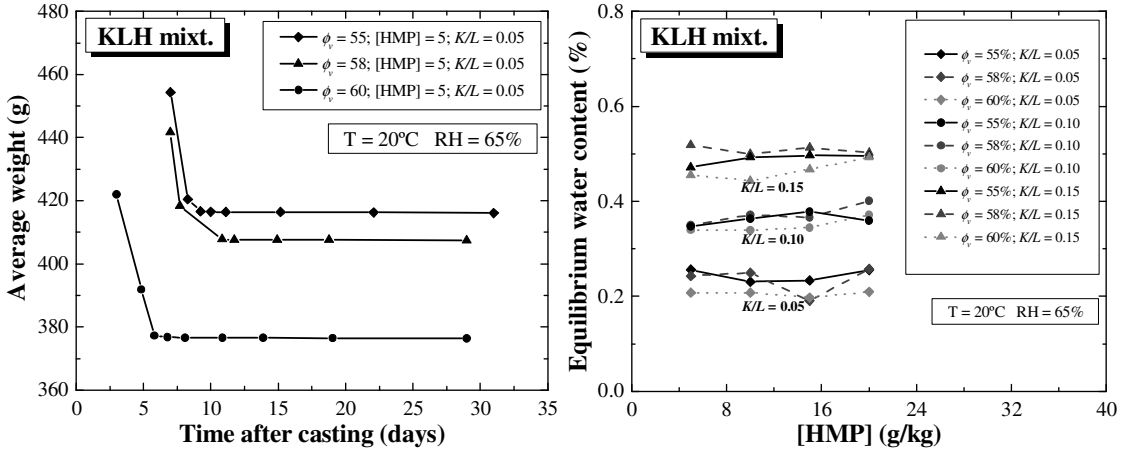

Figure 4.6 – Water content of the beam-specimens: (a) time evolution of the weight of KLH specimens with [HMP]=5g/kg and *K/L*=0.05; and (b) equilibrium water content of all KLH specimens.

Shrinkage

The drying shrinkage of the KLH mixtures was assessed by comparing the volume of the dry beam-specimens with the volume of the mould of the respective specimen. It should be noted that this procedure does not simulate the drying conditions of a mud grout. The drying occurs mostly by sorption caused by the earthen material of the construction, which means that these results should be looked at carefully when addressing the real shrinkage of the mud grout in a repair intervention.

Adhesion

The three mud grouts selected to assess the adhesion capacity (see Table 4.4) were used to repair 18 earthen beams (160x40x40 mm^3) built with three types of soil typically used in the construction of rammed earth houses in Alentejo, Portugal (6 specimens per soil type). Due to the small dimensions of the specimens, the soils were first sieved to remove particles larger than 2 mm, resulting in the properties given in Table 4.5.

The preparation of the specimens consisted in compacting three layers of moistened earth within a typical metallic mould for mortars (see Figure 4.7a), which were immediately demoulded and stored in a controlled ambient room temperature (*T*= 20ºC) and humidity (RH= 65%). The water content for compaction was defined such that in the ball drop test (Minke 2006) the ball would present some cracks without crumbling completely (see Section 2.3.1). The flexural strength of the beams was tested after 23 days (after achieving the equilibrium water content), according to the EN 1015-11 (CEN 1999) procedure.

Table 4.5 – Properties of the soils used in the adhesion tests after sieving (KULeuven).

Soil	% Clay	% Silt	% Sand	PL (%)	LL (%)	PI (%)
A_S1	19	47	34	28	44	16
A_S2	15	37	48	17	32	15
A_S3	18	29	53	20	35	15

Clay: <0.002 mm / silt: ≥0.002 mm and <0.060 mm / sand: ≥0.060 mm and <2.0 mm

Afterwards, the beams were repaired by injecting the mud grouts (2 beams of each soil per mix) into the crack between the two parts of each beam (see Figure 4.7b), which were positioned in a mould to provide an approximate crack width of 5 mm. Before injection, the crack surfaces were scraped to remove loose materials and then wetted to mitigate the sorption of water from the mud grout upon the injection. It should be mentioned that the drying and hardening of the grouts took only a few minutes, showing the high sorption capacity of earthen materials, which can be a drawback in an injection intervention due to a decrease in injectability. The repaired beams were stored in the aforementioned room, and were tested again after 15 days.

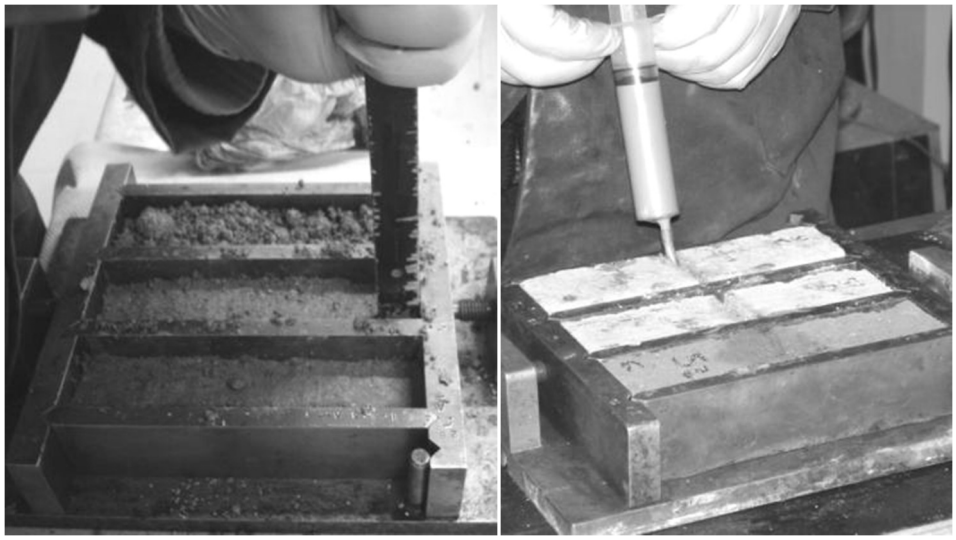

(a) (b)

Figure 4.7 – Preparation of the earthen beams for (a) the adhesion tests and (b) injection of the earthen beams after testing.

Stability

The stability of the aforementioned mud grouts as a suspension of solid particles was also assessed. Bleeding tests carried out according the ASTM C 940 (ASTM 2003) procedure. Moreover, the capacity of the other tested mixtures in maintaining the particles in suspension was evaluated qualitatively during their handling for the other tests. In this case, attention was

4.3 Experimental program at UMinho

The experimental program carried out at University of Minho (UMinho) aimed at confirming and generalising the main findings of the experimental program carried at KULeuven, using materials available locally. This resulted in a simplified version of the composition study carried out at KULeuven, which did not include the measurement of flow curves, time dependent behaviour and the testing of the stability. Moreover, the materials used in this composition study were later used in the composition of mud grouts used to repair rammed earth specimens with larger scale (see Section 6.2), which justifies the partial repetition of the experimental program carried out at KULeuven.

4.3.1 Materials

Kaolin and Limestone powders were also used in the composition study carried out at UMinho. The kaolin Mibal-A was acquired from a local manufacturer (Mibal - Minas de Barqueiros S.A.), which provided a qualitative mineralogical analysis given in Table 4.6. As can be seen, this kaolin is mainly constituted by kaolinite clay minerals. The manufacturer also provided the chemical analysis, which is given in Table 4.7.

Table 4.6 – Mineralogical analysis of the kaolin Mibal-A (provided by Mibal – Minas de Barqueiros S.A.).

Mineral	Kaolinite	Quartz	Feldspar	Mica
Presence	++++	++	+	+

The kaolin Mibal-A is mainly constituted by clay-sized particles, as can be seen in Table 4.8 and Figure 4.8. However, the clay fraction percentage is significantly lower than that of the kaolin RR40. Moreover, the kaolin Mibal-A is less plastic, since the PL and PI are significantly lower than those of the kaolin RR40. This difference can be attributed to several factors, such as: clay fraction percentage, clay mineralogy/chemistry and fineness of the clay fraction.

Table 4.7 – Chemical composition of the kaolin Mibal-A (provided by Mibal – Minas de Barqueiros S.A).

Composition	SiO_2	Al_2O_3	Fe_2O_3	TiO_2	CaO	MgO	Na_2O	K_2O	L.O.I
% mass	47.0	37.1	0.9	0.1	0.1	0.15	0.2	2	12.8

The limestone powder Micro 200-OU was obtained from a local supplier, namely Omya *Comital Minerais e Especialidades S.A.* As can be seen in Table 4.8, this material is mainly composed by silt-sized particles of calcium carbonate ($CaCO_3$> 98%) and has a PSD similar to that of the limestone powder Calcitec 2001 S in terms of the percentages of the size-fractions (see Figure 4.8). Sodium hexametaphosphate (HMP) was again selected to improve the fluidity of the tested suspensions. Tap water was also used to constitute the liquid phase of the mixtures.

Table 4.8 – Properties of the materials composing the solid fraction of the mixtures (Kaolin Mibal-A and limestone powder Micro 200-OU).

Material	% Clay	% Silt	% Sand	Specific gravity	PL (%)	LL (%)	PI (%)
Kaolin Mibal-A	67	33	0	2.65	27	59	32
Micro 200-OU	6	71	23	2.71	-	-	-

Clay: <0.002 mm / silt: ≥0.002 mm and <0.060 mm / sand: ≥0.060 mm and <2.0 mm

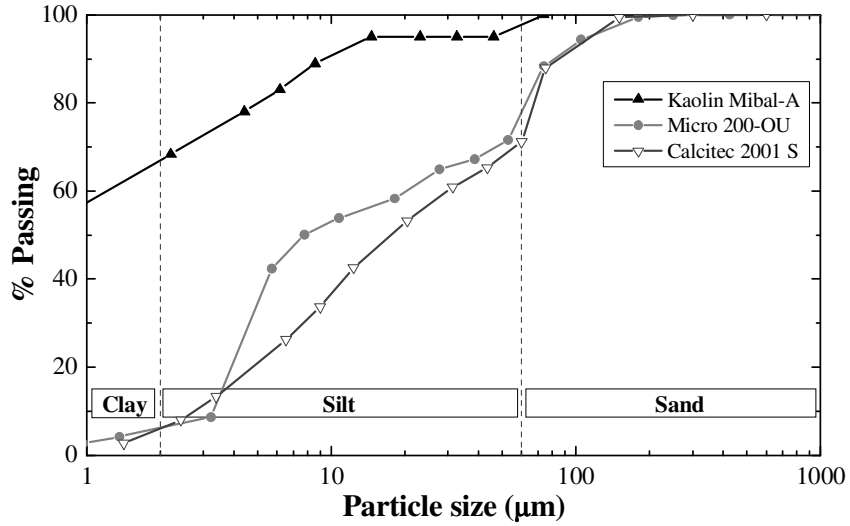

Figure 4.8 – Particles size distribution curves of the kaolin Mibal-A and limestone powder Micro 200-OU (ASTM D 422 - ASTM 1998).

4.3.2 Mixtures and mixing procedure

The experimental program carried out at UMinho included the testing of 83 mixtures, which were defined by varying ϕ_v, [HMP] and *K/L* (see matrix of Figure 4.9). It should be noted that mixtures of the type KL were not included in this composition study. The mixing procedure was the same used in the experimental work developed at KULeuven (see section 4.2.2). The used mixer was again a Hobart N50 planetary mixer with a wire whip paddle.

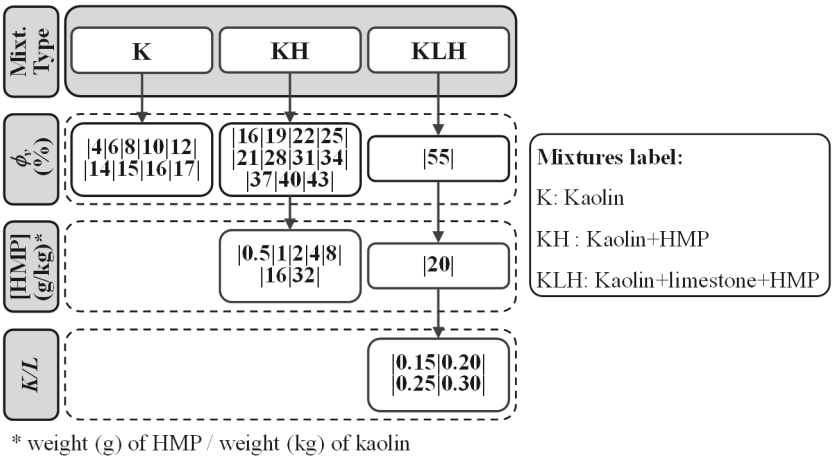

Figure 4.9 – Matrix of the mixtures tested at UMinho.

4.3.3 Experimental procedures

Rheology

The rheological behaviour of the mixtures was tested only by means of Marsh cone tests, where the flow time was determined according the procedure of ASTM C 939 (ASTM 1994). A different Marsh cone from that used at the KULeuven tests was used.

This cone complies with the dimensions provided by the EN 445 (CEN 2007), but it was used the nozzle with 8 mm diameter (see Figure 4.10). The cone has an average flow time of 10.5 s for 1 dm^3 of water at 23ºC. The tests were carried out immediately after finishing the mixing procedure using samples with 1 dm^3 volume.

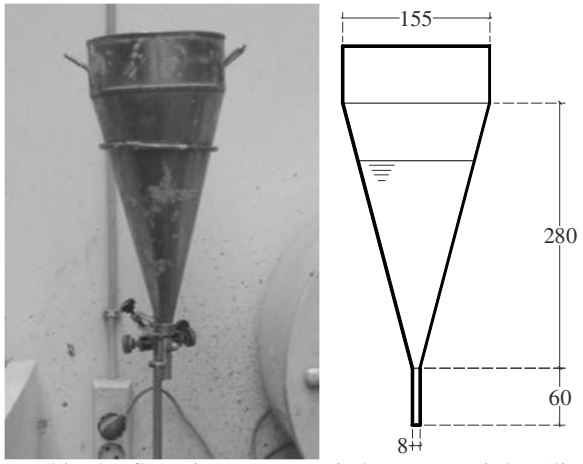

Figure 4.10 – Marsh cone used in the flow time tests carried out at UMinho (dimensions in mm).

Strength

The flexural and compressive strengths were tested on the KLH mixtures according the EN 1015-11 (CEN 1999) procedure. The testing age was about 28 days, which allowed the specimens achieving the equilibrium water content for the storing ambient conditions (T= 20ºC and RH= 57.5%). Figure 4.11 shows the equilibrium water content of the specimens after testing as function of the *K/L* ratio. Again, this parameter is low, but is shown to be directly proportional to the *K/L* ratio, and thus to the clay content.

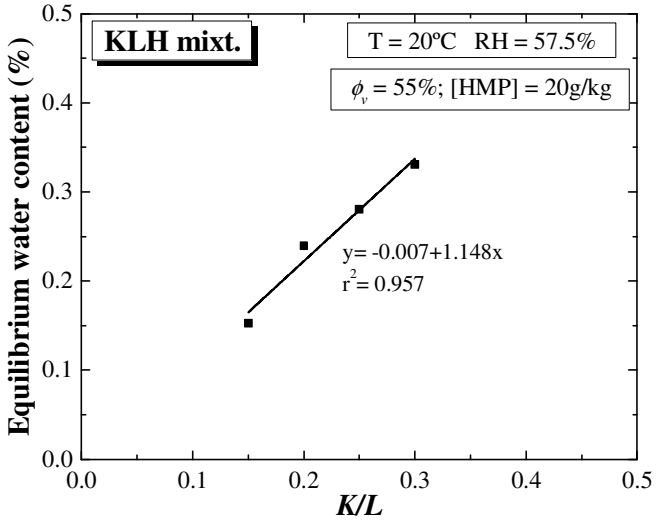

Figure 4.11 – Equilibrium water content of the KLH mixtures specimens tested at UMinho.

Shrinkage

The drying shrinkage of the KLH mixtures was assessed according the procedure followed in the experimental program carried out at KULeuven (Section 4.2.3).

Adhesion

The adhesion tests performed at UMinho assessed the adhesion capacity of the four mud grouts (all tested KLH mixtures), whose compositions are detailed in Table 4.9. The testing procedure was the same adopted at KULeuven (Section 4.2.3). However, the adhesion specimens were prepared by using only one soil, which was also collected from Alentejo, Portugal (Table 4.10). A total of 24 specimens was prepared, which means that 6 specimens were tested per grout.

Table 4.9 – Composition of the KLH mixtures used to test the adhesion capacity.

Mud Grout	[HMP] (g/kg)	*K/L*	ϕ_v (%)	W/S (wt.)	% Clay	% Silt	% Sand
II55MG15	20	0.15	55	0.30	14	66	20
II55MG20	20	0.20	55	0.30	16	65	19
II55MG25	20	0.25	55	0.30	18	64	18
II55MG30	20	0.30	55	0.30	20	62	18

Table 4.10 – Properties of the soils used in the adhesion tests after sieving (UMinho).

Soil	% Clay	% Silt	% Sand	PL (%)	LL (%)	PI (%)
A_S4	19	25	56	16	27	11

Clay: <0.002 mm / silt: ≥0.002 mm and <0.060 mm / sand: ≥0.060 mm and <2.0 mm

4.4 Results and discussion

The discussion of the results is not organised by individualised experimental program (KULeuven or UMinho) as presented previously. Instead, it was preferred to organise the discussion of both programs by properties. Furthermore, the observations of the composition study carried out at UMinho are here discussed as a validation and generalisation of the main conclusions drawn from the composition study carried out at KULeuven.

4.4.1 Rheology

K mixtures

The results of the flow time tests of the K mixtures of both experimental programs are presented in Figure 4.12, where the flow time is shown to increase exponentially with increasing ϕ_v. In the case of the tests carried out at KULeuven, a critical solid fraction (ϕ_{vcr}) is attained for ϕ_v between 9% and 10% (W/S between 3.8 and 3.4), after which the flow through the Marsh funnel is no longer possible. The same behaviour was observed for the tests carried out at UMinho, where ϕ_{vcr} is in between 16% and 17% (W/S between 1.9 and 1.8). It should be noted that both ϕ_{vcr} are not directly comparable, because they result from different Marsh cones. Despite that, both ϕ_{vcr} values correspond to very low solid fractions, which are not suitable for a potential grout since it would result in high shrinkage. On the other hand, adopting a larger ϕ_v would result in a grout with inferior injectability properties, making its injection at low pressure rather difficult or even impossible.

The observed behaviour is explained by the colloidal behaviour of the kaolinite particles in suspension, which interact with each other under Brownian or/and hydrodynamic motion, generating two possible states of the particles: deflocculated or flocculated (Van Olphen 1977). The interaction between kaolinite particles in suspension is governed by DLVO (Derjaguin-Landau-Verwey-Overbeek) forces, namely electrostatic forces (repulsion between like electric double layers and attraction between unlike charged surfaces) and van der Waals attractive forces. The balance between these forces is dictated by several factors, such as the average distance between particles (directly related to the solid fraction of the suspension), the nature (permanent or variable) and the magnitude of the heterogeneous surface charge of the clay particles, the pH, and the ionic strength of the medium, etc. (Tombácz and Szekeres 2006). Therefore, when the attractive forces are favoured, the clay particles tend to flocculate, forming an internal structure (house-of-cards or scaffold structure) that opposes the flow. Practically speaking, increasing the ϕ_v of the mixtures results in smaller average distances between particles, which favours the attractive forces and thus the build-up of the aforementioned internal structure.

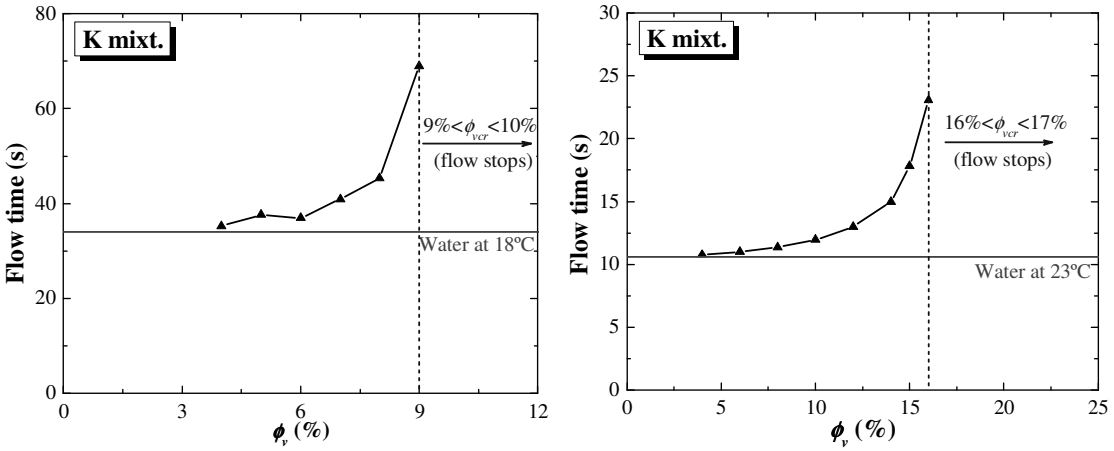

Figure 4.12 – Flow time measurements of the K mixtures carried out at (a) KULeuven and (b) UMinho.

KH mixtures

The addition of HMP is expected to disturb the formation of internal structure of clay particles, which would result in favourable flow behaviour. Figure 4.13 shows exactly this, since the flow time decreases with increasing [HMP]. This behaviour is explained by three deflocculating mechanisms introduced by the addition of HMP: (i) increase in the overall negative surface charge by the adsorption of anionic HMP polymeric chains onto the kaolinite surface, especially at the edges of the kaolinite particles (Andreola *et al*. 2006, Legaly 2006); (ii) stabilisation caused by the steric hindrance effect of the adsorbed HMP chains (Papo *et al*. 2002); (iii) complexing of the dissolved alkaline-earth cations and replacing them by lower valence Na^+ cations, which increases the thickness of the electric double layers of the clay particles surfaces (Andreola *et al*. 2006). Nevertheless, the mixtures incorporating higher HMP concentration had their flow time increased. This can be explained by a concentration of HMP that is above a

critical value, namely the saturation adsorption limit. This results in excess concentration of non-adsorbed HMP chains in solution, which promotes the association of kaolinite particles, instead of their repulsion (Papo *et al.* 2002).

The aforementioned mechanisms allowed also increasing further the ϕ_{vcr}. In the case of the tests carried out at KULeuven, ϕ_{vcr} is in between 21% and 24% (W/S between 1.4 and 1.2), while in the case of the UMinho tests is in between 37% and 40% (W/S between 0.62 and 0.54). The difference between the values of ϕ_{vcr} of each kaolin type can be attributed to the different Marsh cones used, but also to different properties of each one.

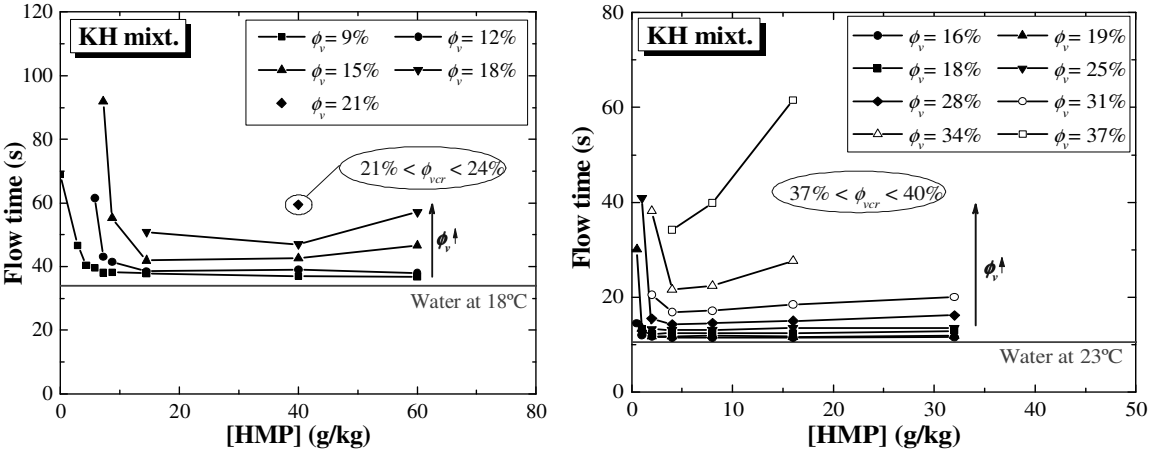

Figure 4.13 – Flow time measurements of the KH mixtures carried out at (a) KULeuven and (b) UMinho.

As referred previously, the KH mixtures with thicker consistency had their rheological behaviour characterized resorting to a Viskomat PC rheometer. It should be noted that 7 to 8 data points were recorded for each step of the flow profile, of which a trimmed average was taken as representative point of the step. However, the output points were constituted by a torque value and a respective angular velocity, which were converted into shear stress and shear rate values by using the Couette analogy theory. The Couette analogy method is based on Bousmina *et al.* (1999) and Aït-Kadi *et al.* (2002), and was proposed in Lootens *et al.* (2004) for cement slurries. This method requires the determination of a fictitious radius R_i of a cylindrical bob, which would experience the same torque as that of the actual paddle. For a Newtonian fluid the ratio between the external radius R_e (0.042 m) and R_i is given by equation (4.2):

$$\frac{R_e}{R_i} = \sqrt{1 + \frac{8\pi^2 L R_e^2 \mu 2\pi N}{T}} \tag{4.2}$$

Where, L is the paddle length (0.063 m), η the viscosity of the fluid, N the rotation speed (in revolutions per unit of time) and T the recorded torque. This ratio was determined using a Newtonian fluid of known viscosity, and was found to be of about 1.154 (see Hendrickx 2009). The shear rate ($\dot{\gamma}$), viscosity (η) and shear stress (τ)

values at the middle of the fictitious gap can be approximately estimated from this radii ratio, according to:

$$\dot{\gamma} = \frac{2\pi N}{\ln\left(\frac{R_e}{R_i}\right)} \tag{4.3}$$

$$\mu = \frac{T}{2\pi N} \frac{\left(\frac{R_e}{R_i}\right)^2 - 1}{4\pi L R_e^2} \tag{4.4}$$

$$\tau = \mu\dot{\gamma} \tag{4.5}$$

It should be noted that in the aforementioned equations, it is assumed that the fluid is Newtonian. However, Hendrickx (2009) shows that their application to cement and lime pastes (exhibiting Bingham behaviour within the tested range of shear rate) produces comparable results to those obtained from a rotational rheometer with a Couette cell.

Figure 4.14 presents the flow curves of the KH mixtures with ϕ_v= 15%, where the effect of the addition of increasing amounts of HMP on the flow resistance is evidenced; the shear stress is decreased by increasing the [HMP].

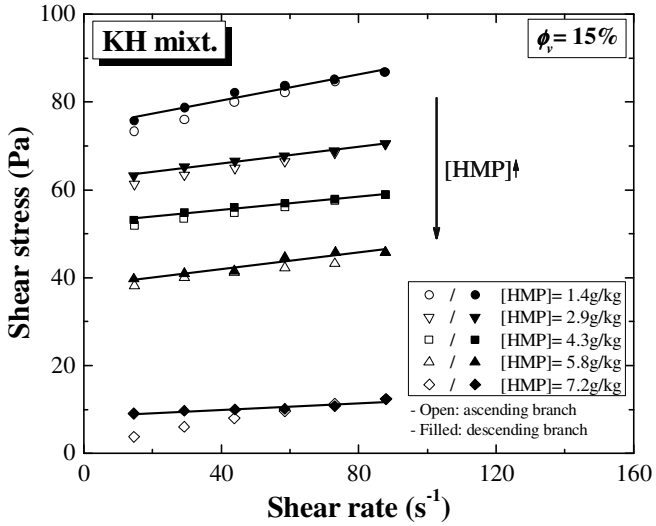

Figure 4.14 – Flow curves of KH mixtures with ϕ_v= 15% (Bingham's model fitted to the descending branch).

It should be noted that, the KH mixtures with [HMP] higher than 7.2 g/kg were rather fluid, whereby the Viskomat PC rheometer was not capable of measuring reliably such relatively low flow resistances. The same occurred for the mixtures with ϕ_v of 9% for all [HMP], and ϕ_v of 12% and 18%, for [HMP] higher than 5.8 g/kg and 14.5 g/kg, respectively. Moreover, the points of the descending branch of the KH mixtures plotted

in Figure 4.14 seem to exhibit Bingham behaviour. This is an observation that can be extended to the other mixtures (see Annex A), whereby the Bingham's model of Equation (3.5) was fitted to the descending branch of all mixtures.

The Bigham's parameters of the KH mixtures with a ϕ_v of 21% are presented in Figure 4.15, which is representative of the behaviour observed for other ϕ_v (see Annex A). Both parameters are substantially reduced by addition of little amounts of HMP. In practical terms, the yield stress is related to the force required to deform and to disrupt the internal house-of-cards or scaffold structure previously mentioned. This structure is formed from the association between clay particles in edge-to-edge (EE) and edge-to-face (EF), in which the more numerous and as stronger these associations are, the higher the yield stress is (Van Olphen 1977). The HMP added to the KH mixtures is mainly adsorbed at the edge surfaces of the clay particles, which increases the magnitude of their negative surface charge, and thus reduces the frequency and strength magnitude of EE and EF associations. The reduction observed for the plastic viscosity is also a consequence of the effect of the HMP, since its addition allows a reduction in the number and size of flocks formed from the EE and EF associations. Therefore, less water is entrapped within them, leading to lower effective volumetric solid fraction (ϕ'_v) in the mixtures with a higher [HMP] (Barnes *et al.* 1989).

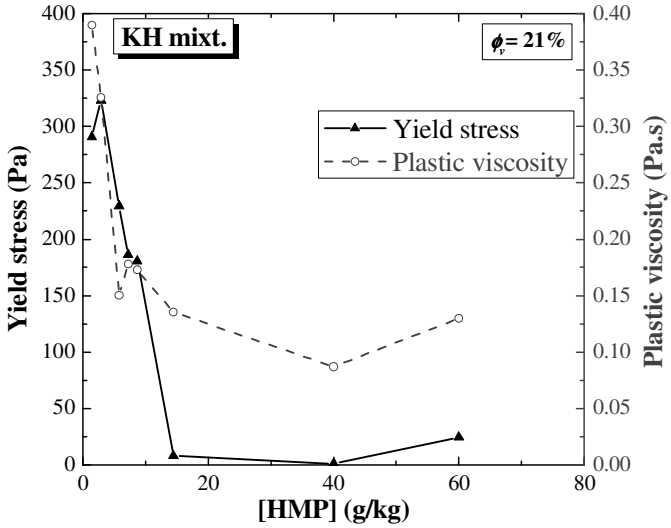

Figure 4.15 – Bingham's parameters of the KH mixtures with ϕ_v= 21%.

However, the yield stress has the greatest contribution to the flow resistance in the tested domain of shear rates. Furthermore, this parameter is the main responsible for the Marsh cone tests that failed. In these failed tests, the flow through the Marsh cone attained a critical situation before the gravity force empties the cone, where the flow rate becomes zero. It should be noted that the nozzle of a Marsh cone is a critical zone for the flow of the mixtures, since the radius of this section is the smallest. The flow will not occur (or will stop) if the condition of the equation (4.6) is not observed at the nozzle during the test (Roussel and Le Roy 2005):

$$\frac{2\tau_0}{Ar} \leq 1 \tag{4.6}$$

where r is the nozzle radius and A the pressure gradient. For the complete flow of the Marsh cone, the pressure gradient assumes its minimum value at the nozzle and, thus it is written as follows:

$$A = \rho g \tag{4.7}$$

Where ρ is the density of the mix and g the gravitational acceleration.

By considering that the density of the KH mixtures tested at KULeuven varied between 1198 kg/m^3 and 1347 kg/m^3 and those tested at UMinho varied between 1264 kg/m^3 and 1710 kg/m^3, results that the maximum yield stress that grants complete flow of the mixtures tested at KULeuven varies between 14 and 16 Pa and that of those tested at UMinho between 25 and 34 Pa. The threshold of the KH mixtures tested at KULuven is represented in Figure 4.16, where all mixtures with shear stress below it flowed through the Marsh funnel.

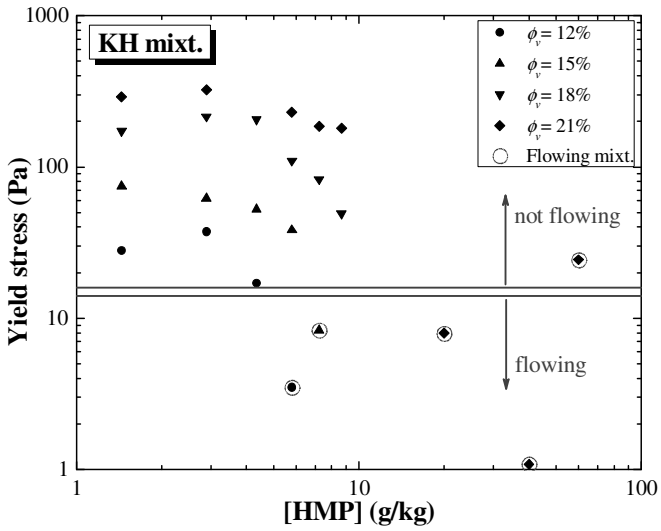

Figure 4.16 – Influence of the shear stress in the flowing capacity of the KH mixtures through the marsh funnel.

Figure 4.15 also demonstrates the effect of exceeding the critical HMP concentration, namely it results in an increase in both Bingham's parameters. Another curious result is that the hysteresis observed for some mixtures indicates an anti-thixotropic behaviour, which is contrary to the expected thixotropic behaviour usually reported for clay suspensions. This is explained by the low shear rate range of the tests (when compared with the range of shear rates usually found in the bibliography on clay suspensions), which is, most probably, promoting the association of clay particles, and thus the build-up of the aforementioned internal structure.

KL mixtures

KL mixtures were only tested in the case of the experimental program carried out at KULeuven in order to investigate the influence of the clay content on the rheological behaviour of fresh mud grouts. The results of the flow time tests are presented in Figure 4.17, where the effect of the clay faction on fluidity is evidenced; as the clay content is increased (increase in *K/L*), the flow time increases. Moreover, it is shown that substituting partially the clay content by a silt size material (limestone powder) increases ϕ_{vcr} significantly when comparing with the K and KH mixtures; ϕ_{vcr} is lower than 40% but higher than 30%.

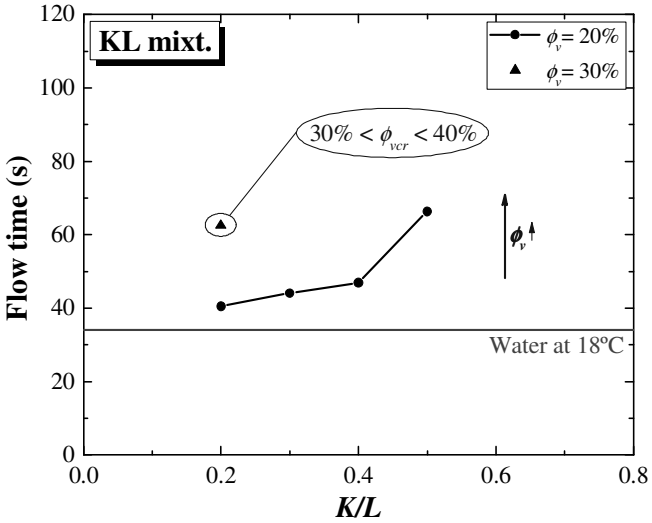

Figure 4.17 – Flow time measurements of the KL mixtures carried out at KULeuven.

KLH mixtures

The KLH mixtures tested at KULeuven allowed testing the combined effect of the addition of HMP with the incorporation of limestone powder. The results showed that this effect makes possible to further increase ϕ_{vcr} relatively to the KH and KL mixtures, since flowing suspensions with ϕ_v from 55% to 60% were obtained (W/S between 0.3 and 0.25). Moreover, all KLH mixtures tested at UMinho (ϕ_v= 55% and W/S= 0.3) flowed thought the respective Marsh cone, which means that the ϕ_v, chosen based on the KULeuven experimental program, seems to be adequate, as is later discussed. However, the flow times increased substantially when compared with those of the K, KH and KL flowing mixtures, as is the case of the mixtures with ϕ_v= 55% presented in Figure 4.18. Moreover, the flow time measurements obtained at KULeuven (Figure 4.18a) show a tendency that seems contrary to that of the KL mixtures, in the sense that the mixtures with lower *K/L* ratios have higher flow times (see also Annex A). On the other hand, the flow time measurements of the KLH mixtures carried out at UMinho disagree with those carried out at KULeuven and follow the same trend of the KL mixtures. This conflicting result can be explained by the fact that [HMP] was defined as a function of the kaolin content, meaning that the lower is the *K/L* ratio, the lower is the effective HMP weight in mixtures. Moreover, the deflocculant/dispersant effect of HMP on clay

suspension (or in general any other compound used with this function) is known to be very dependent on the clay mineralogy, resulting that the HMP concentration that promotes higher fluidity has to be optimized (by testing) for each clay (Van Olphen 1977). This may mean that the fluidity of the KLH mixtures tested at KULeuven were still being limited by the colloid behaviour of the clay fraction and that a [HMP] higher than 20 g/kg would be required to promote their maximum fluidity. It should be noted that part of the HMP added is also expected to contribute for a deflocculating/dispersing effect on the limestone powder. To verify the existence of this effect, the flow time of some additional mixtures (LH mixtures) was tested. The mixtures were composed by limestone powder and HMP, whose weight was defined as a function of the ratio between the weight of HMP and the weight of limestone powder ([HMP]'). The mixtures were tested with ϕ_v of about 50% and the results are given in Figure 4.19, where the addition of HMP is shown to result in decreasing of the flow time. However, after a [HMP]' of 4 g/kg the flow time increases again, which may be explained by a an HMP concentration at the liquid phase above the saturation point.

However, the hypothesis considering the fluidity of the KLH mixtures tested at KULeuven being limited by the clay fraction colloid behaviour is contradicted by the analysis of the flow curves obtained from the Viskomat PC rheometer, as is discussed later. Thus, another hypothesis to explain the odd behaviour of the KLH mixtures tested at KULeuven is probably related to the particles packing within the mixtures. This hypothesis is also discussed later with the analysis of the flow curves of the KLH mixtures.

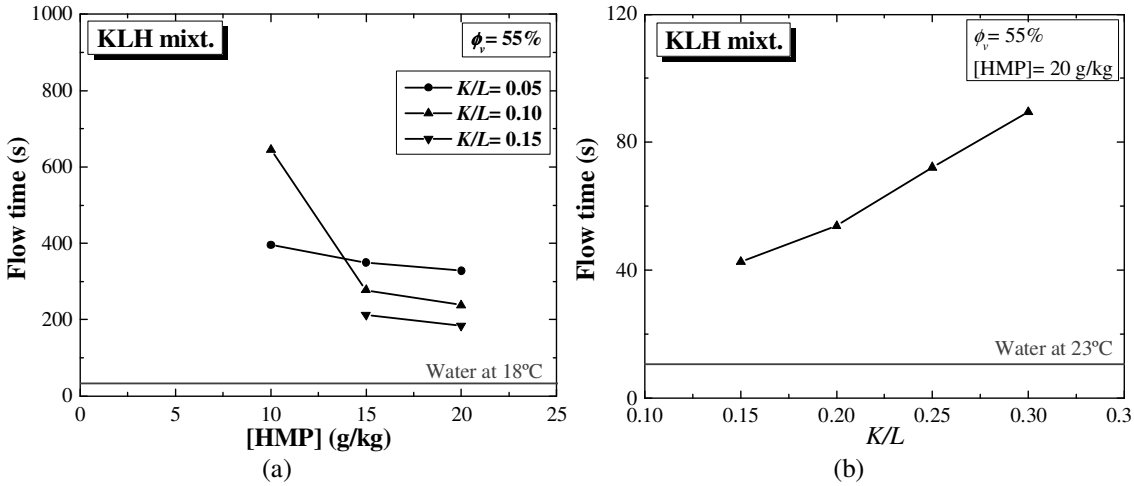

Figure 4.18 – Flow time measurements of the KLH mixtures with ϕ_v=55%: (a) KULeuven (b) UMinho.

Figure 4.20 depicts the flow curves of the KLH mixtures with ϕ_v= 55% and *K/L*= 0.05, whose behaviour is representative of other KLH mixture (see Annex A) and seems to be similar to that of a Bingham´s fluid. Therefore, the Bingham´s parameters were computed in the same way as those computed for the KH mixtures. Some KLH mixtures also exhibit anti-thixotropic behaviour, which revealed tendency to be extensively attenuated with the addition of higher percentages of HMP. In terms of Bingham's parameters, it is shown that the HMP has greater impact on the reduction of

the yield stress than it has on the plastic viscosity (see Figure 4.21). In fact the addition of higher quantities of HMP brings the yield stress to values close to zero, which is an important finding regarding the success of a grouting intervention (Brás and Henriques 2012). This importance resides in the fact that the flow stops if the injection pressure of the mud grout in a crack is not sufficient to keep the shear stress at the head of the injection grout higher than the respective yield stress. Such situation impedes the complete filling of the crack by the grout. This is an identical circumstance to that of the failed Marsh funnel tests, where the flow of the KLH mixtures tested at KULeuven (density between 1931 kg/m^3 and 2019 kg/m^3) an those tested at UMinho (density of about 1931 kg/m^3) according to Equation (4.6) would not occur completely for yield stresses greater than 23-24 Pa and 38 Pa, respectively.

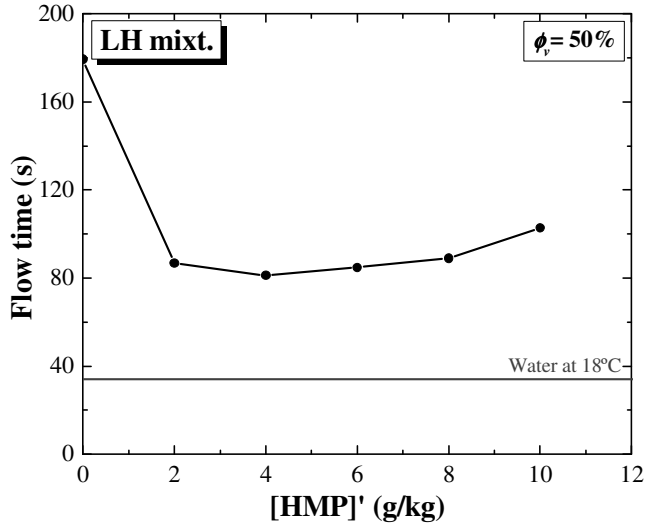

Figure 4.19 – Flow time measurements of the LH mixtures tested at KULeuven.

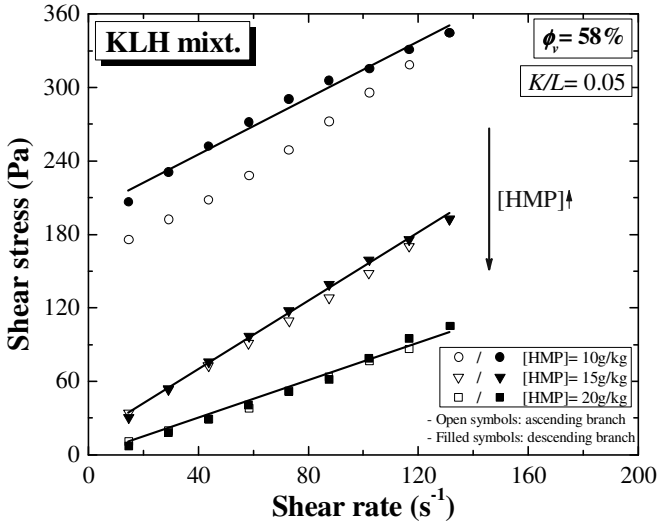

Figure 4.20 – Flow curves of the KLH mixtures with ϕ_v=55% and *K/L*=0.05 (with Bingham's model fitted to the descending branch).

The aforementioned threshold of the KLH mixtures tested at KULeuven is presented in Figure 4.22, where it defines well the limit between flowing and non-flowing mixtures.

It should be noted that the Bingham's parameters of some mixtures could not be obtained because they were so thick that they were out the measuring range of the Viskomat PC rheometer. Moreover, the mixtures with yield stress close to zero are not represented due to the log scale adopted. On the other hand, the plastic viscosity values obtained from the KLH mixtures are substantially higher than those obtained from the KH mixtures, as a result of the substantially higher ϕ_v of the KLH mixtures. The higher ϕ_v of the KLH mixtures also explains the higher flow times measured.

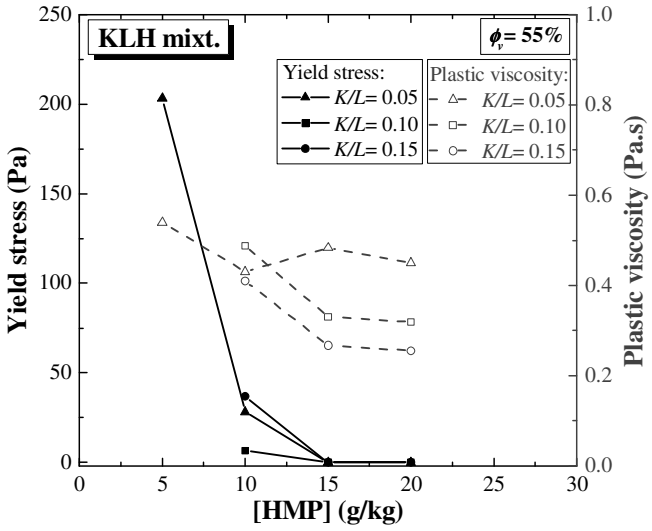

Figure 4.21 – Bingham's parameters of KLH mixtures with ϕ_v=55%.

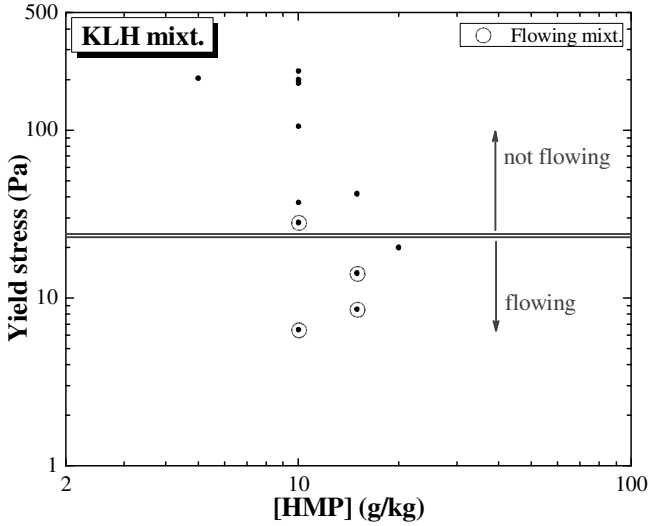

Figure 4.22 – Influence of the shear stress in the flowing capacity of the KLH mixtures through the marsh funnel.

In fact, Figure 4.23 shows that the ϕ_v of the KLH mixtures tested with [HMP]= 20g/kg was approaching to the maximum packing fraction, since the plastic viscosity tends to increase almost exponentially for ϕ_v= 60%. This means that values of ϕ_v greater than or even equal to 60% would produce mixtures that would not present adequate fluidity to be injected in a real injection intervention.

The analysis of the Brigham's parameters of the mixtures with [HMP]= 20g/kg allows verifying that the colloid behaviour of the clay content had little contribution for their flow resistance, since the yield stress of these mixtures was practically zero (except for the mixtures with ϕ_v= 60%). This means that the colloid behaviour of the clay fraction was not limiting the fluidity of the aforementioned KLH mixtures in the Marsh cone tests and that a [HMP]= 20g/kg was sufficient to promote the highest possible fluidity. Therefore, the unexpected behaviour of the KLH mixtures as a function of the *K/L* ratio cannot be explained by the colloid behaviour hypothesis aforementioned. Instead, the plastic viscosity is that contributing mostly for the flow resistance, and it reflects the flow energy dissipation caused by the packing of the solid particles in the mixtures. This means that the PSD of the mixtures with *K/L*= 0.15 results in better packing than that of the mixtures with other *K/L* ratios. However, Figure 4.23 indicates that there is a *K/L* ratio, higher than 0.15, after which the plastic viscosity starts to increase as a function of the increase in *K/L*. This is the case of the KLH mixtures tested at UMinho, where the *K/L* ratio corresponding to the maximum packing seems to be lower than 0.15.

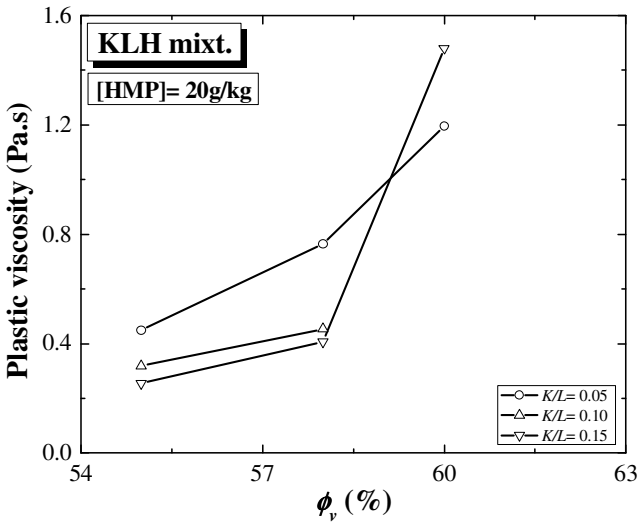

Figure 4.23 – Plastic viscosity of the KLH mixtures with [HMP]= 20g/kg presented as a function of ϕ_v.

The limitations of the Marsh funnel as a rheological apparatus for the complete characterization the flow behaviour are known. However Le Roy and Roussel (2005) proposed the expression of Equation (4.8), which allows computing the flow time (t_V) as function of the geometry of the cone, assuming that the fluid is Newtonian.

$$t_V = \frac{8\mu}{3\rho g r^3 \tan(\alpha)}\left(\left(1+\frac{3h\tan(\alpha)}{r}\right)\left(\tan^2(\alpha)(H_0-H)\left(\frac{H_0-H}{2}+h\right)\right.\right.$$
$$\left.-2\tan(\alpha)(h\tan(\alpha)-r)(H_0-H)+(h\tan(\alpha)-r)^2\ln\left(\frac{H_0+h}{H+h}\right)\right) \qquad (4.8)$$
$$\left.-\frac{r^3}{h\tan(\alpha)-r}\left(\ln\frac{H_0\tan(\alpha)+r}{H\tan(\alpha)+r}-\ln\left(\frac{H_0+h}{H+h}\right)\right)\right)$$

Where, the geometrical parameters of the Marsh cone are given in Figure 4.3 for the case of the cone used in the tests carried out at KULeuven. Since the tested flow times are relative to the complete flow of the material, H is considered to be zero. Later on Roussel and Le Roy (2005) proposed Equation (4.9), where the fluid is assumed to have Bingham's behaviour. The parameter a_V is given by Equation (4.10), where V is the tested volume, while b_V is given by Equation (4.11).

$$t_V = \frac{a_v \mu_p}{\rho - b_v \tau_0} \tag{4.9}$$

$$a_V = \frac{8V\tan(\alpha)(3h(H_0\tan(\alpha)+r)^3 + H_0 r(H_0^2\tan^2(\alpha)+3H_0 r\tan(\alpha)+3r^2))}{(3\pi r^3\tan(\alpha)gr(h+H_0))(H_0\tan(\alpha)+r)^3} \tag{4.10}$$

$$b_V = \frac{\pi r^3(8r\ln(H_0\tan(\alpha)+r) - 8r\ln(r) + 8h\tan(\alpha))}{3\pi r^3\tan(\alpha)gr(h+H_0)} \tag{4.11}$$

The predicted flow times computed from Equation (4.8) and Equation (4.9) were plotted against the measured flow times in Figure 4.24, where can be seen that both equations give reasonable approximation of the flow time.

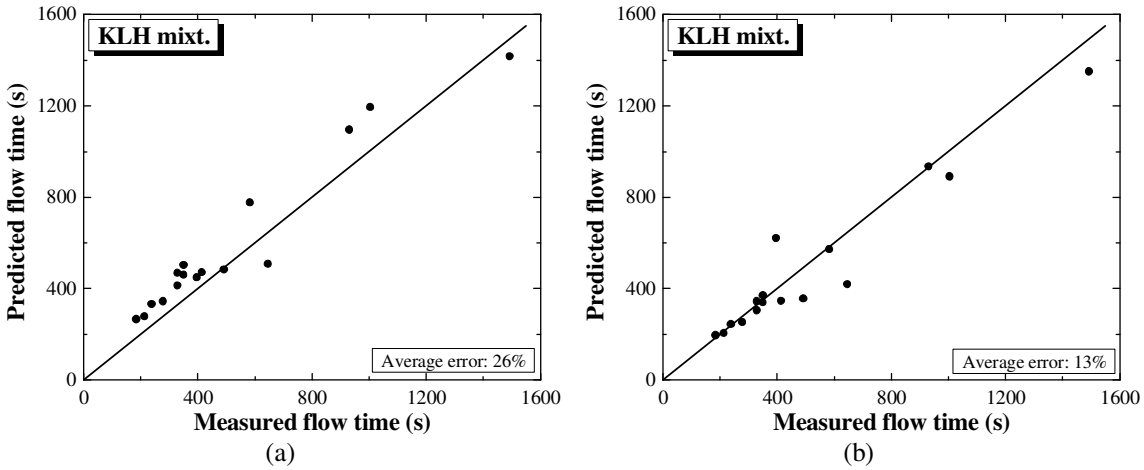

(a) (b)

Figure 4.24 – Comparison between the measured flow time and the predicted flow time using (a) Equation (4.8) and (b) Equation (4.9).

From the application of Equation (4.9) resulted a low average error, which is rather satisfactory since the development of this equation considers the flow constant, which is only valid for the first half of the test (Roussel and Le Roy 2005). Therefore, both equations seem to be adequate for estimation of rheological parameters where no advanced rheological apparatus are available. Being said that, Equation (4.8) was used to estimate the plastic viscosity of the KLH mixtures tested at UMinho. The estimated values are presented in Figure 4.25, where it can be seen that they are within the range

of values obtained for the KLH mixtures tested at KULeuven (0.26-1.5 Pa.s). It should be noted that Equation (4.9) cannot be used to estimate the Bigham's parameters of the KLH mixtures since it requires using two Marsh cones in a procedure similar to that described in Roussel and Le Roy (2005).

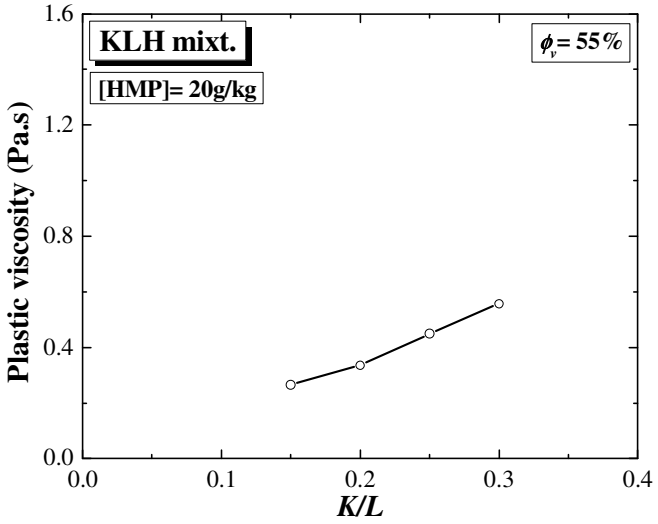

Figure 4.25 – Plastic viscosity of the KLH mixtures tested at UMinho estimated resorting to Equation (4.8).

4.4.2 Time-dependent rheological behaviour

The data collected from the Viskomat PC rheometer for each time period was used to compute the Bingham's parameter. In general, all grouts presented a yield stress of about 0 Pa, while the plastic viscosity is presented in Figure 4.26 as a function of the time.

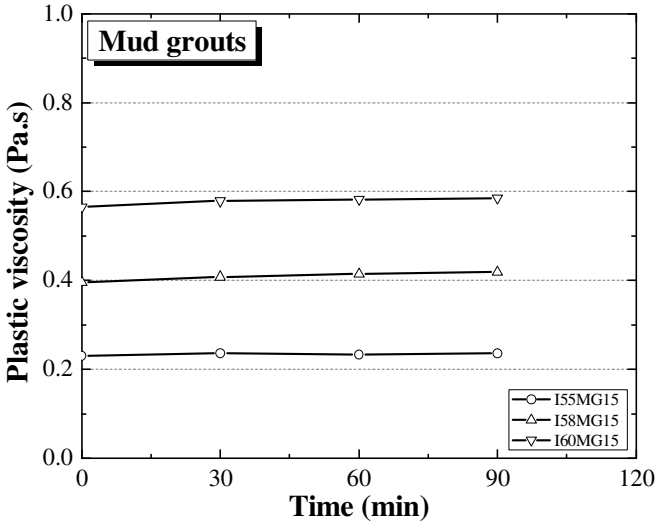

Figure 4.26 – Time-dependent rheological behaviour of the mud grouts tested at KULeuven.

The plotted curves show in general the increase of the plastic viscosity with the time, which is more obvious for the two mud grouts with the highest solid fraction, namely grout I60MG15 and I58MG15. The increase in plastic viscosity after 90 min was less

than 6% for any of the three tested mud grouts, which can be considered insignificant in practical terms. Despite that, some level of gelation of the grouts samples was observed between measurements, which was apparently disturbed by the flow profile applied by the Viskomat PC rheometer, especially in the first 30 s step. This means that the tested mud grouts are able to maintain the initial rheological properties during at least 90 min after mixing, providing that the grouts are sheared before application.

4.4.3 Strength

The average flexural strength values (resulting from three tests) of the KLH mixtures tested at KULeuven with *K/L*= 0.15 are presented as function of ϕ_v in Figure 4.27a. The standard deviation is presented as error bars. There seems to be no relation between the aforementioned parameters with the exception of the mixtures with [HMP] of 20g/kg. On the other hand, the compressive strength seems to be favoured by an increasing ϕ_v (see Figure 4.27b).

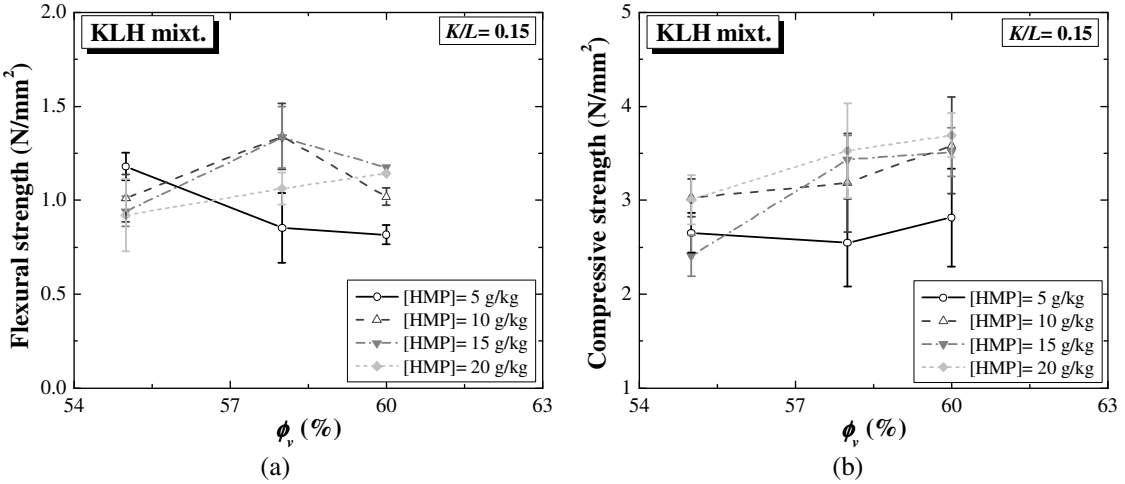

Figure 4.27 – Strength of the KLH mixtures with *K/L*=0.15 tested at KULeuven: (a) flexural strength and (b) compressive strength.

Regarding the effect of clay content on the KLH mixtures tested at KULeuven, the increase in *K/L* promoted a positive development of both strength parameters (Figure 4.28). Furthermore, the mixtures with a low *K/L* ratio developed compressive strengths that are quite satisfactory, since according Houben and Guillaud (2008) a value between 2 N/mm^2 and 2.5 N/mm^2 satisfies the requirements of most standards for earth construction. This gives indication that there is margin to further reduce the clay content (through the decrease in *K/L* ratio) of the mixtures in order to favour the rheological behaviour. However, it should be noted that decreasing the clay content results also in lower water resistance, and thus in lower durability of the material (Minke 2006). Figure 4.27 and Figure 4.28 also show that the addition of HMP also benefits the strength of the KLH mixtures.

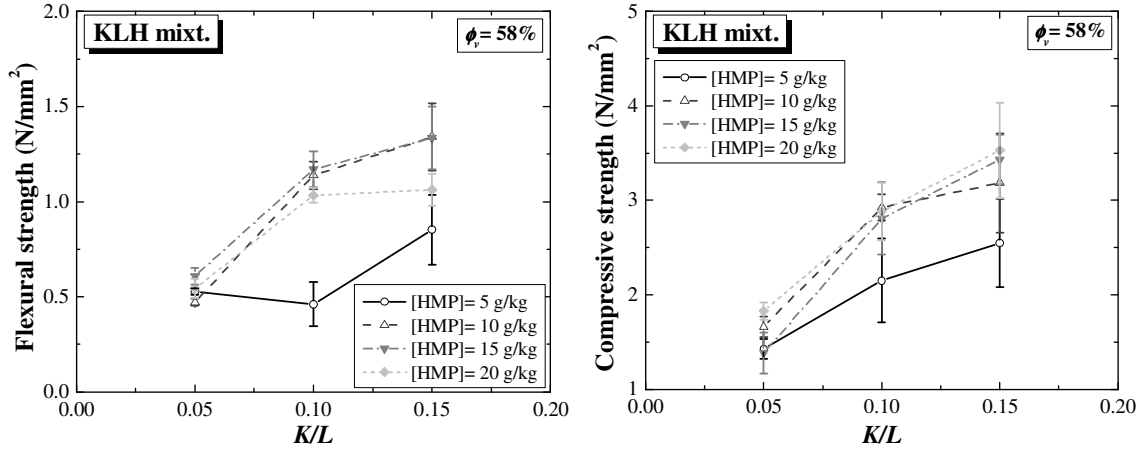

Figure 4.28 – Strength of the KLH mixtures with ϕ_v=58% tested at KULeuven: (a) flexural strength; (b) compressive strength.

The KLH mixtures tested at UMinho confirm the trend of the strength increase with the clay content increase, as is shown in Figure 4.29. However, the strength of the mixtures tested at KULeuven is in general higher than that of the mixtures tested at UMinho, despite the higher *K/L* ratios adopted in this last case. This is explained by the fact that different kaolin powders were used in each experimental program. The higher consistency limits of the kaolin RR40 indicate that this kaolin is expected to promote higher strength that that promoted by the kaolin Mibal-A. This is mainly related to the clay mineralogy of the clay fraction and with its submicron PSD.

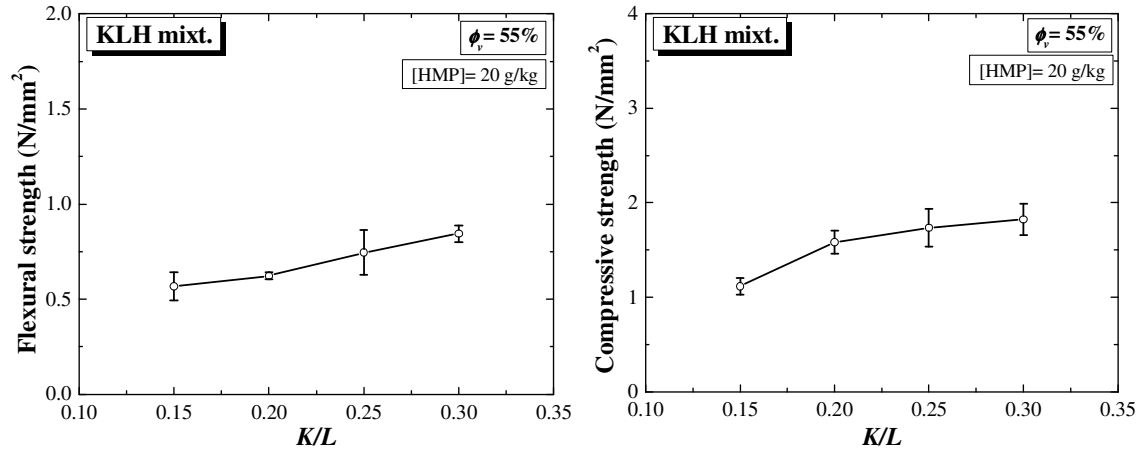

Figure 4.29 – Strength of the KLH mixtures tested at UMinho: (a) flexural strength; (b) compressive strength.

4.4.4 Shrinkage

The average volumetric shrinkage of the KHL mixtures tested at KULeuven with *K/L*=0.15 is presented in Figure 4.30a as a function of ϕ_v. The volumetric shrinkage is lower in the mixtures with higher ϕ_v, as it would be expected (see also Annex A). However, the volumetric shrinkage values seem to be rather high when comparing with cementitious grouts or ternary grouts (Luso 2012), even for the mixtures with higher ϕ_v.

It should be noted however that 60% corresponds to a limit ϕ_v, above which the mixtures present very low fluidity, as discussed previously in Section 4.4.1. This means that increasing ϕ_v above 60% would produce a non-injectable grout even if higher [HMP] is used.

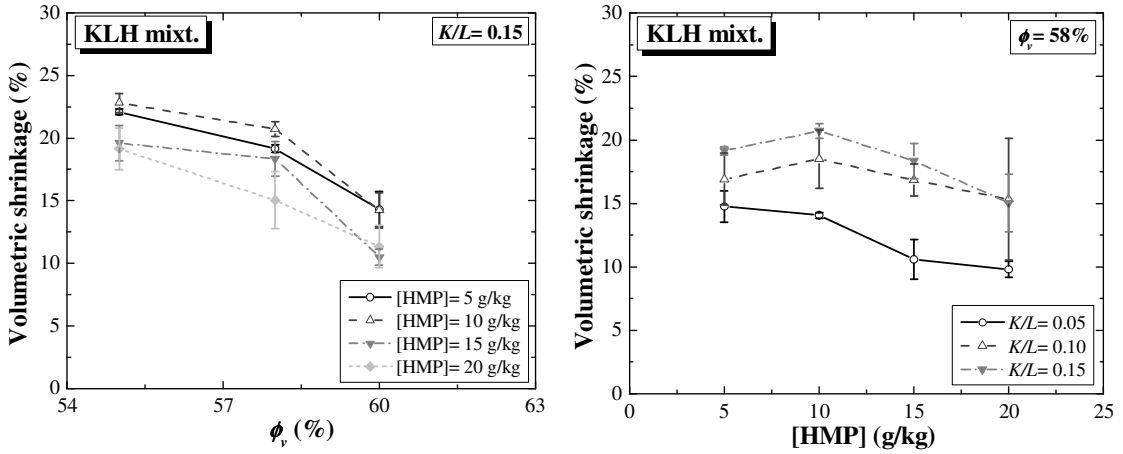

Figure 4.30 – Volumetric shrinkage of the KLH mixtures: (a) as a function of ϕ_v (mixtures with K/L= 0.15); (b) as a function of [HMP] (mixtures with ϕ_v=58%).

Figure 4.30b presents the volumetric shrinkage as a function of [HMP] for the mixtures tested at KULeuven with ϕ_v=58%, where it can be seen that the higher the [HMP], the lower is the volumetric shrinkage. In fact, the lower volumetric shrinkage of the mixtures with higher [HMP] results from the lower dry density of the respective specimens (see Figure 4.31). The effect of the HMP on the colloid interaction between the clay particles is likely to be the probable responsible for this observation.

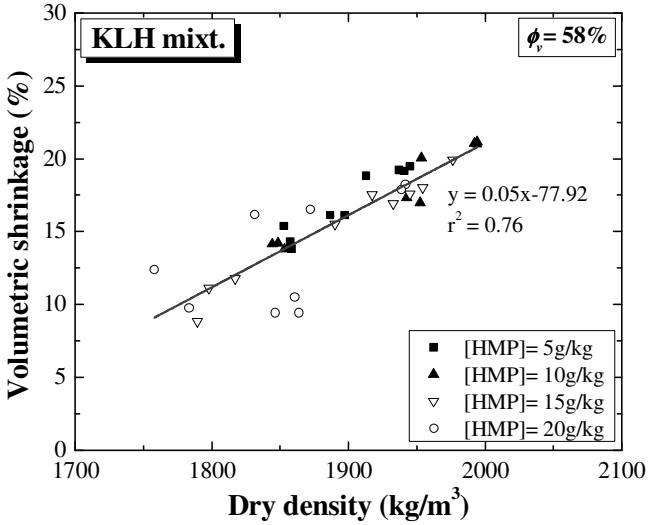

Figure 4.31 – Volumetric shrinkage of the KLH mixtures tested at KULeuven with ϕ_v=58% as a function of the dry density.

Regarding the effect of the K/L ratio on the volumetric shrinkage, Figure 4.30b shows that for the KLH mixtures tested at KULeuven the higher the K/L, the higher is the volumetric shrinkage (see also Annex A). However, this trend is contradicted by

Figure 4.32, where the volumetric shrinkage of the KLH mixtures tested at UMinho are presented. This difference is possibly affected by two possible causes that compete between each other: (i) suction at the capillary pores and (ii) packing of the particles.

In the first case, the inclusion of finer materials (i.e. kaolin powder) promotes thinner voids, which are prone to result in higher suction during the drying of the specimens, promoting higher shrinkage. On the other hand, the shrinkage also depends on the packing promoted by the PSD of the particles constituting each of the mixtures, which depends on the *K/L* ratio. This means that the looser is the packing upon drying, the lower is the resulting shrinkage.

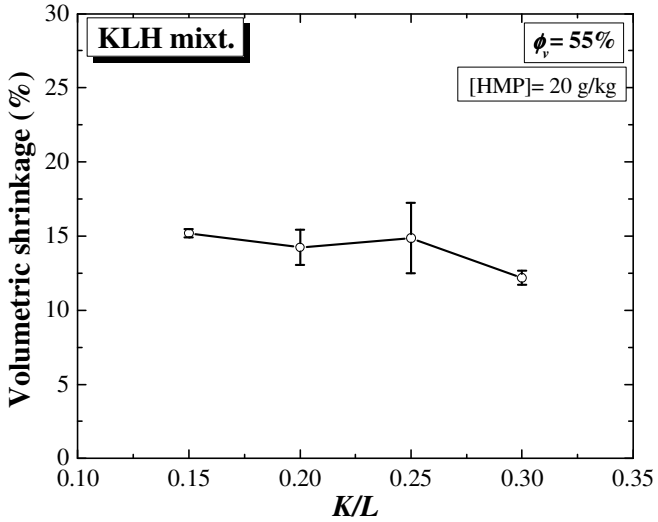

Figure 4.32 – Volumetric shrinkage of the KLH mixtures tested at UMinho.

4.4.5 Adhesion

The properties of the mud grouts used in the adhesion tests carried out at KULeuven are summarised in Table 4.11, while the properties of those used at UMinho are summarised in Table 4.12. It should be noted that the grout I60MG15 is presenting the highest flow time and plastic viscosity. Nevertheless, the injection of this grout, in the gap between the two parts of each beam-specimen, was possible.

Table 4.11 – Rheological and mechanical properties of the grouts used in the adhesion tests carried out at KULeuven (coefficient of variation between brackets).

Mud Grout	Flow time (s)	τ_0 (Pa)	μ_p (Pa.s)	Dry density (kg/m^3)	V. Shrinkage (%)	f_b (N/mm^2)	f_c (N/mm^2)
I55MG15	184	0	0.231	1827 (3%)	19 (9%)	0.92 (21%)	3.01 (12%)
I58MG15	328	0	0.396	1820 (3%)	15 (15%)	1.03 (8%)	3.53 (11%)
I60MG15	525	0	0.565	1843 (2%)	11(15%)	1.14 (und.)	3.63 (6%)

The results of the three-point bending tests carried out at KULeuven and UMinho are presented in Figure 4.33. In general, all grouts had higher flexural strength than that of the beams manufactured with the respective soil, except the case of soils soil A_S2, which resulted in specimens stronger than the mud grouts I55MG15 and I58MG15.

Another curious result is that the beam-specimens tested at KULeuven present higher flexural strength than those tested at UMinho. This is explained by a clay fraction more active in the first case soils, since their consistency limits are in general higher than those of soil A_S4.

Table 4.12 – Rheological and mechanical properties of the mud grouts used in the adhesion tests carried out at UMinho(coefficient of variation between brackets).

Mud Grout	Flow time (s)	Dry density (kg/m^3)	V. Shrinkage (%)	f_b (N/mm^2)	f_c (N/mm^2)
II55MG15	42.6	1798 (1%)	15 (2%)	0.57 (13%)	1.12 (7%)
II55MG20	55.9	1773 (1%)	15 (8%)	0.62 (3%)	1.58 (6%)
II55MG25	72.2	1796 (1%)	14 (16%)	0.74 (16%)	1.74 (9%)
II55MG30	89.5	1785 (1%)	12 (4%)	0.84 (5%)	1.82 (8%)

In the case of the adhesion tests carried out at KULeuven, all grouts failed at re-establishing completely the original strength of the earthen beams. The repair effectiveness (defined by the recovery rate of the initial flexural strength of the specimens) varied between 50% and 93%, which means that that recovery capacity was satisfactory. Moreover, the high volumetric shrinkage observed in the mud grouts seems not to be a limiting issue, but large-scale tests are required to confirm this. In fact, the capacity of the mud grout in maintaining a plastic consistency while it dries is believed to allow it to adapt to volume changes, creating bond bridges of hardened grout between the two sides of the crack (see Figure 4.34).

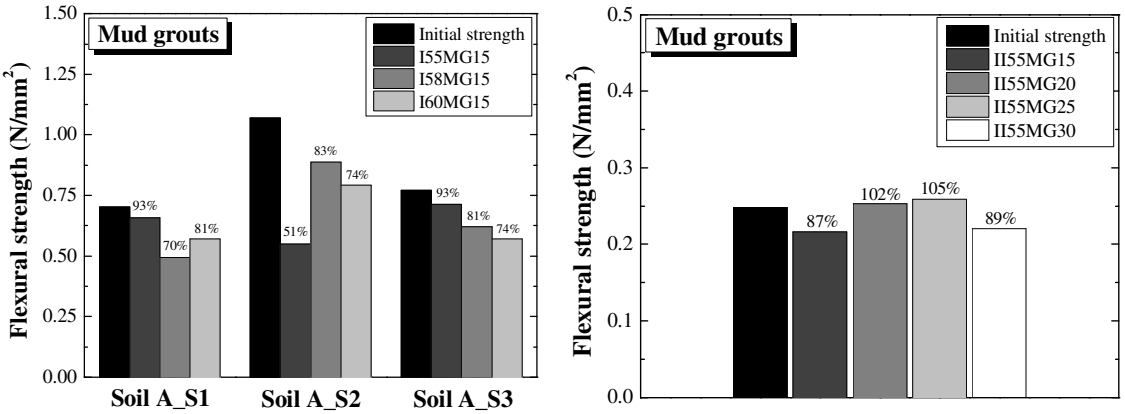

Figure 4.33 – Adhesion capacity of the tested mud grouts and respective repair effectiveness: (a) KULeuven; (b) UMinho.

The plastic behaviour of the mud grout is maintained until de water content drops to the PL of the solid phase, which is about 9% and is the same for all mud grouts tested at KULeuven. Below the PL, any volume change results in internal stresses, which may be responsible by cracking. The drying shrinkage ceases when the SL is attained, which is about 13%, 10% and 7% for the grouts I55MG15, I58MG15 and I60MG15, respectively. The fact the PL and the SL of the mud grouts have similar values may mean that the shrinkage disturbs minimally the adhesion capacity by occurrence of cracking. This means that the tested ϕ_v had apparently low interference on the adhesion

capacity, and thus it indicates that the water content of the mud grouts could be further increased in order to favour their injectability properties. The incipient formation of these bridges was observed during the drying of the grout in the specimens, through the formation of a depression at the top surface of the specimen, as depicted in Figure 4.34.

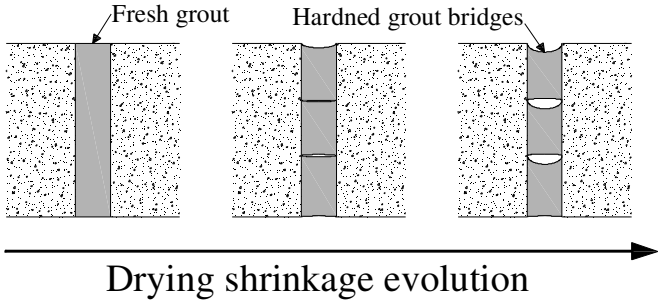

Figure 4.34 – Drying shrinkage evolution of a mud grout used to repair a crack.

In the case of the adhesion tests carried out at UMinho, it should be highlighted that all mud grouts attained a repair effectiveness of almost 100%, where the flexural strengths obtained are relatively low but within the range of what is expectable for historical rammed earth (Jaquin 2008).

Regarding the failure mode of the repaired beams tested at KULeuven, most of them failed within the grout (see Figure 4.35a), however some of the specimens manufactured with soil A_S3, failed at the grout-beam interface (see Figure 4.35b).

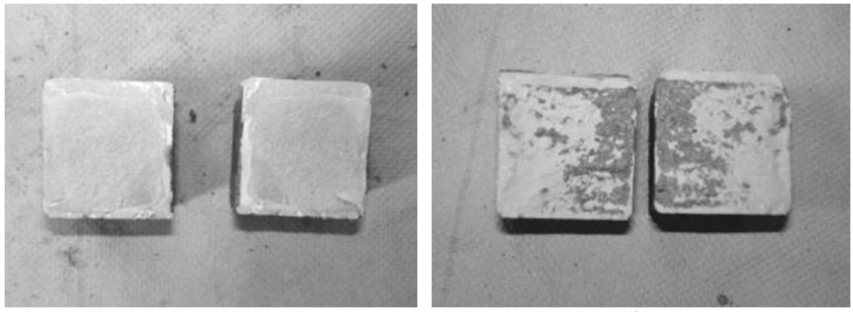

(a) (b)

Figure 4.35 – Failure modes of the adhesion specimens tested at KULeuven: (a) failure by the grout and (b) failure by the interface grout-beam.

The failure of the adhesion specimens tested at UMinho occurred according to all possible failure modes, namely failure by the earthen material, interface and grout, as is illustrated in Figure 4.36.

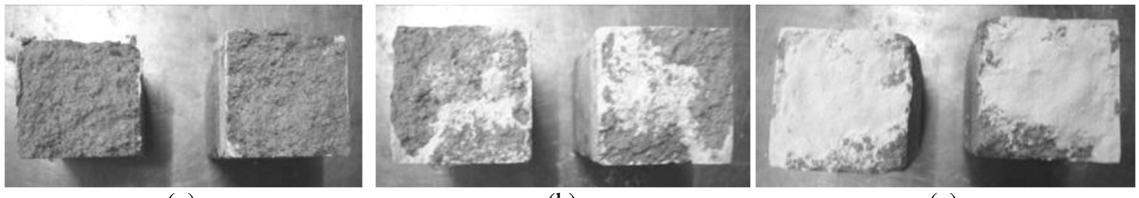

(a) (b) (c)

Figure 4.36 – Failure modes of the adhesion specimens tested at UMinho: (a) by the earthen material; (b) by the interface grout-earthen material and (c) by the grout.

4.4.6 Stability

Qualitatively speaking, none of the KLH mixtures tested at KULeuven presented evidences of bleeding or particle sedimentation during their handling for the other tests. Regarding the bleeding tests carried out on the mud grouts, no bleeding occurred even after 24 hours of testing (see Figure 4.37). This behaviour is probably a consequence of a high content of clay-size particles (<0.002 mm) in the grouts, which have good water retention capacity and are responsible for keeping the larger sand and silt particles in suspension due to Brownian motion. Moreover, it should be noted that gelation was observed in the grouts, which is a typical behaviour of highly concentrated clay suspensions and contributes for the stability in suspension.

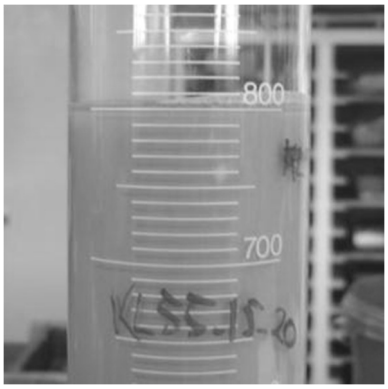

Figure 4.37 – Bleeding test of the grout I55MG15 after 24 hours of mixing.

4.5 Conclusions

The composition study carried out at KULeuven and UMinho allowed clarifying the influence of the composition of an unmodified mud grout on the most important properties governing the application and effectiveness of grout injection interventions in earth constructions.

The results of experimental programs indicated that the clay fraction of an unmodified grout has great influence on its rheological behaviour. Increasing the ϕ_v of aqueous mixtures of clay promotes the flocculation of clay particles, which is responsible for the formation of an internal house-of-cards or scaffold structure. This was observed in the tested K mixtures, where the flow through the Marsh funnel was hindered for ϕ_v higher than ϕ_{vcr} (between 9% and 10% in case of the experimental program at KULeuven and between 16% and 17% in the case of that at UMinho). The addition of HMP to the KH mixtures allowed to further increase ϕ_{vcr} (comprehended between 21% and 24% in case of the experimental program at KULeuven and between 37% and 40% in the case of that at UMinho), which was promoted by the capacity of this compound in increasing the repulsion between clay particles. The flow curves determined for the KH mixtures showed that increasing amounts of HMP decrease the resistance to flow by means of reduction of the Bingham parameters, which is a consequence of the weakening and disruption of the aforementioned internal structure. The addition of limestone powder to

the KL mixtures resulted, as well, in the increase of ϕ_{vcr} (comprehended between 30% and 40% in the case of the experimental program at KULeuven). This is a consequence of the increase in the content of silt-sized particles over those clay-sized, whose colloid interaction of the first in the mixture is considerably less important.

However, designing a mud grout with adequate ϕ_v (to avoid excessive drying shrinkage) demands accounting for the previous two effects as was shown by the results obtained for the KLH mixtures, where it was possible to obtain flowing mixtures up to ϕ_v=60%, in the case of the of the experimental program carried out at KULeuven. The addition of HMP to the KLH mixtures was mainly reflected in the reduction of the yield stress, which for adequate values of [HMP] attained values close to zero. This is a very important feature if a mud grout is to be injected at low pressure. On the other hand, the plastic viscosity of the KLH mixtures revealed to be very high when compared with typical values of cementicious or even ternary grouts (Toumbakari 2002). This was reflected by the high flow times measured for the KLH mixtures, and is directly related to the high values of ϕ_v adopted for the mixtures. It should be noted that the W/S of ternary grouts is typically of about 0.6-1.0 (Luso 2012) while that of the tested KLH mixtures was from 0.25-0.30. In fact, such high ϕ_v are required to minimize the volumetric shrinkage of the mud grouts, which was shown to be high, even for the KLH mixtures with ϕ_v=60% (W/S= 0.25). However, adhesion capacity of the mud grouts tested both at KULeuven and UMinho seemed not to be affected by their high volumetric shrinkage. The grouts were able to recover a substantial percentage of the original strength of the earthen beams of the adhesion tests (higher than 50% in the case of the experimental program at KULeuven and than 87% in the case of that at UMinho). Moreover, the ranges of tested ϕ_v seemed to have no interference on the efficiency of the repair, which may mean that there is margin to reduce ϕ_v for favouring the rheological behaviour, despite of the high shrinkage that may result. It should be noted that the adhesion tests were carried out on small-scale specimens, whereby this property is further investigated in Chapter 6, using specimens of larger scale.

The fresh-state stability of the KLH mixtures tested at KULeuven was also qualitatively evaluated and the bleeding of the of the selected mud grouts was tested. The clay content of the KLH mixtures and mud grouts was found to provide adequate stability against sedimentation and bleeding, respectively.

Regarding the strength of the unmodified mud grouts, it was shown that the higher the clay content, the higher is the flexural and the compressive strengths. Nevertheless, the maximum clay content of a mud grout must be limited, since excessive clay content has negative impact on its rheological behaviour. Therefore, the adequate design of mud should be found with a compromise between the rheological behaviour, adhesion capacity and strength.

In general, the experimental program performed at UMinho confirmed the trends observed in experimental program carried out at KULeuven, namely regarding: (i) the

great contribution of the clay fraction of a mud grout for its flow resistance; (ii) the great improvement capacity of the incorporation of a deflocculated for clays on the rheological behaviour, (iii) the importance of limiting the clay percentage (by addition of a silt-sized material) on the rheological behaviour of a mud grout; (iv) the importance of the clay fraction on the strength of a mud grout; (v) the good effectiveness of the grout injection in repairing small-scale specimens. Therefore, the generalisation of these trends to other similar materials is expected to support the design of a mud grout. Nevertheless, the experimental programs also showed that the properties of the mud grouts also depend greatly on the materials constituting them. This means that the design process may require an optimisation process based on simple tests.

Chapter 5

Assessment of Soils for Unstabilised Rammed Earth Construction

5.1 Introduction

This Chapter deals with the suitability assessment of the soils from Alentejo region (Portugal) for unstabilised rammed earth construction. This assessment emerged from the necessity of selecting a representative soil for manufacturing medium- and large-scale specimens used to test the effectiveness of the injection of unmodified mud grouts. The Alentejo region was picked as case study due to its important rammed earth built stock (see Section 2.2.2). The rammed earth from Alentejo is the Portuguese case that better suits the injection of unmodified mud grouts, since these constructions were built frequently with unstabilised rammed earth. The adobe construction from Aveiro region would be another possible case study. However, this option was discarded because the typical lime stabilisation of these adobes possibly limits the injection technique to the use of modified mud grouts, which were not addressed in the thesis.

This Chapter also intends to contribute to the knowledge on the suitability of the soils from Alentejo for unstabilised rammed earth construction and on the respective mechanical and durability properties. For this purpose, four soils were collected from this region and their suitability for unstabilised rammed earth construction was assessed through testing. The experimental program included the characterization of the soils resorting to both expeditious and laboratory tests, as well as the characterization of the compression behaviour and water resistance capacity of the respective rammed earth.

Finally, a soil was selected being concluded that its use required previous correction of the particles size distribution. Specimens were then prepared and tested accordingly.

5.2 Methodology

The decision on a soil suitability for unstabilised rammed earth construction is based on the assessment of its properties or/and on the performance of rammed earth specimens prepared with such soil. In general, documents on earth construction (Houben and Guillaud 2008, Standards Australia 2002, LNEC 1953, NZS 1998b, Doat *et al.* 1991) outline limit properties of the soil, such as those regarding the texture, consistency, organic content, binding force and compactness, and are determined by means of expeditious and laboratory tests. Thus, if the soil properties fit within limit values, it is assumed that the respective rammed earth will present the required performance.

However, the correlation existing between the soil properties and the performance of the respective rammed is not clear and does not account for the immense diversity existing between soils. This may result in misleading suitability assessments, whose reliability would require testing, in laboratory, the performance of manufactured rammed earth specimens. In this case, the compressive strength and the water erosion resistance of rammed earth are frequently adopted as performance indicators for strength and durability (Ciancio *et al.* 2013). Then, the suitability of the soil is defined by comparing the performance of the specimens with that required by the project or by existing standards or other regulating documents (Standards Australia 2002, NZS 1998b, NMAC 2006).

The suitability for unstabilised rammed earth construction of the four soils from Alentejo (here termed as S1, S2, S3 and S4) was assessed by taking into account the aforementioned methodology. The natural soils S1, S2 and S3 were collected from Serpa, Odemira and S. Luís, respectively. The soil S1 was used in the construction of a rammed earth wall for a commercial exhibition; the soil S2 was going to be used in the construction of a new rammed earth house; and the soil S3 was used to build two houses (in stabilised rammed earth) from a rural tourism place. Soil S4 was a soil with corrected PSD by addition of coarse aggregates, and was being used in the construction of a new rammed earth house in Odemira.

5.3 Soil assessment

The assessment of the four soils for rammed earth construction was carried out by means of both expeditious and laboratory tests. By definition, expeditious tests are of simple execution and only require common tools, making them prone to be carried out on-site. These tests are essentially focused in evaluating the properties of the soil in a qualitative way, while giving indications on its suitability. Despite the qualitative nature of the expeditious tests results, they still assume great importance in documents about earth construction. This is explained by the fact that the expeditious tests are the only

available alternative in many situations, and they are able to provide important parameters featuring the building process. For instance, the drop test is an expeditious test frequently used to determine the compaction water content.

The laboratory tests are more accurate and rigorous than those expeditious. However, their execution requires more resources (tools, equipment, expertise, funding, etc.) that are not always available, and typically include geotechnical characterization. Table 5.1 outlines the expeditious and laboratory tests performed to assess the properties of the soils under study and their suitability for unstabilised rammed earth. It is worth to mention that these tests are frequently used in practice.

Table 5.1 – Expeditious and laboratory tests used to characterize the soils under analysis.

	Test	Property	Reference
Expeditious	Visual inspection	Texture/organic matter	ASTM D 2488 (ASTM 2000a)
	Sedimentation	Texture	HB 195 (Standards Australia 2002)
	Ribbon test	Texture (binding force)	HB 195 (Standards Australia 2002)
	Drop test	Compaction/texture	NZS 4298 (NZS 1998b)
	Dry strength test	Texture	Houben and Guillaud (2008)
Laboratory	Particle size distribution	Texture	LNEC E 196 (LNEC 1966)
	Atterberg limits	Plasticity	NP 143 (LNEC 1969) and ASTM D 4943 (ASTM 1995)
	Standard Proctor	Compaction	LNEC E 197 (LNEC 1967)

5.3.1 Visual inspection

The visual inspection of the soils was carried out with basis on ASTM D 2488 (ASTM 2000a), which allowed evaluating more objectively properties such as colour, angularity, shape and odour of the particles. The results of the visual inspection are summarised in Table 5.2 and Figure 5.1 illustrates some of the fractions composing each soil (fraction-sizes defined according to the standard). The soils S1, S3 and S4 resulted from the weathering of schist, but in this last case river sand and gravel were added (in non-quantified proportions) for thinning the soil clay content. The soil S2 is a transported soil collected from Mira's riverside, which explains its sub-rounded coarse particles. The absence of organic matter in all soils is attested by the absence of colours and odours indicating it.

Table 5.2 – Results from the visual inspection.

Property	S1	S2	S3	S4
Angularity	Mainly angular	Mainly Sub-rounded	Mainly Sub-angular	Mainly Sub-rounded
Shape	Neither flat nor elongated	Neither flat nor elongated	Neither flat nor elongated	Neither flat nor elongated
Colour	Brown	Yellowish brown	Light brown	Reddish brown
Odour	No odour	No odour	No odour	No odour
Texture	Coarse grained	Coarse grained	Coarse grained	Coarse grained

Soil	Gravel (75-4.75 mm)	Coarse sand (4.75-2.00 mm)	Fine sand (0.425-0.075 mm)	Silt + clay (<0.075 mm)
S1	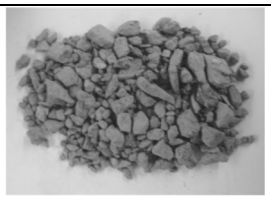	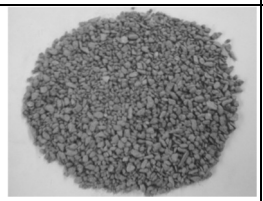		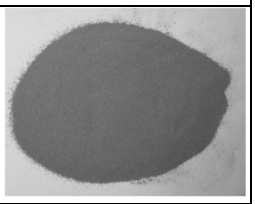
S2	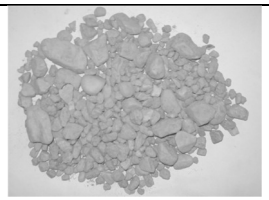	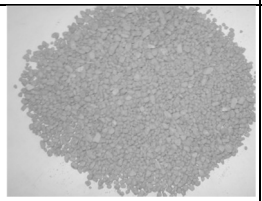	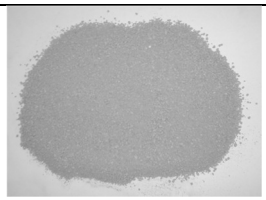	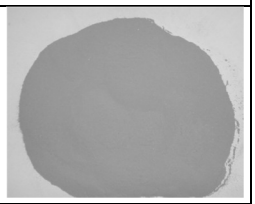
S3	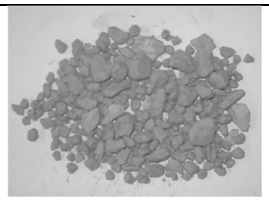	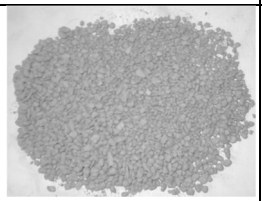	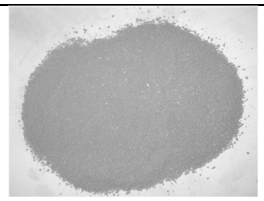	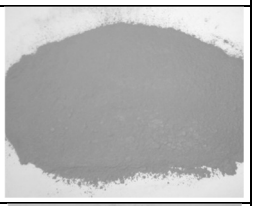
S4	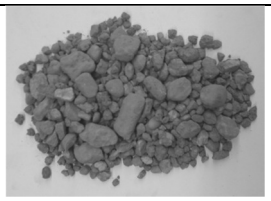	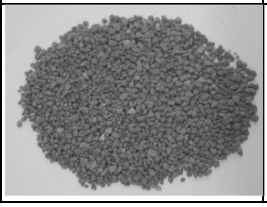	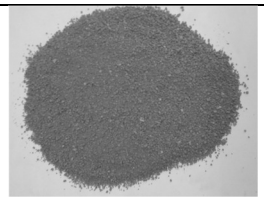	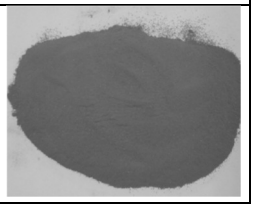

Figure 5.1 - Visual inspection of the assessed soils (fraction sizes defined according ASTM D 2488 (ASTM 2000a)).

5.3.2 Sedimentation test

The sedimentation test allows obtaining qualitatively the proportions between the different size-fractions composing the soils, by visually identifying the respective sedimentation layer, as depicted in Figure 5.2.

Figure 5.2 – Sedimentation test of the soils (S1 to S4 from left to right).

The results of the tests are presented in Figure 5.3 for all soils, where the clay and silt fractions are grouped due to the impossibility of visually differentiating their respective

layers. Soils S2 and S3 are those presenting higher percentages of clay plus silt. According to Houben and Guillaud (2008) the clay plus silt percentage is recommended to be between 21% and 37% (obtained from a PSD envelope), whereby the percentages of soil S2 and S3 are considered to be excessive. Soil S1 complies with this recommendation, while the clay plus silt percentage of soil S4 is slightly below the minimum value. It should be noted that the results of this test are affected by the flocculation of the clay fraction, which occupies a much larger volume than in its unflocculated state and are prone to result in erroneous conclusions.

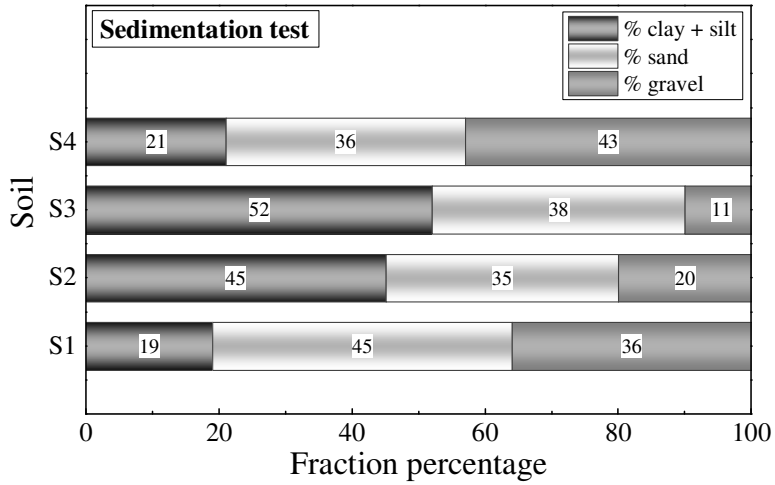

(Gravel: ≥2 mm / sand: ≥0.060 mm and <2 mm / clay + silt: <0.002 mm)

Figure 5.3 – Results from the sedimentation test.

5.3.3 Ribbon test

The ribbon test also allows assessing qualitatively the proportions between the different size-fractions composing the soil. Figure 5.4 illustrates the sequential execution of this test, whose results were interpreted according to Table 2.2. The ribbon length of each soil is given in Table 5.3, where all soils seem to be adequate for rammed earth construction. Moreover, soils S1 and S3 seem to be those presenting higher clay content due to their higher ribbon length.

Figure 5.4 – Sequential execution of the ribbon test.

Table 5.3 – Results of the ribbon tests and respective interpretation.

Soil	Ribbon length (mm)	Interpretation
S1	55	Suitable for rammed earth
S2	41	Suitable for rammed earth
S3	65	Suitable for rammed earth and adobe
S4	37	Probably suitable for rammed earth

5.3.4 Drop test

This test is usually carried out on-site to determine the compaction water content of the earth mixture. Therefore, this requires several trials while adjusting the water content of the mixture to obtain the correct state of the ball after impact on the ground. Figure 5.5 presents the three possible states occurring within the tests. After obtaining a successful trial (i.e. the ball crumbled partly with minor cracks - Figure 5.5b), the water content of the ball was measured for each soil and the results are given in Table 5.4, in terms of drop test water content (DTWC). Later on, these results will be compared with those of the Proctor test.

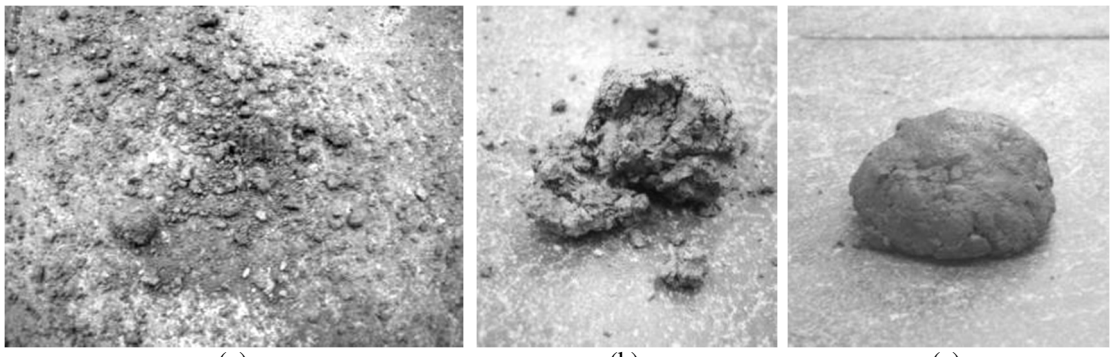

(a) (b) (c)

Figure 5.5 – Possible states of the ball after impact on the ground: (a) completely crumbled, (b) partially crumbled with minor cracks; (c) flattened.

Table 5.4 – Compaction water content obtained from the drop test.

Soil	DTWC (%)
S1	11.7
S2	9.5
S3	17.0
S4	7.5

5.3.5 Dry strength test

The dry strength test was carried out on dry soil pats (fraction below 0.425 mm) with 4 cm diameter and 1 cm thickness (Figure 5.6). The test was carried out by breaking the specimens and crushing them between the thumb and forefinger, and the results were interpreted according to Houben and Guillaud (2008), see Table 2.3. The soils S2 and S3 have moderate dry strength, while the soils S1 and S4 have high dry strength. This means that these two last soils would probably result in rammed earth of higher strength.

Figure 5.6 – Execution of the dry strength test.

5.3.6 PSD analysis

Sieving and sedimentation analyses were carried out in order to quantify all size-fractions composing the soils, which are presented in Table 5.5. The particles size distribution (PSD) curves were plotted in Figure 5.7 and compared against recommended envelopes for rammed earth construction, namely given by Houben and Guillaud (2008), MOPT (1992) and by the Portuguese National Laboratory of Civil Engineering (LNEC 1953).

Table 5.5 – Particles size fractions of the assessed soils (according to the size fractions usually adopted in earth construction).

Soil	Clay (%)	Silt (%)	Sand (%)	Gravel (%)	Pebbles (%)
S1	8	15	24	51	2
S2	10	13	29	41	7
S3	14	23	33	28	2
S4	8	11	33	42	6

(clay < 0.002 mm / 0.002 mm ≤ silt < 0.060 mm / 0.060 mm ≤ sand < 2.0 mm / 2.0 mm ≤ gravel < 20 mm / pebbles≥ 20 mm)

The soils S1, S2 and S4 have very similar PSD curves and follow the lower limit of the envelopes, within or slightly below it. The case of the LNEC (1953) envelope is an exception, where these soils seem to be substantially below the recommended minimum for fines content (clay + silt). This is explained by the fact that this envelope results from the survey of several case studies, which also includes adobe constructions. The manufacture of this type of materials admits higher clay content than that admitted by rammed earth construction.

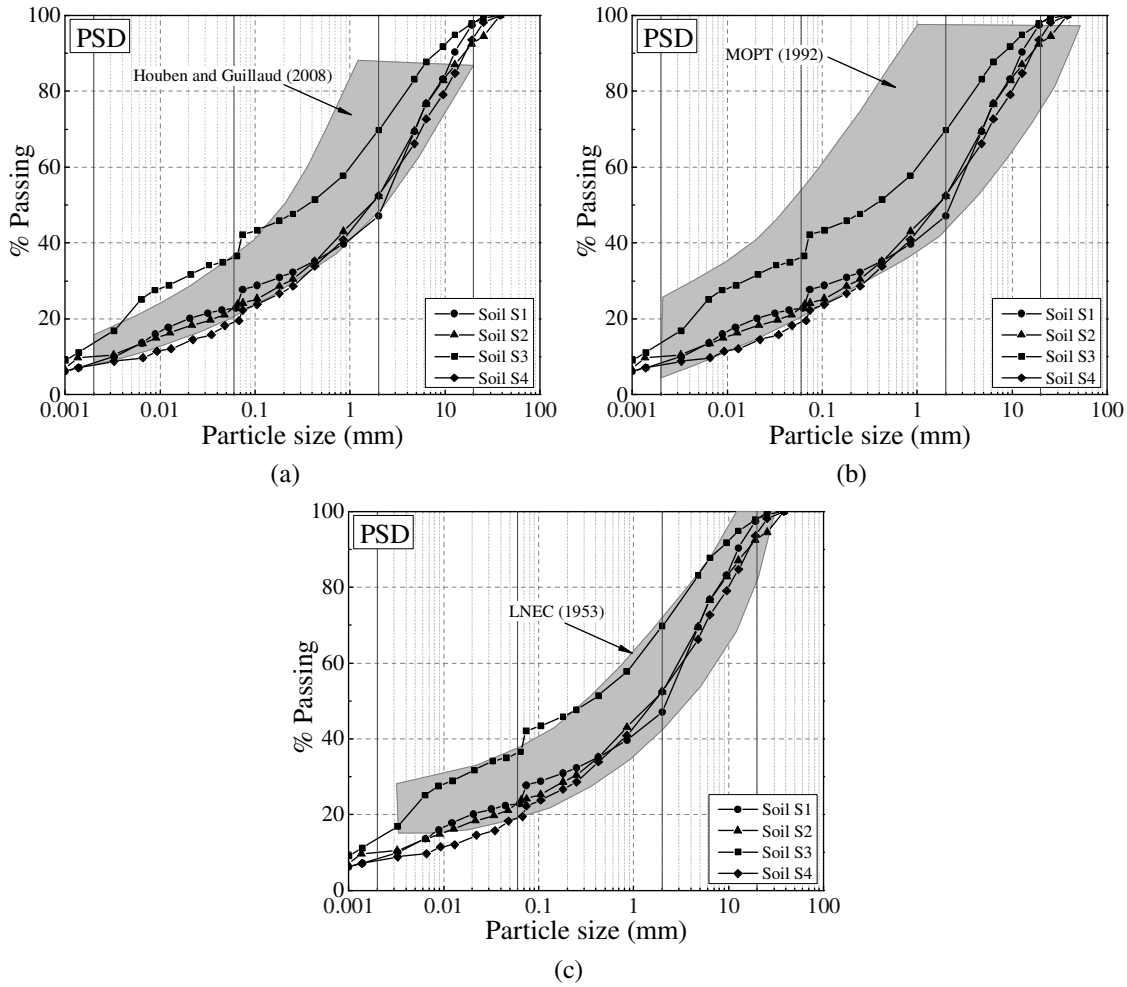

Figure 5.7 – Comparison between the PSD curves of the soils and the envelopes for rammed earth construction recommended by: (a) Houben and Guillaud (2008); (b) MOPT (1992) and; Portuguese National Laboratory of Civil Engineering (LNEC 1953).

On the other hand, the PSD curve of soil S3 is within or slightly above the envelopes. The soils S2 and S3 are those presenting higher percentages of clay content, which goes against the results obtained for the dry strength, but agrees with the results from the sedimentation tests, from a comparative perspective. Given the higher clay fraction percentage of soils S2 and S3, it would be expectable that they would obtain higher dry strength than the other soils. However, this unexpected result can be explained by the type of clay minerals composing the clay fraction of each soil and by its respective submicron PSD, which is not possible to characterize from this test.

By comparison with the results from the sedimentation test, it is shown that this expeditious test fails in giving the exact proportion between the size fractions composing each soil. However, it constitutes a simple and fast method to compare qualitatively the fine fraction percentage among the soils.

5.3.7 Atterberg limits

The liquid limit (LL), plastic limit (PL) and shrinkage limit (SL) were determined for each soil and the results are presented in Table 5.6, as well as the respective unified soil

classification system (USCS) (ASTM 2000b). Despite the reference to the Atterberg limits being frequent in earth construction, only few suggest recommended values for unstabilised rammed earth. In fact, the use of these parameters regards more commonly the selection of a stabilisation technique (chemical), but they also provide information on the mineralogical properties of the fine fraction, which can have consequences on the performance of the rammed earth. Houben and Guillaud (2008) suggest an envelope of recommended values for PI (plasticity index) and LL given in Figure 5.8, where these parameters are plotted for each soil. Soil S1, S2 and S3 fit within the envelope, while soil S4 is outside, because of its low PI and LL. In practical terms, this means that rammed earth prepared with soil S4 may have durability or/and strength problems, whose uncertainty can only be clarified by testing the performance of rammed earth specimens. The low values obtained for the shrinkage index (SI) of the soils indicates that these have low shrinkage/swelling characteristics, which constitutes a good feature when addressing rammed earth construction.

Table 5.6 – Atterberg's limits of the soils and respective USCS classification.

Soil	LL (%)	PL (%)	PI (%)	SL (%)	SI (%)	USCS classification
S1	30	17	13	20	10	Clayey sand with gravel (SC)
S2	27	16	11	18	9	Clayey sand with gravel (SC)
S3	32	18	14	24	8	Clayey sand with gravel (SC)
S4	21	15	6	15	6	Silty, clayey sand with gravel (SC-SM)

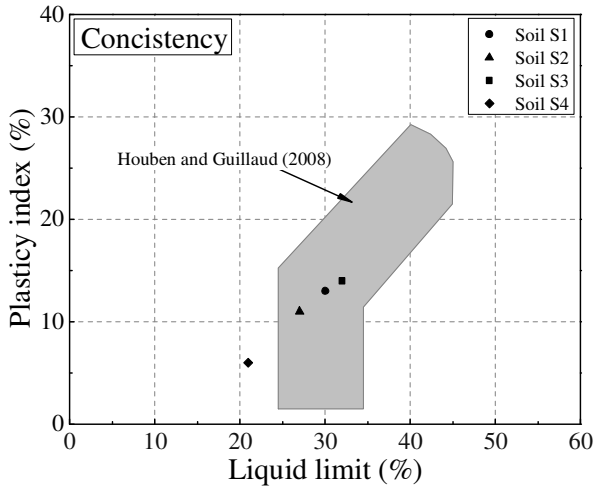

Figure 5.8 – Comparison of the consistency parameters of the soils against the envelope of recommended values by Houben and Guillaud (2008) for unstabilised rammed earth.

5.3.8 Standard Proctor

The compaction properties of the soil are very important in rammed earth construction, because there is a direct relation between dry density and compressive strength of the material; the more compact the material is, the higher is its strength. The standard Proctor test is in general preferred to the modified Proctor (Houben and Guillaud 2008 and NZS 1998b), since the compaction energy of traditional rammed earth is expected

to be closer to that of the first test. The results of the test are summarised in Table 5.7 in terms of maximum dry density (ρ_{dmax}), optimum water contents (OWC), density of the particles (G_s) and DTWC. The compaction curves of the soils are presented together in Figure 5.9, and are individually presented in Annex B. Soils S1, S2 and S4 are those presenting higher maximum dry densities, with similar values among them. On the other hand, the soil S3 presents a substantially lower value for this parameter. According to Doat *et al.* (1991), the soils S1, S2 and S3 are expected to result in earthen materials with very satisfactory performance ($1.76\ g/cm^3 < \rho_{dmax} < 2.10\ g/cm^3$), while soil S4 is expected to result in a material with excellent performance ($2.10\ g/cm^3 < \rho_{dmax} < 2.20\ g/cm^3$).

The lowest OWC of soil S4 means that it is less prone to suffer from shrinkage problems. Another important observation is with respect to the drop test water content (DTWC), which is very similar to the OWC of each soil, and whose difference varies between 0.3% and 1.2%. Therefore, the drop test seems to be an adequate method to obtain compaction water content similar to OWC, at least for these four soils.

Table 5.7 – Compaction properties of the soils.

Soil	ρ_{dmax} (g/cm^3)	OWC (%)	G_s	DTWC (%)
S1	2.06	10.6	2.69	11.7
S2	2.07	9.8	2.73	9.5
S3	1.84	16.4	2.75	17.0
S4	2.12	8.7	2.63	7.5

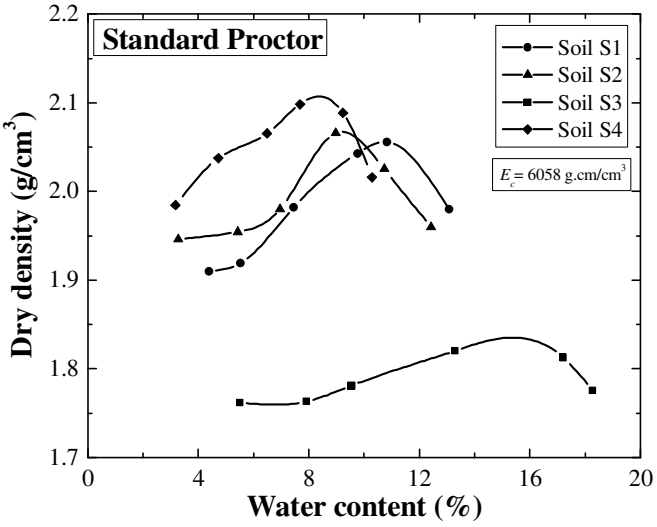

Figure 5.9 – Compaction curves of the soils.

5.4 Rammed earth performance assessment

As referred in Section 5.2, the suitability of a soil for unstabilised rammed earth can only be reliably decided by assessing the performance of the earthen material manufactured with it, which must satisfy project or standard requirements. Both

mechanical and durability requirements are addressed for this purpose, where the compressive strength and water erosion resistance assume the main indicators. Thus, the suitability of the four soils being studied was assessed by means of compression and Geelong tests. With respect to the compression tests, it was also aimed at assessing the influence of the compaction features on the compression behaviour of the rammed earth manufactured with the soils.

5.4.1 Compression behaviour

According to NZS 4298 (NZS 1998b), the moisture content to compact rammed earth should never be 3% below or 5% above the optimum water content. Furthermore, there are rammed earth practitioners defending that the compaction should be carried out on the dry side to facilitate the demoulding, while others defend the wet side to promote higher strength (Minke 2006). In order to investigate the influence of the water content (and consequently of the material density) on the strength of rammed earth, a set of six specimens per soil were prepared and tested under compression (Figure 5.10). Each of the six specimens represented a point of the respective compaction curve resulting from the standard Proctor test. The specimens consisted of three-layered cylinders with dimensions of 100 mm diameter and 200 mm height, compacted in a metallic mould by means of an electrical hammer, and demoulded immediately after compaction.

(a) (b) (c)

Figure 5.10 – Preparation of the rammed earth cylindrical specimens: (a) compaction with electrical hammer; (b) scraping of the surface of the first layer for improving the adhesion with the second layer; (c) disaggregation of one of the specimens prepared with lower water content.

The specimen named as CURES1_1 serves as an example to explain the nomenclature used, where S1 corresponds to soil S1 and 1 to the first point of the standard Proctor test, which is the one with the lowest water content (in opposition 6 is the one with the highest water content). The soils were previously dried and then the amount of water required to perform the desired water content was added and mixed with the soil. Each mixture was stored in a plastic bag, during at least 12 hours, to promote the

homogeneisation of the water content. A sample of each mixture was taken immediately before compaction in order to check the real water content.

The tests were carried out after the specimens achieving their equilibrium water content at 20ºC temperature and 57.5% relative humidity (drying period between 27 and 35 days). The vertical deformations at the middle third of each specimen were measured by means of three LVDTs radially-disposed (see Figure 5.11). The tests were carried out under displacement control at a rate of 0.003 mm/s, applied monotonically. In the day before testing, the specimens had their top and bottom rectified by means of a gypsum capping.

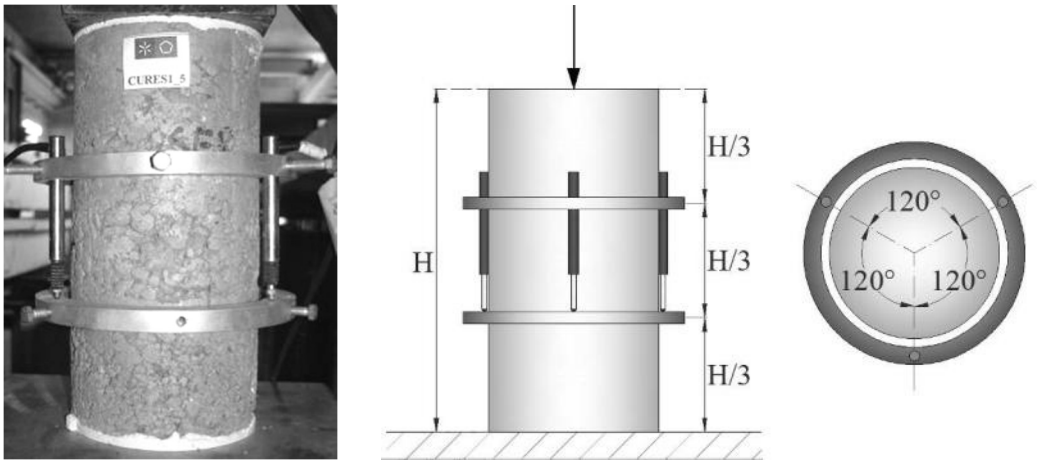

(a) (b)

Figure 5.11 – Compression test: (a) test setup; (b) LVDTs configuration.

Some of the specimens with a low water content (first points of the compaction curve) presented low cohesion and started disaggregating after demolding, whereby they were not tested (Figure 5.10c). The specimen with the highest water content of soil S4 (namely CURES4_6) was lost, since it was unable to auto-sustain after demoulding, due to an excessively high water content (see Annex B).

The stress-strain curves of the specimens are presented in Figure 5.12 for all soils, where it can be seen that the different compaction conditions resulted in substantial differences in terms of compressive strength and deformability. The difference between the minimum and maximum values of the compressive strength obtained among the specimens of each soil varied between 19% and 59%. This confirms the great influence of the compaction features on the strength of the rammed earth. Figure 5.13 highlights this influence, where the higher the dry density the higher is the compressive strength. This relation becomes more evident when each soil is analysed individually, since the strength of the rammed earth also depends on the properties (mineralogy, PSD, etc) of the respective clay fraction.

Regarding the maximum compressive strength, the soil S4 presents the highest value, which seems to result from its higher maximum dry density. In opposition, the soil S3 presents the lowest maximum compressive strength. Although this soil presents the

highest clay content, its maximum dry density is substantially lower than that of the other soils, thus justifying its lower mechanical performance.

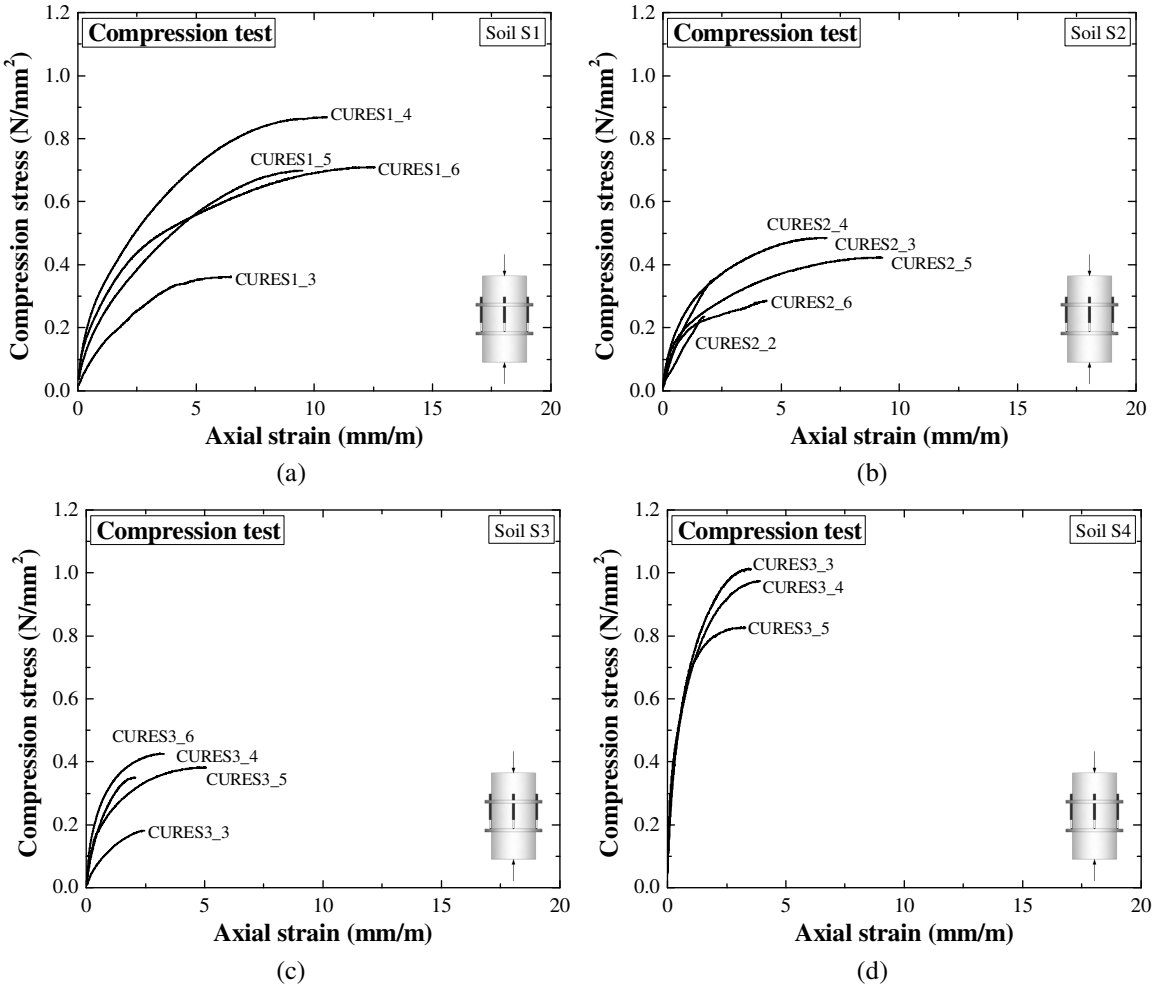

Figure 5.12 – Stress-strain curves of the rammed earth cylindrical specimens: (a) soil S1; (b) soil S2; (c) soil S3; (d) soil S4.

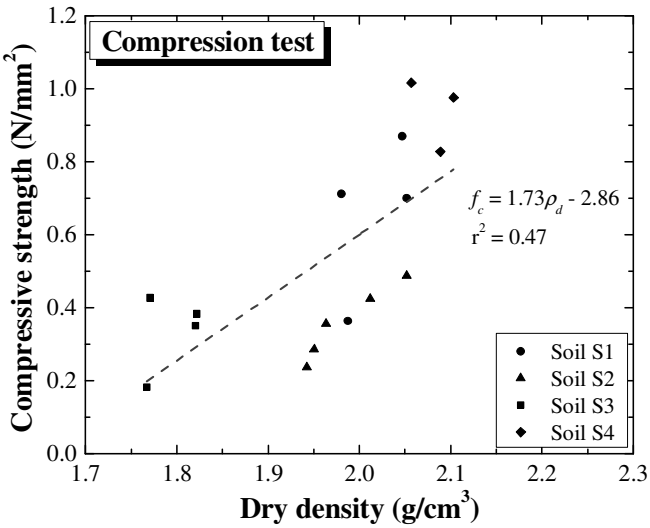

Figure 5.13 – Relation between dry density and compressive strength.

In addition to the influence of the compaction water content and dry density (ρ_d) on the compressive strength (f_c), Figure 5.14 also depicts the influence of these parameters on the Young's modulus (E_0), which was computed between 5% and 30% of f_c by linear fitting.

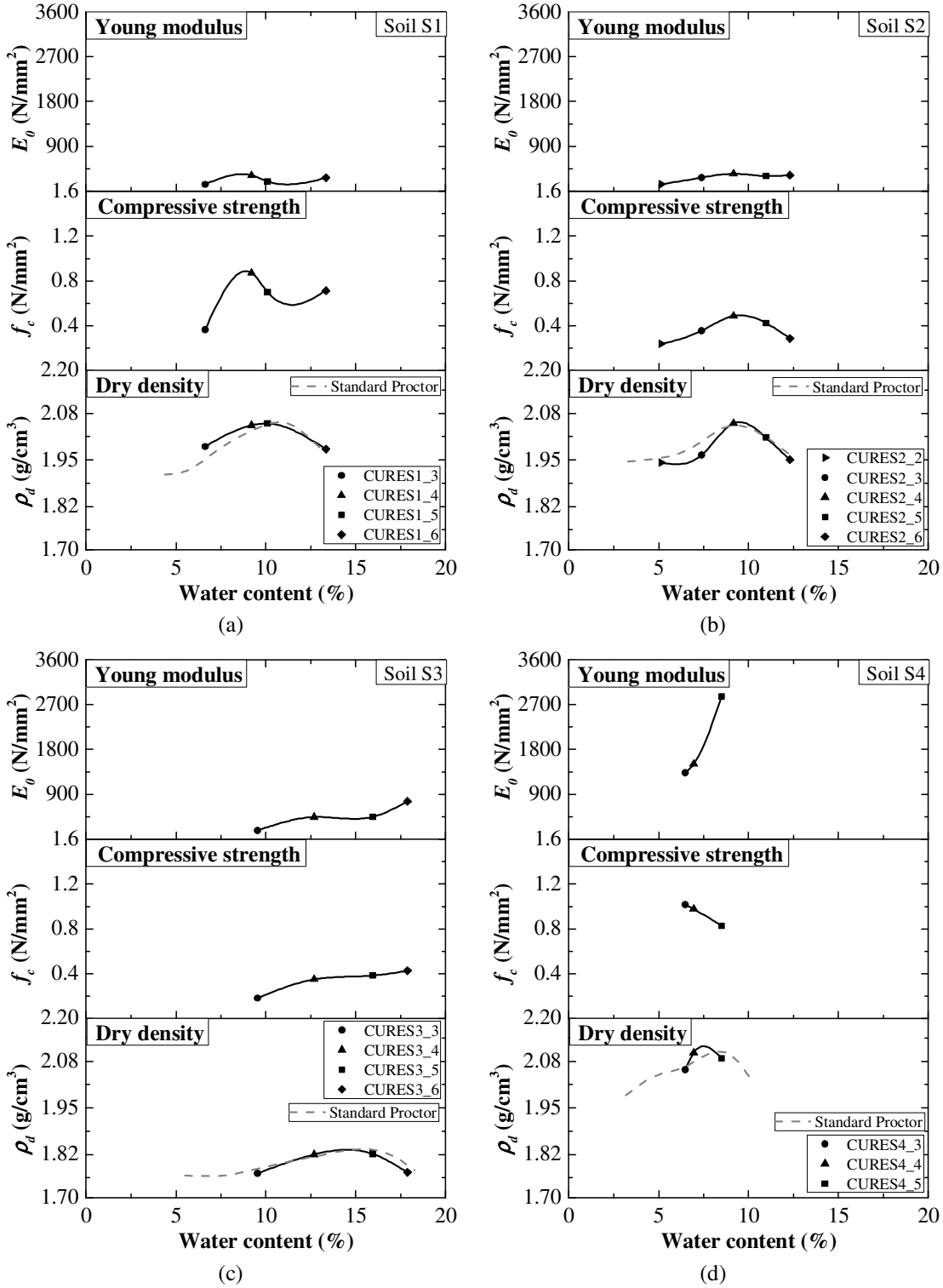

Figure 5.14 – Relation between dry density, compressive strength and Young modulus: (a) soil S1; (b) soil S2; (c) soil S3; (d) soil S4.

For soils S1 and S2, the compressive strength curves seem to follow the tendency of the dry density curves, where the higher the dry density the higher is the strength. Soil S4 also seems to follow this tendency, but it should be noted that each point in the graphic is based on a single test result. On the other hand, this relation is not so evident for soil S3. The specimens from soil S3 with higher water content (CURES3_5 and CURES3_6) are those presenting higher strength, which seems indicating that the wet side of the compaction curve promotes higher strength in this soil. The Young's modulus curves of the soils seem to approximately follow the compressive strength curves tendency. Therefore and generically speaking, the compaction conditions influence the strength and deformability of rammed earth, but this influence seems to be also dependent on the type of soil.

Regarding the suitability of the soils in terms of mechanical performance, it should be noted that none of them deem with the minimum requirements of documents regulating rammed earth construction, as depicted in Table 5.8. The least demanding case corresponds to SNZ 4298 (SNZ 1998b).The required compressive strength for standard grade rammed earth constructions, if corrected by the height-to-thickness factor (2:1) of the tested specimens, is of about 1.14 N/mm^2. This minimum value is not exceeded by any of the tested specimens. Therefore, these soils might be considered unsuitable for unstabilised rammed earth according to the requirements of the documents referred to in Table 5.8. Eventually, chemical stabilisation can be used to improve the performance towards adequate levels.

Table 5.8 – Minimum compressive strength for rammed earth according to standards/recommendations for earth construction.

Standard/recommendation	Country	Compressive strength (N/mm^2)
Standards Australia (2002)	Australia	≥2[a]
CYTED (1995)	-	≥1.2 in 80% of the specimens[b]
NMAC (2006)	USA	>2.1[c]
SNZ (1998b)	New Zealand	>1.3[d]

Notes:

[a] dry unconfined characteristic compressive strength obtained from earth blocks or cylindrical earth specimens. Aspect ratio correction factor must be applied.

[b] Characteristic compressive strength.

[c] on cured rammed earth specimens. No info is provided on the specimens preparation.

[d] lowest of 5 specimens with 1:1 height/thickness ratio.

Bui *et al.* (2009) highlight that a traditional rammed earth wall (about 50 cm thick) is loaded by stresses between 0.1 N/mm^2 and 0.3 N/mm^2. Therefore, a wall built with soils S1 to S4 (considering the average compressive strength of the specimens of each soil) would present, respectively, a safety factor of about 2.2, 1.2, 1.1 and 3.1 for a stress level of 0.3 N/mm^2. In practical terms, this means that a rammed earth dwelling built with any of the soils tested would not collapse under normal conditions (e.g. in the absence of moisture problems and important seismic events).

The failure of the specimens occurred according to two modes: (i) material crushing and consequent disaggregation of the specimen (Figure 5.15a); (ii) main vertical/diagonal

crack formation with spalling of the specimen surface (Figure 5.15b). The first mode occurred mostly in the specimens with lower compaction water content, while the second occurred mostly in those with higher compaction water content.

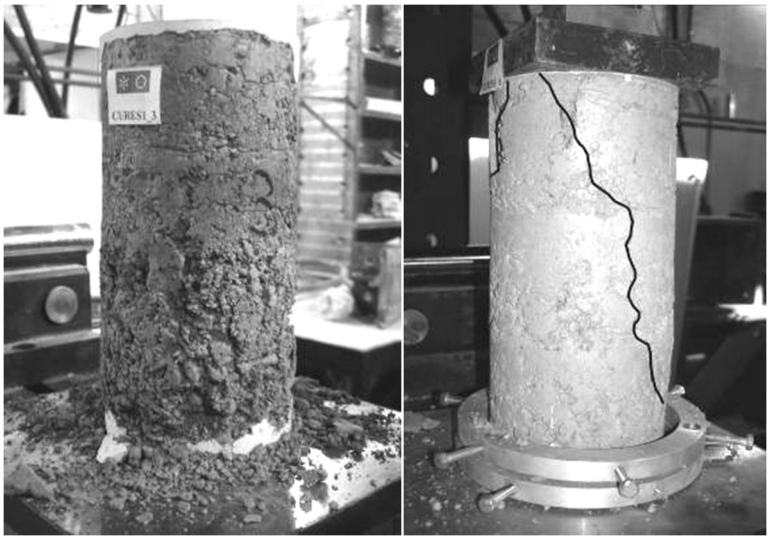

(a) (b)

Figure 5.15 – Failure mode of the rammed earth cylindrical specimens: (a) material crushing and consequent disaggregation of the specimen; (b) main vertical/diagonal crack formation with spalling of the specimen surface.

5.4.2 Durability (Geelong test)

The Geelong test (also known as drip test) was used to assess the durability performance of unstabilised rammed earth manufactured with each of the four soils. The test was carried out on cubic specimens (one per soil), with dimensions 150x150x150 mm^3, compacted in three layers with the maximum dry density and OWC obtained from the Proctor test (Figure 5.16), following the procedure of NZS 4298 (NZS 1998b). The specimens dried in a room with controlled temperature (20ºC) and relative humidity (57.5%) and were tested with 21 days of age. The pitting depth and depth of moisture penetration were measured in each test, see Figure 5.17.

(a) (b) (c)

Figure 5.16 – Preparation of the specimens for the Geelong test: (a) compaction with manual rammer; (b) trimming of the last layer; (c) specimens after drying.

The results of the Geelong test are presented in Table 5.9, where the pitting depth is classified as an erodibility index according to NZS 4298 (NZS 1998b). The moisture penetration depth of all soils is less than 120 mm, as it is required by the standard. All soils have similar results in terms of pitting depth, but soil S4 is that presenting the

lowest value, while soil S3 presents the highest. The use of these soils in unplastered unstabilised rammed earth walls is limited to situations/locals that require erodibility indexes equal or higher than 3. In the case where plasters are used as protection, the erodibility indexes of unstabilised rammed earth preformed with these soils can be improved to 2. It should be referred that the erodibility index requirements are defined specifically for New Zealand in NZS 4297 (NZS 1998a) and depend on regional parameters that are not defined for other regions in the World. Therefore, this standard cannot be applied directly to a rammed earth construction in Alentejo. On the other hand, Standards Australia (2002) has a more practical approach by referring that, in Australia, rammed earth with erodibility index 3 can be used in protected walls. This is the case of traditional rammed earth constructions built in Alentejo, where they are typically protected by lime/earth mortar plasters, which are frequently revitalized in maintenance interventions by limewash painting (Gil *et al*. 2011).

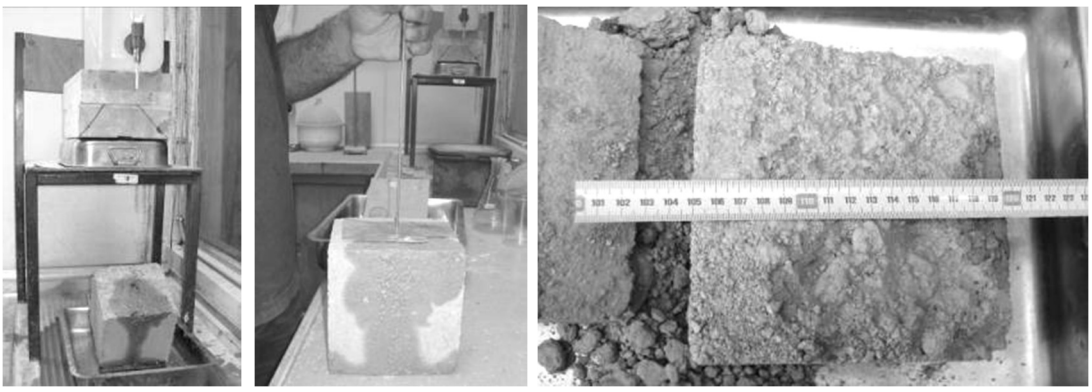

(a) (b) (c)

Figure 5.17 – Geelong test: (a) test setup; (b) pitting depth measurement; (c) depth of moisture penetration measurement.

Table 5.9 – Results of the Geelong test.

Soil	Pitting depth (mm)	Erodibility index	Depth of moisture penetration (mm)
S1	6	3	15
S2	6	3	28
S3	8	3	30
S4	5	3	16

5.5 Characterization of the selected soil

The original soil used in the mixture that resulted into soil S4 was selected to build the rammed earth specimens tested in Chapter 6. Given the mechanical similarity among the four soils, the availability and the transport provided without costs were the main reasons behind the selection. The soil was collected from Amoreiras-Gare in Odemira, Alentejo and was characterized by means of expeditious and laboratory tests, as presented before. These tests were carried out according to the procedures given in Section 5.3, and served to assess the suitability of the soil for rammed earth construction without the aforementioned PSD correction of soil S4. Henceforth, this soil is designated as soil S5.

5.5.1 Sedimentation test

The sedimentation test revealed that the soil S5 presents high clay content, which affected the results. The layers of the fractions that compose the soil are not well defined (Figure 5.18), since the clay in the soil sample was rather mixed with the other fractions, hindering their visual identification and quantification. Therefore, the percentages of the size-fractions composing the sample could not be determined.

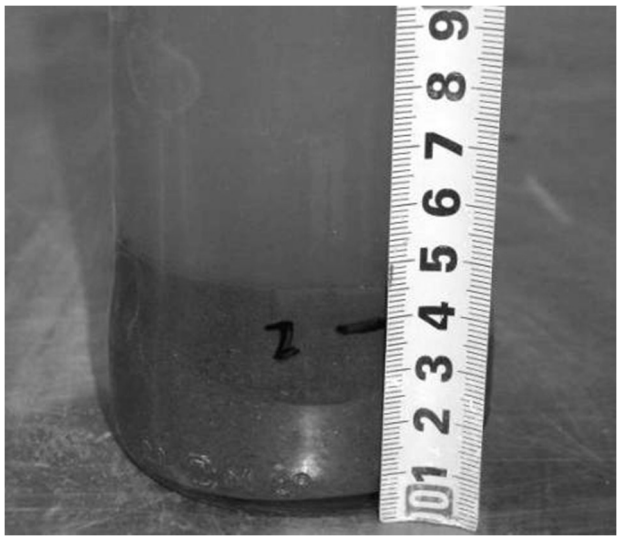

Figure 5.18 – Result of the sedimentation test showing that the fraction layers are hardly identified.

5.5.2 Ribbon test

The ribbon length obtained from the ribbon test was of about 65 mm, which according to Standards Australia (2002) means that soil S5 is adequate for rammed earth construction. The high clay content of the soil was visually detected upon its mixing with water, since the clay was sticking to the hands and formed agglomerates hindering the homogeneisation of the water content of the mixture (see Figure 5.19).

Figure 5.19 – Mixing of the soil with water: clay sticking to the hands and formation of agglomerates.

5.5.3 Drop test

The drop test on the soil S5 resulted on a compaction water content of about 15.9%, which is substantially greater than that of soil S4. This means that the PSD correction applied to soil S4 consisted in the addition of large quantities of river sand and gravel, as later confirmed in Section 5.5.5.

5.5.4 Dry strength test

The results of the dry strength of the soil S5 revealed a high clay content. This means that a relatively good strength performance can be expectable, in agreement with the results obtained for soil S4.

5.5.5 PSD analysis

The particles size distribution (PSD) curves of soil S5 and S4 are plotted in Figure 5.20 against the PSD envelopes recommended by Houben and Guillaud (2008), MOPT (1992) and by the Portuguese National Laboratory of Civil Engineering (LNEC 1953).

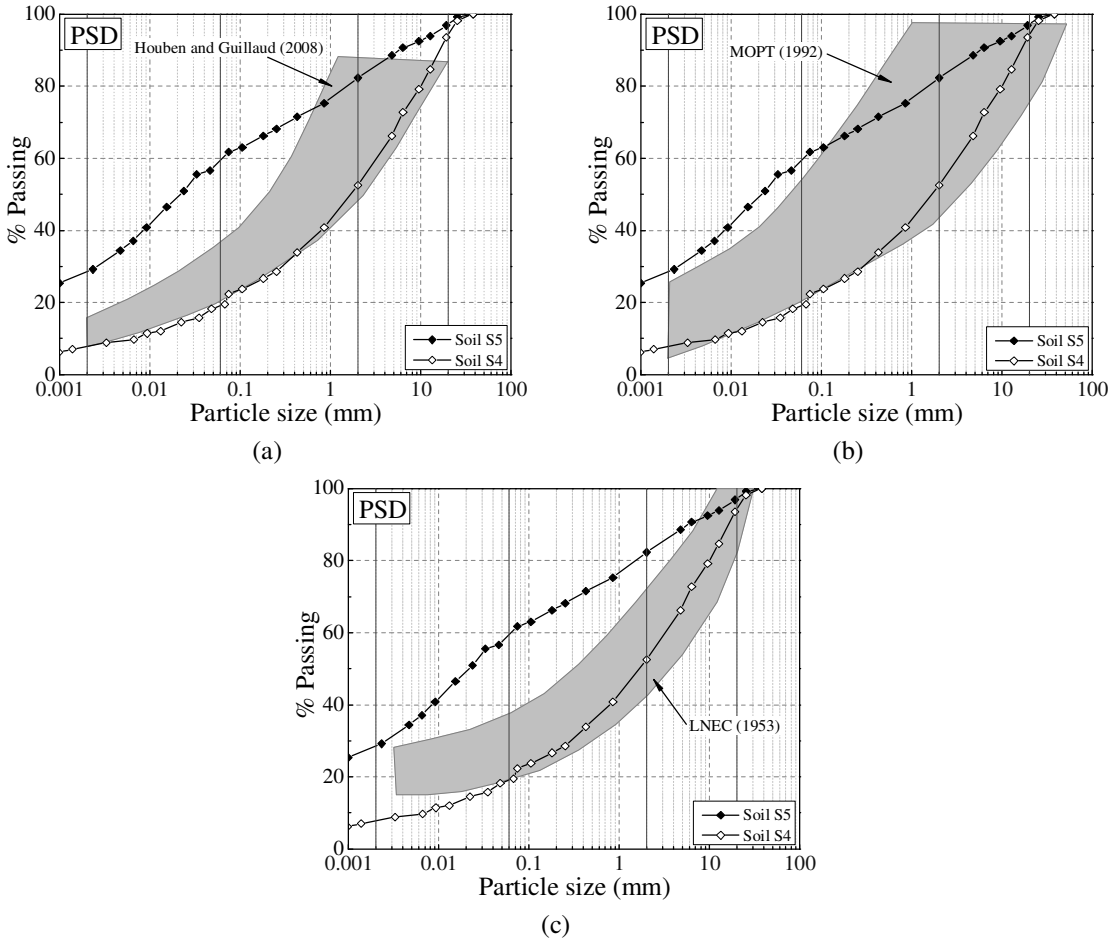

Figure 5.20 – Comparison between the PSD curves of the soils S5 and S4, and the envelopes for rammed earth construction recommended by: (a) Houben and Guillaud (2008); (b) MOPT (1992) and; Portuguese National Laboratory of Civil Engineering (LNEC 1953).

The percentages of the size fractions composing each soil are given in Table 5.10. The results confirm the high clay content identified in the previous tests, which is shown to be excessively high, according to the envelopes of recommended values. The large difference between the PSD curves of soil S5 and S4 indicate that the correction applied included the addition of large quantities of coarse aggregates.

Table 5.10 – Particles size fractions of the soils S5 and S4 (according to the size fractions usually adopted in earth construction).

Soil	Clay (%)	Silt (%)	Sand (%)	Gravel (%)	Pebbles (%)
S5	28	31	23	15	3
S4	8	11	33	42	6

(clay < 0.002 mm / 0.002 mm ≤ silt < 0.060 mm / 0.060 mm ≤ sand < 2.0 mm / 2.0 mm ≤ gravel < 20 mm / pebbles≥ 20 mm)

5.5.6 Atterberg limits

The liquid limit (LL), plastic limit (PL) and shrinkage limit (SL), as well as the plastic index (PI), shrinkage index (SI) and respective USCS classification are given in Table 5.11 for soil S5 and S4. Furthermore, the consistency parameters are plotted in Figure 5.21 against the envelope recommended by Houben and Guillaud (2008), where the soil S5 fits within it. Another important observation is that even without PSD correction the soil S5 presents low SI, meaning that it has low shrinkage/swelling potential.

Table 5.11 – Atterberg's limits of the soils S5 and S4 and respective USCS classification.

Soil	LL (%)	PL (%)	PI (%)	SL (%)	SI (%)	USCS classification
S5	30	18	12	22	8	Sandy lean clay (CL)
S4	21	15	6	15	6	Silty, clayey sand with gravel (SC-SM)

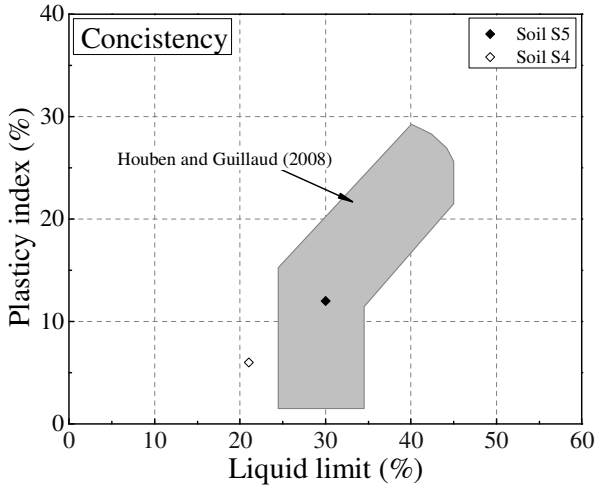

Figure 5.21 – Comparison of the consistency parameters of soils S5 and S4 against the envelope of recommended values by Houben and Guillaud (2008) for unstabilised rammed earth.

5.5.7 Standard Proctor

The results of the standard Proctor test are summarised in Table 5.12 and the compaction curve of soil S5 is presented in Figure 5.22. The maximum dry density of soil S5 is substantially lower than that of soil S4. This is explained by a worse PSD of soil S5 in comparison with that of soil S4, which was corrected by addition of coarse particles. The OWC of soil S5 is higher than that of soil S4, which is a consequence of its higher clay content. The difference between the DTWC and the OWC of soil S5 is high when compared to that obtained for the other soils. This is probably explained by the possibility of the results of the drop test being affected by the rather high clay content of soil S5. Eventually, the drop test only results in a good estimation of the OWC in soils with clay content within or closer to the clay content range of soils S1, S2, S3 and S4 (8-14%).

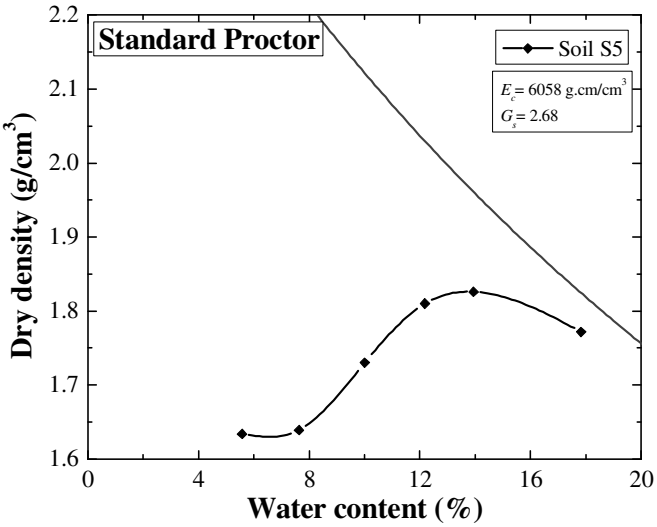

Figure 5.22 – Compaction curve of soil S5.

Table 5.12 – Compaction properties of the soils S5 and S4.

Soil	ρ_{dmax} (g/cm^3)	OWC (%)	G_s	DTWC (%)
S5	1.83	13.4	2.68	15.9
S4	2.12	8.7	2.63	7.5

5.5.8 Suitability for rammed earth construction

In general, the tests performed on soil S5 showed that the clay content is excessively high. Furthermore, the PSD curve of this soil clearly does not respect the recommended PSD envelopes. As a consequence of this faulty PSD, it resulted a maximum dry density that is rather low when compared to that of soil S4, and even to those of soil S1 and S2. For these reasons, the use of soil S5 in rammed earth construction is expected to result in a low strength material and in shrinkage problems. This justifies the decision taken by the contractor in correcting the soil PSD, which resulted into soil S4. Therefore, it was decided not to proceed with the assessment of the performance of rammed earth specimens manufactured with this soil (strength and durability). Instead, it was decided

to proceed directly with the PSD correction of soil S5, as described in detail in the following Section.

5.6 PSD correction of the selected soil

The adjustment of the PSD curve of the soil S5 was carried out by means of the addition of aggregates acquired locally, namely river sand and gravel obtained from crushed granite (Figure 5.23).

(a) (b)

Figure 5.23 – Materials used in the PSD correction of soil S5: (a) river sand; (b) Gravel obtained from crushed granite.

The PSD curves of the aggregates are given in Figure 5.24a. The correction of the PSD consisted in the adjustment of the curve of the mixture of soil, sand and gravel to the fuller curve of Equation (5.1), recommended by Houben and Guillaud (2008). The use of this curve is expected to optimize the density of the material, and thus its strength performance.

$$P = \left(\frac{d}{D} \right)^{0.25} \tag{5.1}$$

where P is the percentage finer than the size being considered, d is the size being considered and D is the maximum size of the particles.

Furthermore, the adjustment took into account the overall envelope resulting from the envelopes recommended by Houben and Guillaud (2008), MOPT (1992) and LNEC (1953). The resulting mixture was called soil S6 and is composed by 50% of soil S5, 28% of river sand and 22% of gravel, in weight (about 50% of added aggregates). The PSD curve of the soil S6 is given in Figure 5.24b and the size-fractions composing it are given in Table 5.13. . It should be noted that the “in-situ” correction resulting in soil S4 seems to have included the addition of an even higher percentage of coarse aggregates.

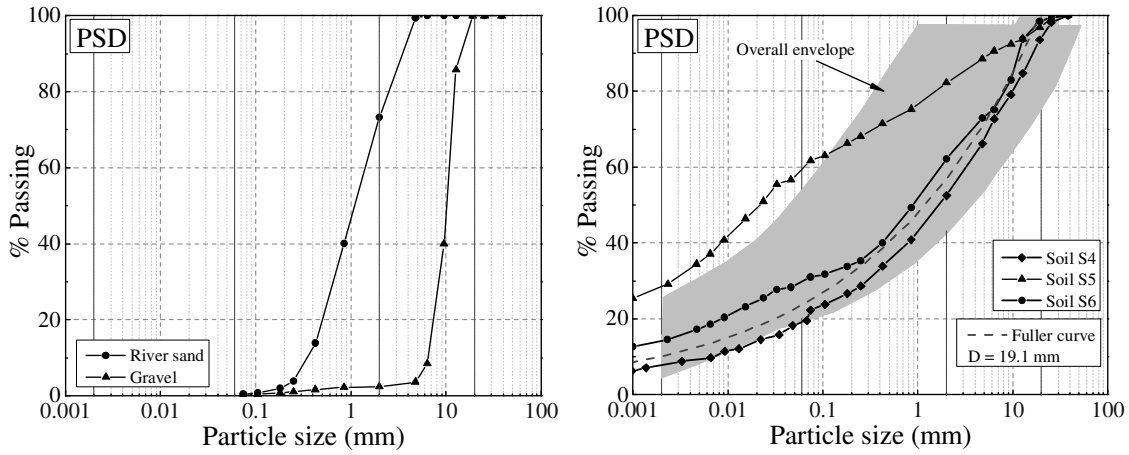

Figure 5.24 – Correction of the soils S5: (a) PSD of the gravel and river sand; (b) correction with 50% of soil S5, 28% of sand and 22% of gravel (soil S6).

Table 5.13 – Particles size-fractions of soil S6 and respective components, namely soil S5, river sand and gravel (according to the size fractions usually adopted in earth construction).

Soil	Clay (%)	Silt (%)	Sand (%)	Gravel (%)	Pebbles (%)
S6	14	16	32	37	1
S5	28	31	23	15	3
River sand	0	0	73	27	0
Gravel	0	0	3	97	0

(clay < 0.002 mm / 0.002 mm ≤ silt < 0.060 mm / 0.060 mm ≤ sand < 2.0 mm / 2.0 mm ≤ gravel < 20 mm / pebbles≥ 20 mm)

5.7 Performance of the corrected soil

Following to the definition of the correction proportions to be applied to soil S5, it was proceeded with the characterization of the corrected soil (S6), which included the execution of the following tests: ribbon test, drop test, dry strength, Atterberg limits and standard Proctor.

The ribbon test showed that soil S6 is adequate for rammed earth construction, since the resulting ribbon length was of about 51 mm. As expected, the reduction of the clay content of the soil resulted in the reduction of the ribbon length.

The dry strength of soil S6 is high as expectable, since the addition of sand and gravel had low impact in the fines fraction (particles smaller than 0.425 mm), which should be similar to that of soil S5.

Regarding the Atterberg limits, the PSD correction resulted in the decrease of LL and PL relative to soil S5, as it can be seen in Table 5.14. The consistency parameters are plotted outside the recommended envelope by Houben and Guillaud (2008) (Figure 5.25).

Table 5.14 – Atterberg's limits of the soils S5 and S6 and respective USCS classification.

Soil	LL (%)	PL (%)	PI (%)	SL (%)	SI (%)	USCS classification
S5	30	18	12	22	8	Sandy lean clay (CL)
S6	23	16	7	-	-	Clayey sand with gravel (SC)

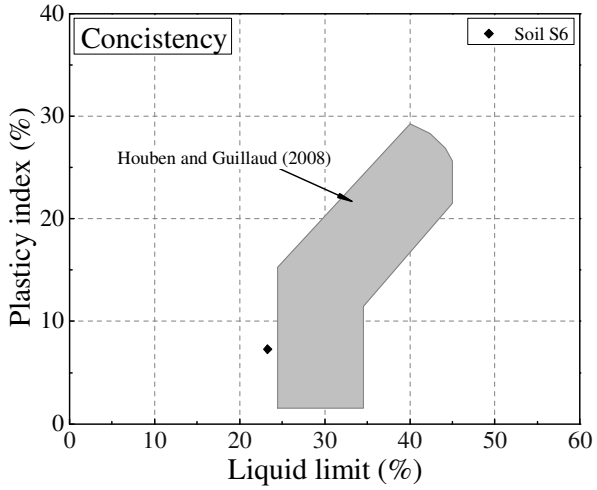

Figure 5.25 – Comparison of the consistency parameters of soil S6 against the envelope of recommended values by Houben and Guillaud (2008) for unstabilised rammed earth.

The results of the standard Proctor test are presented in Figure 5.26 and are summarised in Table 5.15, where is shown that the correction resulted in a substantial increase of the maximum dry density relative to soil S5, as well as, in the decrease of the OWC. Moreover, the DTWC obtained from the drop test, is very similar to the OWC, which is an important finding regarding the construction of the medium- and large-scale specimens, as it will be explained later.

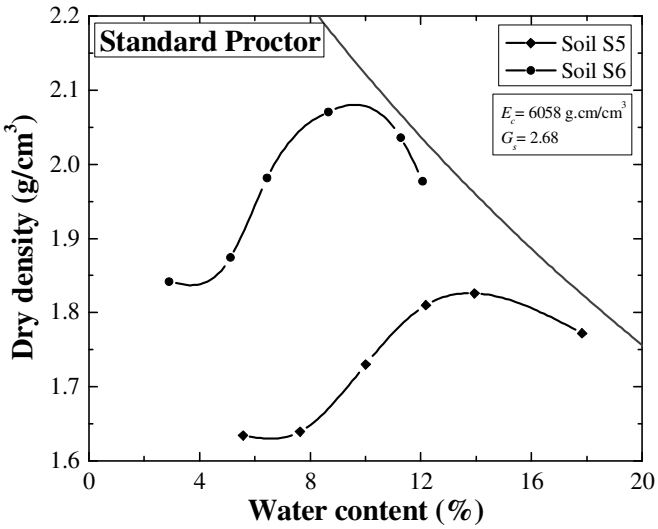

Figure 5.26 – Compaction curves of soils S5 and S6

Table 5.15 – Compaction properties of the soils S5 and S6.

Soil	ρ_{dmax} (g/cm^3)	OWC (%)	G_s	DTWC (%)
S5	1.83	13.4	2.68	15.9
S6	2.10	10.1	2.68	9.7

According to Doat *et al.* (1991) soil S6 is expected to result in a rammed earth with excellent performance (2.10 g/cm^3 < ρ_{dmax} < 2.20 g/cm^3). Both soil S4 and S6 have

similar maximum dry densities, whereby similar compressive strengths are also expected.

5.7.1 Compression behaviour

The compressive behaviour of rammed earth prepared with soil S6 was assessed by performing compression tests on six cylindrical specimens compacted with maximum dry density and OWC. The preparation of the specimens and the testing procedure were similar to those of the specimens prepared with the other soils, presented in Section 5.4.1. The stress-strain curves of the specimens and the respective envelope are presented in Figure 5.27. Table 5.16 summarises the results in terms of density (ρ_d), compaction water content (W), compressive strength (f_c), Young modulus (E_0) and equilibrium water content (W_{eq}). It should be noted that the specimens present a slightly difference relative to the programmed compaction characteristics (dry density and compaction water content), which are a consequence of possible water losses and of the error associated to the method to determine the water content.

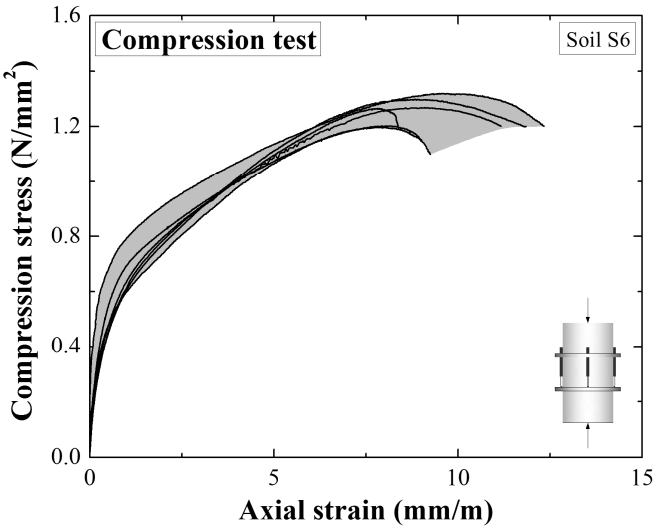

Figure 5.27 – Stress-strain curves of the rammed earth cylindrical specimens manufactured with soil S6.

Table 5.16 – Results of the rammed earth cylindrical specimens tested under compression.

Specimen	W (%)	ρ_d (g/cm3)	f_c (N/mm2)	E_0 (N/mm2)	W_{eq} (%)
CURES6_1	10.1	2.07	1.27	865	1.12
CURES6_2	10.0	2.07	1.20	1408	1.05
CURES6_3	9.5	2.07	1.20	1112	1.04
CURES6_4	9.3	2.08	1.32	3160†	0.98
CURES6_5	10.5	2.06	1.27	960	1.04
CURES6_6	9.9	2.07	1.30	827	1.03
Average	9.9	2.07	1.26	1034*	1.04
COV (%)	4.3	0.4	4.0	22.8*	4.4

†Outlier according to Grubbs and Dixon tests; *Outliers not considered.

The average compressive strength was of about 1.26 N/mm^2 and was obtained for an average equilibrium water content of about 1.04%. This value is significantly higher than the maximum compressive strength obtained for soils S1, S2, S3 and S4, and shows a coefficient of variation relatively low, taking into account the type of material tested. This is explained by the controlled conditions given in laboratory (compaction and drying), whereas the coefficient of variation of rammed earth compacted on-site would be expectedly higher.

The results obtained for the compressive strength deem with the minimum requirements defined by the NZS 4298 (NZS 1998b), even that barely; the least value of the set of six specimens (1.2 N/mm^2) must be greater than 1.14 N/mm^2. This standard also provides a procedure to determine the characteristic compressive strength from a set of tests, which is used for design purposes. The aspect ratio of the specimen has to be taken into account by applying Equation (5.2):

$$f_c' = k_a f_c \tag{5.2}$$

where f_c' is the adjusted compressive strength and k_a is the aspect ratio factor, which assumes a value of 0.8 for a 2:1 height to thickness ratio. The characteristic compressive strength ($f_{c,k}$) is then computed from Equation (5.3):

$$f_{c,k} = \left(1 - 1.5\frac{s}{\overline{f_c'}}\right) f_{c,\min}' \tag{5.3}$$

where $\overline{f_c'}$ is the average adjusted compressive strength, s is the respective standard deviation and $f_{c,\min}'$ is the respective least value. Given this, the resulting characteristic compressive strength was of about 0.90 N/mm^2.

The Young's modulus (E_0) was computed between 5% and 30% of the compressive strength of the respective specimen. It should be noted that the Young modulus of specimen CURES6_4 seems to deviate remarkably from that of the others specimens, whereby the outlier status of this value was tested according Grubbs and Dixon criteria, as described in ASTM E178 (ASTM 2002a).

Both criteria showed that this value is an outlier, and thus it was not considered for statistical analysis of the results regarding the Young's modulus. Therefore, the Young's modulus presents an average value of about 1034 N/mm^2, which is of similar order of magnitude to those obtained for the specimens manufactured with soil S4 (Section 5.4.1). In terms of design value, the HB 195 (Standards Australia 2002) provides an underestimation of the Young's modulus as it recommends a fixed value of about 500 N/mm^2, when tests are not available. Furthermore, the average Young's modulus is about 820 times higher than the compressive strength, which means that standard NZS 4297 (NZS 1998a) provides a slight underestimation of this parameter (700 times higher). The NMAC 14.7.4 (NMAC 2006) is the standard providing the best

approach for this specific case by considering the Young's modulus to be 750 times higher than the compressive strength. Despite that, any of the referred standards provide a good estimation of Young's modulus for the case of soil S6, but it should be noted that this parameter shows high variability.

The failure mode was similar for all specimens and is characterized by the formation of a main diagonal crack that splited the specimens in two wedge-shaped parts (see Figure 5.28).

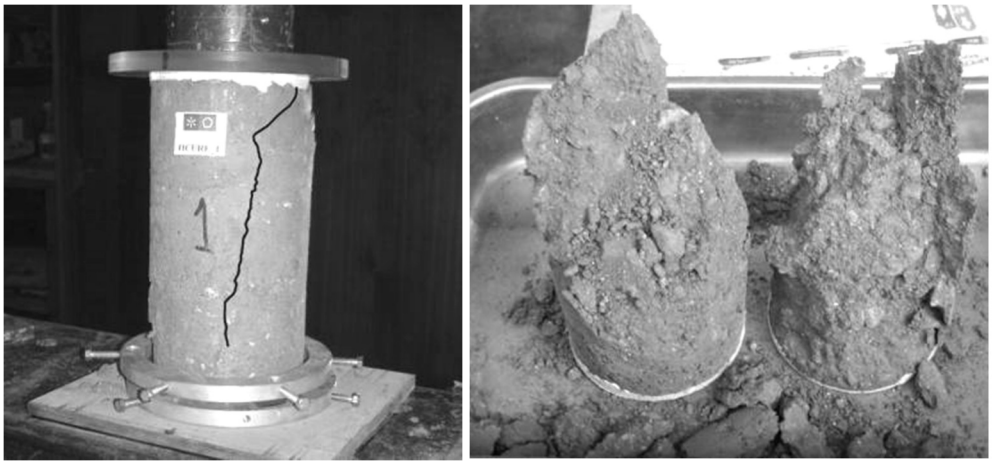

(a) (b)

Figure 5.28 – Failure mode of the rammed earth cylindrical specimens: (a) formation of a diagonal crack; (b) main vertical/diagonal crack formation with spalling of the specimen surface.

5.7.2 Durability (Geelong test)

The durability of the rammed earth preformed with the soil S6 was also tested resorting to the Geelong test. The preparation of the specimens and the testing procedure is similar to those used for the other soils, as described in Section 5.4.2.The pitting depth was of about 2 mm, which means that the erodibility index is 2. The penetration depth was of about 25 mm, and thus is rather inferior to the limiting 120 mm required by NZS 4298 (NZS 1998b). In practical terms and according to Standards Australia (2002), this means that the soil is suitable for exposed rammed walls. In addition, soil S6 seems to have better performance against water erosion than soil S4, which is probably explained by the higher clay content of the first.

5.8 Conclusions

The suitability of four soils for unstabilised rammed earth construction from Alentejo region was assessed first by characterizing the soil properties and then by characterizing the performance of rammed earth specimens. Commonly used expeditious and laboratory tests were carried out in order to assess the properties of the soils. The performance of the rammed earth specimens was assessed resorting to compression tests and to the Geelong test.

The soils S1, S3 and S4 resulted from the weathering of schist, while soil S2 is a transported soil. In the case of soil S4, river sand and gravel were added upon the construction of the rammed earth house where it was used.

The sedimentation test was shown to be a simple and fast method to compare the fraction percentages between soils, however, the quantification of the size-fractions percentages composing each soil were largely affected by clay flocculation. This means that the quantification of the soils size-fractions by this test may not be reliable.

The ribbon test indicated that all soils are suitable for rammed earth construction, and that the clay content of soils S1 and S3 would be expectably higher than that of the other soils. However, the PSD characterization showed that soils S2 and S3 are those presenting higher clay content, which means that the ribbon test may lead to erroneous conclusions.

The drop test allowed determining a compaction water content very similar to the OWC obtained from the standard Proctor test. However, the fact that the ball to perform the drop test could be the moulded means only that the soils present an important percentage of clay, required to give cohesion to the rammed earth.

The dry strength test showed that the strength of rammed earth manufactured with soils S1 and S4 would be expectably higher than that of other soils, as it was confirmed later by the compression tests. Therefore, this test seems to be a useful and practical method to compare the strength performance expected for different soils in an initial approach of the assessment of soils. However, this test does not allow properly concluding on the suitability of the soils.

The PSD curves of the soils were found to be mostly within recommend envelopes for unstabilised rammed earth construction. However, the envelope given by LNEC (1953) is an exception, because it is also applied to adobe construction. Moreover, the higher clay content of soils S2 and S3 would suggest a higher compressive strength of these soils, which was not verified in the compression tests. This can be explained by differences existing at the mineralogical level of the clay fraction of the soils

The determination of the Atterberg limits allows identifying the presence of expansive clay minerals that may result in shrinkage problems in rammed earth. The Atterberg limits of the soils were compared with an envelope of recommended values, and all soils fitted within it, except soil S4. The low values of PI and SI obtained for all soils allowed concluding that expansive clay minerals are practically absent from the soils.

The compaction properties were determined for all soils by means of the standard Proctor test. The soil S4 presented a higher maximum dry density and also an higher performance in terms of compressive strength. It was shown to exist a dependency of the compressive strength on the dry density, i.e., the higher the dry density the higher is the compressive strength.

Regarding the compressive strength performance of unstabilised rammed earth specimens, it was shown that the minimum requirements presented in some regulating documents could not be achieved, even by soil S4 (soil presenting the highest compressive strength). The generalisation of this situation does not mean that the unstabilised rammed earth constructions from Alentejo are unsafe for normal loading conditions. Nevertheless, their seismic behaviour might be compromised by this fact, and thus this topic should be addressed in future work, given the important seismic hazard of the region.

In terms of durability, the rammed earth specimens presented an erodibility index of 3, meaning that they can be used to build protected walls. This is a typical situation found in Alentejo, where traditional rammed earth constructions are protected by lime/earth mortar plasters, frequently limewash painted.

Regarding the characterization of soil S5, it was shown that its clay content was excessively high for rammed earth construction, so its use in rammed earth would require PSD correction. This correction was performed by mixing 50% of soil S5, 28% of river sand and 22% of gravel. In general, the resulting soil S6 presented similar properties to those of soil S4, which also resulted from an empirical PSD correction of soil S5. The compressive strength achieved by soil S6 was the highest obtained, and is higher than the compressive strength required by NZS 4298 (NZS 1998b) for standard grade constructions.

Chapter 6

Repair of Rammed Earth by Means of Mud Grouts Injection

6.1 Introduction

This Chapter presents the results of an experimental campaign where the adhesion capacity of unmodified mud grouts was assessed by means of tests carried out on medium- and large-scale rammed earth specimens. The medium-scale specimens consisted on beams tested under three-point bending, while the large-scale specimens consisted on wallets tested under diagonal compression. These specimens were first tested and then were repaired resorting to three unmodified mud grouts, namely an "artificial" mud grout composed by kaolin and limestone powder and two "natural" mud grouts composed by sieved soil and limestone powder. The adhesion capacity was then assessed by testing again the repaired specimens. The injectability of the tested mud grouts was also assessed during the repair works. In addition, the experimental program also allowed characterizing the behaviour of rammed earth in bending and shear. Finally, the ultrasound pulse velocity (UPV) technique was investigated as a mean to assess the repair effectiveness and quality of the injection technique by means of a non-destructive method.

6.2 Adhesion tests on medium-scale specimens

The medium-scale tests on rammed earth specimens aimed mainly at characterizing the adhesion capacity in tension of two mud grouts, namely an "artificial mud grout" and a "natural mud grout". The "artificial mud grout" was composed by kaolin powder Mibal-

A and limestone powder Micro 200-OU, while the "natural mud grout" was composed by sieved soil S5 corrected with the addition of the aforementioned limestone powder. The purpose of the "natural mud grout" was to test the possibility of using a grout manufactured with the same soil used in the construction, which is a current practice in the manufacturing of repair materials used in other intervention techniques on earth constructions.

The rammed earth specimens consisted of beam-specimens that were tested under three-point bending and then were repaired by grout injection in order be re-tested. This procedure allowed evaluating the recovery ratio promoted by the grouts, which is intimately related to its adhesion capacity. In addition, the injectability capacity of the mud grouts through a crack was also assessed during the repair of the specimens by injection. The injectability capacity was evaluated in the injection of cracks with 2 mm and 8 mm width.

6.2.1 Manufacture of the specimens

The flexural behaviour of the rammed earth beams preformed with soil S6 and then the adhesion capacity of the mud grouts was assessed by means of three-point bending tests carried out on twelve medium-scale specimens, namely with dimensions 150x150x600 mm^3. The large quantity of material required to perform each of the specimens made unpractical its drying before mixing, which required an alternative procedure in order to taking into account the water content of the materials composing soil S6, namely the soil S5, the sand and the gravel described in Section 5.6. The determination of the water content of these materials by the traditional oven method would normally take 16-24 hours (LNEC 1965), which means that part of the water would evaporate before obtaining these results. As a consequence, it was decided to determine the water content by means of a much faster method, namely the microwave oven heating method described in ASTM D 4643 (ASTM 2000c). The water content determined by this method was used to define each mixture, but in addition, the water contents were also determined by the oven method. The water contents (W) are compared in Figure 6.1, where good agreement is observed for the case of the sand and gravel. However, both methods slightly disagree for the case of soil S5 and the resulting corrected soil S6 upon the compaction of the beam-specimens, where the microwave method provides a water content higher than the oven method. The effect of the microwaves on the clay fraction is the probable responsible for this observation, namely by promoting a better drying of the interlayer space of the clay minerals composing the clay fraction of both soils, whose percentages are known to be substantial.

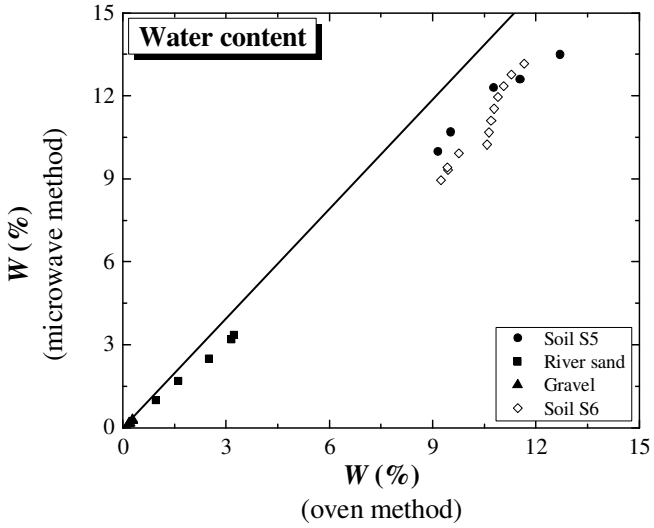

Figure 6.1 – Comparison between the oven and microwave oven heating methods for determination of the water content in the manufacture of the medium-scale specimens.

The weighing of components of the soil S6 included an excess of 10% relative to the weight required to prepare each specimen. The preparation of the specimens is illustrated in Figure 6.2, where the solid components were first mixed manually, resorting to a hoe and a shovel. The water required to perform the OWC was calculated with basis on the individual water contents of the components. The water was added by means of a watering can with the soil spread over the ground, and then the soil-water mixture was again mixed manually. This method aimed at allowing a better distribution of the water and at avoiding the formation of lumps. After this procedure, the soil mixture showed a dry appearance, which means that the calculated water quantity was insufficient to allow moulding a ball of soil required for the drop test, whereas a successful iteration of the test would be the expectable result. This situation can be explained by several reasons, such as water losses during the mixing, heterogeneity of the materials (especially of the soil) and the error associated to the microwave method to estimate the water content. Since the drop test was shown to result into compaction water contents similar to OWC (see Section 5.7), it was decided to keep adding and mixing extra water until obtaining a successful iteration of the test. This procedure was then followed for all the mixtures performed.

(a) (b) (c) (d) (e)

Figure 6.2 – Preparation of the mixture to compact the specimens: (a) component materials of soil S6; (b) dry mixing; (c) addition of the water with a watering can; (d) wet mixing and (e) compaction of a specimen.

The soil mixture was compacted in a steel mould using an electrical hammer equipped with a compaction plate of dimensions 145x145x5 mm^3. The specimens were composed by three layers of similar thickness (about 50 mm) and were demoulded immediately after compaction. The weight of soil-water mixture was defined by taking into account the wet density of the soil S6 corresponding to the maximum dry density and OWC. Thus, the weight of soil-water mixture per layer was fixed as 10.42 kg.

6.2.2 Testing procedure

After drying for 6 weeks at a room temperature of about 22±2ºC, the beam-specimens were tested under three-point bending. The load was applied at middle span and the distance between supports was of about 500 mm (see Figure 6.3). The application of the load was carried out under monotonic displacement control at a rate of 0.001 mm/s. The testing procedure of the specimens after injection was similar, but the tests were carried out 3 weeks after the repair. The drying was processed under a room temperature similar to that of the specimens before testing.

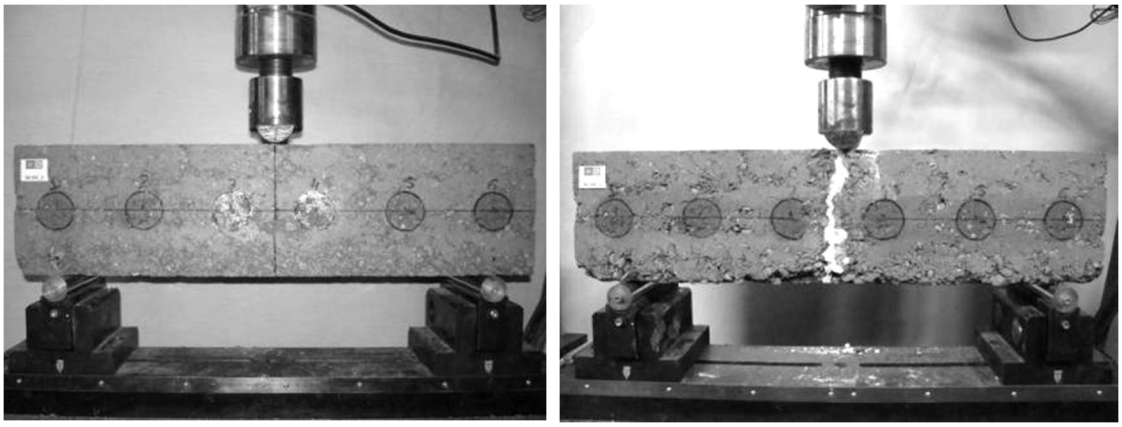

(a) (b)

Figure 6.3 – Test setup of the bending test carried out on the rammed earth medium-scale specimens (layers in the horizontal direction): (a) specimen before injection; (b) specimen after injection.

6.2.3 Repair procedure

The failure mode of specimens tested under three-point bending consisted in the formation of a middle-span crack that split the specimen into two parts. These parts were then bonded together by a mud grout that was injected in the crack (gap) between them. Before injection, the crack surfaces were brushed to remove loose debris, and were sprayed with water to mitigate the water sorption during the injection (Figure 6.4a). Then a line of sealant silicone was applied at the base (next to the crack) of each specimen part. The specimens' parts were placed on a plywood board and squeezed against it to spread the silicone line (Figure 6.4b and Figure 6.4c). The plywood board surface was first oiled to avoid fully adhesion with the silicone sealant. The specimens' parts were positioned on the board such that the gap width (crack to be injected) would be of about 2 mm or 8 mm. It should be noted that the first test of the beam-specimens

resulted in material losses in the top and bottom faces nearby the crack, due to crushing and tension cracking, respectively. Thus, the crack widths near these regions were larger than planned.

The same sealing procedure was then used for the side faces, but in this case, Plexiglas plates were pressed against the specimen by means of two screw clamps. The gaps between the Plexiglass plates and the plywood board were also sealed with silicone. This procedure allowed visualising the rising of the mud grout within the crack during the injection.

(a) (b) (c)

Figure 6.4 – Preparation of the beam-specimens for injection: (a) water spraying; (b) line of silicone sealant being applied at the bottom face; (c) line of silicone sealant being applied at a side face.

The "artificial grout" used to repair the specimens corresponds to the mud grout named II55MG25, which was that obtaining the highest adhesion capacity in the tests carried out at UMinho on small-scale specimens, as discussed in Section 4.4.5. On the other hand, the "natural grout" was composed by sieved soil S5, limestone powder 200-OU, and HMP was used as deflocculant/dispersant. The sieved soil S5, named as S5#80, consisted in the material passing through the ASTM sieve nº80 (size below 0.180 mm), whose sieving had to be carried out by the wet method, since the high clay percentage of the soil resulted in the formation of aggregates of fine particles. After sieving, the passing slurry was left to settle, the supernatant water was decanted, the sediment was oven dried and then was manually broken into powder using a steel rammer. The PSD curves of the materials involved in the composition of the grouts are given in Figure 6.5 and the respective size fractions are summarised in Table 6.1.

The high clay content of S5#80 shows the need in correcting its PSD with limestone powder in order to produce a suitable mud grout. This decision is supported by the conclusions drawn from the composition studies on mud grouts discussed in Chapter 4, namely regarding the incorporation of limited percentage of clay to obtain adequate fluidity. Furthermore, the correction applied to S5#80 was based on the PSD curve of grout II55MG25. Therefore, limestone powder was added in adequate amounts to bring down the clay content to a value slightly higher than that of grout II55MG25, namely of about 20%. An higher clay content was adopted for the "natural" mud grout, since it results directly from a natural soil without processing or purification treatment. Thus, the resulting grout was composed by 40% of S5#80 and 60% of limestone powder, and was named as II55NMG40-60. Despite that, the PSD curves of both grouts are shown to

be very similar in Figure 6.6, where the size-fractions percentages also assume similar values (see Table 6.2).

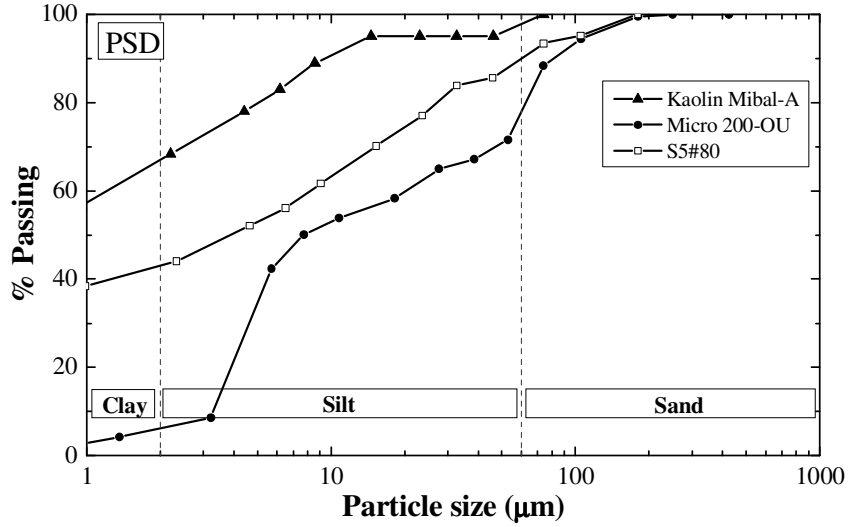

Figure 6.5 – PSD curves of the materials composing the mud grouts.

Table 6.1 – Size-fractions percentages of the materials used to compose the mud grouts and respective particles specific gravity.

Material	% Clay	% Silt	% Sand	Specific gravity
Kaolin Mibal-A	67	33	0	2.65
Micro 200-OU	6	71	23	2.71
S5#80	43	47	10	2.68

Clay: <0.002 mm / silt: ≥0.002 mm and <0.060 mm / sand: ≥0.060 mm and <2.0 mm

Table 6.2 – Size-fractions percentages of the grouts II55MG25 and IINMG40-60.

Mud Grout	% Clay	% Silt	% Sand
II55MG25	18	64	18
II55NMG40-60	21	62	17

Clay: <0.002 mm / silt: ≥0.002 mm and <0.060 mm / sand: ≥0.060 mm and <2.0 mm

The solid fraction adopted for grout II55NMG40-60 was also of about 55%. Regarding the addition of HMP, it was based on the ratio between weight of HMP and that of the clay fraction of the grout (HMP/C), which is of about 0.022 g/g. It should be noted that the HMP weight of grout II55MG25 was previously defined (in the composition study) as function of the weight of the incorporated kaolin powder. The composition of both mud grouts is summarised in Table 6.3, while the respective properties are given in Table 6.4, in terms flow time of 1 dm^3 of the grout (ASTM C 939: ASTM 1994), dry density (ρ_d), volumetric shrinkage (S_v), flexural strength (f_b) and compressive strength (f_c) (EN 1015-11: CEN 1999). It should be noted that the grout II55NMG40-60 presents higher mechanical properties and lower flow time than grout II55MG25.

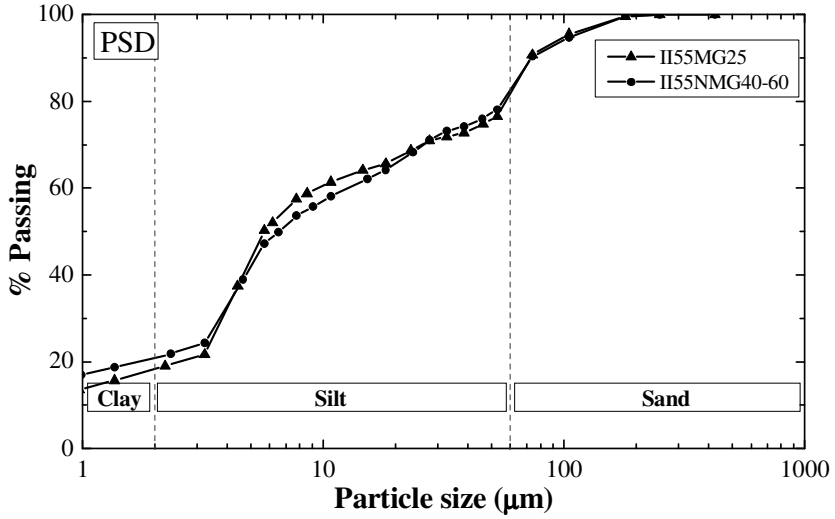

Figure 6.6 – PSD curves of the mud grouts II55MG25 and IINMG40-60.

Table 6.3 – Composition of the mud grouts injected in the medium-scale specimens.

Mud Grout	K. Mibal-A (wt.%)	S5#80 (wt.%)	L. 200-OU (wt.%)	HMP/C (g/g)	ϕ_v (%)	*W/S*
II55MG25	20	-	80	0.022	55	0.30
II55NMG40-60	-	40	60	0.022	55	0.30

A syringe of 100 ml capacity was used to inject the grouts into the crack of the specimens, by inserting it into a 6 mm diameter plastic tube attached at one of the Plexiglas plates covering the sides of the specimens. Furthermore, the tube was located near the bottom, and all grout was injected from it till it reached the top. An excess of grout was given in order to compensate possible leakages (see Figure 6.7). Regarding the injectability of the grouts during the injection of the specimens, none of the grouts registered difficulties in penetrating through the two types of cracks considered. This means that, despite the high flow time of grout II55MG25, both grouts presented adequate fluidity and water retention capacity to allow their injection without experiencing excessive water sorption by the rammed earth specimens. However, the high water sorption capacity of the rammed earth specimens was thoroughly observed, since the grouts presented a hardened-state in about 10 minutes after their injection. This means that the working time to inject the grout into the injection tube was less than 10 minutes.

Table 6.4 – Properties of the mud grouts injected in the medium-scale specimens.

Mud Grout	Flow time (s)	ρ_d (kg/m^3)	S_v (%)	f_b (N/mm^2)	f_c (N/mm^2)
II55MG25	85.9	1802	12.7	0.62	1.48
II55NMG40-60	36.5	1789	13.2	0.92	2.44

(a) (b) (c)

Figure 6.7 – Injection of the rammed earth beam-specimens: (a) injection with a 100 ml syringe from one of the sides; (b) rising of the mud grout at the opposite side of the injection; (c) crack completely filled.

Table 6.5 summarises the injection conditions of each specimen in terms of crack width (d_{cr}) and injected grout. Each mud grout was used to inject two sets of six specimens, three from which had a crack width of about 2 mm and the other three of about 8 mm. Regarding the injectability of both grouts, it should be mentioned that the grouts raised without difficulties in all specimens.

Table 6.5 – Injection conditions of the medium-scale specimens.

Specimen	d_{cr} (mm)	Injected grout
BURE_1	2	II55MG25
BURE_2	2	II55MG25
BURE_3	2	II55MG25
BURE_4	8	II55MG25
BURE_5	8	II55MG25
BURE_6	8	II55MG25
BURE_7	2	II55NMG40-60
BURE_8	2	II55NMG40-60
BURE_9	2	II55NMG40-60
BURE_10	8	II55NMG40-60
BURE_11	8	II55NMG40-60
BURE_12	8	II55NMG40-60

6.2.4 Results and discussion

The results of the tests carried out on the medium-scale specimens are summarised in Table 6.6, in terms of compaction water content determined by the oven method (W), dry density (ρ_d), initial flexural strength (f_{bi}), flexural strength after grout injection (f_{bg}) and the flexural strength recovery rate f_{bg}/f_{bi}. It should be noted that the dry density of the specimens deviate from the maximum dry density of soil S6 because of errors associated with the microwave oven method for estimating the water content, which have consequences on the reproduction of the PSD of soil S6, resulting in different compaction properties between mixtures. However, the greatest contribution for this difference came from the fact that the beam-specimens were manufactured by fixing a reference wet weight of soil S6, which is shown to present, in general, water contents that are higher than OWC upon its compaction as a specimen.

Regarding the results of the tests, grout II55MG25 shows poor recovery rate for both tested gap widths, where for d_{cr}= 2 mm the average recovery rate was of about 26%, while that for d_{cr}= 8 mm was of about 17%. On the other hand, grout II55NMG40-60 shows very satisfactory adhesion capacity by presenting an average recovery rate of about 55% for d_{cr}= 2 mm and of about 74% for d_{cr}= 8 mm. Even though grout II55NMG40-60 is stronger than grout II55MG25, this fact does not justifies the unsatisfactory results obtained for this last grout. Probably this difference can be explained by differences in the clay fraction of both grouts, where that of grout II55NMG40-60 is similar to that of the beam-specimens, since it is composed by the respective soil. Therefore, this result seems to encourage the use of the same soil used in the construction to compose a mud grout in a repair intervention. Moreover, the unsatisfactory result obtained for grout II55MG25 justifies the decision of not considering this grout for repairing the wallet-specimens, as is later described.

Table 6.6 – Results of the tests carried out on the medium-scale specimens.

Specimen	W (%)	ρ_d (g/cm^3)	d_{cr} (mm)	Injected grout	f_{bi} (N/mm^2)	f_{bg} (N/mm^2)	f_{bg}/f_{bi} (%)
BURE_1	10.6	2.03	2	II55MG25	0.26	0.07	27
BURE_2	10.6	1.93	2	II55MG25	0.21	0.06	31
BURE_3	10.7	2.00	2	II55MG25	0.18	0.04	20
Average	10.6	1.99	-	-	0.22	0.06	26
BURE_4	10.8	2.04	8	II55MG25	0.23	0.03	13
BURE_5	10.9	2.01	8	II55MG25	0.22	0.05	21
BURE_6	11.1	1.95	8	II55MG25	0.18	0.03	18
Average	10.9	2.00	-	-	0.21	0.04	17
BURE_7	11.3	1.94	2	II55NMG40-60	0.19	0.13	69
BURE_8	11.7	1.95	2	II55NMG40-60	0.17	0.09	55
BURE_9	9.5	2.04	2	II55NMG40-60	0.24	0.09	39
Average	10.8	1.98	-	-	0.20	0.11	55
BURE_10	9.8	2.05	8	II55NMG40-60	0.26	0.16	59
BURE_11	9.4	2.07	8	II55NMG40-60	0.23	0.19	83
BURE_12	9.2	2.07	8	II55NMG40-60	0.30	0.24	79
Average	9.5	2.06	-	-	0.26	0.20	74

Figure 6.8 presents the load-deflection curves of the medium-scale specimens both before and after being repaired by injection. For the case of the specimens repaired with grout II55MG25, the low performance of the strength recover is evident, but the curves also show a strong reduction in stiffness. Regarding the curves of the specimens repaired with grout 55IINMG40-60, this reduction is present, but it is not so evident, especially in the case of specimens with d_{cr}= 8 mm. Another important observation to be made is that the specimens before and after injection present similar deformability capacity (see Annex C for more details).

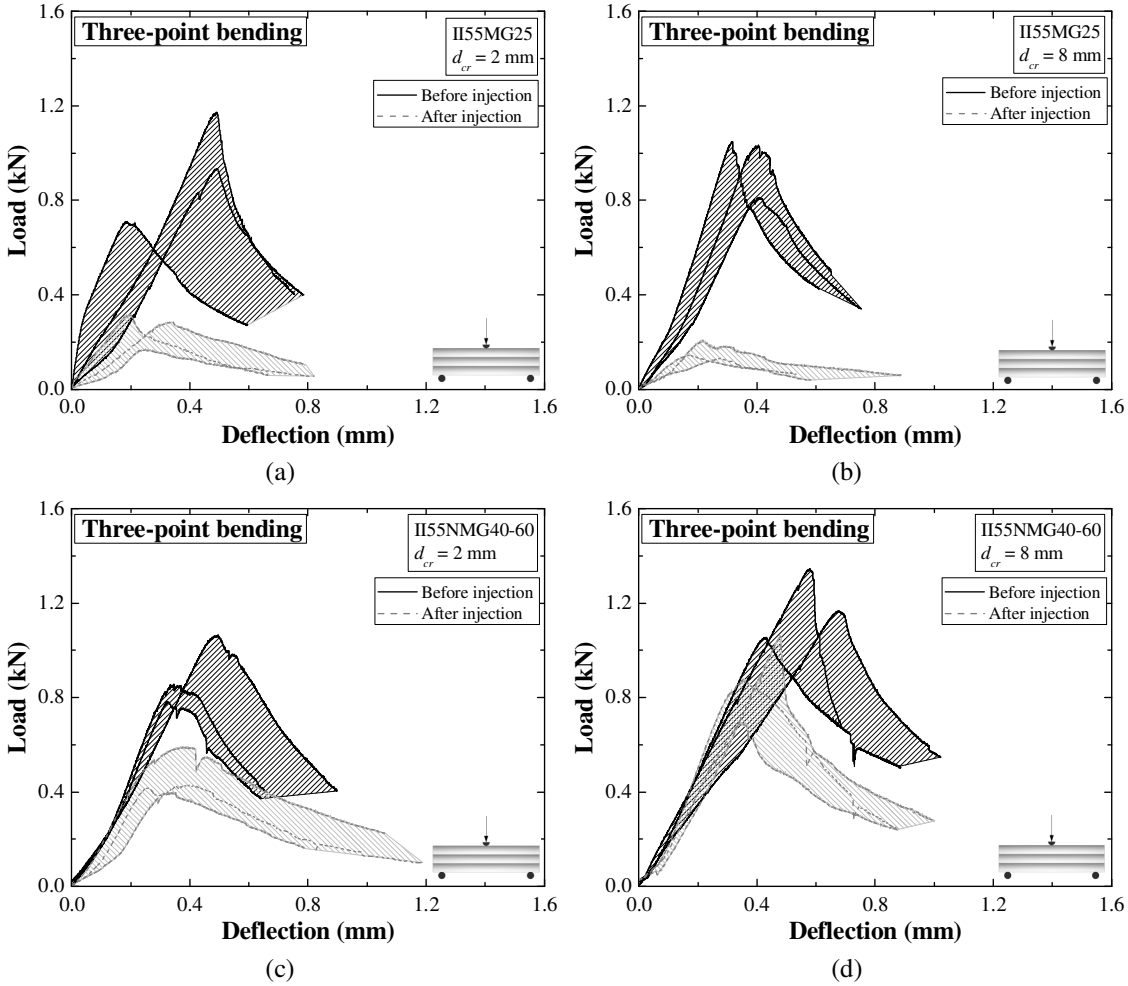

Figure 6.8 – Load–deflection curves of the medium-scale specimens: (a) grout II55MG25 and d_{cr} = 2 mm; (b) grout II55MG25 and d_{cr} = 8 mm; (c) grout II55NMG40-60 and d_{cr} = 2 mm; (d) grout II55NMG40-60 and d_{cr} = 8 mm.

Table 6.7 to Table 6.10 present illustrations of the failure surfaces of the beam-specimens tested after repair and provide comments about the failure surfaces at the tensile zone of each specimen (corresponds to the interior zone of the photo of the failure surface, as is highlighted). It should be noted that all specimens presented full injection of the crack and that no gaps were detected.

Regarding the specimens repaired with grout II55MG25, it is shown that the failure occurs mostly at the interface mud grout/rammed earth, but there are cases where it occurs inside the grout. In the first situation, this means that the adhesion capacity of the grout was the limiting property, while the second situation means that the tensile strength of the mud grout was the limiting property. However, the flexural strength of grout II55MG25 fairly exceeds the flexural strength of the rammed earth specimens in about 2.8 times, whereby failure through the grout should not be happening. The occurrence of cracking due to shrinkage may explain a reduction of the strength of the grout and thus its poor performance for the situations imparting this failure mode.

Table 6.7 – Failure surfaces of the medium-scale specimens repaired with grout II55MG25 and d_{cr} = 2 mm (the tensile zone is highlighted).

Specimen	Failure surface photos	f_{bg}/f_{bi} (%)	Comments
BURE_1	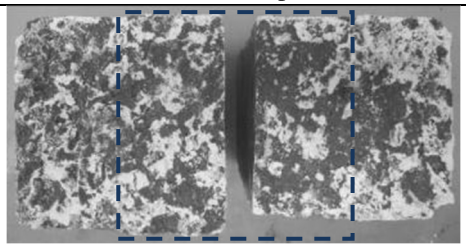	27	Failure at the tensile zone occurring mostly at the interface mud grout/rammed earth.
BURE_2	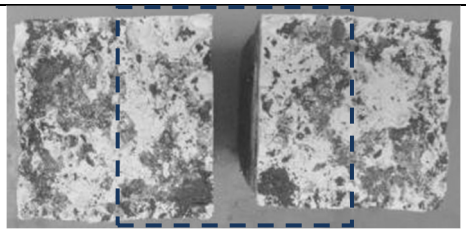	31	Failure at the tensile zone occurring mostly inside the mud grout.
BURE_3	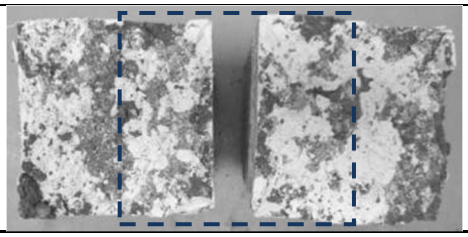	20	Failure at the tensile zone occurring mostly by the mud grout.

Table 6.8 – Failure surfaces of the medium-scale specimens repaired with grout II55MG25 and d_{cr} = 8 mm (the tensile zone is highlighted).

Specimen	Failure surface photos	f_{bg}/f_{bi} (%)	Comments
BURE_4	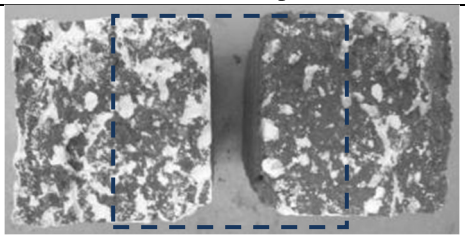	13	Failure at the tensile zone occurring mostly at the interface mud grout/rammed earth.
BURE_5	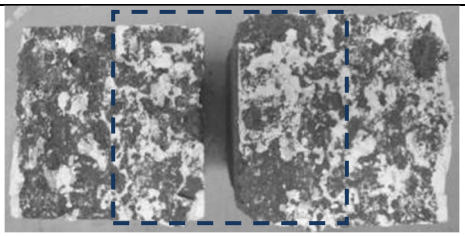	21	Failure at the tensile zone occurring inside the mud grout and at the interface mud grout/rammed earth.
BURE_6	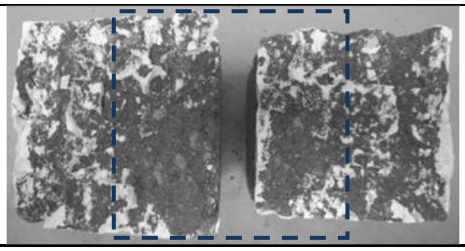	18	Failure at the tensile zone occurring mostly at the interface mud grout/rammed earth.

Table 6.9 – Failure surfaces of the medium-scale specimens repaired with grout II55NMG40-60 and d_{cr} = 2 mm (the tensile zone is highlighted).

Specimen	Failure surface photos	f_{bg}/f_{bi} (%)	Comments
BURE_7	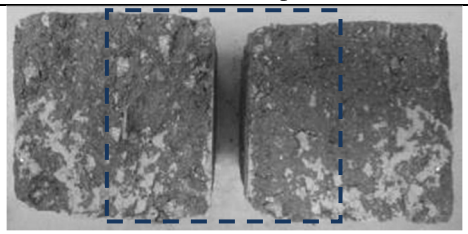	69	Failure at the tensile zone occurring mostly inside the rammed earth.
BURE_8	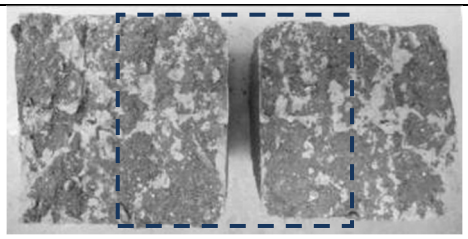	55	Failure at the tensile zone occurring partially inside the rammed earth and mud grout, and at the interface grout/rammed earth.
BURE_9	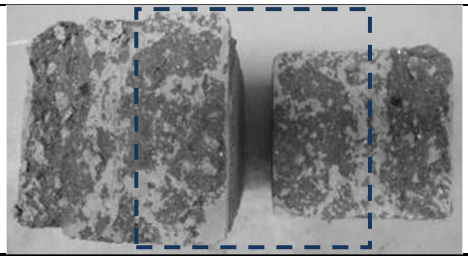	39	Failure at the tensile zone occurring partially inside the rammed earth and mud grout, and at the interface grout/rammed earth.

Table 6.10 – Failure surfaces of the medium-scale specimens repaired with grout II55NMG40-60 and d_{cr} = 8 mm (the tensile zone is highlighted).

Specimen	Failure surface photos	f_{bg}/f_{bi} (%)	Comments
BURE_10	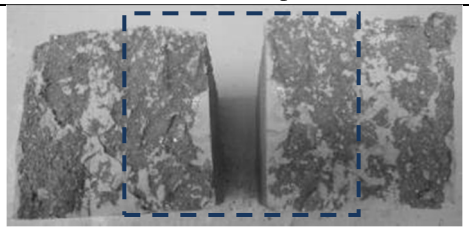	59	Failure at the tensile zone occurring partially inside the rammed earth and mud grout.
BURE_11	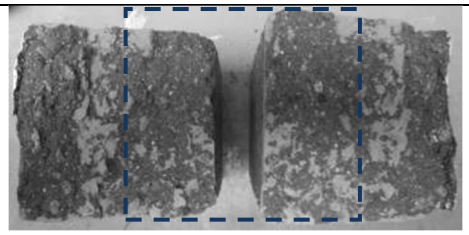	83	Failure at the tensile zone occurring partially inside the rammed earth and at the interface mud grout/rammed earth.
BURE_12	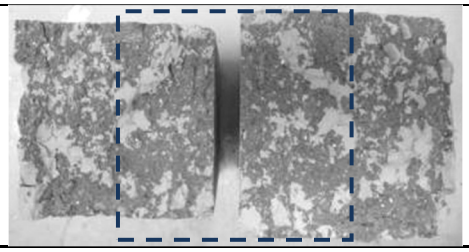	79	Failure at the tensile zone occurring partially inside the rammed earth and at the interface mud grout/rammed earth.

The situations imparting failure at the interface mud grout/rammed earth are the most frequent and evidence a very limited adhesion capacity. This may be explained by the

discussed shrinkage cracking or by the poor adhesion capacity of the clay fraction composing the grout, which is acknowledged to differ from that of the rammed earth specimens. Therefore and taking into account that the strength recovery rate of the medium-scale specimens was very low, this may lead to conclude that grout II55MG25 may not be adequate for a repair intervention on rammed earth manufactured with soil S6.

The failure of the specimens repaired with grout II55NMG40-60 occurred mostly by failure of the rammed earth, mixed in some cases with failure at the interface mud grout/rammed earth. The occurrence of the first failure mode means that the grout II55NMG40-60 presents a great adhesion capacity, which would theoretically indicate total recovery of the flexural strength of the specimens. However and despite the satisfactory recovery rate achieved by this mud grout, all specimens were far from achieving 100%. This aspect is mostly probably related to a weakness of the rammed earth material nearby the crack during the first test.

6.3 Adhesion tests on large-scale specimens

The large-scale tests carried out on rammed earth specimens aimed mainly at characterizing the adhesion capacity in shear of two mud grouts. Due to the poor performance of the "artificial" mud grout II55MG25, another "natural" mud grout was considered instead. This new grout II55NMG50-50 incorporated the same components of grout II55NMG40-60, but different proportions of sieved soil S5 and limestone powder Micro 200-OU were adopted.

The large-scale rammed earth specimens consisted of wallet-specimens tested under diagonal-compression and then repaired by grout injection in order to be later on re-tested. Again, this procedure allowed evaluating the recovery ratio promoted by each grout, which is intimately related to its adhesion capacity.

6.3.1 Manufacture of the specimens

The shear behaviour of the rammed earth preformed with soil S6 was assessed by means of diagonal-compression tests carried out on eleven wallet-specimens with dimensions 550x550x200 mm^3. Again, the water contents of the materials composing soil S6 were considered by the microwave oven method (ASTM D 4643: ASTM 2000c) in the several mixtures prepared to manufacture the specimens. Figure 6.9 presents a comparison between the oven and the microwave oven methods to determine the water content in the manufacture of the wallet- specimens. This confirms that both methods diverge slightly for the materials with higher clay content, as previously discussed in Section 6.3.1.

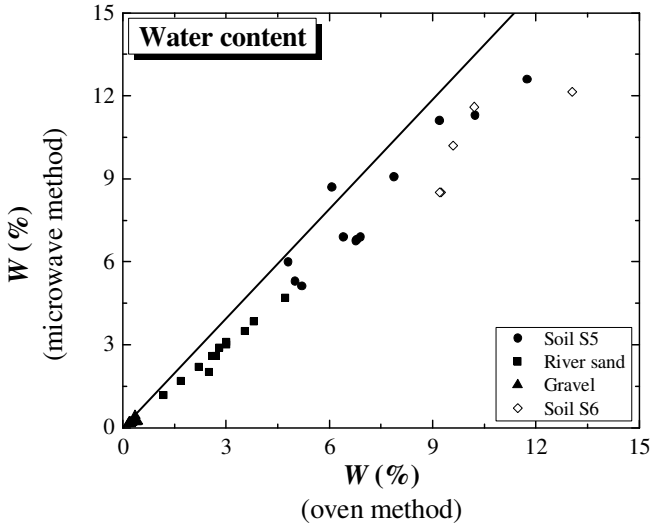

Figure 6.9 – Comparison between the oven and microwave oven heating methods for determination of the water content in the manufacture of the large-scale specimens.

The manufacture of each specimen corresponded to the preparation of a soil mixture, which was carried out manually according to the same procedure adopted for manufacturing the medium-scale specimens (see Section 6.2.1). The addition of water to the soil mixture (soil S6) was also controlled by means of the drop test.

Figure 6.10 illustrates the manufacture process of the large-scale specimens. The wallets were compacted in a high density plywood formwork, which was assembled by tightening its elements resorting to screw clamps. The formwork shutters were reinforced and stiffened by means square timber poles placed horizontally tightened to them. The formwork was of easy assembling and disassembling, which allowed demoulding the specimens immediately after compaction and to reuse the formwork in the manufacture of the next specimen. Only the base plywood board was not reused, as it was kept with each specimen for transportation purposes within the laboratory.

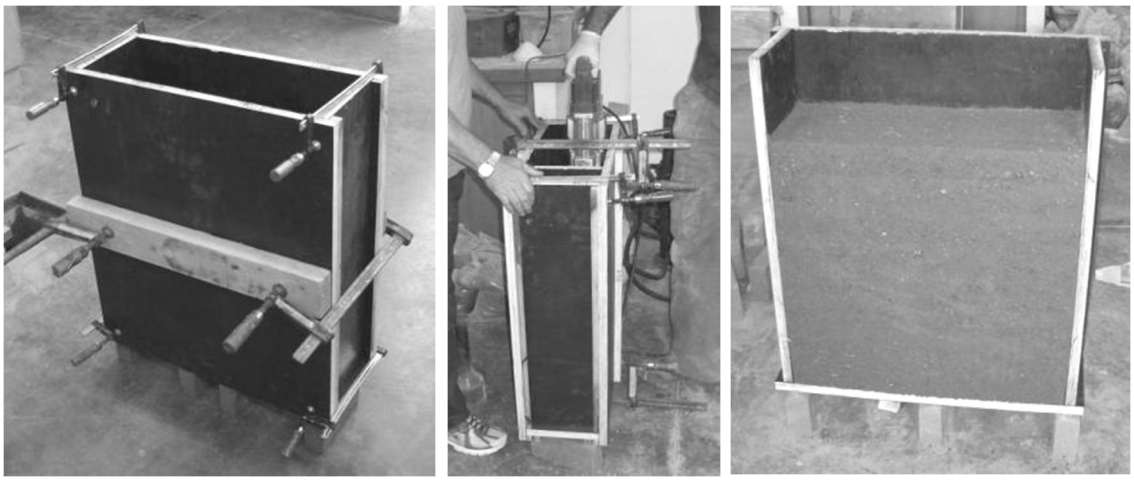

(a) (b) (c)

Figure 6.10 – Manufacture of the wallet-specimens: (a) plywood formwork; (b) compaction by electric rammer; (c) demoulding.

The formwork was oiled in advance and the compaction of the specimen was carried out by means of an electric rammer equipped with a compaction plate of dimensions 145x145x5 mm^3. Each specimen was compacted in nine layers by controlling both the layer thickness and its weight of wet soil S6. The layers thickness was similar for all layers (about 61 mm) and the weight of wet soil was fixed as 15.45 kg for each layer, independently of the water content of the mixture.

6.3.2 Testing procedure

The wallets were first tested under diagonal-compression after drying for about 12 weeks at a room temperature of about 22±2ºC. The test setup is presented in Figure 6.11 and the testing procedure was carried out according to ASTM E 519 (ASTM 2002b). The supports were made of steel, with a width of about 100 mm, and the contact with the specimens was uniformed by means of neoprene rubbers introduced between the specimens and the supports. The load was applied under monotonic displacement control at a rate of 0.002 mm/s and the vertical and horizontal displacements were measured in both faces of the wallets, resorting to LVDTs attached to the middle third of each diagonal (see Figure 6.11). The same testing procedure was followed for the repaired wallets, which were tested 5 weeks after injection.

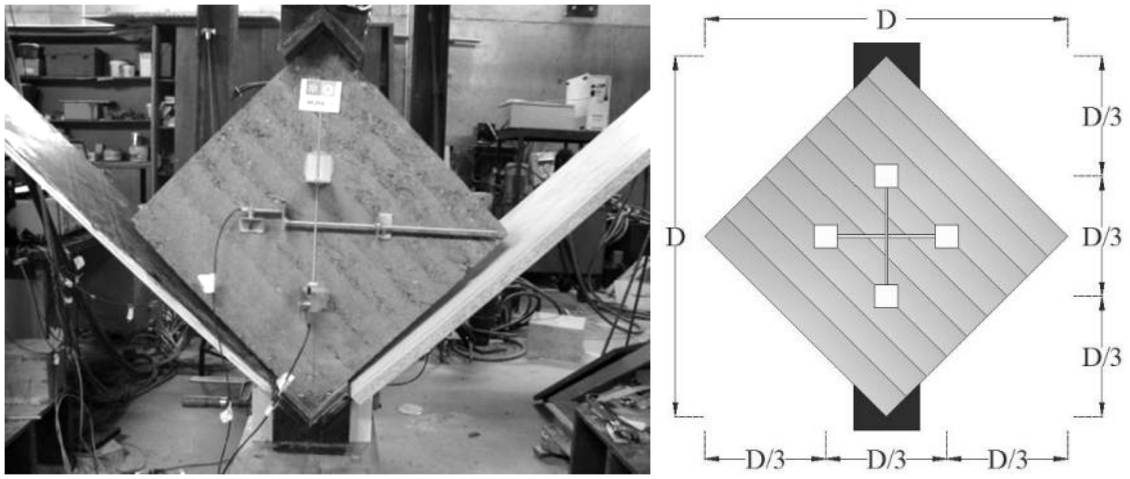

Figure 6.11 – Test setup of the diagonal compression tests carried out on the rammed earth large-scale specimens.

6.3.3 Repair procedure

The failure of the wallets resulted in its division into some parts, which were removed from the testing apparatus and remounted together on the respective base plywood board. Before the wallets being remounted, the loose debris were removed from the failure surfaces. The assembling of the specimens was carried out with the aid of an earth mortar prepared with soil S5 sieved through the ASTM sieve #4 (particles size below 4.75 mm). The remounting was performed by simple putting piece by piece like masonry whenever possible (Figure 6.12a), and when the specimen presented instability it was tied by means of two plywood boards (Figure 6.12b).

The abovementioned mortar was also used to seal the cracks (gaps between the specimen parts), by penetrating about 20 mm from the respective face surface of the wallets (Figure 6.12c). Flexible plastic tubes with 6 mm diameter were installed in one of the sides of the specimens in such way that they would penetrate about 4 cm in the wallet. It should be noted that in a real intervention, the injection tube should deliver the grout at the middle of the wall, meaning that the injection tube should penetrate up to the middle thickness of the wall. However, by delivering the grout near the surface of the wallets and from a single side, it was intended to evaluate eventual difficulties relative to the penetration of the mud grout in the crack, namely in the injection of real walls that are in general thicker than the tested wallets. The injection tubes were installed first in the intersection of cracks and then along the cracks, in such way that the spacing between injection tubes would be less than 100 mm. In the case of horizontal cracks, additional injection tubes were installed in the other side of the wallets in order to merely facilitate the air evacuation, whereby they were not used for injection of the respective mud grouts.

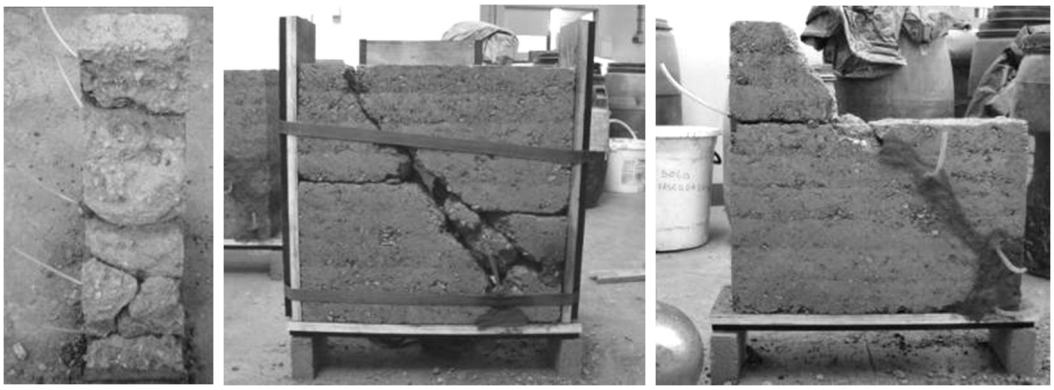

(a) (b) (c)

Figure 6.12 – Remounting of the specimens: (a) simple remounting by application of mortar at the cracks near the surface and introduction of injection tubes; (b) tying by two opposite boards; (c) sealing of the cracks with earth mortar.

Two “natural” mud grouts were used to repair the wallets, namely the mud grouts II55NMG40-60 and II55NMG50-50. The first was also used to repair part of the medium-scale specimens (see Section 6.2.3) and the second was introduced to substitute the “artificial” mud grout II55MG25, which had poor performance. Both “natural” grouts incorporate the same materials, but in the case of grout II55NMG50-50 an higher percentage of sieved soil S5#80 over the limestone powder Micro 200-OU percentage was included. The composition of both grouts is summarised in Table 6.11, the respective PSD curves are plotted in Figure 6.13 and the respective size-fractions percentages are summarised in Table 6.12. The clay percentage of the mud grout II55NMG50-50 is obviously higher than that of grout II55NMG40-60, whereby its inclusion in the experimental program intended to assess if this feature improves the performance of the repair by grout injection. The solid fraction and HMP/C ratio of the grout II55NMG50-50 were similar to those of grout II55NMG40-60, respectively 55% and 0.022 g/g.

Table 6.11 – Composition of the "natural" mud grouts used to repair the large-scale specimens.

Mud Grout	S5#80 (wt.%)	L. 200-OU (wt.%)	HMP/C (g/g)	ϕ_v (%)	*W/S*
II55NMG40-60	40	60	0.022	55	0.30
II55NMG50-50	50	50	0.022	55	0.30

Table 6.12 – Size-fractions percentages of the mud grouts IINMG40-60 and IINMG50-50.

Mud Grout	% Clay	% Silt	% Sand
II55NMG40-60	21	62	17
II55NMG50-50	25	59	16

Clay: <0.002 mm / silt: ≥0.002 mm and <0.060 mm / sand: ≥0.060 mm and <2.0 mm

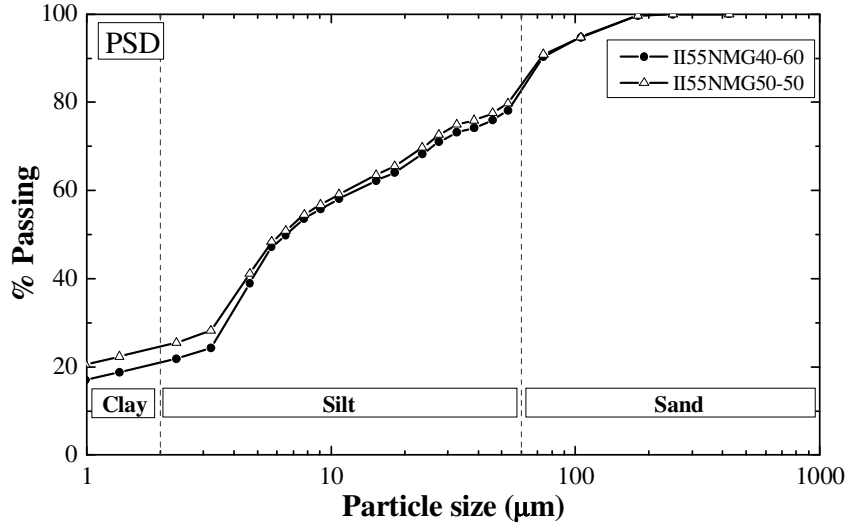

Figure 6.13 – PSD curves of the mud grouts IINMG40-60 and IINMG50-50.

The preparation of each grout mixture required first weighing the solid components into a plastic bucket in order to prepare a grout volume of about 5 dm^3. The HMP was dissolved in the water necessary to prepare the grout, which was then added completely to the solid components in the bucket. This blend was first hand mixed (with a trowel) just to allow the water involving the solid components, and then was mixed with an electrical hand grout mixer at maximum rotation speed (about 700 rpm) by 5 minutes (Figure 6.14a). The mixtures were then sieved through ASTM sieve #10 (aperture size of about 2 mm) to remove agglomerates of particles.

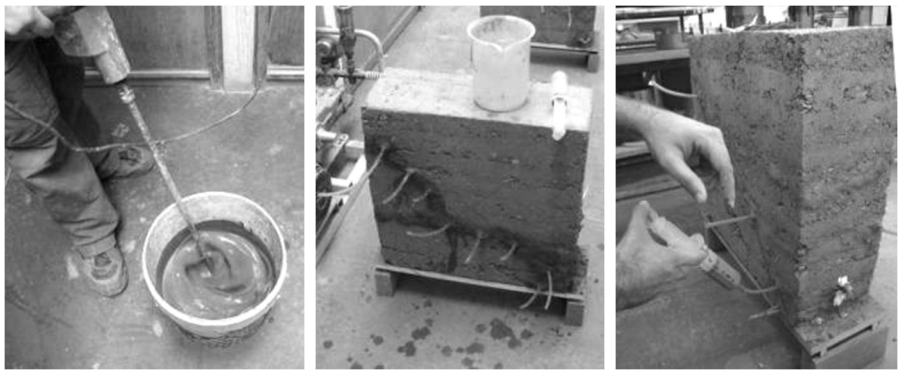

(a) (b) (c)

Figure 6.14 – Repair of the wallets by grout injection: (a) mud grout mixing; (b) injection of water; (c) injection of the mud grout.

The properties of both "natural" mud grouts were tested and the average results are summarised in Table 6.13, in terms flow time of 1 dm^3 of the grout (ASTM C 939: ASTM 1994), dry density (ρ_d), volumetric shrinkage (S_v), flexural strength (f_b) and compressive strength (f_c) (EN 1015-11: CEN 1999). It should be noted that the higher clay content of grout II55NMG50-50 had almost no interference on the flow time, when comparing with grout II55NMG40-60. Regarding the mechanical properties, grout II55NMG50-50 is clearly stronger than grout II55NMG40-60, but the volumetric shrinkage is also higher.

Table 6.13 – Properties of the mud grouts used to repair the large-scale specimens.

Mud Grout	Flow time (s)	ρ_d (kg/m^3)	S_v (%)	f_b (N/mm^2)	f_c (N/mm^2)
II55NMG40-60	36.5	1789	13.2	0.92	2.44
II55NMG50-50	37.0	1814	15.6	1.15	3.47

Before injecting the wallets with the respective mud grout, 100 ml of water were injected in each injection tube, using a 100 ml capacity syringe (Figure 6.14b). This procedure intended to mitigate the water sorption by the wallets and to test if the injection tubes were active. This procedure is an important step to be carried out in a real intervention, since excessive water sorption by the rammed earth material may cause clogging at the head of the injection grout in a crack. The wallets were then injected with the mud grouts one hour after injecting the water. The previously referred 100 ml syringe was also used to inject the wallets with the mud grouts. The injection started by the lowest tube up to the top of the wallet. The tube being injected was sealed once the grout leaked from the next injection tube (normally that immediately above). The injection was then carried out from the leaking tube, and so on (Figure 6.14c). The occurrence of leakages from the sealing mortar was not very frequent and was easily solved using toilet paper pressed against the leaking crack.

Table 6.14 presents the injection conditions of the wallets, where it can be seen that a total of five wallets were repaired with grout II55NMG40-60 and six wallets with grout II55NMG50-50. Moreover, the total length of injected cracks (L_{cr}) and the volume of injected grout (V_{mgi}) are reported for each wallet.

The L_{cr} is shown to be very variable (87-218 cm), meaning that the wallets also presented very different levels of damage after the first test. The average crack width (d_{acr}) was computed assuming that the cracks were completely filled by the grout, that the leaked mud grout was insignificant (meaning that the total gap volume is considered as equal to V_{mgi}) and that the effective thickness of the injected material at the crack was of about 16 cm (by discounting two times the penetration length of the sealing mortar to the thickness of the wallets). In average terms d_{acr} is of about 1.0 cm, however it should be noted that the width along the cracks is very variable, as can be seen in Figure 6.12b. This means that cracks much thicker or thinner than 1.0 cm were injected, as is highlighted in the next Section.

Table 6.14 – Injection conditions of the wallets.

Wallet	Grout	L_{cr} (cm)	V_{mgi} (cm^3)	d_{acr} (cm)
WURE_1	II55NMG40-60	146	2300	1.0
WURE_2	II55NMG40-60	146	1980	0.8
WURE_3	II55NMG40-60	100	1974	1.2
WURE_4	II55NMG40-60	104	1542	0.9
WURE_5	II55NMG50-50	118	1400	0.7
WURE_6	II55NMG50-50	218	3974	1.1
WURE_7	II55NMG50-50	111	2150	1.2
WURE_8	II55NMG50-50	116	2300	1.2
WURE_9	II55NMG50-50	87	1990	1.4
WURE_10	II55NMG50-50	120	1922	1.0
WURE_11	II55NMG40-60	115	1408	0.8

6.3.4 Results and discussion

The results of the tests carried out on the sets of large-scale specimens injected with grout II55NMG40-60 and grout II55NMG50-50 are summarised in Table 6.15 and Table 6.18, respectively, in terms of compaction water content determined by the oven method (W), dry density (ρ_d), initial shear strength (f_{si}), shear strength after grout injection (f_{sg}) and the shear strength recovery rate f_{sg}/f_{si}, shear modulus before injection (G_{0i}), shear modulus after injection (G_{0g}) and shear modulus recovery rate (G_{0g} /G_{0i}).

Both shear stresses (f_{si} and f_{sg}) were computed according to ASTM E519 (ASTM 2002), by using Equation (6.1):

$$f_s = \frac{0.707P}{\left(\frac{w+h}{2}\right)t} \tag{6.1}$$

where f_s is the shear strength, P the maximum applied load, w the width, h the height and t the thickness of the specimen.

Both shear modulus values (G_{0i} and G_{0g}) were computed by linear fitting of the respective shear stress - shear strain curve between 5% and 30% of the shear strength, where the shear strain was computed using Equation (6.2):

$$\gamma = \frac{\Delta V + \Delta H}{\left(\frac{L_v + L_h}{2}\right)} \tag{6.2}$$

where γ is the shear strain, ΔV the average vertical shortening, ΔH the average horizontal extension, L_v the average gauge length of the vertical LVDTs and L_h the average gauge length of the horizontal LVDTs.

Table 6.15 – Results of the diagonal-compression tests carried out on the wallets repaired with grout II55NMG40-60.

Wallet	W (%)	ρ_d (g/cm^3)	f_{si} (N/mm^2)	f_{sg} (N/mm^2)	f_{sg}/f_{si} (%)	G_{0i} (N/mm^2)	G_{0g} (N/mm^2)	G_{0g}/G_{0i} (%)
WURE_1	10.0	2.02	0.17	0.07	39	659	67	10
WURE_2	9.2	2.06	0.16	0.15	93	705	53	8
WURE_3	9.2	2.04	0.13	0.06	43	413	47	11
WURE_4	10.2	2.03	0.14	0.09	68	341	54	16
WURE_11	10.7	2.04	0.14	0.12	89	732	142	19
Average	9.9	2.04	0.15	0.10	66	570	73	13
COV (%)	6	1	10	40	38	32	54	37

Table 6.16 – Results of the diagonal-compression tests carried out on the wallets repaired with grout II55NMG50-50.

Wallet	W (%)	ρ_d (g/cm^3)	f_{si} (N/mm^2)	f_{sg} (N/mm^2)	f_{sg}/f_{si} (%)	G_{0i} (N/mm^2)	G_{0g} (N/mm^2)	G_{0g}/G_{0i} (%)
WURE_5	9.6	2.01	0.11	0.09	77	464	89	19
WURE_6	13.1	1.97	0.14	0.07	52	646	33	5
WURE_7	10.6	2.02	0.17	0.09	55	640	29	5
WURE_8	11.4	2.03	0.13	0.09	68	1036	73	7
WURE_9	11.7	2.02	0.14	0.07	54	807	66	8
WURE_10	9.1	2.04	0.19	0.09	46	661	45	7
Average	10.9	2.01	0.15	0.08	59	709	56	8
COV (%)	13	1	19	10	20	27	43	64

Regarding the dry density of the rammed earth wallets, it is shown to also deviate from the maximum dry density of soil S6. This difference can be explained by difficulties in reproducing the PSD of soil S6 (errors associated to estimation of the water content by the microwave oven method), compaction water contents different from OWC and deformations of the plywood formwork.

The average shear strength before injection in both sets of wallets was of about 0.15 N/mm^2, but the results present some variability when comparing with the results obtained for the compressive strength. The shear strength of rammed earth is a topic almost absent from specialized references. However, Lacouture *et al.* (2007) report an average value of about 0.04 N/mm^2 from an experimental program carried out in Colombia, which is considerable lower than that reported in this experimental program. It should be noted that the compressive strength reported by Lacouture *et al.* (2007) was also considerably lower (0.55 N/mm^2) than that reported in Section 5.7.1. The shear strength here reported for rammed earth is also significantly higher than that reported for adobe masonry by Lacouture *et al.* (2007) and Varum *et al.* (2011), which varied between 0.02 N/mm^2 and 0.03 N/mm^2. This low performance of adobe masonry is obviously explained by the fact that the mortar joints constitute a weak point of preferential failure, where the adhesion capacity of the mortar is a limiting property.

The shear strength of the wallets after being repaired by injection is in average of about 0.10 N/mm^2 and 0.08 N/mm^2, respectively for the case of the set of wallets repaired

with grout II55NMG40-60 and that repaired with II55NMG50-50. The average shear strength recovery rate was of about 66% for the first grout and of about 59% for the second, distant from the total shear strength recovery (100%). However, it should be noted that, in practice, this goal can be hardly achieved, since the wallets are expected to present damage at a micro level (ex: micro-cracking), which was not possible to be repaired with the injection. Despite that, both grouts presented a satisfactory performance regarding the adhesion capacity. Another important observation to be highlighted is that the grout II55NMG50-50 did not promote a higher recovery rate, as it would be expected due to its higher strength. Instead, both grouts presented similar performance, indicating that a higher clay percentage in the grout did not promote higher adhesion capacity.

The shear stress-shear strain curves of the wallets before and after injection are presented in Figure 6.15. Regarding the behaviour of both sets of wallets before repair (Figure 6.15a and c), it is observed that most of the wallets present an early peak shear stress, after which the shear strain has a fast increase. This early peak shear stress is thought to be related to cohesion (or in other words, to the binding capacity) promoted by the clay fraction. In fact, the shear behaviour of the wallets up to this peak stress results from the contribution of the clay fraction cohesion, and friction and interlocking capacity of the gravel-size (or larger) aggregates. After this point, the contribution of the cohesion is lost and the shear behaviour of the wallets relies only on the friction and interlocking. Moreover, some wallets present a hardening behaviour after this stress, which can be explained by a superior interlocking occurring in these wallets. Another important contribution of the friction and interlocking to the shear behaviour of the wallets is that all wallets (with exception of WURE_4) present large deformation capacity, and thus good ductility. This is an important feature for rammed earth in the case of a seismic event, which is expected to contribute for the energy dissipation.

Regarding the shear stress-shear strain curves of the wallets after injection (Figure 6.15b and d), it is observed a substantial decrease in stiffness relative to the performance before injection, no matter the grout used. According to Table 6.15 and Table 6.16, the average G_{0g} corresponds to an overall decrease of about one order of magnitude with respect to G_{0i} (see Annex C for more details). This important decrease may be explained by a less efficient interlocking and friction mechanisms in the wallets after repair. In fact, the interlocking at the failure surface in the first test of the wallets was provided by coarse aggregates, which were then lost in the reassembling of the specimens and not reintroduced by the injection. Therefore, this potential failure surface was smoothed by the first test reducing the friction of what is an obvious preferential failure surface for the second test. Moreover, the lower interlocking and friction of the repaired wallets can also be pointed out as a reason to explain a shear strength recovery that was shown to be relatively inferior to the total recovery.

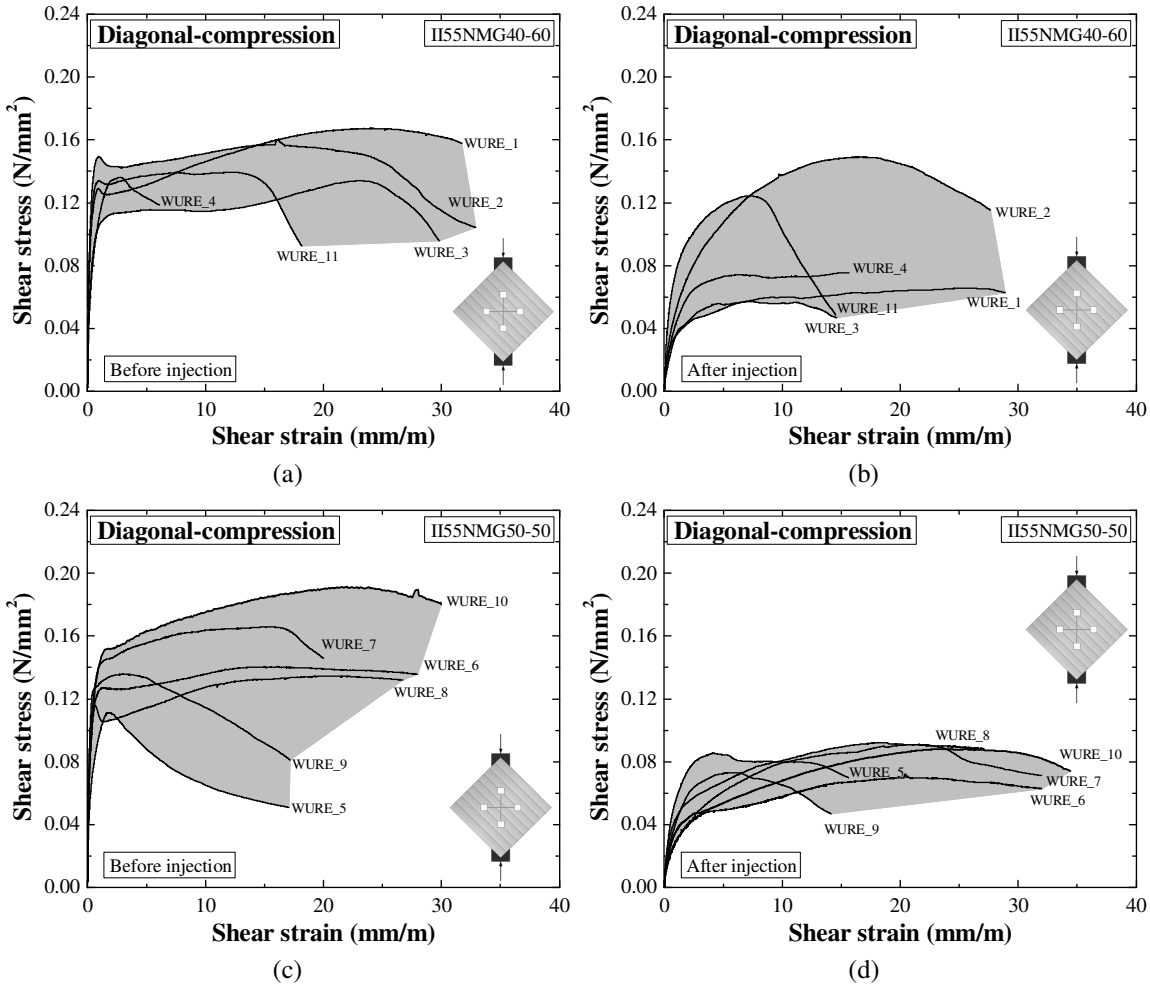

Figure 6.15 – Shear stress–shear strain curves of the wallets: (a) set repaired with grout II55NMG40-60 before injection; (b) set repaired with grout II55NMG40-60 after injection; (c) set repaired with grout II55NMG50-50 before injection; (d) set repaired with grout II55NMG50-50 before injection.

The failure crack patterns at the same face of the wallets before and after injection are illustrated in Figure 6.16 and Figure 6.17, respectively, for the sets repaired with grout II5NMG40-60 and II55NMG50-50. The failure of the wallets before injection occurred as consequence of the formation of a main crack or set of cracks with vertical orientation, which crossed diagonally the entire specimen. The formation of these cracks or set of cracks was observed visually to start before the peak load, at the middle of the specimens, and then they developed heading to the edges next to the top and bottom support. The cracking initiation of the specimens is given in Table 6.17 and Table 6.18, where $f_{s1cr,i}$ is the shear stress at the first crack initiation in the wallets before injection and $f_{s1cr,g}$ is the respective shear stress in the wallets after injection. The percentage relative to the shear strength of the wallets is also given and called $f_{s1cr,i}/f_{si}$ and $f_{s1cr,g}/f_{sg}$, respectively for the tests carried out before and after injection. Regarding the average $f_{s1cr,i}/f_{si}$, is shown to be very similar in both sets of wallets, respectively 86% and 84% for the wallets repaired with grout II55NMG40-60 and II55NMG50-50.

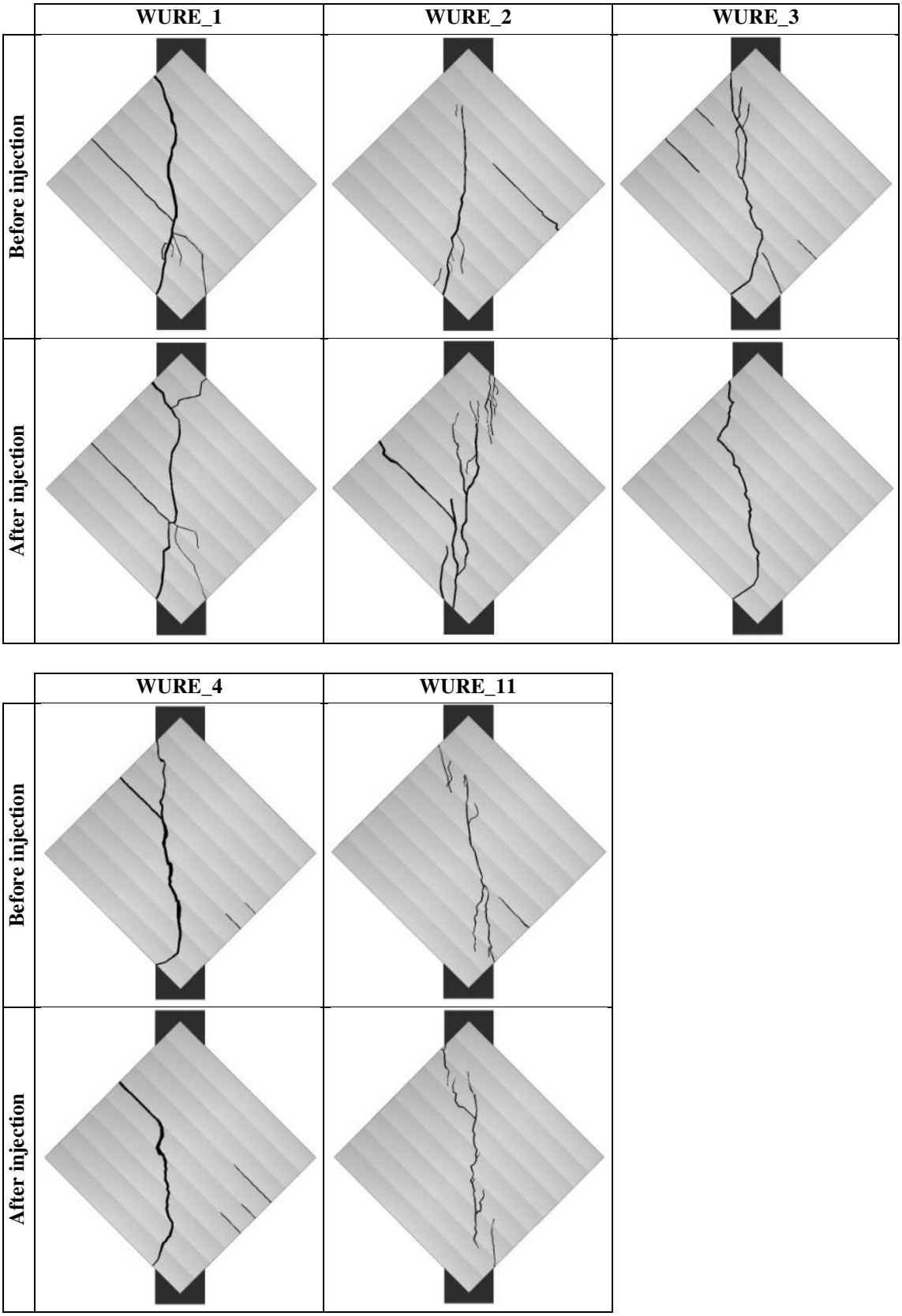

Figure 6.16 – Failure crack patterns of the wallets repaired with grout II55NMG40-60, before and after injection.

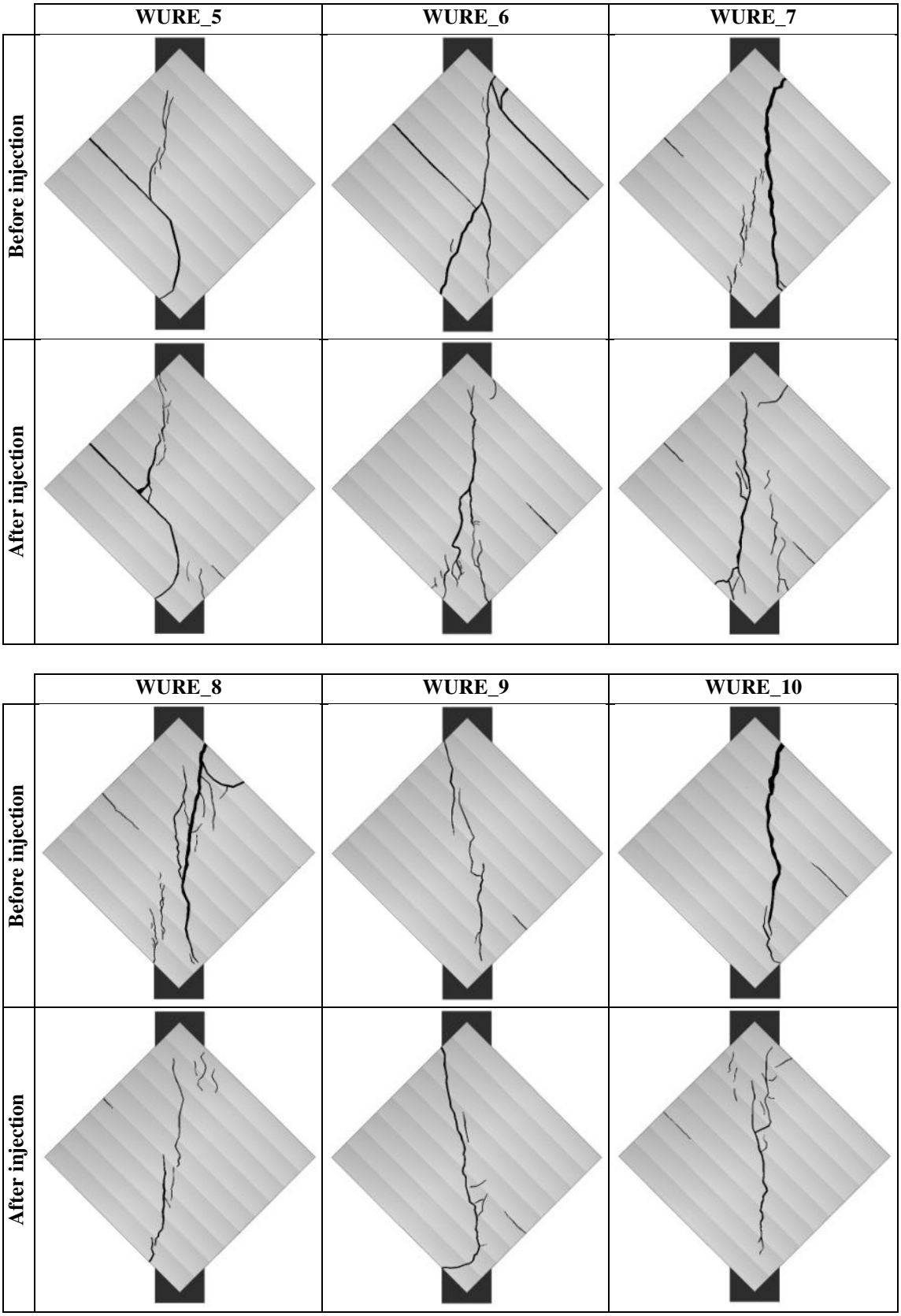

Figure 6.17 – Failure crack patterns of the wallets repaired with grout II55NMG50-50, before and after injection.

The illustrations of the crack patterns of the wallets also show some cracks occurring at the interface between layers, which propagate from the edges to the interior of the

wallets. This means that these interfaces constitute weak surfaces when the rammed earth is subjected to tension in the respective perpendicular direction, and thus the adhesion between layers is far from being perfect. It should be noted that the onset formation of these cracks occurred just before the failure of the specimens. However, this feature seems to have little importance regarding the shear behaviour of the wallets, since the previously referred main vertical crack or set of cracks, characterizing the failure, did not tend to follow these interfaces.

Table 6.17 – First crack initiation of the wallets repaired with grout II55NMG40-60 before and after injection.

Wallet	f_{si} (N/mm^2)	$f_{s1cr,i}$ (N/mm^2)	$f_{s1cr,i}/f_{si}$ (%)	f_{sg} (N/mm^2)	$f_{s1cr,g}$ (N/mm^2)	$f_{s1cr,g}/f_{sg}$ (%)
WURE_1	0.17	0.13	76	0.07	0.05	77
WURE_2	0.16	0.14	88	0.15	0.10	64
WURE_3	0.13	0.11	82	0.06	0.03	56
WURE_4	0.14	0.13	94	0.09	0.06	68
WURE_11	0.14	0.13	92	0.12	0.05	41
Average	0.15	0.13	86	0.10	0.06	61
COV (%)	10	9	8	40	40	22

Table 6.18 – First crack initiation of the wallets repaired with grout II55NMG50-50 before and after injection.

Wallet	f_{si} (N/mm^2)	$f_{s1cr,i}$ (N/mm^2)	$f_{s1cr,i}/f_{si}$ (%)	f_{sg} (N/mm^2)	$f_{s1cr,g}$ (N/mm^2)	$f_{s1cr,g}/f_{sg}$ (%)
WURE_5	0.11	0.10	86	0.09	0.06	74
WURE_6	0.14	0.12	88	0.07	0.05	69
WURE_7	0.17	0.14	85	0.09	0.05	57
WURE_8	0.13	0.10	77	0.09	0.05	56
WURE_9	0.14	0.13	95	0.07	0.06	79
WURE_10	0.19	0.14	73	0.09	0.05	58
Average	0.15	0.12	84	0.08	0.05	65
COV (%)	19	16	9	10	10	15

The repair by injection mainly consisted in injecting the cracks represented on the failure crack pattern of the first test. However, it should be noted that further cracks were injected, since other cracks (not detected visually) were revealed during the dismounting of the specimens (especially cracks at the interfaces between layers). The crack patterns of the wallets tested after injection seem to follow that of the respective wallet in the test before injection. This shows that the region around the injected cracks (includes rammed earth, mud grout and mud grout/rammed earth interface) is a region of preferential failure in the second test. This is a consequence of the impossibility of the mud grout in repairing the micro-damage in the rammed earth caused by the first test, and the partially lost interlocking and the friction capacity, as previously discussed. Regarding the cracking initiation, it should be referred that it occurred sooner than in the first test, since $f_{s1cr,g}/f_{sg}$ is of about 61% and 65% for the set repaired with grout II55NMG40-60 and II55NMG50-50, respectively.

Table 6.19 and Table 6.20 illustrate the failure surfaces of the wallets repaired with grout II55NMG40-60 and II55NMG50-50, respectively. Moreover, comments on these surfaces are given, namely regarding the material by which the failure occurred, minimum width of the injected cracks and existence of gaps or non injected cracks.

Table 6.19 – Failure surfaces of the wallets repaired with grout II55NMG40-60.

Wallet	Photos of the failure surfaces	f_{sg}/f_{si} (%)	Comments
WURE_1	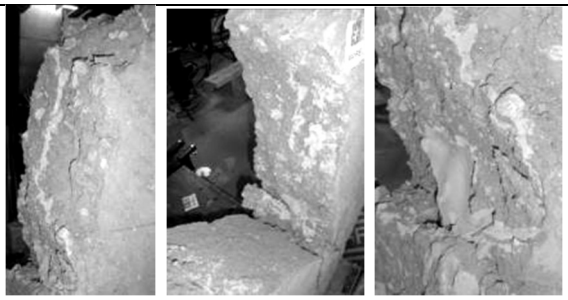	39	Failure occurred both in the rammed earth and at the grout/rammed earth interface. Observation of the injection of cracks with a minimum width of about 4 mm. Observation of a gap in the grout caused by its migration.
WURE_2	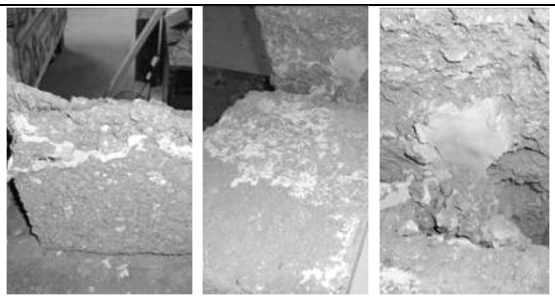	93	Failure occurred mainly in the rammed earth, but also occurred at the grout/rammed earth interface at one of the interfaces between layers. Observation of the injection of cracks with a minimum width of about 4 mm. Observation of a gap in the grout caused by its migration.
WURE_3	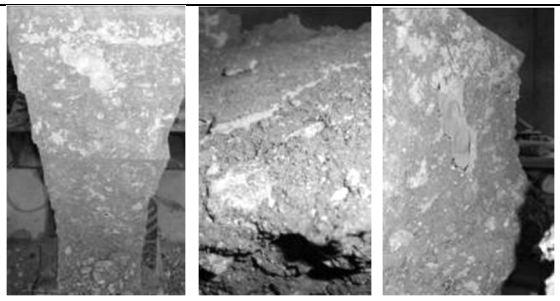	43	Failure occurred both in the rammed earth and at the grout/rammed earth interface. Observation of the injection of cracks with a minimum width of about 2 mm. Observation of a gap in the grout caused by its migration.
WURE_4	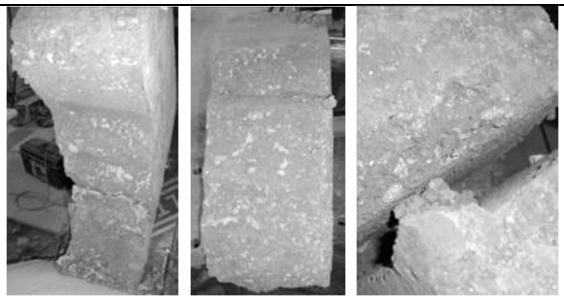	68	Failure occurred both in the rammed earth and at the grout/rammed earth interface. Observation of the injection of cracks with a minimum width of about 2 mm. The repaired interface between layers was only partially injected. No gaps in the grout were observed.
WURE_11	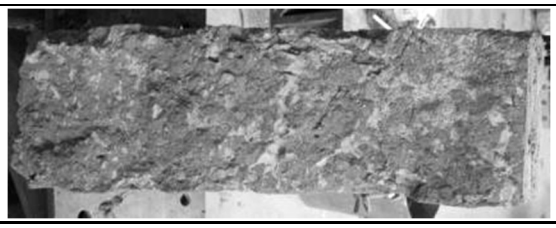	89	Failure occurred both in the rammed earth and at the grout/rammed earth interface. Observation of the injection of cracks with a minimum width of about 4 mm. No gaps in the grout were observed.

Table 6.20 – Failure surfaces of the wallets repaired with grout II55NMG50-500.

Wallet	Photos of the failure surfaces	f_{sg}/f_{si} (%)	Comments
WURE_5		77	Failure occurred mainly in the rammed earth, but also at the grout/rammed earth interface. Observation of the injection of cracks with a minimum width of about 1-2 mm. Observation of a minor gap in the grout caused by its migration.
WURE_6	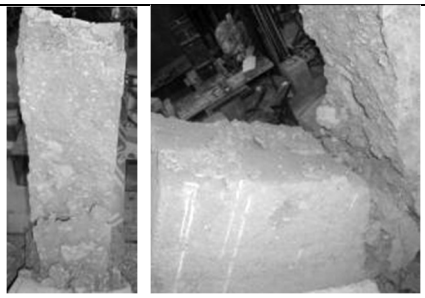	52	Failure occurred mainly in the rammed earth. Observation of the injection of cracks with a minimum width of about 2 mm. An important gap was detected in the grout.
WURE_7	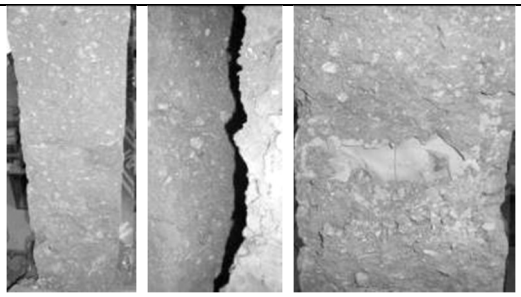	55	Failure occurred mainly in the rammed earth. Observation of the injection of cracks with a minimum width of about 2 mm. Observation of a gap in the grout caused by its migration, located at one of the failure surfaces.
WURE_8	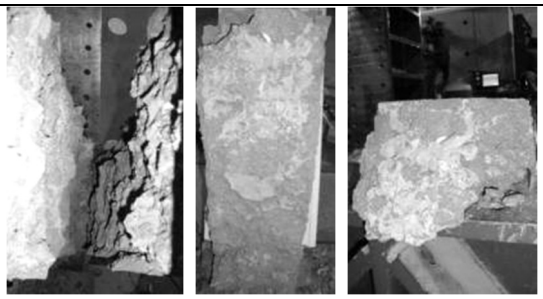	68	Failure occurred both in the rammed earth and grout/rammed earth interface. Observation of the injection of cracks with a minimum width of about 4 mm. Observation of a minor gap in the grout caused by its migration.
WURE_9	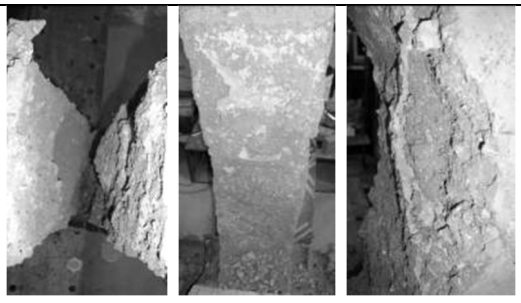	54	Failure occurred mainly in the rammed earth, but also at the grout/rammed earth interface. Observation of the injection of cracks with a minimum width of about 4 mm. Observation of a minor gap in the grout caused by its migration.
WURE_10	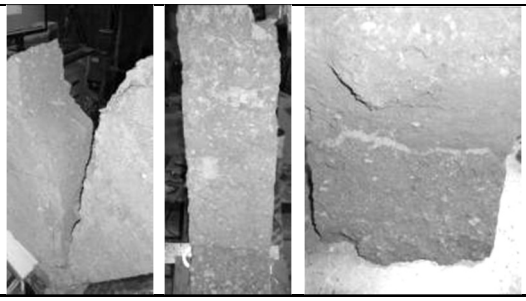	46	Failure occurred mainly in the rammed earth, but also at the grout/rammed earth interface. Observation of the injection of cracks with a minimum width of about 4 mm. Observation of minor gaps in the grout caused by its migration.

In general, the failure occurred both in the rammed earth and at the grout/rammed earth interface, but in some wallets the first case was predominant. This means that both grouts presented, in general, a good adhesion capacity and that the shear strength of the wallets was probably limited by micro-damage introduced during the first test.

The failure at the interface grout/rammed earth occurred mainly at the cracks in interfaces between layers. In these cases, the grouts were found to be always bonded to the bottom face of the crack. This is explained by the building process of the rammed earth, where the compaction of a layer results in a top region where the material is denser than that in the bottom region. Thus, the top region tends to be stronger than that of the bottom (Bui and Morel 2009). Moreover, it is reasonable to think that the top region is also stronger due to a migration of clay particles dragged by the water during the compaction of the layer. This also gives a higher cohesion to the top region surface than that in the bottom region surface, which is thus more prone to have the grout detached from it.

The observation of the failed wallets also allowed assessing the great difficulty in injecting the cracks at the interfaces between layers, which resulted from the first test of the wallets. The injection of these horizontal cracks is critical because of the difficulty in evacuating the air, as stated for wallet WURE_4. This wallet had one crack in an interface between layers that was only partially injected, despite the care taken in the injection process.

Gaps in the mud grout were also detected in the wallets, which probably contributed for a lower performance of some wallets after repair, since the failure surfaces tended to cross them. These gaps are probably associated to the injection of horizontal cracks, as they appear immediately above these cracks. The grout missing in the gap probably flowed towards these horizontal cracks, while the air was being evacuated by the pores of the rammed earth and sealing mortar, and while the mud grout was still fluid. The migration of the grout from the gaps may also have the contribution of compensations for possible volumetric shrinkage of the grout in regions of larger crack width, which thus demand larger volumes of grout. Nevertheless, its importance may be little when compared with the first reason, since a distributed gap presence along the injected cracks would be the expectable result.

Regarding the minimum width of the injected cracks, it was observed to vary between 1 mm and 4 mm. However, this does not mean that thinner cracks cannot be injected by the tested grouts. According to Miltiadou (1990), only cracks with width larger than three times the maximum particle size of the grout are injectable, which in the case of the tested grouts corresponds to 0.54 mm (3x0.180 mm). This shows a good penetrability capacity of the grouts employed.

6.4 Repair effectiveness assessment by means of UPV

One of the major challenges in an intervention involving grout injection is the assessment of its final quality and performance, i.e., to verify existence of non-filled gaps and cracks, and to estimate the repair/strengthening effectiveness. This assessment can be carried out by inspecting visually the injected region and by testing mechanically the injected elements. However, this requires, in general, damaging these elements, which is not desirable to occur by obvious reasons. In the last years, non-destructive techniques (NDT) and procedures have been developed with the aim of allowing an assessment of the quality and performance without destructive means.

In the case of two- and three-leaf masonry walls, their injection involves filling with grout gaps between leaves or a network of voids of an inner leaf (Toumbakari 2002). The success of the grout injection is then dictated by the complete filling of these gaps and voids, which can be assessed resorting to several NDTs, such as geo-electrical measurements (Schueremans *et al.* 2003), infrared thermography (Bosiljkov *et al.* 2010), radar (Cotic *et al.* 2013) and sonic tests (Binda *et al.* 2001). The assessment of the quality and effectiveness of the repair of cracks crossing masonry walls by NDTs is a topic not frequently addressed in literature. However, information can be found in the bibliography dedicated to the conservation of concrete structures (e.g. Van Tittelbooma *et al.* 2010). The ultrasound pulse velocity (UPV) is probably one of the most used NDTs regarding this purpose, due to their relative low cost and flexibility. By having this into account, the UPV technique was tested as a method to assess the quality and effectiveness of interventions involving injection of cracks in rammed earth constructions and was carried out during the testing of the medium-scale specimens.

6.4.1 Testing procedure

The ultrasonic pulse measurements were carried out by resorting to a testing equipment provided by MATEST, composed by a central pulse generator unit with a measuring range of approximately 0 to 3000 μs, with an accuracy of about ±0.1 μs (Figure 6.18a). The ultrasonic pulse was transmitted and received by piezoelectric probes of a natural resonance frequency of about 55 kHz, whose contact surface is circular, with a diameter of 40 mm. It should be noted that this equipment is typically used for inspection of concrete structures, namely in damage detection and estimation of mechanical properties.

The UPV measurements of the rammed earth medium-scale specimens was done immediately before the three-point bending test preceding the repair by injection, and then immediately before the test after repair. The indirect method was used for this purpose, which means that the transmission and receiver probes were placed on the same surface at a given distance between them. Ultrasound gel was used to promote a better contact between the probes and the specimens, whose surface presented gaps that would not allow full contact and thus would influence negatively the results.

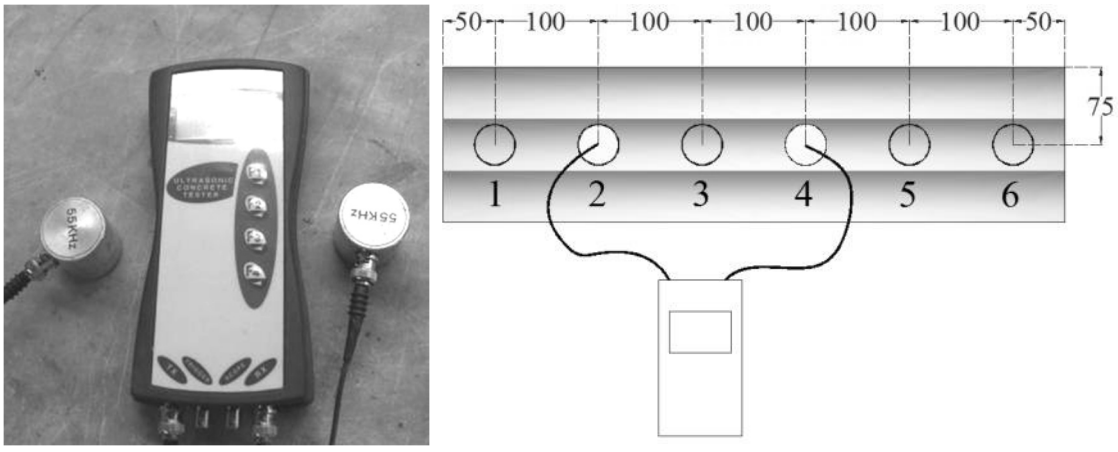

(a) (b)

Figure 6.18 – UPV measurements: (a) equipment used; (b) test setup (dimensions in mm).

The measurements on the specimens were taken just from one side surface, which was marked with six measuring points according to Figure 6.18b. The taken UPV measurements included all the possible combinations between the six measuring points, which means that the covered distances between probes were 100, 200, 300, 400 and 500 mm. Figure 6.19 illustrates the execution of the UPV measurements, where each reading was only taken upon the stabilisation of the ultrasonic pulse transition time (UPTT).

Figure 6.19 – UPV measurements on the medium-scale specimens.

6.4.2 Results and discussion

Figure 6.20 presents the UPTT for the medium-scale specimens before the first test, as a function of the distance between the transmission and receiver probes. The UPTT results show in general high scattering, but it becomes even higher as the distance between probes increases. This is probably a consequence of the high porosity of rammed earth, especially when compared with that of materials over which the UPV equipment is typically used (ex: concrete), and to the fact that the soil composing the specimens is a granular material with particles of large dimension (sand and gravel). This also contributes to a deviation of the points with higher distance between probes from a linear relation between transmission distance (d_{up}) and UPTT, which theoretically corresponds to the UPV, see Equation (6.3). Therefore, all measurements

involving a distance between probes of 400 and 500 mm were not considered for computing the average UPV of each specimen. Moreover, combinations that did not intersect the middle span cracks resulting from the first three-point bending test were not considered. Thus, the combinations used to compute the average UPV were: 1-4, 2-4, 2-5, 3-4, 3-5 and 3-6 (see Figure 6.18b).

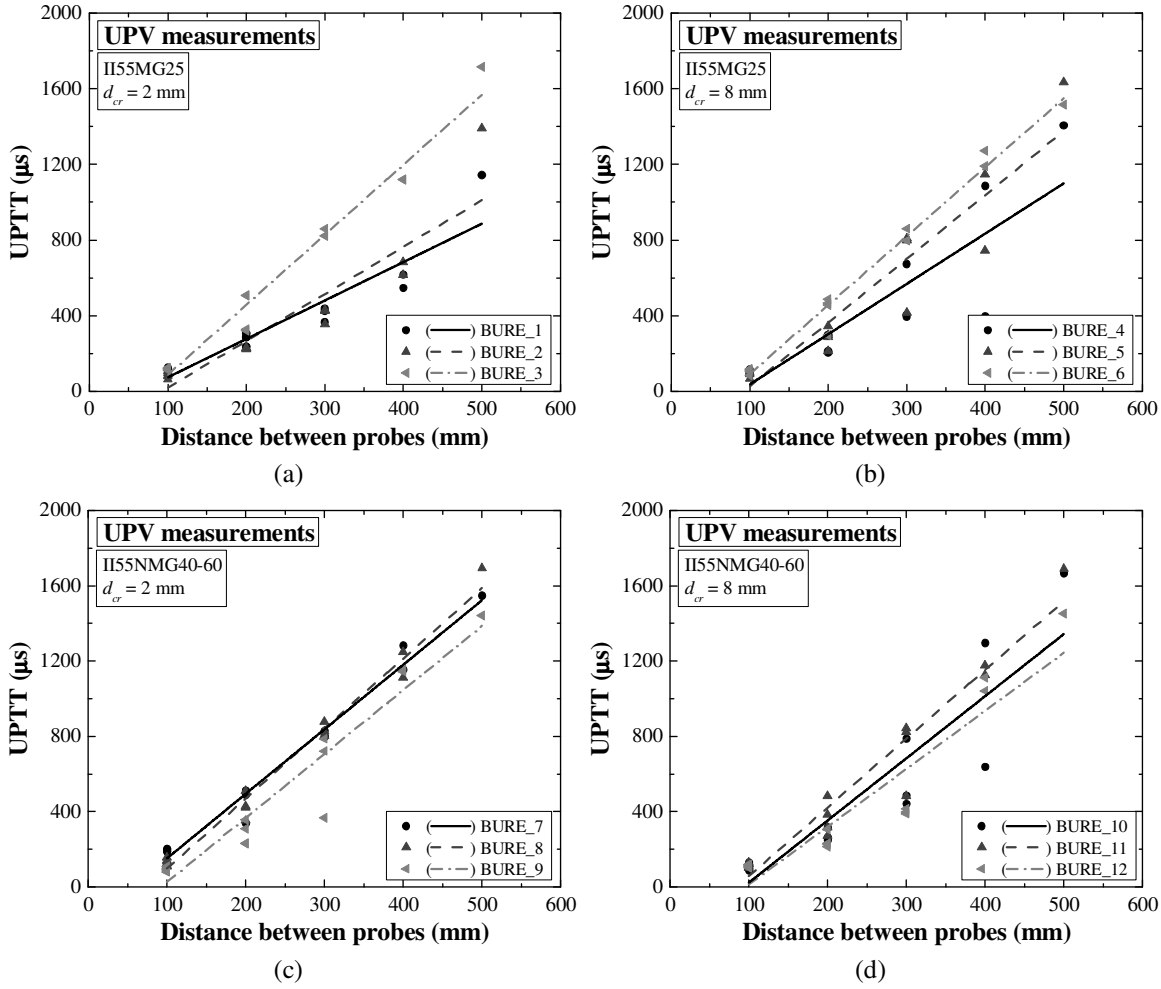

Figure 6.20 – Ultrasonic pulse transmission time (UPTT) of the medium-scale specimens (before the first test) as a function of distance between probes: (a) set of specimens repaired with grout II55MG25 and d_{cr} = 2 mm; (b) set of specimens repaired with grout II55MG25 and d_{cr} = 8 mm; (c) set of specimens repaired with grout II55NMG40-60 and d_{cr} = 2 mm; (d) set of specimens repaired with grout II55NMG40-60 and d_{cr} = 8 mm.

$$UPV = \frac{d_{up}}{UPTT} \tag{6.3}$$

Figure 6.21 presents the relation between the initial flexural strength of the specimens (first three-point bending test) and the average UPV. There seems to be a correlation between the flexural strength and the UPV, where the higher the UPV the higher is the flexural strength. It should be noted that this trend must be looked at carefully since the obtained correlation coefficient is low and is probably affected by the scattering of the UPV measurements. However, it agrees with the trends found by Varum *et al.* (2006) and Bandeira (2009) between the compressive strength and the UPV of other earthen

materials. Moreover, this shows that the UPV measurements can constitute a useful tool in inspection works on earth constructions, namely in the mapping of regions with different mechanical properties in rammed earth walls.

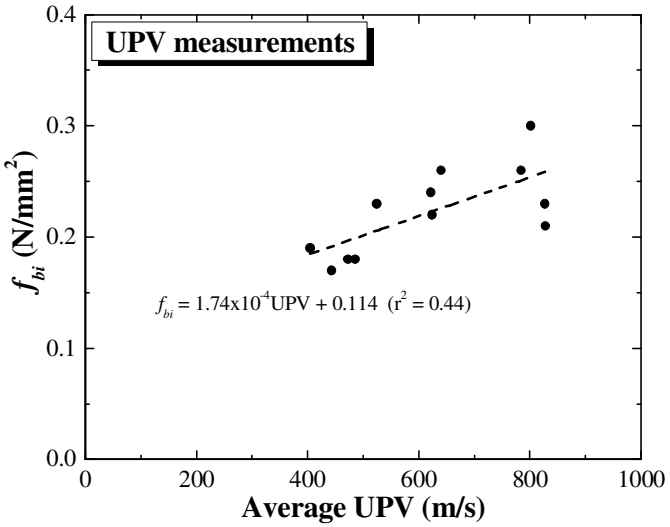

Figure 6.21 – Initial flexural strength as a function of the average UPV of the medium-scale specimens.

The UPV variation between the repaired and the initial state was computed for each of the combinations used to compute the average UPV. The resulting average value was then compared against the flexural strength recovery rate of the twelve medium-scale specimens, as depicted in Figure 6.22.

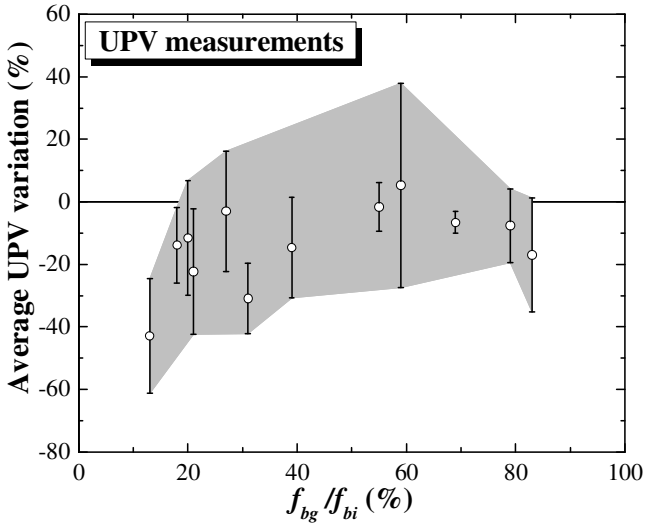

Figure 6.22 – Average UPV variation (the standard deviation is represented as error bars) as a function of the flexural strength recovery rate.

The error bars illustrated in the graph represent the standard deviation of the UPV variation. In general, there seems to be a relation between the recovery rate and the UPV variation, i.e., the higher the average UPV variation the higher is the recovery rate. However, the high scattering of the UPV makes this relation a little unclear and does not allow defining a reliable relationship between this parameter and the recovery rate.

6.5 Conclusions

In this chapter, medium- and large-scale rammed earth specimens were built and tested in order to assess the performance of an "artificial" mud grout and two "natural" mud grouts in the repair of structural cracks. The medium-scale specimens consisted of twelve beam-specimens, which were first tested under three-point bending, then repaired with an "artificial" and a "natural" mud grout (II55MG25 and II55NMG40-60, respectively), and, finally, tested again. Moreover, the injected cracks had a width of 2 mm and 8 mm. The large-scale specimens consisted of eleven wallets tested under diagonal-compression. The wallets were then repaired by injection of two "natural" mud grouts (II55NMG40-60 and II55NMG50-50) and tested again. Moreover, the UPV technique was tried as a non-destructive method to assess the quality and effectiveness of the repair of rammed earth cracks by mud grout injection.

The injection of the medium-scale specimens showed that the injectability properties (fluidity, penetrability and water retention capacity) of both grouts tested was adequate to fill completely both crack widths. In terms of adhesion capacity, the grout II55MG25 presented lower performance than grout II55NMG40-60, whichever was the width of the injected crack. Moreover, the performance of the grout II55MG25 was considered very low, as the average recovery rate was of about 26% and 17%, respectively for the specimens with crack width of 2 mm and 8 mm. On the other hand, the grout II55NMG40-60 presented an acceptable adhesion performance, since the average recovery rate was of about 55% and 74%, respectively for the specimens with crack width of 2 mm and 8 mm.

The poor adhesion capacity of the grout II55MG25 was patent on the failure surface of the respective specimens, which was mainly characterized by failure at the interface mud grout/rammed earth. On the other hand, the failure of the specimens repaired with grout II55NMG40-60 was mainly characterized by failure in the rammed earth. In general, the obtained results seem to indicate that the same soil used in the construction should be incorporated in the composition of the mud grout in order to optimize the adhesion capacity. This also means that the development of a commercial mud grout only based on standard materials, such as kaolin and limestone powder, may be a less efficient solution to solve the problem of injection interventions in rammed earth constructions.

The injection of the large-scale specimens also showed that both mud grouts used also presented adequate injectability properties, since it occurred without major problems. In fact, the penetrability of the mud grouts was evidenced upon the analysis of the collapsed specimens after the second test, where the injection of cracks of width from 1 mm onwards was observed. The analysis of the failed specimens also allowed detecting some grout gaps, which is thought to be related to the injection of horizontal cracks, namely the associated difficulties in evacuating the air. Probably, this problem

can be solved or mitigated in a practical situation, by increasing the number of injection tubes in the regions where the crack assumes a horizontal orientation.

Regarding the adhesion capacity, both “natural” mud grouts presented similar performance, since the average shear strength recovery rate was of about 66% and 59% for grout II55NMG40-60 and II55NMG50-50, respectively. This shows that a stronger grout may not be a synonymous of higher adhesion capacity, and that the formulation of the mud grout may prefer to be focused on the fresh-state rheological properties, instead. Moreover, this level of recovery can be considered as very satisfactory, because probably it was partially limited by damage at the micro-level of the rammed earth, resulting from the first test, and by the presence of the aforementioned grout gaps. On the other hand, the injection repair was unable to recover the initial shear stiffness of the wallets. In fact, the shear modulus of the wallets after injection was about one order of magnitude lower that the initial shear modulus. This seems to be an inherent limitation of the repair of cracks in rammed earth walls by grout injection, since this technique is unable to re-establish the interlocking and friction provided by the coarser aggregates.

The UPV measurements carried out on the medium-scale specimens were characterized by high scattering, which is an intrinsic consequence of the characteristics of rammed earth, namely its high porosity and incorporation of coarse particles. Nevertheless, a direct relation between the UPV and the rammed earth strength was found, which means that this technique may constitute a useful tool in inspection works. Finally, there seems to be a relation between the recovery rate and the UPV variation, but the high scattering did not allow clearly validating this hypothesis.

Chapter 7

Shear Behaviour Modelling of Rammed Earth

7.1 Introduction

References on the modelling of rammed earth constructions by the finite element method (FEM) are hardly found in literature. In fact, the few known studies on the modelling of rammed earth resorting to the FEM (Jaquin *et al.* 2004, Jaquin *et al.* 2006 and Gomes *et al.* 2012) adopted very simple models, which include very simple constitutive laws for the materials (such as linear elastic isotropic and elastic-perfectly plastic behaviour). In general, these models were used to predict stress levels and to simulate possible collapse mechanisms. The simulation of the deformability and shear behaviour of rammed earth constructions are topics usually not addressed. However, these are fundamental for understanding and predicting the behaviour of rammed earth construction in the case of a seismic event. Moreover, when these constructions are subjected to a seismic event of important intensity, their structural behaviour is expected to be mainly governed by the non-linear behaviour of the rammed earth material, which is consequence of its general low strength.

On the other hand, the use of complex constitutive laws requires detailed information on the properties of rammed earth materials, which is not always available or is available from a limited quantity of experimental tests. Moreover, the variability found in raw earthen materials brings up even more uncertainties regarding the characterization of the materials and thus to the modelling. Therefore, a compromise should be found between representativeness, reliability, accuracy and complexity of the constitutive model with

respect to the material behaviour, namely regarding the computational demand of the analysis.

This chapter deals with the numerical modelling of rammed earth wallets tested under compression and diagonal-compression by BAM-ZRS (German Federal Institute for Materials Research and Testing and Ziegert Seiler Ingenieure) within the framework of the NIKER FP7 project (New Integrated Knowledge based approaches to the protection of cultural heritage from Earthquake-induced Risk).

The non-linear constitutive law adopted is based on the Total Strain Fixed Crack Model (TSFCM) implemented in DIANA software (TNO 2009). This model has been used successfully, for example, to capture the global seismic behaviour of historical masonry (Mendes and Lourenço 2009), and is relatively common in software of FEM analysis.

Both macro- and micro-modelling approaches were considered for the simulation of the experimental tests, and the respective FEM models were calibrated accordingly to the experimental results. The micro-modelling approach was intended to evaluate the influence of apparent weakness of the interfaces between layers on the shear behaviour of rammed earth.

Then, a sensitivity analysis of the parameters involved was carried out in order to investigate the influence of the variability of the properties of rammed earth on the FEM models. Finally, the diagonal-compression tests carried out at University of Minho (Chapter 6) were also modelled.

7.2 Experimental data

BAM-ZRS tested five rammed earth wallets under compression, while other five were tested under diagonal-compression (Miccoli *et al.* 2011). The dimensions planned for wallets were 500x500x110 mm^3 (width x height x thickness). Their manufacture was carried out with a soil provided by a local manufacturer of prefabricated earthen materials (Berlin, Germany). The manufacture process consisted in compacting six layers within a plywood mould, resorting to a timber rammer (see Figure 7.1). The resulting average layer thickness after compaction was of about 84 mm. The drying of the specimens was carried out in a climate room at 23ºC of temperature and 50% of RH.

Figure 7.1 – Manufacture of the rammed earth wallets tested by BAM-ZRS.

7.2.1 Compression tests

Before testing the specimens under compression, their top and bottom surfaces were rectified by means of a low strength cement mortar. The load applied to the specimens was then distributed with the aid of two I steel profiles placed at the top and bottom surfaces. The five compression tests were carried out under displacement control, where the testing speed was defined such that the failure occurred within 20-30 min. The deformations were measured resorting to LVDTs placed in each side, according to the disposition presented in Figure 7.2a. Figure 7.2b presents the axial stress-strain curves obtained from the compression tests of the specimens, as well as the respective envelope. These curves thoroughly highlight the non-linear behaviour of rammed under compression, which starts from low stress levels.

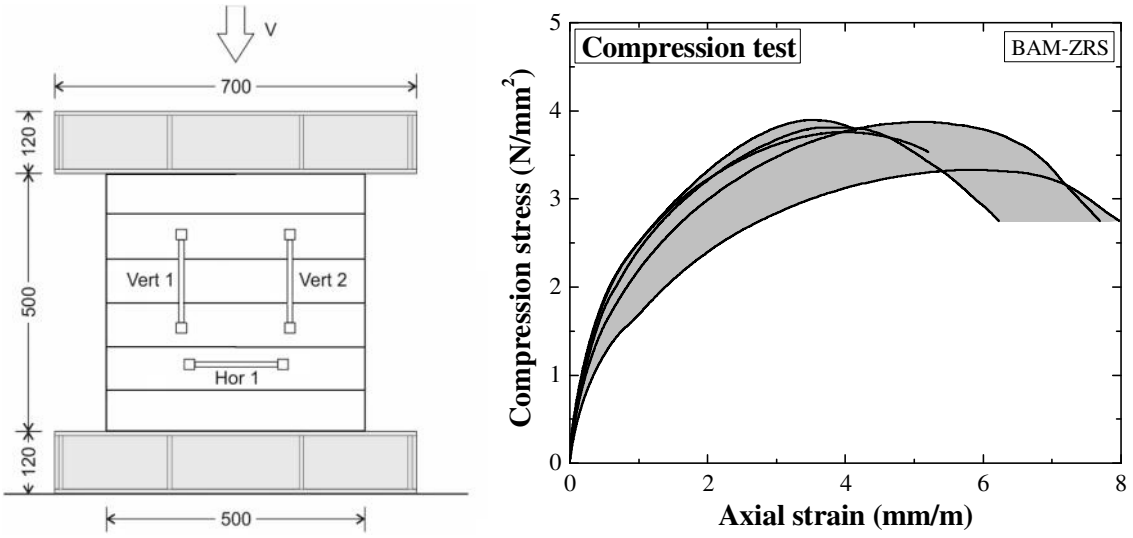

(a) (b)

Figure 7.2 – Compression tests carried out by BAM-ZRS: (a) test setup; (b) compression stress – axial strain curves and respective envelope.

Table 7.1 summarises the mechanical properties obtained from compression tests in terms of compressive strength (f_c) and Young's modulus (E_0), where this last parameter was computed between 5% and 30% of f_c by linear fitting. It should be noted that f_c showed relatively low scattering and varied between 3.3 N/mm^2 and 3.9 N/mm^2, while E_0 presented relatively high scattering and varied between 2844 N/mm^2 and 5048 N/mm^2.

Table 7.1 – Results of the compression tests carried out by BAM-ZRS.

Wallet	f_c (N/mm^2)	E_0 (N/mm^2)
BCWURE_1	3.9	4794
BCWURE_2	3.8	5048
BCWURE_3	3.3	2844
BCWURE_4	3.9	3682
BCWURE_5	3.8	4666
Average	3.7	4207
COV (%)	6	22

7.2.2 Diagonal-compression tests

The five diagonal-compression tests were performed following the procedure given in ASTM E 519 (ASTM 2002b). The test setup is presented in Figure 7.3a, from which is highlighted the geometry of the supports and disposition of the LVDTs placed on both surfaces of the specimens. The contact between the specimens and the supports was regularized by means of a low strength cement mortar. The tests were carried out under force control at a rate of about 130 N/s up to failure. Figure 7.3b presents the shear stress – shear strain curves of the specimens, as well as the respective envelope. In general, the wallets exhibited an early peak shear stress, which was followed by shear hardening. It should be noted that the shear hardening phase imparts most of the shear deformations occurring in the tested specimens.

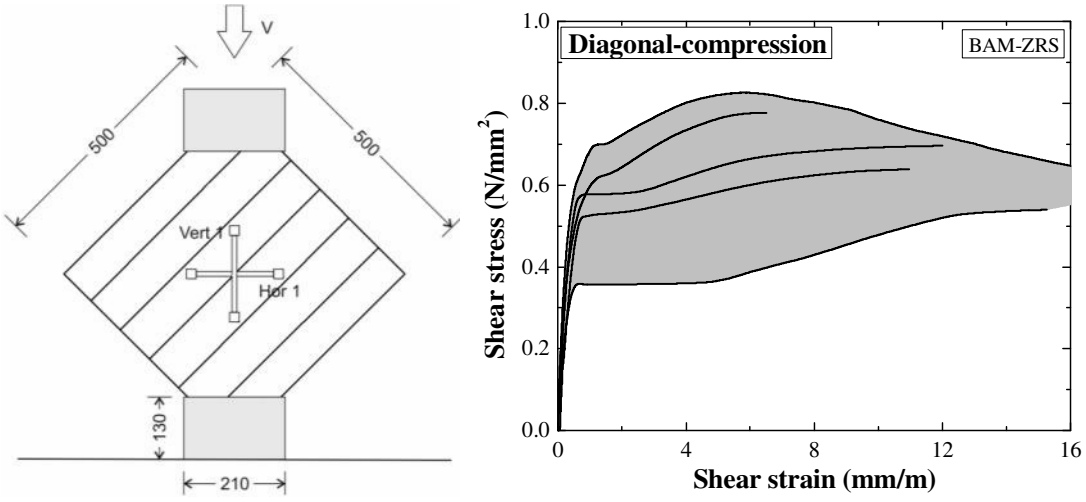

(a) (b)

Figure 7.3 – Diagonal-compression tests carried out by BAM-ZRS: (a) test setup; (b) shear stress – shear strain curves and respective envelope.

Table 7.2 summarises the mechanical properties obtained from the diagonal-compression tests, in terms of shear strength (f_s) and shear modulus (G_0), where this last parameter was computed between 5% and 30% of f_s by linear fitting. It should be noted that both f_s and G_0 showed relatively high scattering, where f_s varied between 0.54 N/mm^2 and 0.83 N/mm^2 and G_0 between 1260 N/mm^2 and 2146 N/mm^2.

Table 7.2 – Results of the diagonal-compression tests carried out by BAM-ZRS.

Wallet	f_s (N/mm^2)	G_0 (N/mm^2)
BDWURE_1	0.54	1260
BDWURE_2	0.64	1476
BDWURE_3	0.83	2146
BDWURE_4	0.78	1530
BDWURE_5	0.70	1499
Average	0.70	1582
COV (%)	16	21

The failure of the specimens was typically preceded by the appearance of a crack close to the early peak shear stress. Then, further cracks developed forming a system of running cracks that crossed diagonally the specimen from the top to the bottom support (see Figure 7.4). Cracking at the interface between layers was also observed, where the diagonal systems of cracks tended to follow partially this interface. Moreover, Figure 7.4 also shows that a crack also appeared at one of the interfaces between layers, nearby the borders of the specimens, developing towards the middle. This shows that these interfaces can behave as weakness surfaces for delamination failure.

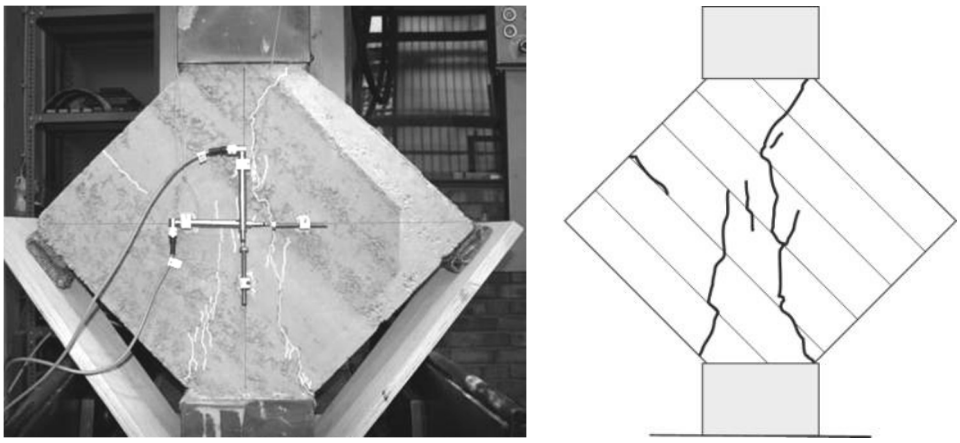

Figure 7.4 – Crack pattern of one of the rammed earth wallets tested by BAM-ZRS under diagonal-compression.

7.3 Modelling of the tests carried out by BAM-ZRS

Rammed earth walls are usually considered to be monolithic, but they also can be seen as masonry built with very large blocks (macro-blocks). These blocks are simply stacked together by ramming the following block on the previous one. Other materials can be included or not in the joints blocks, which include lime-earth mortar, stones, fired bricks and adobes. At the block level, rammed earth can be seen as a layered material. The interfaces between layers constitute weakness planes, which may fail by delamination when the material is sheared or tensioned during, for example, a seismic event. If this is the case, the rammed earth material should be taken as anisotropic, rather than as isotropic (Bui and Morel 2009).

The delamination failure mechanism of rammed earth walls experiencing concentrated loadings was previously modelled by Jaquin *et al.* (2006), using a micro-modelling approach. This model used two layers of different elements to represent each rammed earth layer. One layer of elements simulated the rammed earth as a soil mass, and the respective material properties were assigned resorting to direct shear box and triaxial tests. The other layer simulated the interface between the compacted layers of rammed earth by considering reduced material properties (Mohr-Coulomb failure criterion). The micro-modelling approach was used to capture possible delamination failure occurring in the diagonal-compression tests carried out by BAM-ZRS. The interfaces between rammed earth layers were simulated resorting to interface elements in a multi-layered

FEM model. In addition, the capacity of the macro-modelling approach in capturing the behaviour of rammed earth was also assessed.

7.3.1 Geometry, boundary conditions and loading

The average dimensions of the tested specimens were taken as the dimensions of the preformed models, namely 499x505x117 mm^3 (width x height x thickness). A plane stress state was assumed for all FEM models. Quadrilateral elements of eight nodes (CQ16M) were used to simulate the rammed earth material in both macro- and micro-modelling approaches. The interfaces between layers were simulated, in the micro-modelling approach, resorting to zero thickness interface elements of six nodes (CL12I).

The finite element mesh of the macro-model used to simulate the compression tests was constituted by 400 quadrilateral elements. The micro-model was constituted by 480 quadrilateral elements and 100 interface elements, where the thickness of the layers was assumed as 84 mm (see Figure 7.5).

The macro-model used to simulate the diagonal-compression tests was constituted by 400 quadrilateral elements, while the micro-model was constituted by 460 quadrilateral elements and 100 interface elements (see Figure 7.6).

The boundary conditions adopted in the models simulating the compression tests assumed perfect confinement. The load was applied by imposing uniformly distributed vertical displacements on the constrained nodes at the top of the FEM models.

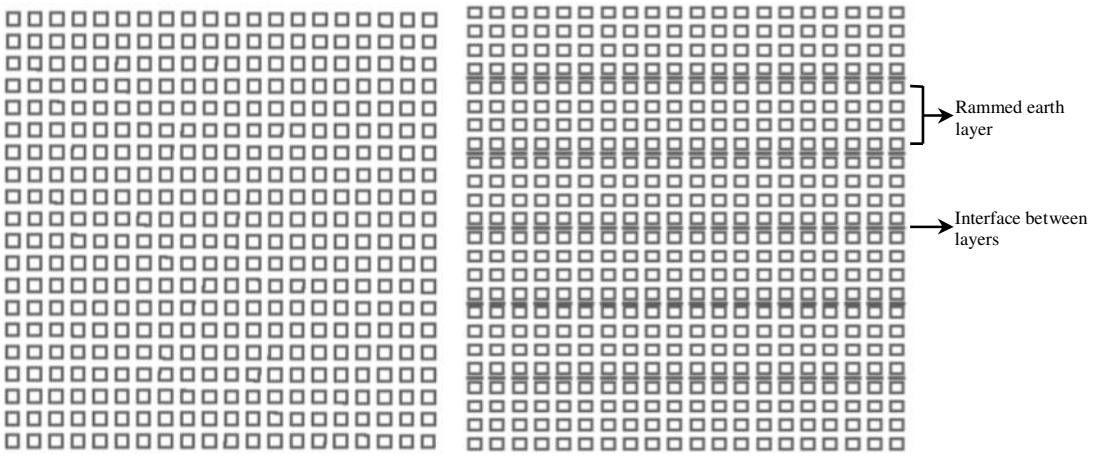

Figure 7.5 – FEM models used to simulate the compression tests carried out by BAM-ZRS: (a) macro-model; (b) micro-model.

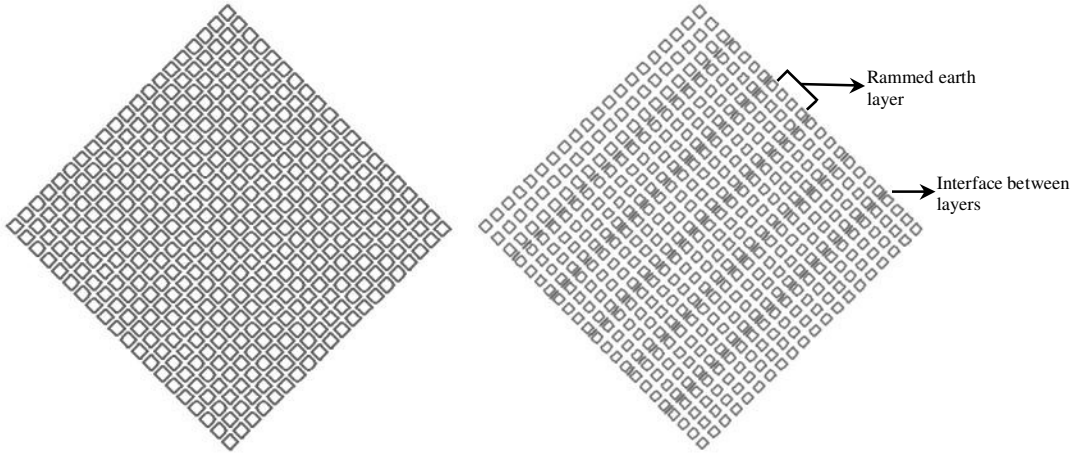

(a) (b)

Figure 7.6 – FEM models used to simulate the diagonal-compression tests carried out by BAM-ZRS: (a) macro-model; (b) micro-model.

The modelling of the diagonal-compression tests was carried out in a similar way to that of the compression tests. The boundary conditions were defined by considering a width of the supports of about 125 mm. The supports were considered as providing full confinement and the load was applied by imposing vertical displacements on constrained nodes at the top of the FEM model.

Finally, none of the analysis considered the self-weight of the material, since its contribution for the stress state was expected to be marginal.

7.3.2 Constitutive laws

The Total Strain Fixed Crack Model (TSFCM) was selected in order to simulate the behaviour of the rammed earth material (TNO 2009). The TSFCM corresponds to a model of distributed and fixed cracks based on total strains. The cracks are fixed according to the principal directions of the strains and remain invariant during the loading of the material. Furthermore, this material model is limited to a maximum of two orthogonal cracks opening in each integration point (Figueiras 1983, Damjamic and Owen 1984 and Póvoas 1991).

The TSFCM implemented in DIANA software (TNO 2009) integrates several possible non-linear stress-strain relationships according to the type of stress involved, namely in compression, tension and shear. These relationships were assumed to be parabolic in compression (Figure 7.7a), exponential in tension (Figure 7.7b) and linear in shear (Figure 7.7c). However, it should be noted that the parabolic relationship in compression was later changed to a multi-linear relationship, as discussed in the next Section.

The crack bandwidth (h) of the elements was assumed to be dependent of the area of the element (A), according to Equation (7.1). This allows making the results of the numerical analysis independent from the size of the finite element mesh. The unloading

and reloading of the TSFCM is simulated by a secant approach, see TNO (2009) and Mendes (2012) for more detail.

$$h = \sqrt{A} \tag{7.1}$$

Table 7.3 presents the initial values assumed for the parameters required by the TSFCM. The average results obtained from the compression tests carried out by BAM-ZRS were used to define the parameters in compression, namely in terms of compressive strength (f_c) and Young's modulus (E_0). The Poisson ratio (ν) was also determined experimentally (Miccoli *et al.* 2011).

The values of the remaining parameters were initially assumed with basis on recommended values for masonry. The compressive fracture energy (G_c) was estimated as $1.6 f_c$. The tensile strength (f_t) was assumed to be 10% of the compressive strength, and the respective mode-I tensile fracture energy (G_f^I) as $0.029 f_t$. Finally, the shear retention factor (β) was assumed to be 1%.

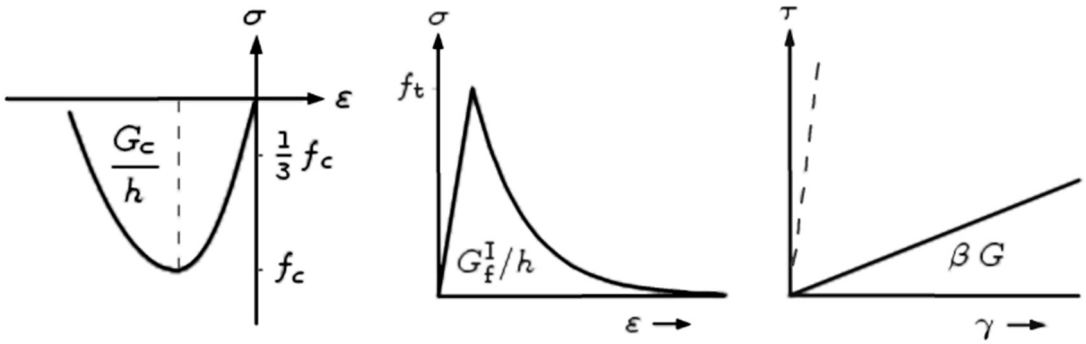

(a) (b) (c)

Figure 7.7 – Stress-strain relationships adopted in the TSFCM: (a) compression; (b) tension; (c) shear.

Table 7.3 – Initial parameters assumed for the TSFCM used to simulate the rammed earth material.

Material	E_0 (N/mm^2)	ν (-)	f_c (N/mm^2)	G_c (N/mm)	f_t (N/mm^2)	G_f^I (N/mm)	β (-)
Rammed earth	4207	0.27	3.7	5.98	0.37	0.0109	0.01

The interface elements of the micro-models were modelled using the non-linear Coulomb friction model (see Figure 7.8) implemented in DIANA software (TNO 2009). The parameters required by this model were neither determined experimentally nor available in the bibliography for the case of rammed earth. This means that these parameters had to be prudently estimated and the initial values are presented in Table 7.4. The values of the normal stiffness (k_n) and of the interface shear stiffness (k_s) were firstly assumed to be very high, in order to avoid concentrating the elastic deformation of the models in the interface elements. Therefore, k_n was assumed as

$100E_0$ and k_s was estimated resorting to Equation (7.2). The cohesion (c) was estimated as a function of the tensile strength estimated for the rammed earth, namely as $1.5f_t$. The friction angle (ϕ) was assumed to be 37º and the dilatancy angle (ψ) as zero. The tensile strength of the interfaces (f_t^i) was defined as $2/3f_t$, while taking into account that the maximum value mathematically allowed by the model is $c/\tan(\phi)$. Finally, the tensile behaviour of the interfaces was assumed as to be brittle.

$$k_s = \frac{k_n}{2(1+\nu)} \tag{7.2}$$

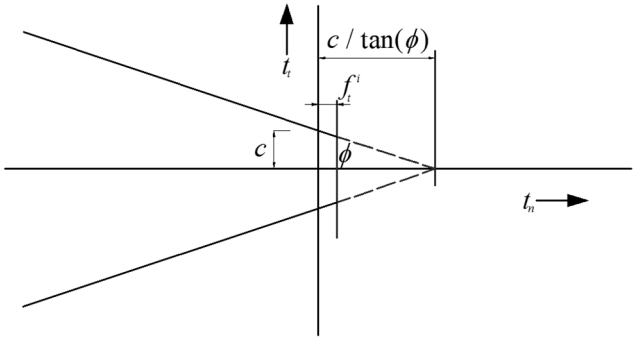

Figure 7.8 – Coulomb friction model used in the modelling of the interfaces between rammed earth layers.

Table 7.4 – Initial parameters assumed for the Coulomb friction model used to simulate the interfaces.

Material	k_n (N/mm^3)	k_s (N/mm^3)	c (N/mm^2)	$\tan(\phi)$ (-)	$\tan(\psi)$ (-)	f_t^i (N/mm)
Interface	4.21x10^5	1.66x10^5	0.561	0.754	0	0.249

7.3.3 Calibration of the models and results

First, the values adopted for the stiffness of the interface elements were assessed by comparing the macro- and micro-model of the compression tests. This was carried out by considering the initial values of the parameters, and by increasing and decreasing both in about one order magnitude. Figure 7.9 presents the compression stress – axial strain curves of the models, where the compressive stress was computed by taking into account the sum of the vertical reactions at the top nodes. The strains were computed by taking into account the relative displacements of the nodes located at the positions of the instrumentation setup used in the experimental tests.

The values of the stiffness adopted for the interfaces of the reference micro-model (Micro_ref) seem to be compatible with the deformability of the reference macro-model (Macro_ref), since the curves were almost coincident. Adopting a stiffness one order of magnitude higher than the reference value (Micro_10k) seems to bring the curves even closer. However, it was observed that adopting very high values of interface stiffness caused convergence problems in the models of the diagonal-compression tests. On the

other hand, a value of stiffness one order of magnitude lower than the reference value (Micro_0.1k) deviates considerably the curve from that of the macro-model. This means that in this case the deformation of the model concentrated mainly in the interfaces. Therefore, it was decided to keep the initial values adopted for the stiffness.

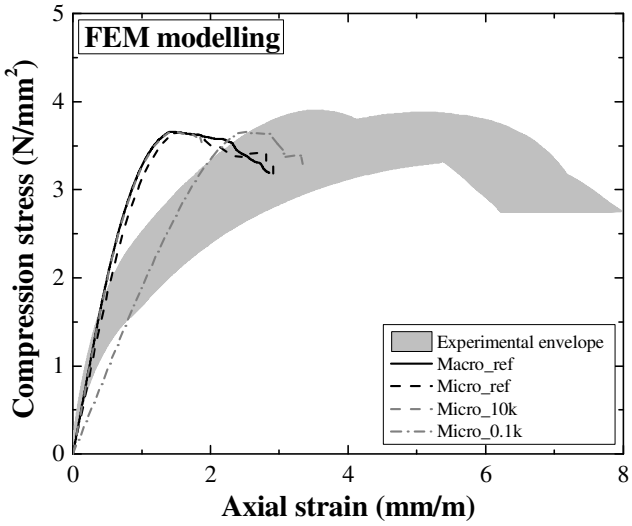

Figure 7.9 – Influence of the stiffness of the interface elements on the deformability of the micro-model of the compression tests.

Another important observation taken from Figure 7.9 is that the models seem to be excessively stiff for simulating the compression behaviour of rammed earth. In fact, the numerical curves present good fitting with experimental envelope up to about 1/3 of the maximum compressive stress (corresponds to about 1.2 N/mm^2), where the experimental behaviour is apparently linear-elastic. After this point, the numerical models do not follow the behaviour depicted by the experimental envelope, which emphasises the importance of the non-linear behaviour of rammed earth. The parabolic relationship available in DIANA software (TNO 2009) does not allow adjusting the pre-peak behaviour, in terms of deformability, to overcome this limitation. This aspect makes the parabolic relationship unsuitable to simulate the behaviour of rammed earth. Therefore, it was decided to adopt a multi-linear relationship, instead. This relationship was built by taking into account the average curve of the compression tests, resulting in the curve of Figure 7.10. It should be noted that the second point of the relationship was defined for $0.3f_c$ by taking into account the experimental Young's modulus.

Figure 7.11 presents the numerical compression stress – axial strain curves, using the multi-linear relationship in compression. As can be seen, this relationship forces the macro- and micro-model to be within the experimental envelope and promotes a non-linear behaviour closest to that of the experimental curves. Furthermore, both models present an almost coincident behaviour.

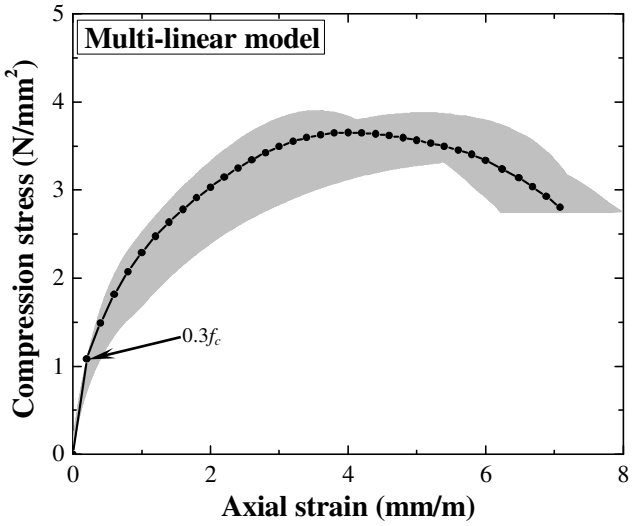

Figure 7.10 – Multi-linear relationship in compression adopted in the FEM models.

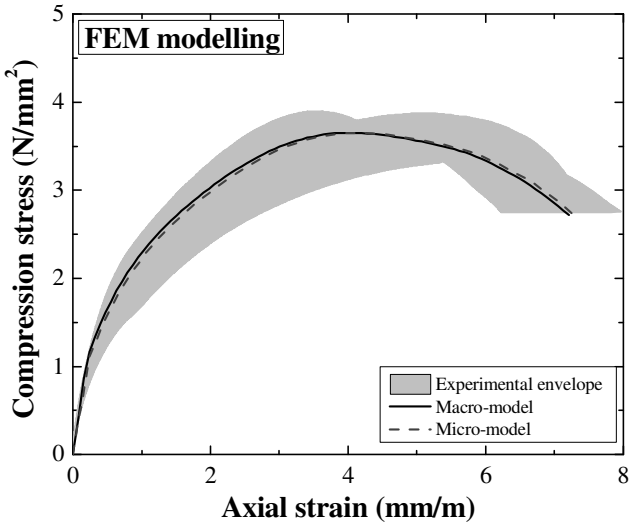

Figure 7.11 – Compression stress – axial strain curves of the macro- and micro-models using the multi-linear relationship in compression and the reference parameters.

Figure 7.12 presents the shear stress – shear strain curves of the macro- and micro-model of the diagonal-compression tests, using the reference values of the parameters and the multi-linear relationship in compression. The shear stresses were computed by taking into account the sum of the vertical reactions at the top support, which was used as input force in Equation (6.1). The shear strains were computed resorting to Equation (6.2), taking into account the relative displacements of the nodes located at the positions of the instrumentation setup in the experimental tests. Both models present similar curves and a behaviour much more brittle than that of the experimental curves.

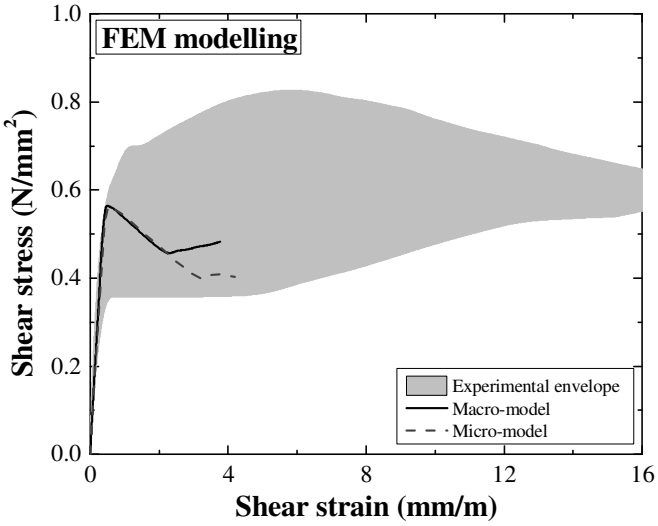

Figure 7.12 – Behaviour of the macro- and micro-model of the diagonal-compression tests with reference parameters.

Therefore, it was decided to adjust the mode-I tensile fracture energy by increasing it one and two orders of magnitude, which resulted in the curves of Figure 7.13. Increasing G_f^I promoted a more ductile behaviour of both models. Eventually, this means that the mode I fracture energy of rammed earth is substantially higher than typical values adopted for masonry. The rammed earth features a broad PSD, which is thought to have great contribution for the interlocking at the crack surface, by promoting its roughness. This enhances the fracture energy of rammed earth relative to historical masonry, where cracking occurs mostly at less rough surfaces, namely the interfaces between mortar and masonry units. However, an increase of G_f^I in about two orders of magnitude seems to be excessive, whereby the increase in one order of magnitude was adopted as the new reference value for this parameter.

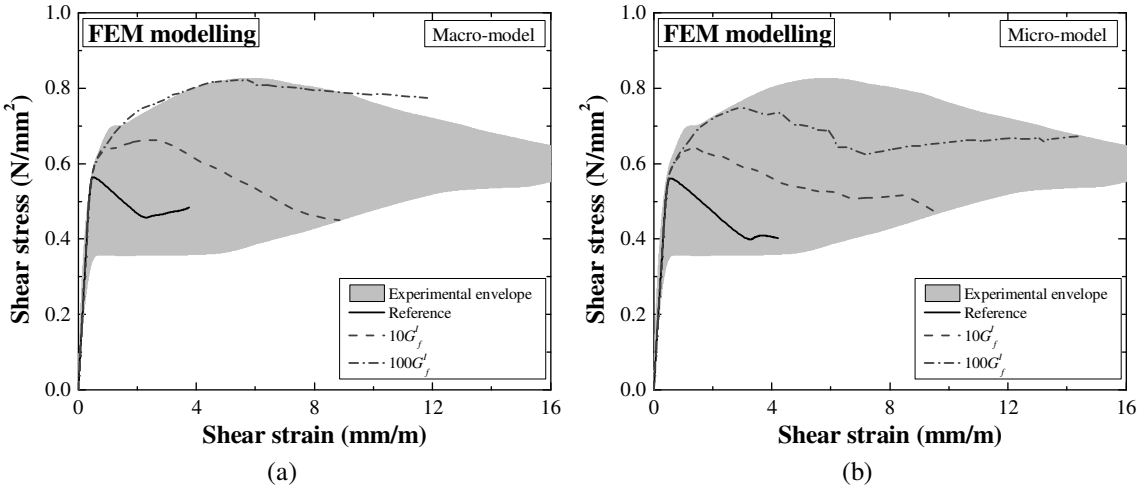

(a) (b)

Figure 7.13 – Effect of the mode-I tensile fracture energy (G_f^I) on the behaviour of the models of the diagonal-compression tests: (a) macro-model; (b) micro-model.

On the other hand, the numerical post-peak behaviour still seems excessively brittle when compared with the experimental curves. This is probably a consequence of the low shear retention factor adopted in the models. In fact, the enhanced roughness of the crack surfaces of rammed earth is also expected to contribute for promoting the mode II friction effect. Thus, it was decided to increase the shear retention for 5%, which resulted in the calibrated curves presented in Figure 7.14.

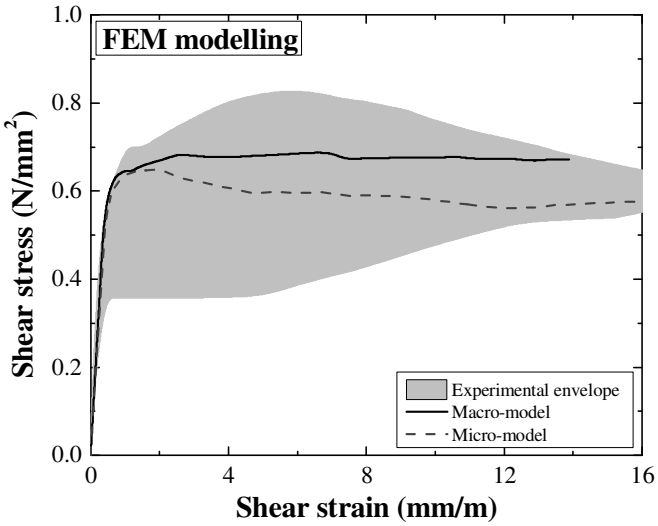

Figure 7.14 – Behaviour of macro- and micro-model of the diagonal compression tests after adjustment of G_f^I (x10) and β (=5%).

The curve of the macro-model is characterized by an early peak shear stress, followed by a small shear hardening until the maximum shear stress is achieved. On the other hand, the curve of the micro-model presents a different behaviour, in the sense that the early peak shear stress is not observed. Instead, the model achieves first the maximum shear stress, followed by a drop in stress with a subtle shear softening. Possibly this drop in stress is related to the failure of interface elements, which is then compensated with stress redistribution. However, the development of the of the macro-model curve is more closer to those obtained from experimental tests. Both models present similar values in terms of maximum shear stress. In the case of the macro-model it was of about 0.69 N/mm^2 and in the case of the macro-model it was of about 0.65 N/mm^2. These values correspond to a minor underestimation of the average shear strength obtained from the experimental tests (0.70 N/mm^2).

In general, it is shown that both curves present good ductility and fit within the experimental envelope, meaning that the utilization of the TSFCM may provide good results when used in the modelling of full rammed earth structures.

The failure modes of both models were also analysed. Figure 7.15 presents the evolution of the principal tensile strains obtained for the macro-model. The principal tensile strains are presented for two stages of imposed vertical displacements, namely 0.40 mm and 1.00 mm. This allows giving an indication of the evolution of the damage in the model. Figure 7.15 also locates these stages in the shear stress-shear strain curve.

The damage is shown to initiate at the middle of the model, due to the development of tensile stresses, and at the supports, due to stress concentration. The damage is also shown to develop from the middle of the model towards the supports. This corresponds to the evolution of the system of cracks observed in the experimental tests. Furthermore, damage is also observed to occur at the four borders of the model in the second stage.

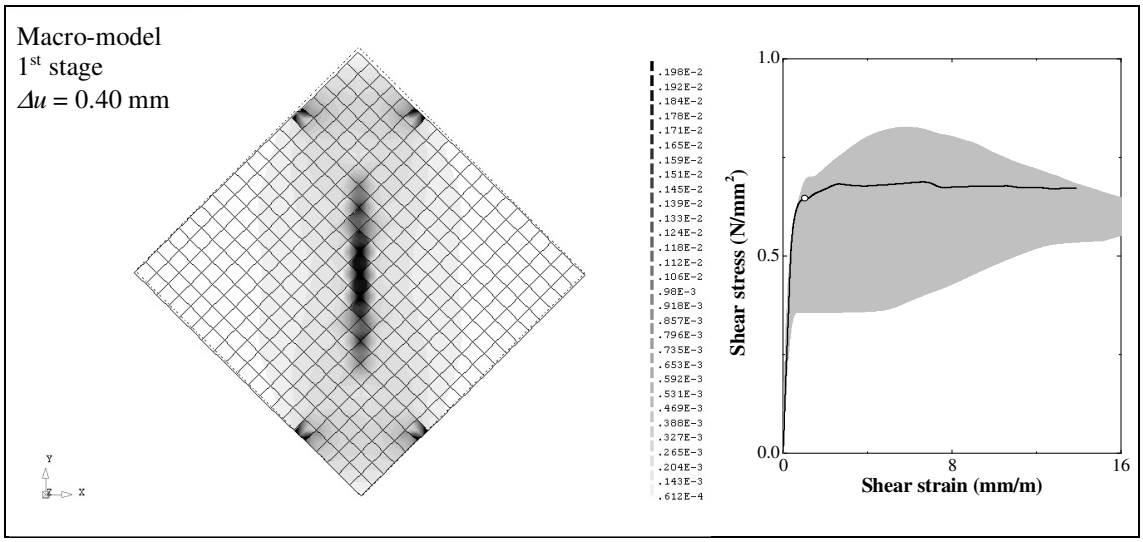

(a)

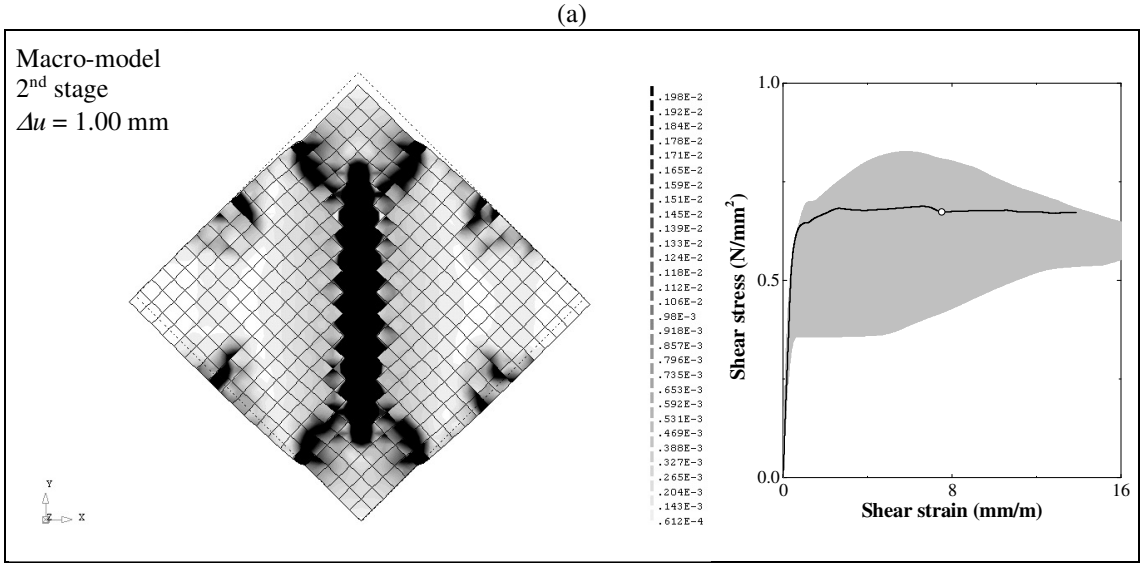

(b)

Figure 7.15 – Principal tensile strains of the macro-model for an imposed vertical displacement (Δu) of: (a) 0.40 mm; (b) 1.00 mm.

Figure 7.16 presents the evolution of the principal tensile strains obtained for the micro-model, while considering the same stages considered for the macro-model. The damage is initiated at the supports and at the middle of the model. Then the damage at the middle of the model develops towards the supports, corresponding to the evolution of the system of cracks observed in the experimental tests. Moreover, it is possible to observe failure by delamination of the interfaces between layers in the second stage. This type of failure is shown to occur nearby the borders and at the zone of concentration of damage at the middle of the model.

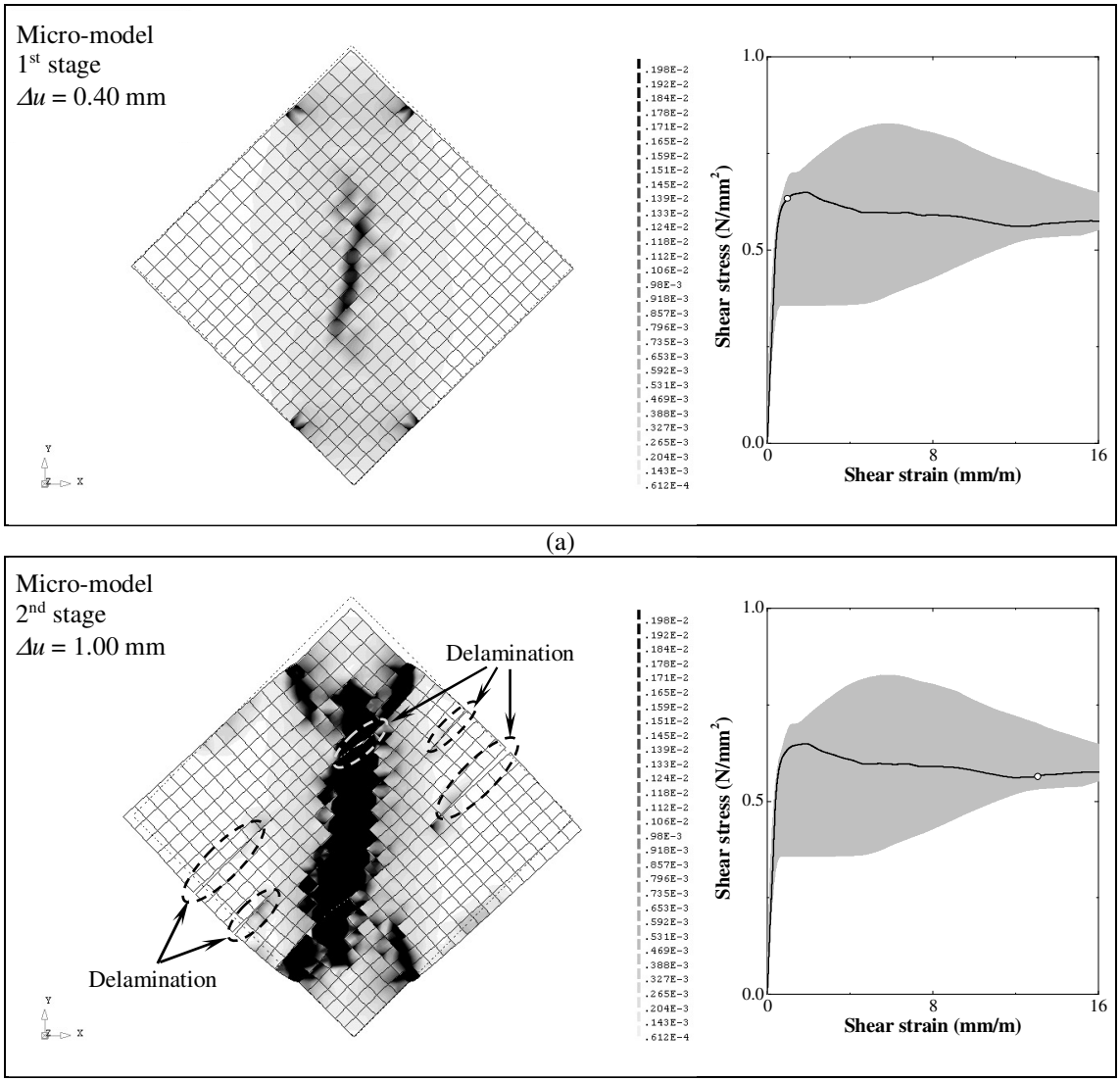

Figure 7.16 – Principal tensile strains of the micro-model for an imposed vertical displacement (Δu) of: (a) 0.40 mm; (b) 1.00 mm.

The fact that the failure of the interfaces did not occur for the vertical displacement of 0.40 mm seems to indicate that, this type of failure was responsible for the drop in shear strength observed in the micro-model. Furthermore, there seems to be a correspondence between the second stages of the macro- and micro-model regarding the damage at the borders, which seems to occur in the same region. This means that both models are capable of detecting potential zones of failure by delamination. However, the macro-model does not allow controlling this failure mode, neither allows differentiating it from the failure of the rammed earth material.

7.4 Sensitivity analysis

A sensitivity analysis was performed in order to assess the influence of the variability associated with the mechanical properties of rammed earth on its shear behaviour. The definition of some of these properties in the macro- and micro-model lacked on reliable sources for their definition, especially in the definition of the properties of the interface

elements. Thus, the main objective of the sensitivity analysis was to assess the importance of these parameters on the response of the macro- and micro-model of the diagonal-compression tests, calibrated in Section 7.3.3. The sensitivity analysis was performed by changing parameters accounting compression, tension, shear, interface and geometrical properties, as summarised in Table 7.5.

Table 7.5 – Parameters considered in the sensitivity analysis.

Parameter	Reference value	Lower value	Upper value
Young's modulus*	$E_{0,ref}$ = 4207 N/mm^2	$0.5E_{0,ref}$ = 2104 N/mm^2	$2E_{0,ref}$ = 8414 N/mm^2
Poisson ratio	ν_{ref} = 0.27	ν_{low} = 0.1	ν_{upp} = 0.4
Compressive strength**	$f_{c,ref}$	$0.8f_{c,ref}$	$1.2f_{c,ref}$
Tensile strength	$f_{t,ref}$ = 0.37 N/mm^2	$0.5f_{t,ref}$ = 0.19 N/mm^2	$2f_{t,ref}$ = 0.74 N/mm^2
Tensile fracture energy	$G^I_{f,ref}$ = 0.109 N/mm	$0.2\,G^I_{f,ref}$ = 0.022 N/mm	$5\,G^I_{f,ref}$ = 0.545 N/mm
Shear retention factor	β_{ref} = 5%	$0.5\,\beta_{ref}$ = 2.5%	$2\,\beta_{ref}$ = 10%
Cohesion	c_{ref} = 0.561 N/mm^2	$0.5c_{ref}$ = 0.281 N/mm^2	$2c_{ref}$ = 1.122 N/mm^2
Friction angle	tan(ϕ_{ref}) = tan(37º)	tan(ϕ_{low}) = tan(20º)	tan(ϕ_{upp}) = tan(50º)
Interface tensile strength	$f^i_{t,ref}$ = 249 N/mm^2	$0.5\,f^i_{t,ref}$ = 125 N/mm^2	$2\,f^i_{t,ref}$ =498 N/mm^2
Layer thickness	$t_{lay,ref}$ = 84 mm	$0.5t_{lay,ref}$ = 4.2 mm	$1.5t_{lay,ref}$ = 12.6 mm

* the value of the Young's modulus was changed in the multilinear relationship by considering only the first point ($0.3f_c$), being the rest of the curve translated.

** the value of the compressive strength value was changed by applying a scale factor to the multilinear relationship, While keeping the reference value of the Young's modulus.

7.4.1 Young modulus

The influence of the Young's modulus on the shear behaviour of the macro- and micro-model was evaluated by reducing the reference Young's modulus two times ($0.5E_{0,ref}$) and by increasing it two times ($2E_{0,ref}$). Figure 7.17 presents the resulting shear stress – shear strain curves of the both models.

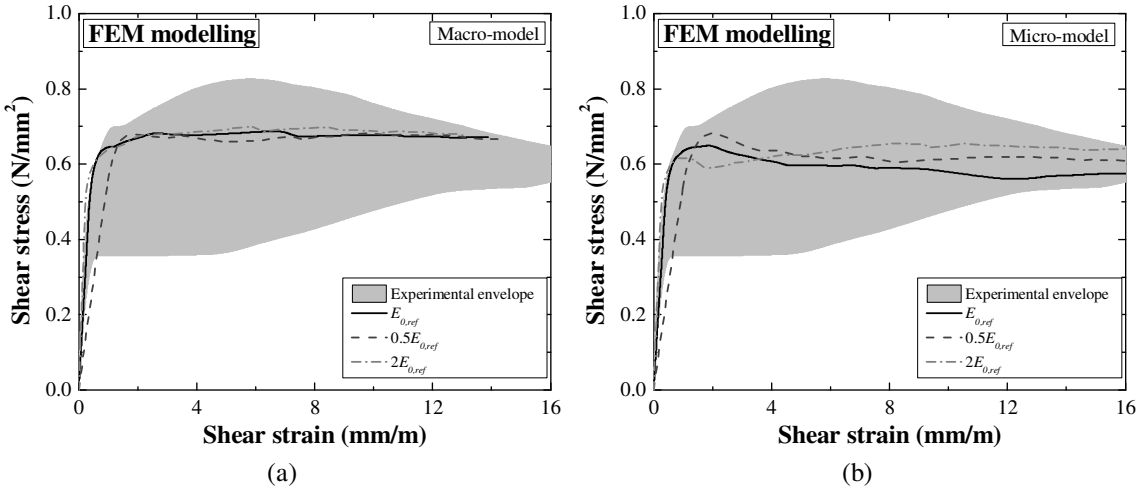

(a) (b)

Figure 7.17 – Shear stress – shear strain curves after varying the Young's modulus: (a) macro-model; (b) micro-model.

The Young's modulus is shown to have little influence on the maximum shear strength. Regarding the macro-model, the maximum shear stress decreases 0.4% and 2.1% for $0.5E_{0,ref}$ and $2E_{0,ref}$, respectively. In the case of the micro-model, the maximum shear stress increases 5.1% for $0.5E_{0,ref}$ and 0.9% for $2E_{0,ref}$. On the other hand, changing the Young's modulus affected mainly the pre-peak behaviour of the models. Reducing this parameter resulted in decreasing shear stiffness, while increasing it resulted in increasing shear stiffness.

7.4.2 Poisson ratio

The influence of the Poisson ratio on the shear behaviour of the macro- and micro-model was evaluated by adopting a lower value of 0.1 (υ_{low}) and an upper value of 0.4 (υ_{upp}). In Figure 7.18, both models are shown to be greatly dependent on the Poisson ratio.

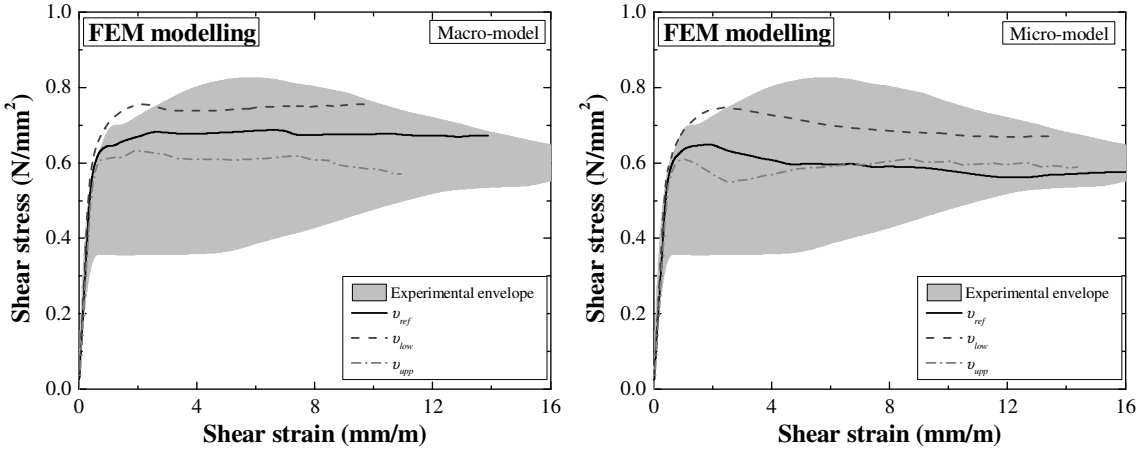

Figure 7.18 – Shear stress – shear strain curves after varying the Poisson ratio: (a) macro-model; (b) micro-model.

In the case of the macro-model, decreasing the Poisson ratio for 0.1 resulted in an increase of about 10.5% in the maximum shear stress, while increasing the Poisson ratio for 0.4 resulted in a decrease of about 7.6%. The same situation occurs for the micro-model, where the increase was of about 15.1% and the decrease of about 6.0%. In fact, a lower value of the Poisson ratio delays the non-linear behaviour in tension in the models and thus the occurrence of damage by tension stress, and vice-versa.

7.4.3 Compressive strength

The influence of the compression strength on the shear behaviour was assessed by reducing and increasing this parameter in 20%. Figure 7.19 shows that the compressive strength has great impact on the shear behaviour of the models. In the case of the macro-model, decreasing the compressive strength resulted in a decrease of the maximum shear stress of about 13.3%, while increasing it resulted in an increase of

about 17.2%. A similar situation occurred for the micro-model, but the decrease was of about 9.9% and the increase of about 16.3%. Moreover, the models seem to lose ductility when the compressive strength is reduced.

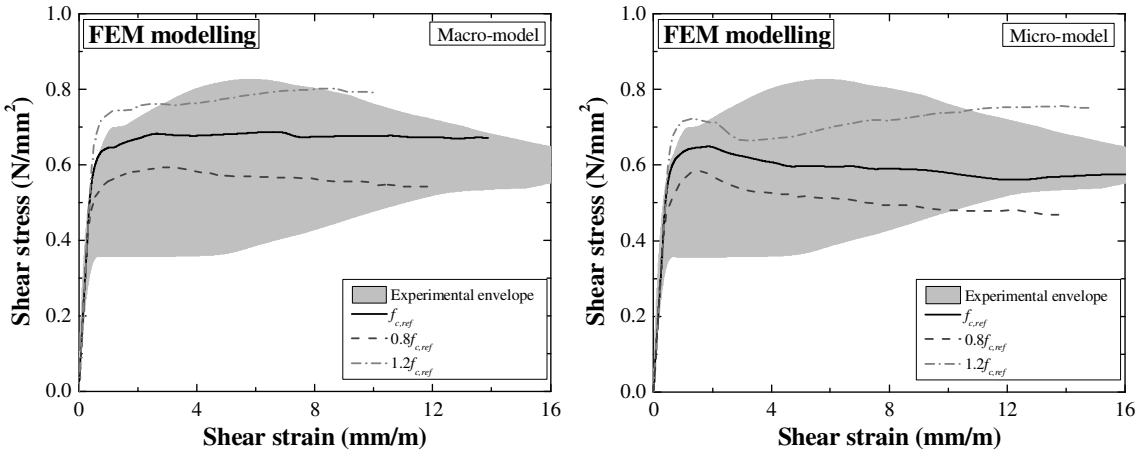

Figure 7.19 – Shear stress – shear strain curves after varying the compressive strength : (a) macro-model; (b) micro-model.

7.4.4 Tensile strength

The influence of the tensile strength on the shear behaviour of the macro- and micro-model was evaluated by reducing the reference tensile strength two times ($0.5f_{t,ref}$) and by increasing it two times ($2f_{t,ref}$). Figure 7.20 shows that the increase in tensile strength resulted in an important increase in terms of the maximum shear stress, which was of about 25.1% in the case of the macro-model and 18.0% in the case of the micro-model.

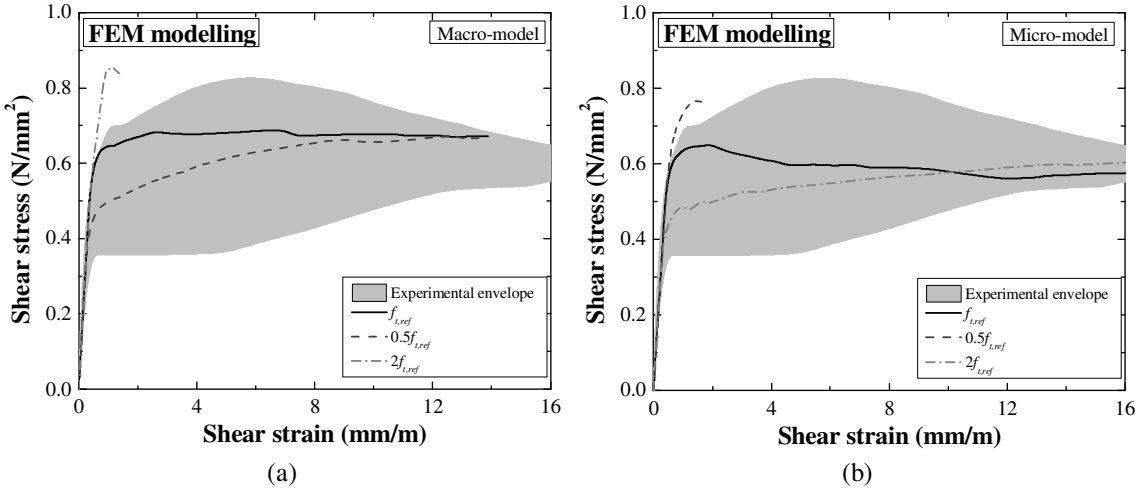

Figure 7.20 – Shear stress – shear strain curves after varying the tensile strength: (a) macro-model; (b) micro-model.

However, the models became very brittle, as a consequence of the decrease of the ratio between the fracture energy and the tensile strength (0.147 mm). On the other hand, this ratio is increased (0.574 mm) when the tensile strength was decreased. This resulted in a more ductile behaviour of both macro- and micro model, where the shear strain at the

maximum shear stress increased significantly. The maximum shear strength was reduced in about 1.9% and 6.8% for the case of the macro- and micro-model, respectively.

7.4.5 Tensile fracture energy

The influence of the tensile fracture energy on the shear behaviour of the macro- and micro-model was evaluated by reducing ($0.2G^{I}_{t,ref}$) and increasing ($5G^{I}_{t,ref}$) the reference value five times. The increase in fracture energy resulted in the increase of the maximum shear stress, which was of about 17.7% in the case of the macro-model and of about 10.9% in the case of the micro-model (Figure 7.21). Decreasing the fracture energy resulted in a decrease of the maximum shear stress of about 13.2% in the case of the macro-model and of about 9.2% in the case of the micro-model. Moreover, it also resulted in an increase of the brittleness of the models. Like was highlighted in the analysis of tensile strength (Section 7.4.4), this brittle behaviour is related with the ratio between the fracture energy and the tensile strength. The lower this ratio is the greater is the brittleness of the model.

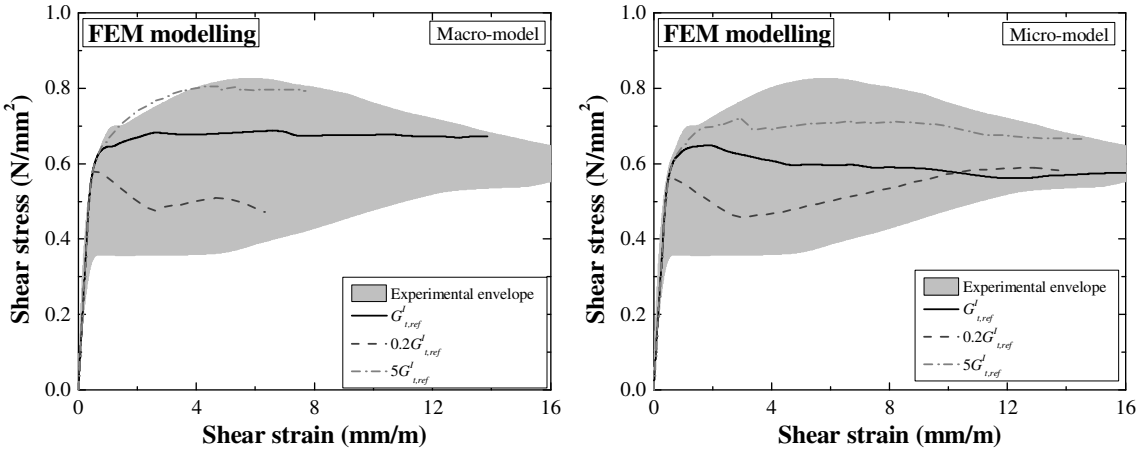

Figure 7.21 – Shear stress – shear strain curves after varying the tensile fracture energy: (a) macro-model; (b) micro-model.

7.4.6 Shear retention factor

The influence of the shear retention factor on the shear behaviour of the macro- and micro-model was evaluated by reducing ($0.5\beta_{ref}$) and increasing ($2\beta_{ref}$) the reference value two times. Figure 7.22 presents the resulting shear stress – shear strain curves of both models, where is shown that this parameter has little influence. In the case of the macro-model, decreasing the shear retention factor resulted in a decrease of the maximum shear stress of 0.2%, while increasing it resulted in an increase of 1.7%. Regarding the micro-model, decreasing and increasing the shear retention factor resulted in a decrease of the maximum shear stress of 0.2% and 1.2%, respectively. Furthermore, the shear retention factor seems not to affect significantly the post-peak

behaviour. However, it should be recalled that a shear retention factor of 1% (or lower value) may result in a more brittle behaviour, as was observed during the calibration of the models.

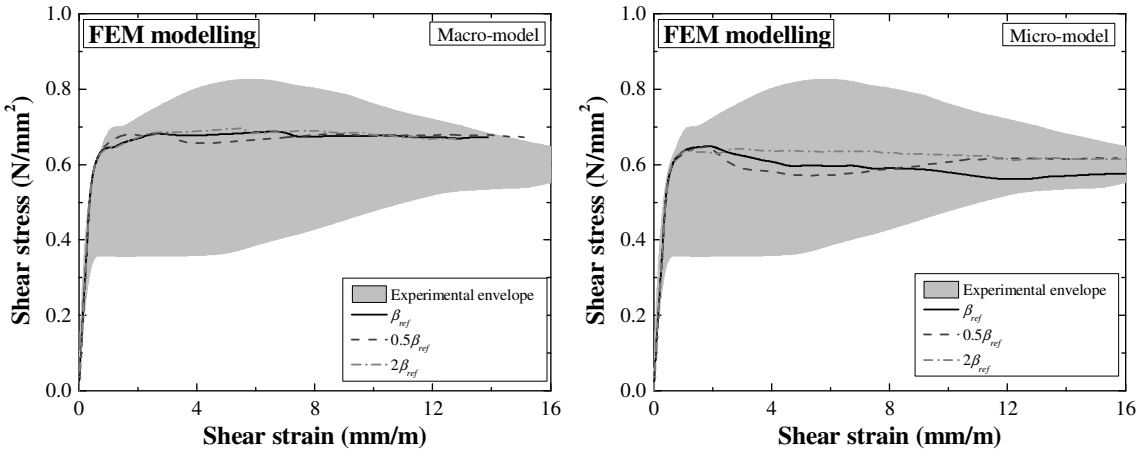

(a) (b)

Figure 7.22 – Shear stress – shear strain curves after varying the shear retention factor: (a) macro-model; (b) micro-model.

7.4.7 Cohesion

The influence of the cohesion of the interface elements on the shear behaviour of the micro-model was evaluated by reducing ($0.5c_{ref}$) and increasing ($2c_{ref}$) the reference value two times. Figure 7.23 presents the resulting shear stress – shear strain curves. Increasing the cohesion has almost no influence on the behaviour of the reference model up to the peak, but deviates from the reference behaviour after this point. Moreover, it produced a residual increase in the maximum shear stress of about 0.1%. On the other hand, decreasing the cohesion resulted in important decrease of the maximum shear stress, which was of about 23.9%. Furthermore, the model presents a more brittle behaviour, which is related with the early yielding failure of the interface elements.

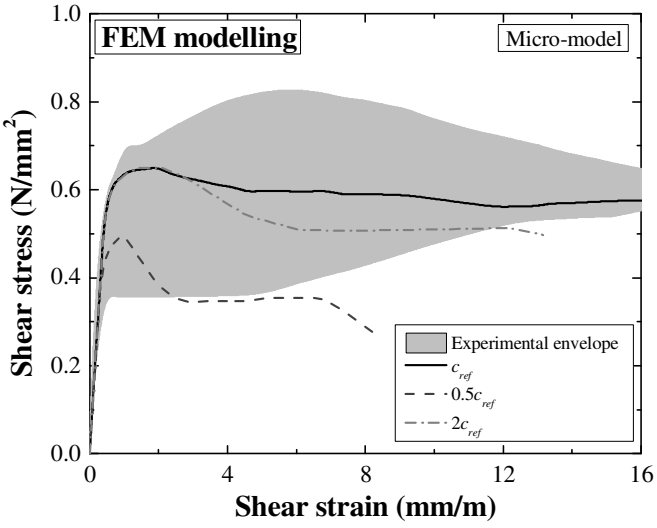

Figure 7.23 – Shear stress – shear strain curves after varying the cohesion of the interfaces.

The variation of the interface parameters is expected to have influence on the failure mode of the micro-model. Thus, the influence of the increasing and decreasing of the cohesion on the damage of the models is depicted Figure 7.24. This figure presents the principal tensile strains of both cases after an imposed displacement of 0.60 mm, as well as the respective deformed mesh. The model with increased cohesion shows only failure by delamination at the interfaces and has similar level of damage to that of the reference micro-model (see Figure 7.25). On the other hand, the model with decreased cohesion presents a higher level of damage, in the sense that sliding between layers is also observed. This results from the plastification of interface elements.

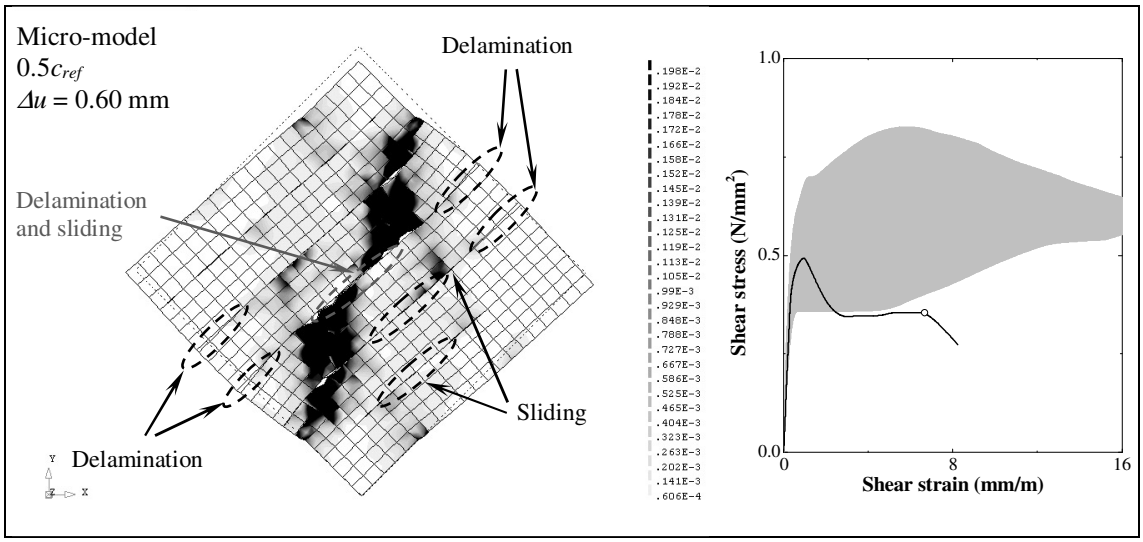

(a)

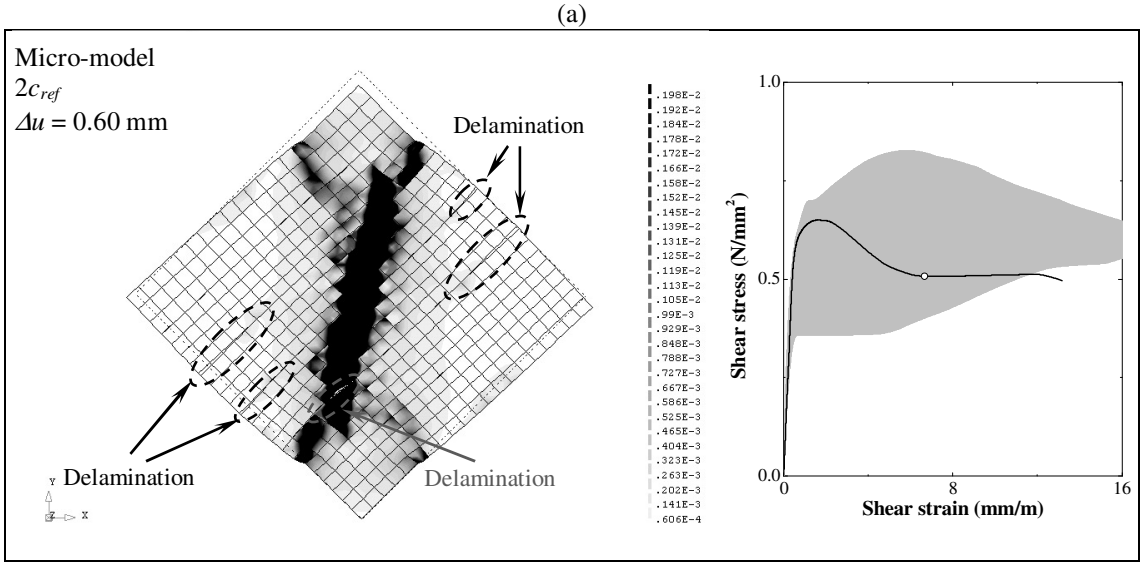

(b)

Figure 7.24 – Principal tensile strains of the micro-model for a vertical displacement Δu = 0.60 mm and after varying the cohesion: (a) 0.5c_{ref}; (b) 2c_{ref}.

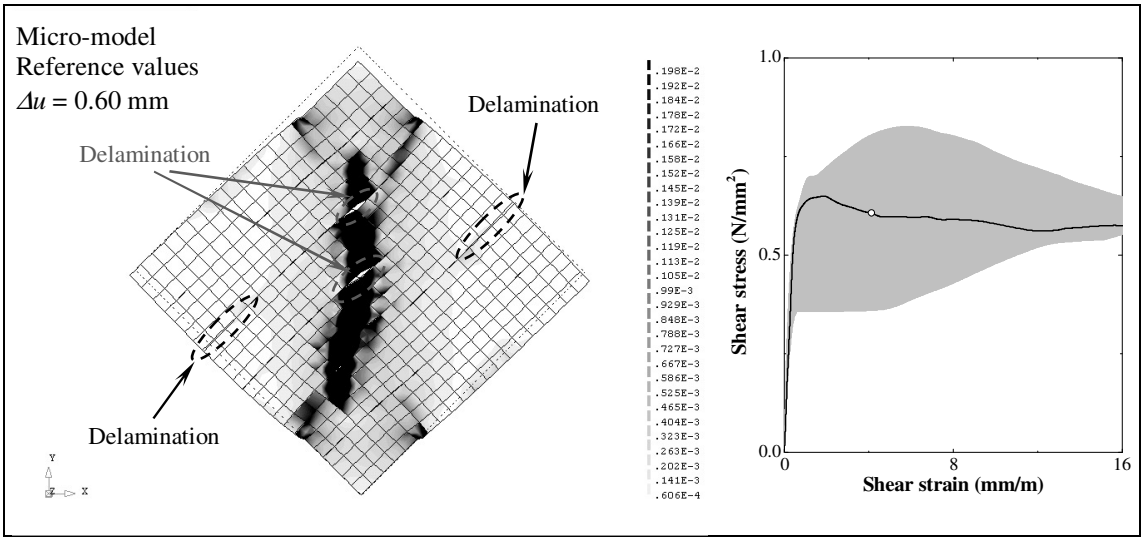

Figure 7.25 – Principal tensile strains of the reference micro-model for a vertical displacement Δu = 0.60 mm.

7.4.8 Friction angle

The influence of the friction angle of the interface elements on the shear behaviour was evaluated by decreasing this parameter to a lower value of 20º (tan(ϕ_{low})) and by increasing it to an upper value of 50º (tan(ϕ_{upp})). As can be seen in Figure 7.26, the decrease in the friction angle resulted in a slightly decrease of the maximum shear stress of 5.3%. However, the brittleness of the model increased substantially. On the other hand, the increase in friction angle seems to have much less influence on the shear behaviour, where the maximum shear stress increased 1.2%.

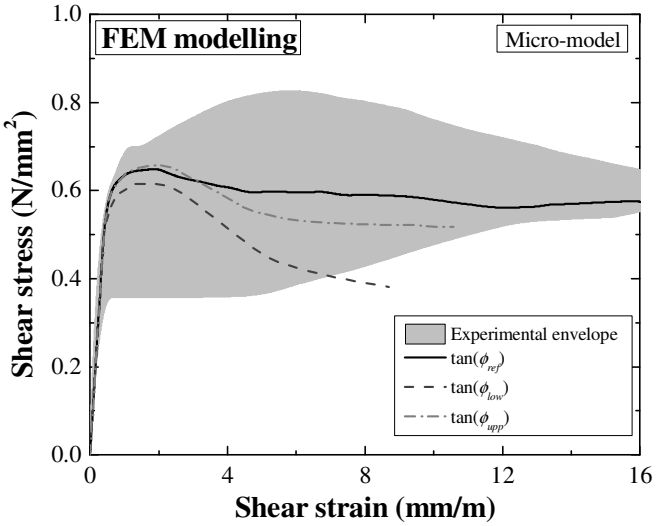

Figure 7.26 – Shear stress – shear strain curves after varying the friction angle of the interfaces.

The influence of the increasing and decreasing of the friction angle on the damage of the models is depicted Figure 7.27. The damage of the model with decreased friction angle is shown to be similar to that of the model with decreased cohesion. It is possible to observe failure by delamination and sliding, which is thought to be the main

responsible for the brittle behaviour exhibited by the model. Regarding the model with increased friction angle, the damage at the interfaces occurs only by delamination and presents a similar level to that of the reference model (Figure 7.25).

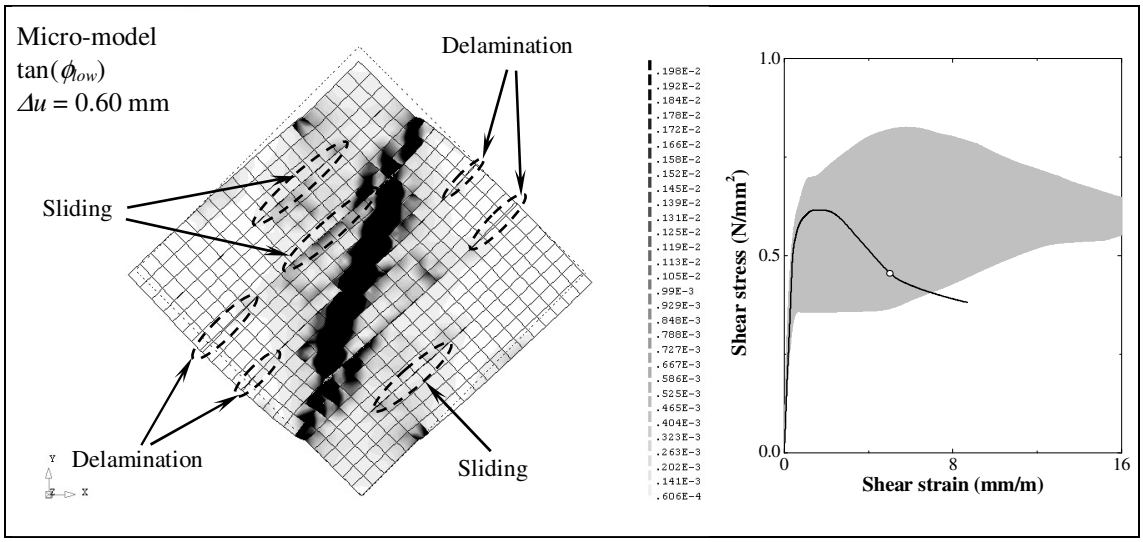

(a)

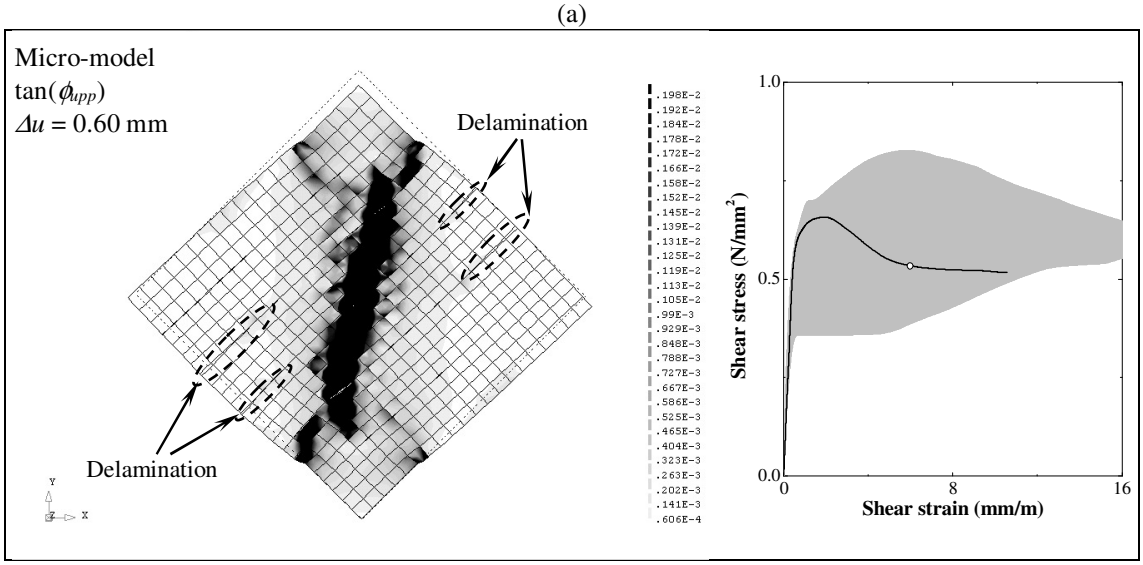

(b)

Figure 7.27 – Principal tensile strains of the micro-model for a vertical displacement Δu = 0.60 mm and after varying the friction angle: (a) tan(ϕ_{low}); (b) tan(ϕ_{upp}).

7.4.9 Interface tensile strength

The influence of the tensile strength of the interface elements on the shear behaviour was evaluated by decreasing ($0.5\, f^{i}_{t,ref}$) and increasing ($2\, f^{i}_{t,ref}$) the reference value two times. Figure 7.28 shows that the tensile strength of the interfaces has little influence on the development of the shear stress – shear strain curves. Decreasing this parameter resulted in a decrease of the maximum shear stress of 1.4%, while increasing it resulted in a 2.0% increase. The variation of the tensile strength of the interfaces also did not introduce major variation in the distribution of damage in the models (see Figure 7.29), as it concentrates at the middle of the models, resembling to the reference model.

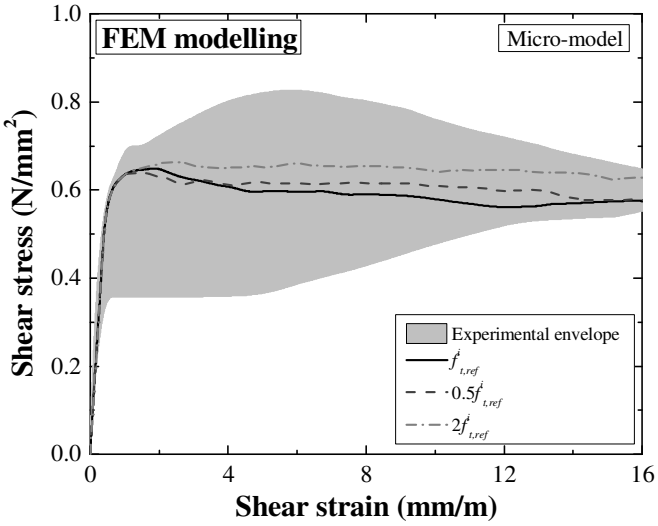

Figure 7.28 – Shear stress – shear strain curves after varying the tensile strength of the interfaces.

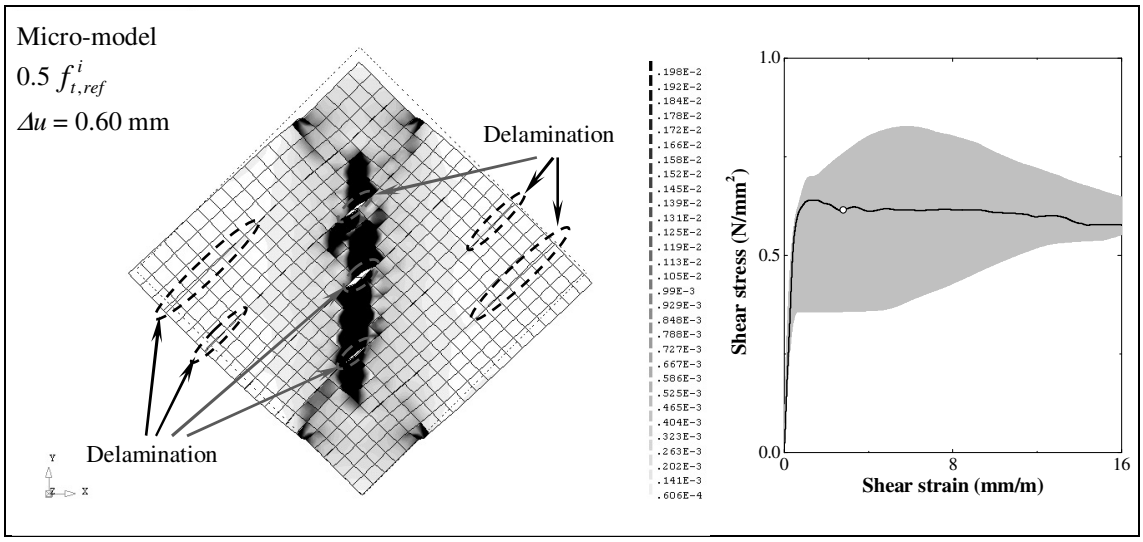

(a)

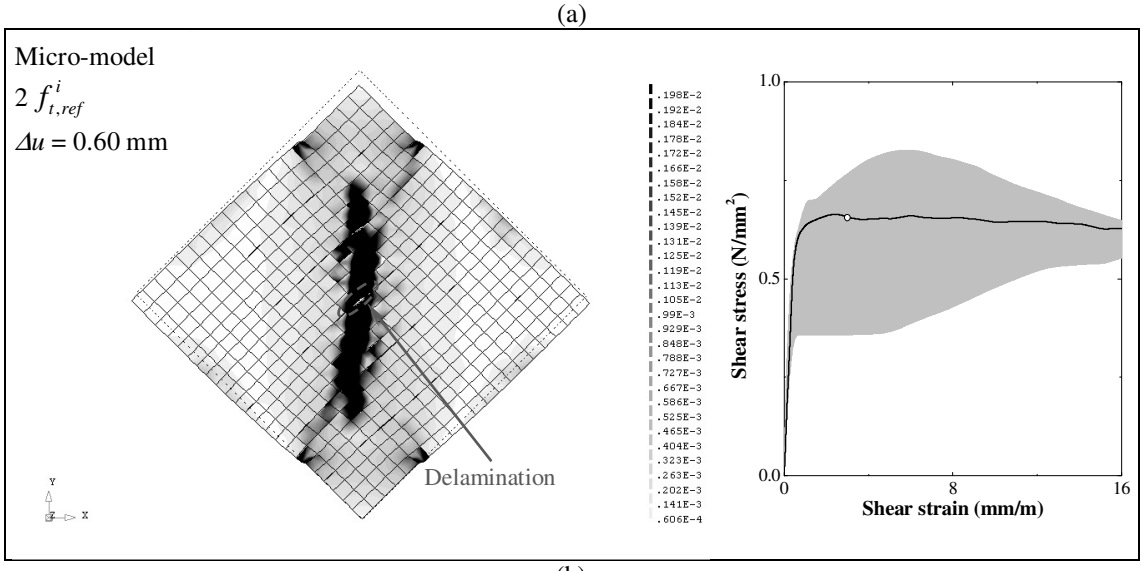

(b)

Figure 7.29 – Principal tensile strains of the micro-model for a vertical displacement Δu = 0.60 mm and after varying the tensile strength of the interface elements: (a) 0.5 $f^i_{t,ref}$; (b) 2 $f^i_{t,ref}$.

However, increasing the tensile strength hindered (or at least delayed) the formation of the delamination cracks. On the other hand, the model with reduced tensile strength of the interfaces presented a much higher level of damage by delamination. Despite that, this parameter seems to have little impact on the shear behaviour of the model, especially when comparing with impact of the other interface parameters.

7.4.10 Layer thickness

The influence of the thickness of the rammed earth layers on the shear behaviour was evaluated by decreasing the reference value to 4.2 mm ($0.5t_{lay,ref}$) and by increasing it to 12.6 mm ($1.5t_{lay,ref}$). The first case corresponds to a model with twelve layers, while the second corresponds to a model with four layers. Figure 7.30 presents the respective shear stress – shear strain curves, which do not show significant deviation from that of the reference model. However, reducing the thickness slightly reduced the shear stiffness of the model, and vice-versa. This is a consequence of the number of layers of each model. The variations of the maximum shear stress were also insignificant. Increasing the thickness resulted in 1.0% decrease, while increasing it resulted in a 0.4% increase.

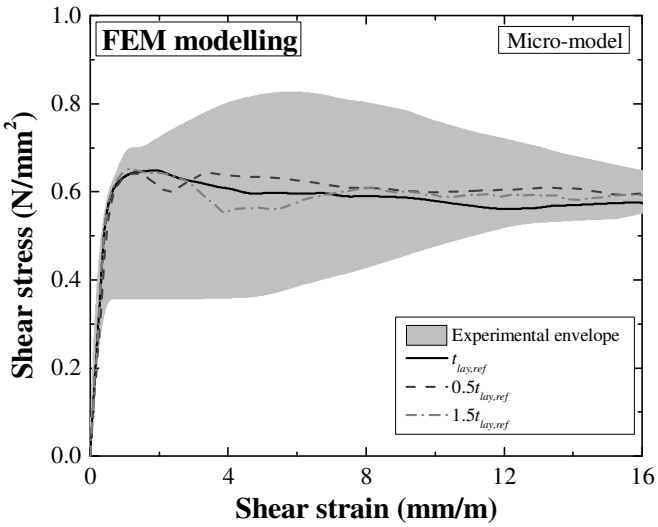

Figure 7.30 – Shear stress – shear strain curves after varying the thickness of the rammed earth layers.

Figure 7.31 shows that the distribution of the damage in the models was not affected significantly by the variation in thickness of the layers. In fact, both models show the same trends of the reference model regarding the damage constituting the system of diagonal cracks and the failure by delamination. The only difference is that the delamination failure occurs more frequently in the case of the model with $0.5t_{lay,ref}$, since it is provided with more interfaces.

Thus, the thickness of the layers of the rammed seems to be a non-limiting parameter of its shear behaviour. However, this conclusion requires a practical analysis to be made. In fact, increasing the thickness of the layers of rammed earth is prone to result in a

material with inferior mechanical properties, due to an also lower quality of the compaction. Therefore, it is reasonable to think that in practice the shear behaviour would be also lower.

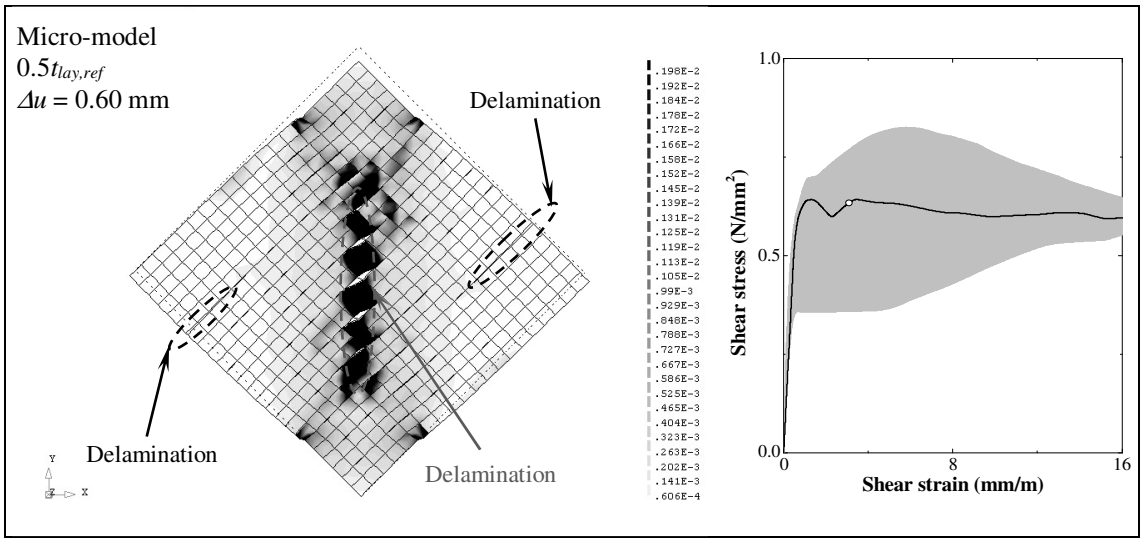

(a)

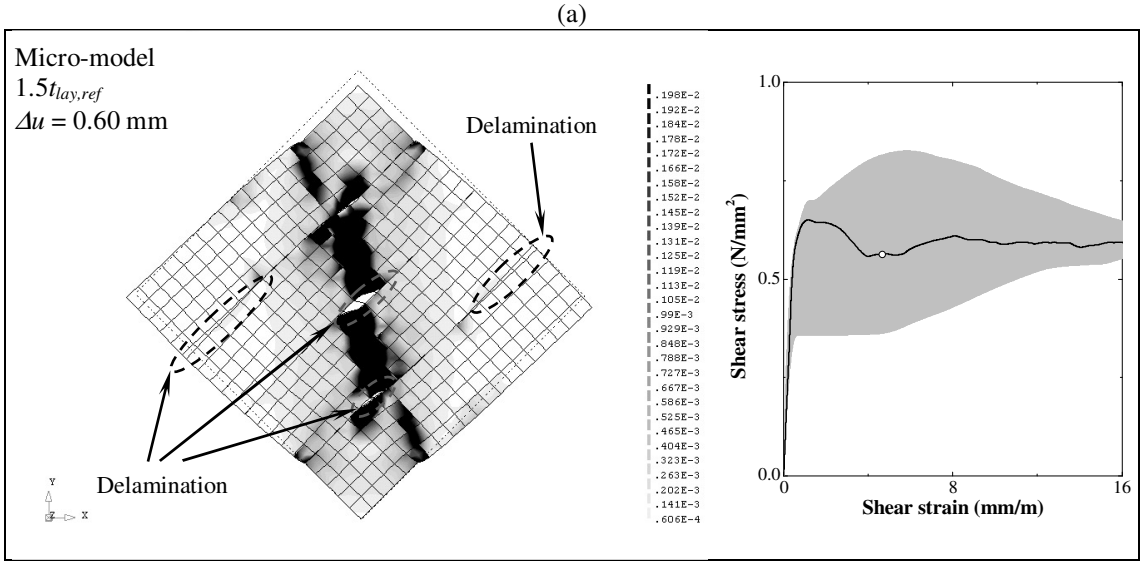

(b)

Figure 7.31 – Principal tensile strains of the micro-model for a vertical displacement Δu = 0.60 mm and after varying the thickness of the rammed earth layers: (a) 0.5$t_{lay,ref}$; (b) 1.5$t_{lay,ref}$.

7.4.11 Discussion

Table 7.6 and Table 7.7 summarize the results of the sensitivity analysis in terms maximum shear stresses obtained for the macro- and micro-model, respectively. In the case of the macro-model, the Poisson ratio, the compressive strength, the tensile strength and the tensile fracture energy are the parameters with the highest influence on the maximum shear stress. This can be easily visualized in Figure 7.32, where the non-dimensional maximum shear stress (normalised by the maximum shear stress of the reference model – $f_s/f_{s,ref}$) is compared with the non-dimensional parameters tested in the sensitivity analysis (normalised by the respective parameter of the reference model – x/x_{ref}).

Table 7.6 – Maximum shear stresses obtained from the sensitivity analysis of the macro-model.

Parameter	Maximum shear stress (N/mm^2)	
	Lower value	Upper value
Young's modulus (E_0)	0.68	0.70
Poisson ratio (υ)	0.76	0.63
Compressive strength (f_c)	0.59	0.80
Tensile strength (f_t)	0.67	0.86
Tensile fracture energy (G^I_t)	0.59	0.81
Shear retention factor (β)	0.68	0.70

Table 7.7 – Maximum shear stresses obtained from the sensitivity analysis of the micro-model.

Parameter	Maximum shear stress (N/mm^2)	
	Lower value	Upper value
Young's modulus (E_0)	0.68	0.66
Poisson ratio (υ)	0.75	0.61
Compressive strength (f_c)	0.59	0.76
Tensile strength (f_t)	0.61	0.77
Tensile fracture energy (G^I_t)	0.59	0.72
Shear retention factor (β)	0.65	0.64
Cohesion (c)	0.49	0.65
Friction angle (tan(ϕ))	0.62	0.66
Interface tensile strength (f^I_t)	0.64	0.66
Layer thickness (t_{lay})	0.64	0.65

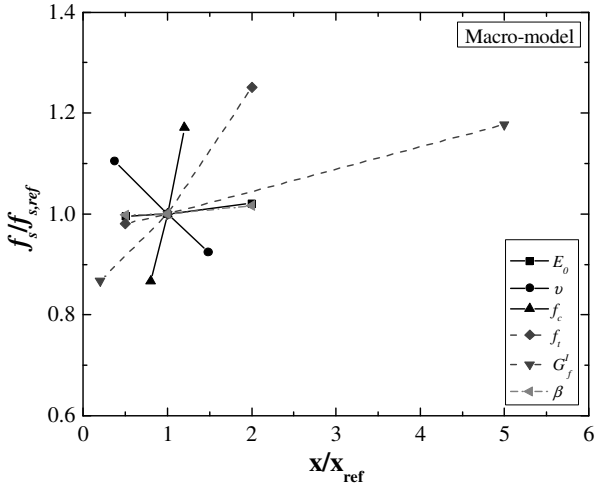

Figure 7.32 – Non-dimensional relationship between the maximum shear stress and the parameters assessed (x) for the macro-model in sensitivity analysis.

The Poisson ratio, the compressive strength, the tensile strength and the tensile fracture energy are also the parameters of the rammed earth layers found to have the greatest influence on the maximum shear stress of the micro-model, as depicted in Figure 7.33a. Regarding the parameters of the interface elements, the cohesion is that with the greatest influence, especially when it is decreased. The friction angle showed little influence in terms of maximum shear stress. However, decreasing this parameter resulted in an increase in brittleness of the model, caused by the appearance of sliding failure. The

variation of tensile strength of the interface and the thickness of the rammed earth layers were shown to have little influence on the shear behavior, especially when compared with that of the two other interface parameters. With respect to this last parameter, it should be noted the varying the layer thickness has also practical implications on the quality of the compaction and thus on the mechanical properties of the final rammed earth.

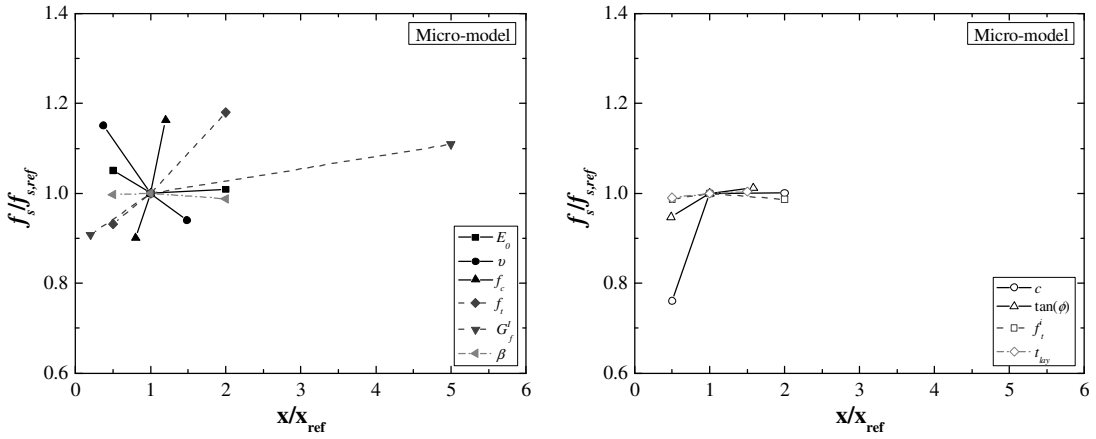

(a) (b)

Figure 7.33 – Non-dimensional relationship between the maximum shear stress and the parameters assessed (x) for the micro-model in sensitivity analysis: (a) layer parameters; (b) interface parameters.

7.5 Modelling of the tests carried out at UMinho

The properties presented by the rammed earth tested by BAM-ZRS are substantially different from those of the rammed earth used in the experimental program discussed in Chapter 6. Therefore, it was decided to model also the shear behaviour of wallets tested at UMinho under diagonal-compression. This aimed at evaluating the approach used for modelling the BAM-ZRS tests when applied to rammed earth with different features. Both the macro- and micro-modelling approaches were used for this purpose.

The models were built with dimensions 550x550x200 mm^3 (width x height x thickness). The boundary condition and the application of the load was similar to that of the modelling of the BAM-ZRS tests. The width of the supports was of 100 mm and the load was applied by means of an imposed vertical displacement at the top support. Moreover, the micro-model was constituted by nine layers with a thickness of about 61 mm.

The material behaviour was simulated resorting to the TSFCM with the multi-linear function in compression. The initial input parameters were defined with basis on the results of the compression tests (see Section 5.7.1) and on the calibration of models of the tests carried out by BAM-ZRS (see Section 7.3). The calibration of the models was then proceeded and resulted in the input parameters of Table 7.8 and Table 7.9. It should be noted that the calibration process resulted in an input compressive strength inferior to that obtained from the compression tests. This means that the original multi-linear relationship obtained from the average compression stress-axial strain curve of

the compression tests was scaled by a factor of 0.7, as depicted in Figure 7.34. The necessity of reducing the compressive strength is explained by the fact that this parameter was obtained from cylindrical specimens compacted with an average dry density 2.2% higher than that of the wallets (see Table 5.16 and Annex B). As depicted in Section 5.7.1, a lower dry density results in a lower compressive strength. In the case of the tests carried out by BAM-ZRS, this reduction was not considered, since the specimens tested under compression and diagonal-compression were compacted under similar conditions.

Table 7.8 – Calibrated parameters assumed for the TSFCM used to simulate the rammed earth material of the tests carried out at UMinho.

Material	E_0 (N/mm^2)	ν (-)	f_t (N/mm^2)	G_f^I (N/mm)	β (-)
Rammed earth	1034	0.27	0.08	0.255	0.05

Table 7.9 – Calibrated parameters of the Coulomb friction model used to simulate the interfaces used in the micro-model of the tests carried out at UMinho.

Material	k_n (N/mm^3)	k_s (N/mm^3)	c (N/mm^2)	$\tan(\phi)$ (-)	$\tan(\psi)$ (-)	f_t^i (N/mm)
Interface	1.03x10^5	0.41x10^5	0.200	0.754	0	0.059

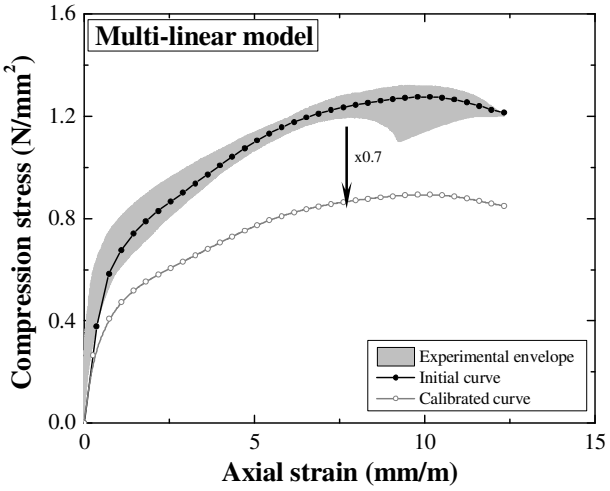

Figure 7.34 – Multilinear relationship adopted for the modelling of the diagonal-compression tests carried out at UMinho.

The shear stress – shear strain curves of the calibrated models are presented in Figure 7.35 and they fit within the experimental envelope. The macro-model overestimates the average shear strength in about 5.0%, while the micro-model underestimates it in about 4.7%. It should be noted that the tensile fracture energy was increased one order of magnitude relative to the initial value. This was required in order to simulate the important ductility observed in the experimental tests. This agrees with the modelling of the tests carried out by BAM-ZRS, in the sense that rammed earth seems to present a relatively good ductility in shear. The failure mode of both models

was also analyzed. Figure 7.36 presents the principal tensile strains obtained for an imposed vertical displacement of about 3.5 mm.

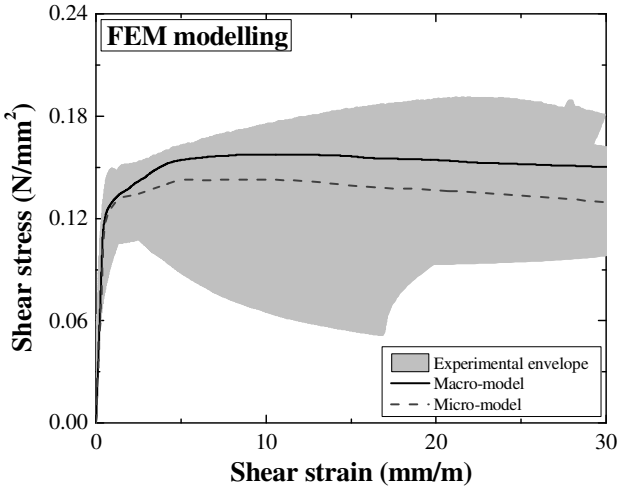

Figure 7.35 – Shear stress – shear strain curves of the macro- and micro-model after calibration.

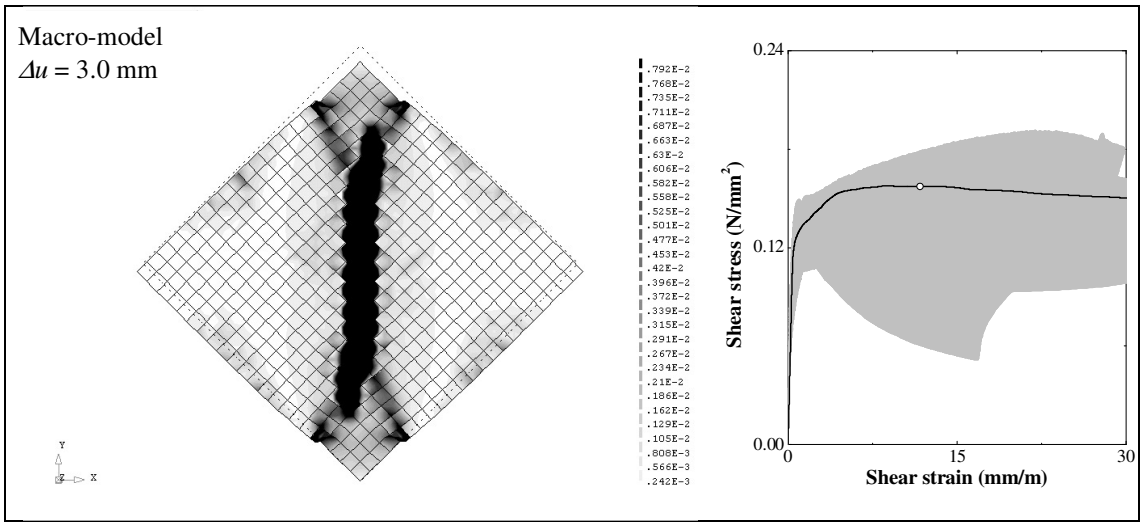

(a)

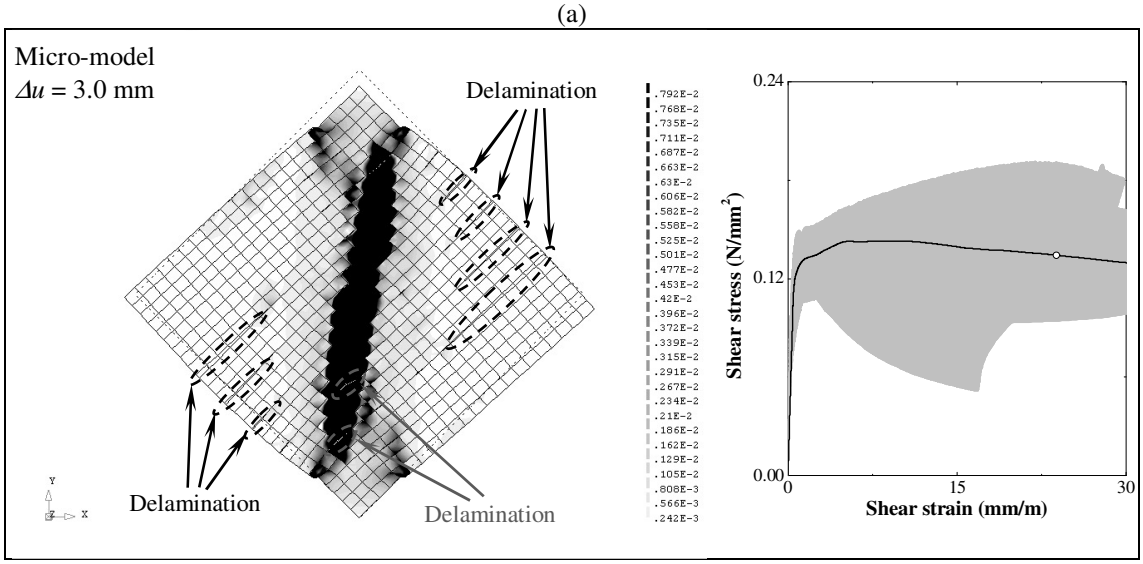

(b)

Figure 7.36 – Principal tensile strains for an imposed vertical displacement of 3.0 mm: (a) macro-model; (b) micro-model.

In the case of the macro-model, the damage is shown to concentrate at the middle of the model and to cross it from one support to the other. This corresponds to the formation of the diagonal system of cracks that characterized the failure mode of the experimental tests. The same is observed for the micro-model, but in addition, it is possible to observe the failure by delamination of some interfaces between layers. A slight deviation of the orientation of the damage diagonal seems also to be a consequence of this failure mode.

7.6 Conclusions

This Chapter deals with the numerical simulation of the shear behaviour of rammed earth walls, where both the macro- and micro-modelling approaches were used. The non-linear behaviour of rammed earth was modelled resorting to the Total Strain Fixed Crack Model (TSFCM) and to interfaces with the Mohr-Coulomb failure criterion.

The models of the BAM-ZRS unstabilised rammed earth wallets were calibrated using the experimental results of compression and diagonal-compression tests. Then, a sensitivity analysis was carried out, taking into account the uncertainties of the parameters involved in the models. Finally, the numerical simulation of the diagonal-compression tests carried out at UMinho was performed.

The compression behaviour of the wallets was simulated resorting to a multi-linear relationship and a good agreement with the compression tests was achieved. Regarding the simulation of the diagonal-compression tests, it was found that the parameters adopted with basis on recommendations for historical masonry promote a shear behaviour excessively brittle, when compared with the experimental results. Therefore, the calibration of the macro- and micro model required changes in the inelastic parameters. This means that ductility of rammed earth is better than typically assumed. Furthermore, the calibrated macro- and micro-model demonstrated a behaviour in agreement with the experimental envelope of the shear stress – shear strain curves.

Both models were able to capture the evolution of the damage during the test, characterized by the formation of the diagonal system of cracks. The micro-model allowed capturing the failure by delamination of the interfaces between layers, like observed in the experimental tests. This revealed to be the main advantage of the micro-modelling approach.

The sensitivity analysis performed on both models showed that the Poisson ratio, the compressive strength, the tensile strength and the tensile fracture energy are the parameters with the greatest influence on the maximum shear stress. Regarding the parameters of the interface elements, the cohesion is that with the greatest influence. The cohesion and the friction angle of the interfaces were found to be critical parameters regarding the occurrence of sliding failure. On the other hand, the tensile strength of the interface and the thickness of the rammed earth layers were shown to

have little influence on the shear behaviour. With respect to this last parameter, it should be noted that its variation has also practical implications in terms of compaction.

Finally, the modelling approach followed for the case of the BAM-ZRS was shown to be suitable to model the tests carried out at UMinho. Furthermore, it allowed confirming the important shear ductility of rammed earth and the capacity of the micro-model in simulate delamination failure.

Chapter 8

Conclusions and Future Work

8.1 Main conclusions

This thesis addresses the topic of the repair of earth constructions by means of the injection of unmodified mud grouts. The aim was to develop knowledge on this type of grouts when applied to rammed earth and to contribute for the characterization and numerical simulation of rammed earth construction.

The fulfilment of the aforementioned objectives led to the execution of an experimental program at both departments of Civil Engineering of the Catholic University of Leuven (KULeuven) and University of Minho (UMinho).

First, a composition study about the behaviour of unmodified mud grouts was carried out at both institutions. This experimental work involved several variables of the grout composition (volumetric solid fraction, percentage of clay deflocculant and percentage of the clay fraction) and the characterization of important properties governing the injection technique (rheology, shrinkage, adhesion, fresh-state stability and strength). Different proportions of kaolin and limestone powders, and sodium hexametaphosphate (HMP) constituted the mixtures tested, representing each a possible mud grout. The results showed a great dependency of the properties of the mixtures on their clay fraction. The rheological behaviour was shown to be affected negatively by flocculation of the clay particles, which was responsible for the formation of an internal house-of-cards or scaffold structure. The presence of this structure increased the flow resistance of the mixtures, namely in terms of a yield stress increase. The addition of HMP improved substantially the fluidity, mainly by decreasing the yield stress to values close to zero. This was found to be an important feature regarding the injection of mud grouts

under low pressure. The fluidity of the mixtures was enhanced by limiting the clay content with the addition of a silt-sized material, namely limestone powder. In general, it was shown that the design of a mud grout requires accounting for both the limitation of the clay content and the effect of the addition of a deflocculant. Otherwise, obtaining a mud grout with adequate fluidity would require a W/S ratio excessively high, which would promote excessive drying shrinkage.

The volumetric shrinkage of the KLH mixtures tested (composed by kaolin, limestone and HMP) was found to be very high, despite the relative low values set for the W/S, namely between 0.25 and 0.30. Nevertheless, the adhesion capacity of the selected mud grouts tested in small-scale specimens did not seem to be compromised by this fact. The mud grouts were able to allow recovering a substantial percentage of the original strength of the small-scale specimens (higher than 50% in the case of the experimental program at KULeuven and higher than 87% in the case of that at UMinho).

Regarding the fresh-state stability, the clay content of the selected grouts provided adequate stability against sedimentation and bleeding. In practical terms, this may mean that a mud grout is capable of featuring adequate stability, providing that adequate clay content is included.

The strength of the unmodified mud grouts was also influenced by its clay content; the higher the clay content, the higher the flexural and the compressive strengths.

The experimental program continued with the suitability assessment of four soils from Alentejo (Portugal) for unstabilised rammed earth construction. The aim of this step was the selection of a representative soil for manufacturing rammed earth specimens used for assessing the repair effectiveness of the injection of mud grouts. The suitability assessment was carried out resorting to the soil characterization by means of expeditious and laboratory tests, and to the performance assessment of the rammed earth manufactured with them, namely regarding the compressive strength and resistance to water erosion. Furthermore, the influence of the compaction conditions on the compression behaviour was also assessed.

The characterization of the soils was compared with recommendations from the bibliography, which in general deemed the soils as adequate for unstabilised rammed earth construction. However, the performance assessment revealed that the requirements for minimum strength where not respected for none of the regulating documents addressed. This shows that a suitability assessment relying only on soil characterization might produce erroneous conclusions. The compaction conditions were also shown to have great influence on the compression behaviour of each soil: the higher the dry density, the higher is the strength.

The soil (S5) selected for manufacturing the rammed earth specimens required PSD correction due to excessive clay content. The corrected soil (S6) was composed by 50% of soil S5, 28% of river sand and 22% of gravel. The compressive strength performance of the rammed earth manufactured with soil S6 deemed the NZS 4298 (NZS 1998b)

requirements, but not the thumb rule of a minimum strength of about 2.0 N/mm^2 (Houben and Guillaud 2008).

The soil S6 was used to manufacture medium- (beam-specimens) and large-scale (wallets) rammed earth specimens tested under three-point bending and diagonal-compression, respectively. These specimens were used to assess the repair effectiveness of three unmodified mud grouts, namely one "artificial" (composed by kaolin and limestone powders) and two "natural" (composed by natural sieved soil and limestone powder). The results indicated that the injection of mud grouts is capable of attaining adequate repair effectiveness, providing that the same soil used in the construction is incorporated in the grout. Another important observation taken consisted in the inability of the grout injection in recovering the initial shear stiffness of the wallet-specimens.

Furthermore, the ultrasound pulse velocity (UPV) technique was tried as a non-destructive method to assess the quality and effectiveness of the repair of rammed earth cracks. The results showed high scattering, but there seemed to be a promising relation between the recovery rate and the UPV variation between the damage and the repaired state.

Finally, the shear behaviour of rammed earth wallets tested under diagonal-compression was modelled resorting to the finite element method (FEM), where both macro- and micro-modelling approaches were used. The material behaviour was modelled resorting to the Total Strain Fixed Crack Model and to interfaces with the Mohr-Coulomb failure criterion. Both approaches provided an adequate simulation of the non-linear shear behaviour, where the enhanced shear ductility of rammed earth became patent. The advantage of the micro-modelling approach was the simulation of the delamination failure of the interfaces between layers. The sensitivity analysis performed showed that the Poisson ratio, the compressive strength, the tensile strength and the tensile fracture energy were the parameters with the greatest influence on the results. Therefore, further attention should be taken regarding these parameters in future works on the mechanical characterization of rammed earth.

8.2 Recommendations for the injection of rammed earth walls

The experimental program presented in the thesis promoted a better understanding of the behaviour of unmodified mud grouts and of the difficulties that may be found when they are used to repair cracks in rammed earth. Therefore, a set of recommendation was elaborated regarding the composition, the required properties and the injection procedure of unmodified mud grouts. To some extent, the proposed recommendations complement the design approach for mud grouts presented in Section 3.3.2. Furthermore, these recommendations are based on the experience acquired during the experimental work developed, yet they should be regarded as indicative and not as strict limits.

Regarding the composition of an unmodified mud grout, the following recommendations are presented:

- The same soil used in the construction should be incorporated in the mud grout;
- The maximum particle size of the mud grout should be limited to a value of about 0.180 mm. This is required in order to avoid sedimentation/segregation of the solid phase and to promote the injection of thin cracks, but larger than 0.540 mm;
- The clay percentage should be bounded between 15% and 30%. A clay percentage inferior to 15% may result in a grout with insufficient strength and adhesion capacity. On the other hand, a grout with clay percentage superior to 30% may limit the fluidity required;
- The W/S ratio should be defined between 0.25 and 0.35. A grout with very low W/S may compromise its fluidity and thus its injectability in cracks. On the other hand, a grout with high W/S may result in excessive drying shrinkage which hinders the establishment of the bond required;
- The percentage of HMP should be superior to 2% of the weight of the clay fraction of the grout. However, the optimization of the deflocculant percentage should be carried out for each case.

Despite these recommendations on the composition of a mud grout, its design process demands obtaining a material with adequate properties. The design process and further optimisation should be based on a set of tests where these properties are addressed. Thus, the following recommendations are given regarding the required properties of an unmodified mud grout:

- The flow time of 1 dm^3 grout through a Marsh cone with a 8 mm diameter nozzle (EN 445 (CEN 2007)) should be inferior to 1 min. Mud grouts with higher flow time may result in a non-injectable material;
- The volumetric shrinkage should be inferior to 16%. Despite this high limit, the mud grouts tested in the thesis with close values presented good adhesion capacity. The adhesion capacity was mainly controlled by the shrinkage mode, rather than by its magnitude;
- The flexural strength of the mud grout should be in between 0.5 N/mm^2 and 1.5 N/mm^2. A flexural strength inferior to the minimum limit may compromise the repair efficiency, while a flexural strength superior to the maximum limit may deem the grout as mechanically incompatible;
- The compressive strength of the mud grout should be in between 0.5 N/mm^2 and 4 N/mm^2. A compressive strength inferior to the minimum limit may indicate a grout with insufficient tensile strength, while a compressive strength superior to the maximum limit may deem the grout as mechanically incompatible;

- An adhesion value superior to 0.05 N/mm^2 (flexural strength from three-point bending tests on repaired specimens) can be suggested. However, the great dependency of this property on the characteristics of the repaired material advice considering this limit as a function of the recovery percentage. Thus, the recovery percentage of the mud grout should be higher than 50%.

Regarding the injection procedure of an unmodified mud grout, the following recommendations are provided:

- Before sealing the cracks, all debris within them and at the surface of the walls (eg.: plasters) should be removed resorting to compressed air. The use of water for this procedure should be avoided, since it may have an important negative impact on the strength of the construction;
- An earth mortar manufactured with the same soil of the construction is recommended to be used in the sealing of the cracks. If the strength of the mortar is expected to be unable to handle the injection pressure, the stabilisation with mineral binders should be accounted for. The drying/hardening of the sealing mortar is in general very fast and is controlled by the sorption promoted by the repaired material.
- In the case of very large cracks (eg.: width larger than 30 mm) gravel-sized aggregates should be introduced in the crack in order to mitigate the effects of the shrinkage;
- The installation of the injection tubes (6-10 mm diameter) should be carried out with a maximum spacing of about 100 mm. This aims at avoiding the hardening of the grout (by drying) before filling the cracks between injection tubes. Special attention should be given in the application of injection tubes in cracks orientated horizontally, where the air evacuation during the injection should be accounted for;
- Water should be injected in all injection tubes one hour before the injection of the grout, and in sufficient volume for mitigation of the water sorption by the repaired material;
- The injection of the mud grout should start from the lowest level tubes up to the top resorting to 100-500 ml syringes or to a pressure pot apparatus. In the first case, careful should be taken to not overpressure the syringe. In the second case, the injection pressure should be inferior to 0.02 N/mm^2. Possible leakages can be stopped resorting to an earth mortar with an important percentage of clay;
- The injection of mud grouts should be avoided under severe hot and dry conditions. If not possible, the injection should be carried out early in the morning or later in the evening.

8.3 Future work

The injection of unmodified mud grouts and the experimental and numerical behaviour of rammed earth were studied within the framework of this thesis, but these topics still need further investigation. In addition, a set of questions regarding the development of other type of repair/strengthening solutions for earth constructions and the numerical simulation of rammed earth should be addressed in further research. Thus, a listing of future works is proposed as follows:

- Application of the mud grout design approach to real case studies or to large-scale models in laboratory (eg.: injection of reduced-scale building models tested at shaking table);
- Further investigation on the behaviour of unmodified mud grouts, namely regarding the use of other deflocculants for clay (other than HMP), the repair effectiveness on adobe masonry, the understanding of the adhesion mechanisms associated to the mud grouts and durability assessment;
- Investigation on the behaviour of modified mud grouts with low percentages of mineral binders, namely regarding the investigation of adequate fluidity promoters (deflocculants for clays and cement superplasticizers) and the repair effectiveness on rammed earth and adobe masonry;
- Testing NDT-based methods (other than the UPV technique) for non-destructive evaluation of the injection repair effectiveness of cracks in earth constructions (eg.: bender element tests);
- Investigation on adequate solutions for repairing basal erosion of earthen walls, with special focus on the further development of the projected earth technique;
- Investigation on the seismic performance of rammed earth construction and on possible strengthening solutions, with special focus on the reinforced plaster technique;
- Application and validation of the numerical approach presented in real rammed earth constructions.

References

AFNOR (1992) NF P 18-891: "*Produits spéciaux destines aux constructions en béton hydraulique - Produits pour injections dans des structures en béton - Essai d'injectabilité à la colonne de sable en milieux sec et humide"*. France (in French)

AFNOR (2001). XP P13-90: Compressed earth blocks for walls and partitions: definitions – Specifications – Test methods – Delivery acceptance conditions. Saint-Denis La Plaine Cedex: AFNOR.

Aït-Kadi A., Marchal P., Choplin L., Chrissemant A. and Bousmina M. (2002). Quantitative analysis of mixer-type rheometers using the couette analogy. Canadian journal of chemical engineering, 80, pp. 1166-1174.

Andreola F., Castellini E., Ferreira J.M.F., Olhero S. and Romagnoli M. (2006) Effect of sodium hexametaphosphate and ageing on the rheological behaviour of kaolin dispersions, Applied Clay Science, 31, pp. 56-64.

Ashurst J. and Ashurst N. (1988) Practical building conservation, English Heritage Technical Handbook. Volume 1, 2 and 3., Gower Technical Press Ltd.

ASTM (1994) ASTM C 939-94: Standard test method for flow of grout for preplaced-aggregate concrete (flow cone method, American Society for Testing and Materials, West Conshohocken, PA.

ASTM (1995) ASTM D 4943: Standard Test Method for Shrinkage Factors of Soils by the Wax Method. American Society for Testing and Materials, West Conshohocken, PA.

ASTM (1998) ASTM D 422-63: Standard test method for particle size analysis of soils, American Society for Testing and Materials, West Conshohocken, PA.

ASTM (2000a) ASTM D 2488: Standard Practice for Description and Identification of Soils (Visual-Manual Procedure). American Society for Testing and Materials, West Conshohocken, PA.

ASTM (2000b) ASTM D 2487: Standard Practice for Classification of Soils for Engineering Purposes (Unified Soil Classification System). American Society for Testing and Materials, West Conshohocken, PA.

ASTM (2000c) ASTM D 4643: Standard test method for the determination of water (moisture) content of soil by the microwave oven method. American Society for Testing and Materials, West Conshohocken, PA.

ASTM (2002a) ASTM E 178-02: Standard practice for dealing with outlying observations. American Society for Testing and Materials, West Conshohocken, PA.

ASTM (2002b) ASTM E 519: Standard Test Method for Diagonal Tension (Shear) in Masonry Assemblages. American Society for Testing and Materials, West Conshohocken, PA.

ASTM (2003) ASTM C 940-98a Standard test method for expansion and bleeding of freshly mixed grouts for preplaced-aggregate concrete in the laboratory. American Society for Testing and Materials, West Conshohocken, PA.

ASTM (2010) C 953: Standard Test Method for Time of Setting of Grouts for Preplaced-Aggregate Concrete in the Laboratory. American Society for Testing and Materials, West Conshohocken, PA.

Ashurst J. and Ashurst N. (1988) Practical Building Conservation. Brick, Terracotta and Earth. Aldershot, Gower Press.

Bandeira R. (2009) Study of the correlation between mechanical strength and ultrasound speed for an earthen material. Msc. Thesis, Federal University of Minas Gerais, Brazil. (in Portuguese)

Barbosa N. and Mattone R. (2002). Building with raw earth. I Seminário Ibero-Americano de Construção com terra, Salvador, Brazil, pp. 41-50. (in Portuguese)

Barnes H. A., Hutton J. F. and Walters K. (1989) An Introduction to Rheology, Rheology Series Vol. 3, Elsevier, Amesterdam.

Binda L., Saisi A. and Tiraboschi C. (2001) Application of sonic tests to the diagnosis of damaged and repaired structures. NDT & E International, 34(2), pp. 123-138.

Binda L., Saisi A. and Tedeschi C. (2006) Compatibility of materials used for repair of masonry buildings: research and applications, *In* Fracture and Failure of Natural Building Stones: Applications in the Restoration of Ancient Monuments, Kourkoulis S.K. ed., Springer, Dordrecht, Netherlands, pp. 167-182.

Binda L., Saisi A. and Tiraboschi C. (2000) Investigation procedures for the diagnosis of historic masonries. Construction and Building Materials, 14, pp 199-233.

Blondet M., Garcia G. and Brzev S. (2003) Earthquake-Resistant Construction of Adobe Buildings: A Tutorial. Earthquake Engineering Research Institute, Oakland, California.

Bosiljkov V., Uranjek M. and Bokan-Bosiljkov V. (2010) An integrated diagnostic approach for the assessment of historic masonry structures. Journal of Cultural Heritage, 11 (3), pp. 239-249.

Bousmina M., Aït-Kadi A. and Faisant J. (1999). Determination of shear and viscosity from batch mixer data. Journal of rheology, 43(2), pp. 415-433.

Brady P.V., Cygan R.T. and Nagy K.L. (1996) Molecular controls on kaolinite surface charge. J. Colloid Interface Sci., 183, pp. 356-364.

Brás A. (2011) Grout optimization for masonry consolidation. PhD Thesis, Universidade Nova de Lisboa, Lisbon, Portugal.

Brás A. and Heriques F.M.A. (2012) Natural hydraulic lime based grouts – The selection of grout injection parameters for masonry consolidation. Construction and Building Materials, 26, pp. 135-144.

Bui Q.B., Morel J.C. (2009) Assessing the anisotropy of rammed earth. Construction and Building Materials, 23, pp. 3005-3011.

Bui Q.B., Morel J.C., Hans S. and Meunier N. (2009) Compression behaviour of non-industrial materials in civil engineering by three scale experiments: the case of rammed earth. Materials and Structurres, 42, pp. 1101-1116.

Cabral J. L. (2006) Training in Restoration and Conservation. In Houses and Cities Built With Earth - Conservation, Significance and Urban Quality, Argumentum, Lisbon, Portugal. (in Portuguese)

Camilloni H.R. (2003) Quincha architecture: The development of an antiseismic structural system in seventeenth century Lima. Proceedings of the First International Congress on Construction History, Madrid, Spain, pp. 1741-1752.

CEN (1999) EN 1015-11: 1999: Methods of test for mortar for masonry – Part 11: Determination of flexural and compressive strength of hardened mortar, European Committee for Standardization, Brussels.

CEN (2007) EN 445: Grout for prestressing tedons – Test methods, European Committee for Standardization, Brussels.

Ciancio D., Jaquin P. and Walker P. (2013) Advances on the assessment of soil suitability for rammed earth. Construction and Building Materials, 42, pp. 40-47.

Cizer O. (2009) Competition between carbonation and hydration on the hardening of calcium hydroxide and calcium silicate binders. PhD Thesis, Catholic University of Leuven, Belgium.

Cóias V. (2006) *"Inspecções e Ensaios na Reabilitação de Edifícios"*, IST, Lisbon, Portugal.

Cóias V. and Costa J.P. (2006) Projected Earth: a new method for rehabilitation of rammed earth constructions. In Houses and Cities Built with Earth: Conservation, Significance and Urban Quality, Eds. Achenza M., Correia M., Cadinu M., Serra A., Argumentum, Lisboa, pp. 59-61. (in Portuguese)

Cointeraux F. (1791). *"Traite dês Constructions Rurales et e Leur Disposition"*. Paris, France. (in French).

Collepardi M. (1999) Thaumasite formation and deterioration in historic buildings. Cement and concrete composites, 21, pp. 147-154.

Correia M. (2004) *"Fortificações islâmicas em taipa militar"*, Pedra & Cal, 24, pp. 16. (in Portuguese)

Correia M. (2007) Rammed Earth in Alentejo. Argumentum, Lisbon, Portugal.

Costa J.P. Cóias V. and Pifano A. (2008) *"Avantages de l aterre projetée dans la conservation structurelle du patrimoine en terre"*. In *"Séminare: Le Patrimoine Architectural d'Origine Portugaise au Maroc: Apports à sa Conservation"*, Rabat, Marrocos. (in French)

Cotic P., Jaglicic Z., Niederleithinger E., Effner U., Kruschwitz Z., Trela C. and Bosiljkov V. (2013) Effect of moisture on the reliability of void detection in brickwork masonry using radar, ultrasonic and complex resistivity tomography. Materials and Structures, DOI: 10.1617/s11527-012-0011-3.

CYTED (1995) *"Recomendaciones para la elaboración de normas técnicas de edificaciones de adobe, tapial, ladrillos y bloques de suelo-cemento". Sistematización del uso de la tierra en viviendas de*

interés social. Red Temática XIV.A HABITERRA-CYTED, Ottazzi, P., Martins, C., Vargas, N., Ribas, J., San Bartolomé, A. and de Silva, S. (in Spanish)

Damjamic F. and Owen D. (1984) Practical considerations for modeling of post-cracking concrete behavior for finite element analysis of reinforced concrete structures. In proceedings of the International Conference on Computer Aided Analysis and Design of Concrete Structures, pp. 693-706.

De Jongh S. and Van Wijnendaele (2009) Earthquakes and other damaging mechanisms to earth structures (Cuenca, Ecuador). Msc thesis, Catholic University of Leuven, Belgium.

De Sensi B. (2003) *"Terracruda, La Diffusione Dell'architettura Di Terra – Soil"*, Dissemination of Earth Architecture. (in Italian)

Delgado M. and Guerrero, I. (2007) The selection of soils for unstabilised earth building: A normative review, Construction and Building Materials, 21(2), 237-351.

De Wit P. (1995) Liquefaction of cohesive sediments caused by waves. PhD thesis, Technical University of Delft, The Netherlands.

Doat P., Hays A., Houben H., Matuk S. and Vitoux F. (1991). Building with earth. The Mud Village Society, New Delhi, India.

Encyclopaedia Brittannica (2013) www.britannica.com (assessed in 07/10/2013)

Fernandes M. (2008). Rammed Earth in the World. *Seminário de Construção e Recuperação de Edifícios em Taipa*, Almodôvar, Portugal. (in Portuguese)

Ferretti D., Bažant Z.P. (2006) Stability of ancient masonry towers: Moisture diffusion, carbonation and size effect. Cement and Concrete Research 36, pp. 1379-1388.

Figueiras J. (1983) Ultimate load analysis of anisotropic and reinforced concrete plates and shells. PhD Thesis, University of Wales, UK.

Flegmann A.W., Goodwin J.W. and Ottewill R.H. (1969) Rheological studies on kaolinite suspensions. Proc. Brit. Ceram. Soc., 13, pp. 31-45.

García R.M. (2010) *"Construcciones de Tierra. El Tapial. Nuevo Sistema para Construcción y Restauración Mediante la Técnica de "Tierra Proyectada""*, PhD thesis, University of Gra-nada, Granada, Spain. (in Spanish)

Getty (2007) Interdisciplinary Experts Meeting on Grouting Repairs for Large-scale Structural Cracks in Historic Earthen Buildings in Seismic Areas. The Getty Conservation Institute.

Gil M., Veiga R., Aguiar J., Seruya A., Carvalho L., Vargas H., Mirão J. and Candeias A. (2008) Color essays: an inside look into Alentejo traditional limewash paintings and colored lime mortars. In proceedings HMC08 – 1st Historical Mortars Conference: Characterization, Diagnosis Conservation, Repair and Compatibility, Lisbon, LNEC.

Gomes I. (2008) Earthquake-Resistant Construction with Raw Earth. Msc. Thesis, Instituto Superior Técnico, Lisbon, Portugal. (in Portuguese)

Gomes I., Lopes M. and Brito J. (2012) Seismic resistance of earth construction in Portugal. Engineering Structures, 33(3), pp. 932-941.

Gouy G. (1910). *"Sur la constitution de la charge électrique à la surface d'un électrolite"*. Ann. Phys. (Paris), 4 (9), pp. 457-468. (in French)

Gouy G. (1917) *"Sur la fonction électrocapillaire"*. Ann. Phys. (Paris), 9(7), pp. 129-184. (in French)

Hendrickx R. (2009) The Adequate Measurement of the Workability of Masonry Mortar, PhD Thesis, Katholieke Universiteit Leuven, Leuven, Belgium.

Houben H. and Guillaud H. (2008) Earth Construction: A Comprehensive Guide. CRATerre – EAG, Intermediate Technology Publication, London, United Kingdom.

ICCROM (1982). Proceedings of International Symposium on Mortars, cements and grouts used in the conservation of historic buildings. Rome, 414 pp.

Ignoul S., Van Rickstal F., Van Gemert D. (2005) Application of mineral grouts. Case study and impact on structural behaviour: Church of St. Catharina at Duisburg (B), Strutural Analysis of Historical Constructions, Modena, Lourenço & Roca (eds), London.

Jäger W. and Fuchs C. (2008) Reconstruction of the Sistani House at Bam Citadel after the collapse due to the earthquake 2003. In proceedings of VI International Conference on Structural Analysis of Historic Constructions 2008, D'Ayala D. and Fodde E. Eds., Vol. 2, Bath, UK, pp. 1181-1187.

Jaquin P.A. (2008) Analysis of Historic Rammed Earth Construction. PhD Thesis, Durham University, Durham, UK.

Jaquin P.A. (2013) One third of world's population live in earth buildings? Personal communication in http://historicrammedearth.com/one-third-of-worlds-population-live-in-earth-buildings/ (accessed in 11/10/2013).

Jaquin P.A., Augarde C.E. and Gerrard C.M. (2004) Analysis of Tapial structures for modern use and conservation. In proceedings of the 4th International Seminar on Structural Analysis of Historical Constructions, 10–13 November, Padova, Italy, pp. 1315-1321.

Jaquin P.A., Augarde C.E. and Gerrard C.M. (2006) Analysis of Historical Rammed Earth construction. In proceeding of 9th Young Geotechnical Engineers Conference 2006, Belfast, UK.

Jaquin P.A., Augarde C.E. and Gerrard C.M. (2008) Chronological Description of the Spatial Development of Rammed Earth Techniques. International Journal of Architectural Heritage, 2(4), pp. 377-400.

Jeffs A. (2001) Core Consolidations of Heritage Struture Masonry Walls & Foundations using Grouting Techniques – Canadian Case Studies. In proceedings of 9th Canadian Masonry Symposium, Canada.

Johansen R.T. and Dunning H.N. (1957) Water-vapor adsorption on clays, Clays and clay minerals, 6(1), pp. 249-258.

Keefe L. (2005) Earth Building: Methods and materials, repair and conservation, Taylor & Francis, London, UK.

Lacouture L., Bernal C., Ortiz J. and Valencia D. (2007) *"Estudios de vulnerabilidad sísmica, rehabilitación y refuerzo de casas en adobe y tapia pisada"*, Apuntes, 20(2), pp. 286-303. (in Spanish)

Legaly G. (2006) Colloid clay science, In: Bergaya F., Theng B.K.G. and Lagaly G. (Eds.) Developments in Clay Science: Handbook of Clay Science, Elsevier, Netherlands, pp. 141-245.

Lehmbau Regeln (1999). Begriffe; Baustoffe; Bauteile. Braunschweig/Wiesbaden, Germany: Friedr. Vieweg & Sohn Verlagsgesellscahaft mbH. (in German)

Le Roy, R. and Roussel N. (2005) The Marsh cone as viscometer: theoretical analysis and practical limits. Materials and Structures, 38 (1), pp. 25-30.

LNEC (1953). The use of earth as a building material. Laboratório Nacional de Engenharia Civil, Lisbon, Portugal. (in Portuguese)

LNEC (1965). NP 84: Soils: water content determination. Laboratório Nacional de Engenharia Civil, Lisbon, Portugal. (in Portuguese)

LNEC (1966). LNEC E196: Particle size distribution analysis. Laboratório Nacional de Engenharia Civil, Lisbon, Portugal. (in Portuguese)

LNEC (1967). LNEC E197: Compaction test. Laboratório Nacional de Engenharia Civil, Lisbon; Portugal. (in Portuguese)

LNEC (1969). NP 143: Soils: determination of the consistency limits. Laboratório Nacional de Engenharia Civil, Lisbon, Portugal. (in Portuguese)

Lootens D., Hébraud P., Lécolier E. and Van Damme H. (2004). Gelation, shear-thinning and shear-thickening in cement slurries, Oil and gas science and technology - Rev. IFP, 59(1), pp. 31-40.

Luckham P.F. and Rossi S. (1999) The colloidal and rheological properties of bentonite suspensions. Advances in Colloid and Interface Science, 82, pp. 43-92.

Luso E. (2012) Experimental Analysis of lime based grouts for injection of ancient masonry. PhD Thesis, University of Minho, Guimarães, Portugal. (in Portuguese)

Ma C. and Eggleton R.A. (1999a) Surface layer types of kaolinite: a high-resolution transmission electron microscope study. Clays Clay Miner., 47, pp. 181-19.

Ma C. and Eggleton R.A. (1999b) Cation exchange capacity of kaolinite. Clays and Clay Minerals, 47, pp. 174-180.

Mazzon N. (2010) Influence of grout injection on the dynamic behaviour of stone masonry buildings. PhD Dissertation, University of Padova, Italy.

Mendes N.M. (2012) Seismic Assessment of Ancient Masonry Buildings: Shacking Table Tests and Numerical Analysis. PhD Thesis, University of Minho, Guimarães, Portugal.

Mendes N.M. and Lourenço P.B. (2009). Seismic Assessment of Masonry ''Gaioleiro'' Buildings in Lisbon, Portugal. Journal of Earthquake Engineering, 14(1), pp. 80-101.

Miccoli L., Perrone C., Müller U., Gardei A. And Ziegert (2011). Structural performances of earthen building materials. A comparison between different typologies. In proceedings of the 2nd WTA – International PhD symposium – Building materials and building technology to preserve the built heritage, Brno, Czech Republic, pp. 85-95.

Mileto C., Vegas F. and López J.M. (2011) Criteria and Intervention Techniques in Rammed Earth Structures. The Restoration of Bofilla Tower at Bétera. Informes de la Construcción, vol. 63, pp. 81-96.

Miltiadou A. (1990) *"Contribution à l'étude des coulis hydrauliques pour la réparation et le renforcement des structures et des monuments historiques en maçonnerie"*, PhD Thesis, ENPC, Paris. (in French)

Minke G. (2006). Building with earth: Design and technology of a sustainable architecture. Birkhäuse-Publishers for Architecture, Basel-Berlin-Boston.

MOPT (1992). *"Bases Para el Diseño y Construcción con Tapial". Centro de Publicaciones, Secretaría General Técnica, Ministerio de Obras Públicas y Transportes*, Spain. (in Spanish)

Neto A., Repette W., Cincotto M. (2003) *"Influência do teor de ativador e da idade de exposição na retração por secagem de argamassas com cimentos de escória ativada com silicato de sódio". Boletim Técnico da Escola Politécnica da USP*, *Departamento de Engenharia de Construção Civil*, São Paulo, Brasil. (in Portuguese)

NMAC (2006). NMAC 14.7.4: Housing and Construction: Building Codes General: New Mexico Earthen Building Materials Code, New Mexico Regulation and Licensing Department, Santa Fe, New Mexico.

NZS (1998a). New Zealand Standard 4297:1998, Engineering design of earth buildings. Wellington: Standards New Zealand, Wellington.

NZS (1998b). New Zealand Standard 4298: 1998, Materials and workmanship for earth buildings,: Standards New Zealand, Wellington.

NZS (1998c). New Zealand Standard 4299:1998. Earth buildings not requiring specific design. Wellington: Standards New Zealand, Wellington.

OIA (1970). Handbook for building homes of earth. Department of housing and urban development, Office of International Affairs (OIA), Washington, DC 20410.

Oliveira D.V., Silva R.A., Lourenço P.B. and Garbin E. (2012) Strengthening of three-leaf stone masonry walls under compression: an experimental research. Materials and Structures, 45(8), pp. 1259-1276, DOI 10.1617/s11527-012-9832-3

Oliveira D. V., Varum H., Silva R. A., Pereira H., Lourenço P. B. and Costa A. (2007) Experimental characterization of the time-dependent behaviour of adobe masonry. V Seminário de Arquitectura Em Terra em Portugal, Aveiro, Portugal. (in Portuguese)

Oliver A. (2008) Conservations of nondecorated earthen materials. *In* Terra Literature Review: An overview of research in earthen architecture conservation, Avrami E., Guillaud H. and Hardy M. (Eds.), The Getty Conservation Institute, Los Angeles, pp. 108-123.

On Yee L. (2009) Study of earth-grout mixtures for rehabilitation. MSc Thesis, University of Minho, Guimarães, Portugal.

Paillère A., Bem Bassat M. and Akman S. (1992) Guide for use of admixtures in concrete. Materials and Structures, 25, pp. 49-56.

Papo A., Piani L. and Riceceri R. (2002) Sodium tripolyphosphate and polyphosphate as dispersing agents for kaolin suspensions: rheological characterization, Colloids and Surfaces A: Physiochemical and Engineering Aspects, 201, pp. 219-230.

Parreira D.J (2007). Análise Sísmica de uma Construção em Taipa. MSc Thesis, Instituto Superior Técnico, Lisbon, Portugal.

Pearson G.T. (1997) Conservation of Clay and Chalk Buildings. Shaftsbury, Donhead Pub-lishing Ltd.

Pérez C., Valencia D., Barbosa S., Saavedra P., Escamilla J. and Díaz E. (2007) *"Rehabilitación sísmica de muros de adobe de edificaciones monumentales mediante tensores de acero"*. Apuntes, 20(2), pp. 369-383. (in Spanish)

Perret S. (2002) *"Rôle du degré de saturation dês sables fins à moyens sur leur injectabilité par dês coulis de ciment microfin"*. PhD Thesis, Sherbrooke University, Quebec, Canada. (in French)

Perret S., Ballivy G., Palardy D. and Laporte R. (2003) Formulation of high-performance cement grouts for the rehabilitation of heritage masonry structures. In proceeding of Third International Conference On Grouting and Grout Treatment, New Orleans, Louisiana.

Pinto A. (2004) *"Sistemas ligantes obtidos por activação alcalina do metacaulino"*. PhD Thesis, University of Minho, Guimarães, Portugal. (in Portuguese)

Pinto J., Varum H., Cruz D., Sousa D., Morais P., Tavares P., Lousada J., Silva P. and Vieira J. (2010) Characterization of traditional tabique constructions in Douro North Valley region. WSEAS Transactions on Environment and Development, 6 (2), pp. 93-102.

Póvoas R. (1991) Non-linear models of analysis and design. PhD Thesis, University of Porto, Portugal. (in Portuguese)

Rand B. and Melton I.E. (1977) Particle interactions in aqueous kaolinite suspensions: I. Effect of pH and electrolyte upon the mode of particle interaction in homoionic sodium kaolinite suspensions. J. Colloid Interface Sci., 60, pp. 308-320.

Rocha M. (2005) Rammed earth in traditional architecture: construction techniques. In Earth architecture in Portugal. Argumentum, Lisboa, Portugal, pp. 22-26.

Rodriges Neto J.B., Novaes de Oliveira A.P., Alarcon O.E., Pozzi P. and Andreola F. (2002) Comparative study of deflocculation mechanisms in coloidal clay suspensions. In proceedings of Qualicer 2002, Castellón, Spain, pp. 283-300.

Roque J. (2002) Structural rehabilitation of ancient masonry walls. Msc Thesis, University of Minho, Portugal. (in Portuguese)

Roselund N. (1990) Repair of cracked walls by injection of modified mud. In proceedings of the 6th International Conference on the Conservation of Earthen Architecture: Adobe 90 Preprints, Las Cruces, New Mexico, pp. 336-341.

Roussel, N. and Le Roy, R. (2005) The Marsh cone: a test or a rheological apparatus?. Cement and Concrete Research, 35, pp. 823-830.

SAZS (2001). Standards Association Zimbabwe Standard 724:2001: Standard Code of Practice for Rammed Earth Structures. Harare: Standards Association of Zimbawbe.

Schofield R.K. and Samson H.R. (1953) The deflocculation of kaolinite suspensions and the accompanying change over from positive to negative chloride adsorption. Clay Minerals Bulletin, 2, pp. 45-51.

Schueremans L., Van Rickstal F., Verderickx K., Van Gemert D. (2003) Evaluation of masonry consolidation by geo-electrical relative difference resistivity mapping. Materials and Structures, 36 (1), pp. 46-50.

SENCICO (2000). *"Norma Técnica Edificación NTE E 0.80 Adobe". Reglamento Nacional de Construcciones*. Lima: SENCICO, Peru. (in Spanish)

Sepulcre-Aguilar A. and Hernandez-Olivares F. (2010) Assessment of phase formation in lime-based mortars with added metakaolin, Portland cement and sepiolite, for grouting of historic masonry. Cement and Concrete Research, 40, pp. 66-76.

Silva R.A. (2008) Experimental characterization of ancient masonry: strengthening and long-term effects. Msc Thesis, University of Minho, Guimarães, Portugal. (in Portuguese)

Silva R.A., Schueremans L. and Oliveira D.V. (2010). Grouting as a mean for repairing earth constructions. In proceedings of *6º Seminário de arquitectura em Portugal/9º seminário Ibérico Americano de construção e arquitectura com terra*, Correia M., Fernandes M. and Lopes M.C. (Eds.), Argumentum, Portugal, pp. 82-86.

Svermova L., Sonebi M. and Bartos P.J.M. (2003) Influence of mix proportions on rheology of cement grouts containing limestone powder. Cement and Concrete Composites, 25, pp. 737-749.

Standards Australia (2002). HB 195: The Australian earth building handbook. Sydney (Australia): Standards Australia.

Stern O. (1924) *"Zur Theorie der Elektrolytischen Doppelschicht. Z. Elektrochem"*. 30, pp 508-516.

Sybertz F. and Reick P. (1991) Effect of fly ash on the rheological properties of cement paste. In proceedings of International conference on rheology of fresh cement and concrete, E.& F.N. Spon, pp. 13-22.

TNO (2009) – Displacement method analyser (DIANA) User's Manual. Release 9.4, Netherlands.

Tolles E., Kimbro E. and Ginell W. (2002) Planning and Engineering Guidelines for the Seismic Retrofitting of Historic Adobe Structures, The Getty Conservation Institute, Los Angeles, USA.

Tolles E.L., Webster F.A., Crosby A. and Kimbro E.E. (1996) Survey of Damage to Historic Adobe Buildings after the January 1994 Northridge Earthquake. The Getty Conservation Institute Scientific Program Report, Los Angeles.

Tombácz E. and Szekeres M. (2004) Colloidal behavior of aqueous montmorillonite suspensions: the specific role of pH in the presence of indifferent electrolytes. Applied Clay Science, 27, pp. 75-94.

Tombácz E. and Szekeres M. (2006) Surface charge heterogeneity of kaolinite in aqueous suspension in comparison with montmorillonite, Applied Clay Science, 34, pp. 105-124.

Toumbakari E. (2002) Lime-Pozzolan-Cement Grouts and their Structural Effects on Composite Masonry Walls. PhD Thesis, Catholic University of Leuven, Leuven, Belgium.

Valluzi M. (2000) *"Comportamento Meccanico di Murature Consolidate Con Materiali e Tecniche a Base di Calce"*. PhD thesis, University of Trieste, Italy. (in Italian)

Valluzzi M., Da Porto F. and Modena C. (2003) Admixtures requirements for the injection of stone masonry walls. In proceedings of International Conference on Performance of Construction Materials, Cairo, Egypt, volume 1, pp. 393-402.

Valluzzi M.R., Da Porto F., Modena C. (2004) Behavior and modeling of strengthened three-leaf stone masonry walls, Materials and structures, 37(3), pp. 184-192.

Van Hees R.P.J, Binda L., Papayianni I. and Toumbakari E. (2004) Characterisation and damage analysis of old mortars. Materials and Structures, 37, pp. 644-648.

Van Olphen H. (1977) Clay colloid chemistry: for clay technologists, geologists, and soil scientists, 2nd ed., Wiley-Interscience, New York.

Van Rickstal F. (2000) Grout injection of masonry, scientific approach and modelling. PhD Thesis, Catholic University of Leuven, Leuven, Belgium.

Van Rickstal F. (2001) Grout injection of masonry, scientific approach and modeling. International Journal for Restoration of Buildings and Monuments, 7(34), pp. 407-432.

Van Rickstal F, Toumbakari E. Ignoul S. And Van Gemert D. (2003) Development of mineral grouts for consolidation injection. In Consolidation of Masonry, Advances in Materials Science and Restoration, Van Gemerts Eds, 1, Freiburg Aedificatio Publishers.

Van Tittelbooma K., De Beliea N., De Muyncka W., Verstraeteb W. (2010) Use of bacteria to repair cracks in concrete. Cement and Concrete Research, 40 (1), pp. 157-166.

Vargas J., Blondet M., Cancino C., Ginocchio F., Iwaki C. and Morales K. (2008) Experimental results on the use of mud-based grouts to repair seismic cracks on adobe walls. In proceedings of the VI International Conference on Structural Analysis of Historic Constructions 2008, D'Ayala D. and Fodde E. Eds., Bath, UK, pp. 1095-1099.

Varum H., Costa A., Pereira H. and Almeida J. (2006) Characterization tests of the structural behaviour of existing adobe constructions. V SIACOT: *Seminario Iberoamericano de Construcción con Tierra / I SAACT: Seminario Argentino de Arquitectura y Construcción con Tierra*, Mendoza, Argentina, pp. 48-51. (in Portuguese)

Varum H, Silveira D, Carvalho J, Figueiredo A, Costa A (2011) Characterization of the mechanical behaviour of adobe masonry walls. *Construcción com tierra. Tecnologia y Arquitectura. Congresso de tierra en Cuenca de Campos 2011*, Valladolid, pp. 225-228. (in Portuguese)

Velosa A. (2006) *"Argamassas de cal com pozolanas para revestimento de paredes antigas"*. PhD thesis, University of Aveiro, Portugal. (in Portuguese)

Vintezileou E. (2006) Grouting of three-leaf stone masonry: types of grouts, mechanical properties of masonry before and after grouting. Structural Analysis of Historical Constructions 2006, New Delhi.

Vintzileou E. and Miltiadou-Fezans A. (2008) Mechanical properties of three-leaf stone masonry grouted with ternary or hydraulic lime-based grouts. Engineering Structures, 30(8), pp. 2265-2276.

Vintzileou E. and Tassios T.P. (1995) Three-leaf stone masonry strengthened by injecting cement grouts. Journal of Structural Engineering, 121(5), pp. 848-856.

Warren J. (1999) Conservation of Earth Structures, Butterworth Heinemann, Bath, UK.

Williams D.J.A. and Williams K.P. (1978) Electrophoresis and zeta potential of kaolinite. J. Colloid Interface Sci., 65, pp. 79-87.

Williamson W. O. (2008) Flocculation. *In* Encyclopedia of Soil Science, Cheswoth W. (Ed.), Springer

Zhou Z. and Gunter W.D. (1992) The nature of the surface charge of kaolinite. Clays Clay Miner, 40, pp. 356-368.

Annex A

Mud Grouts Behaviour

A.1 Drying of the KLH specimens

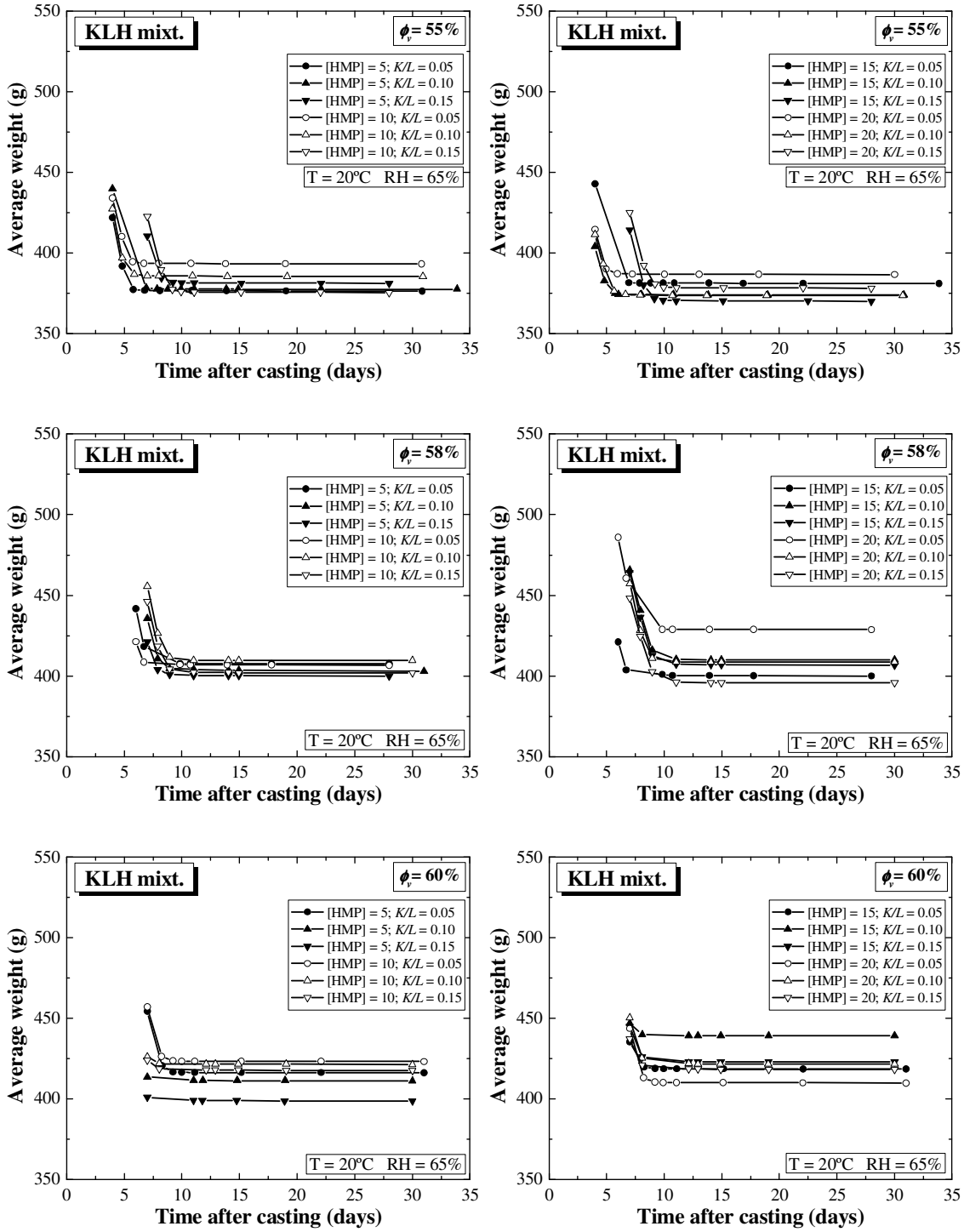

Figure A.1 – Drying of the KLH specimens.

A.2 Flow time measurements

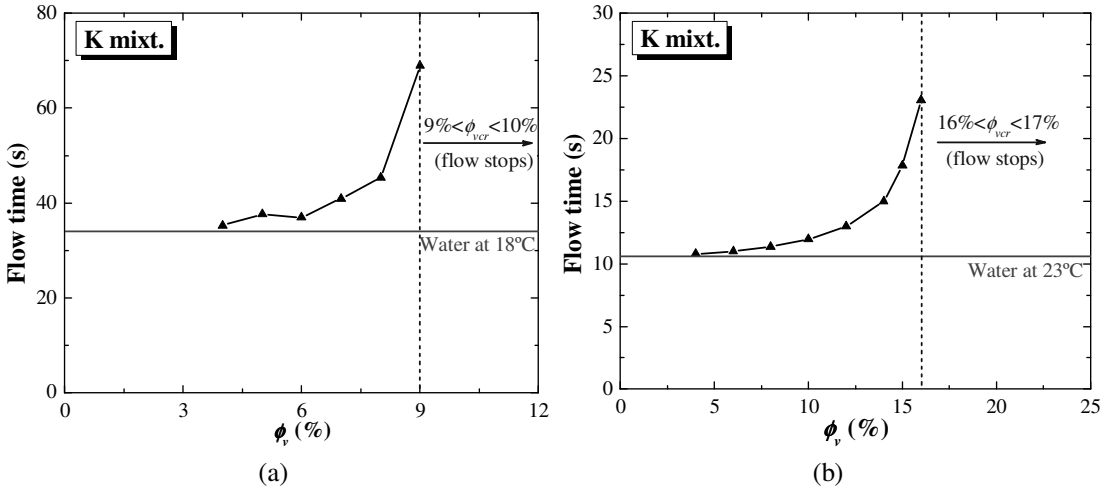

(a) (b)

Figure A.2 – Flow time measurements of the K mixtures: (a) KULeuven; (b)UMinho.

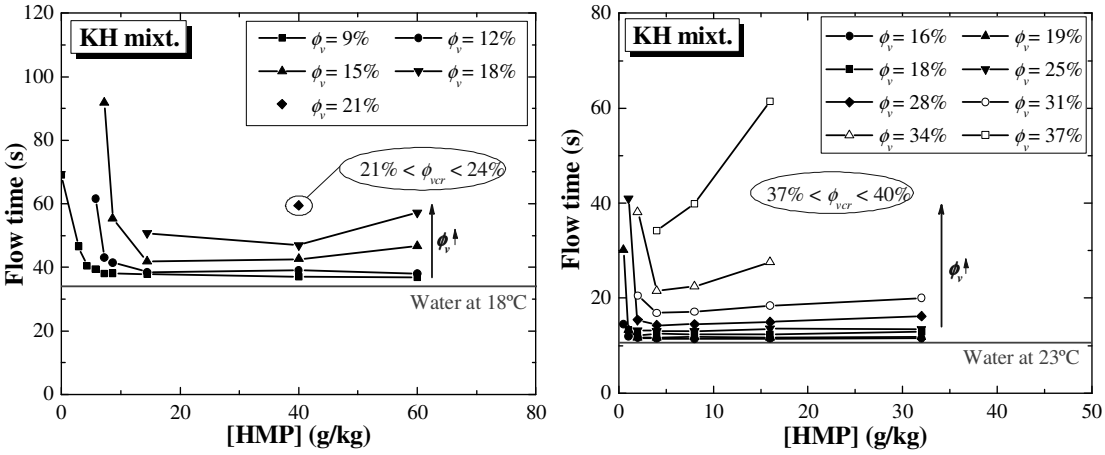

(a) (b)

Figure A.3 – Flow time measurements of the KH mixtures: (a) KULeuven; (b)UMinho.

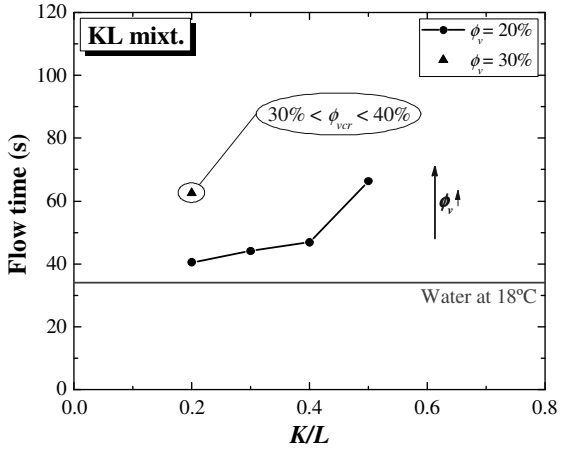

Figure A.4 – Flow time measurements of the KL mixtures tested at KULeuven.

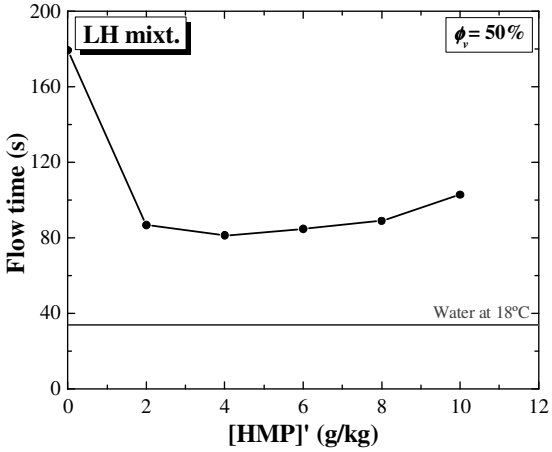

Figure A.5 – Flow time measurements of the LH mixtures tested at KULeuven.

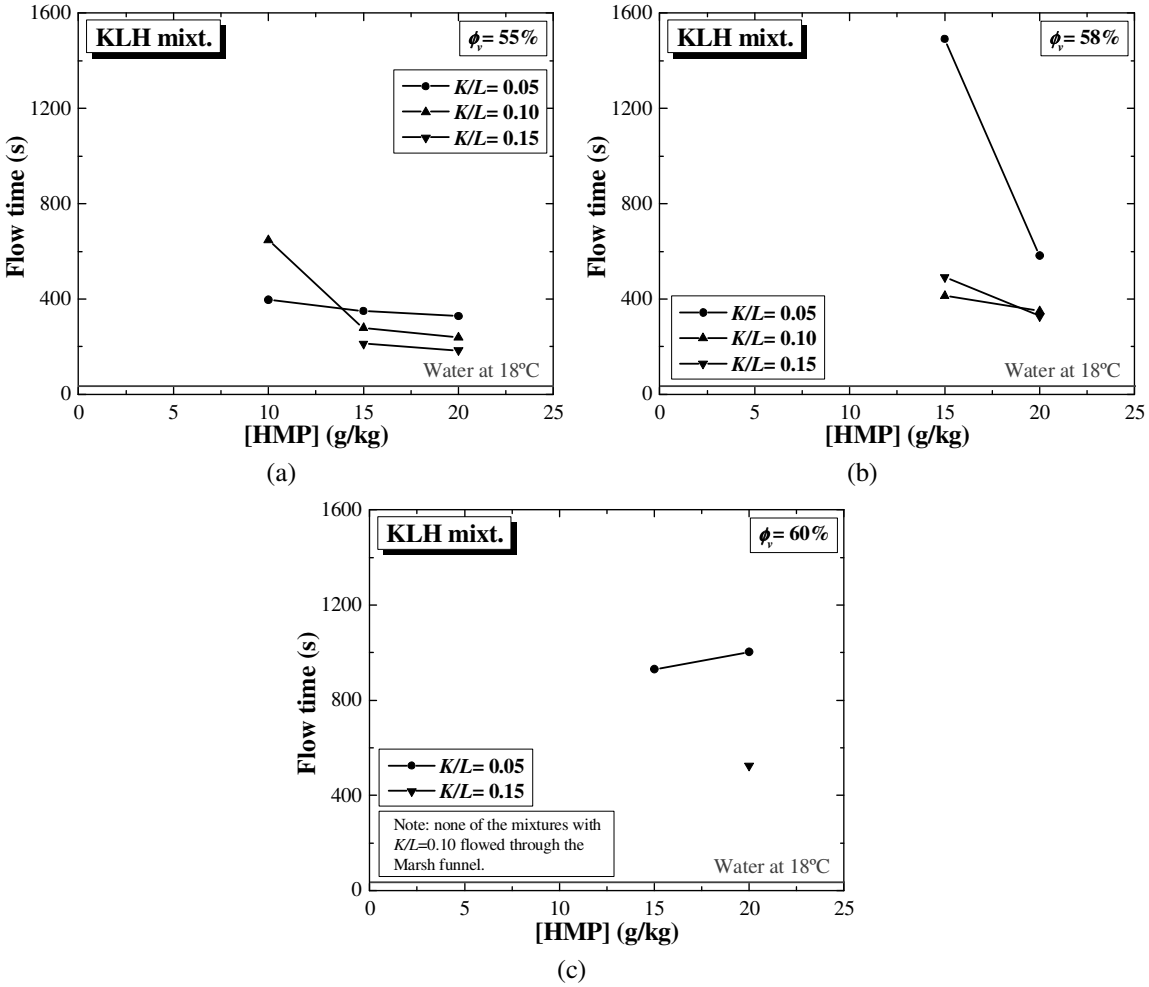

Figure A.6 – Flow time measurements of the KLH mixtures tested at KULeuven: (a) ϕ_v= 55%; (b) ϕ_v = 58%; (c) ϕ_v = 60%.

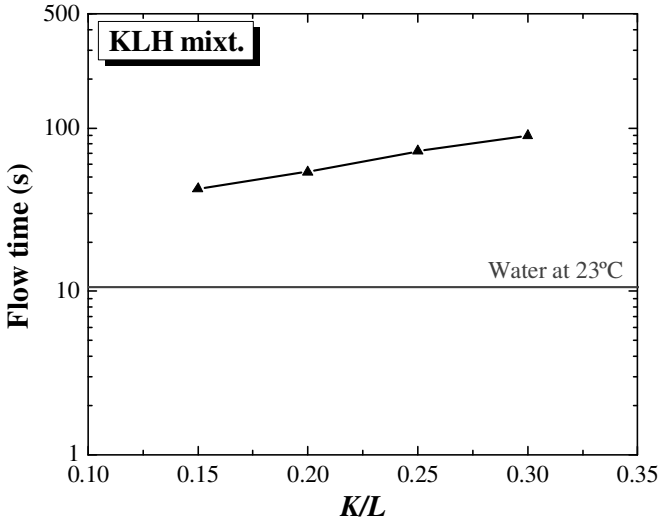

Figure A.7 – Flow time measurements of the KLH mixtures tested at UMinho (ϕ_v= 55%).

A.3 Flow curves

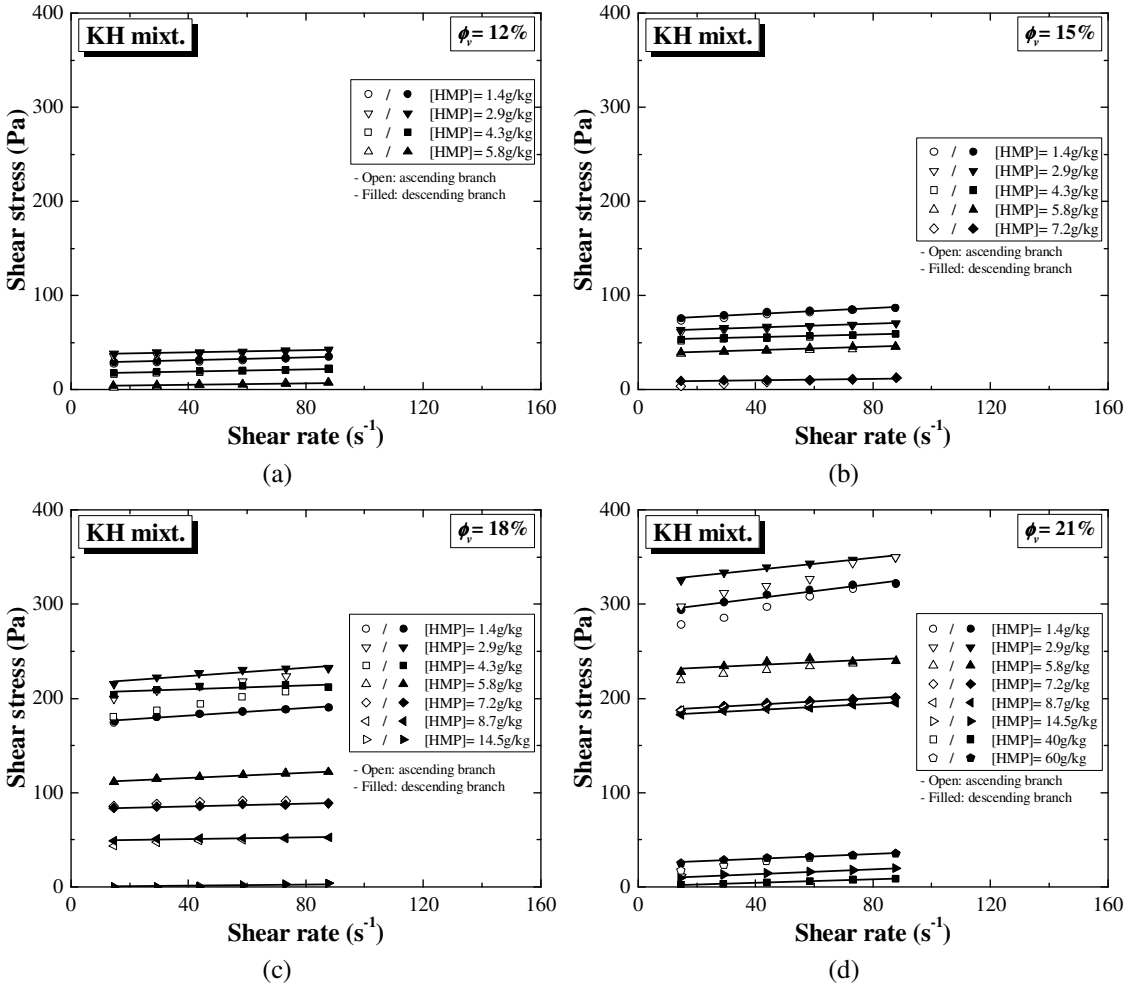

Figure A.8 – Flow curves of the KH mixtures (Bingham's model fitted to the descending branch): (a) ϕ_v= 12%; (b) ϕ_v = 15%; (c) ϕ_v = 18%; (d) ϕ_v = 21%.

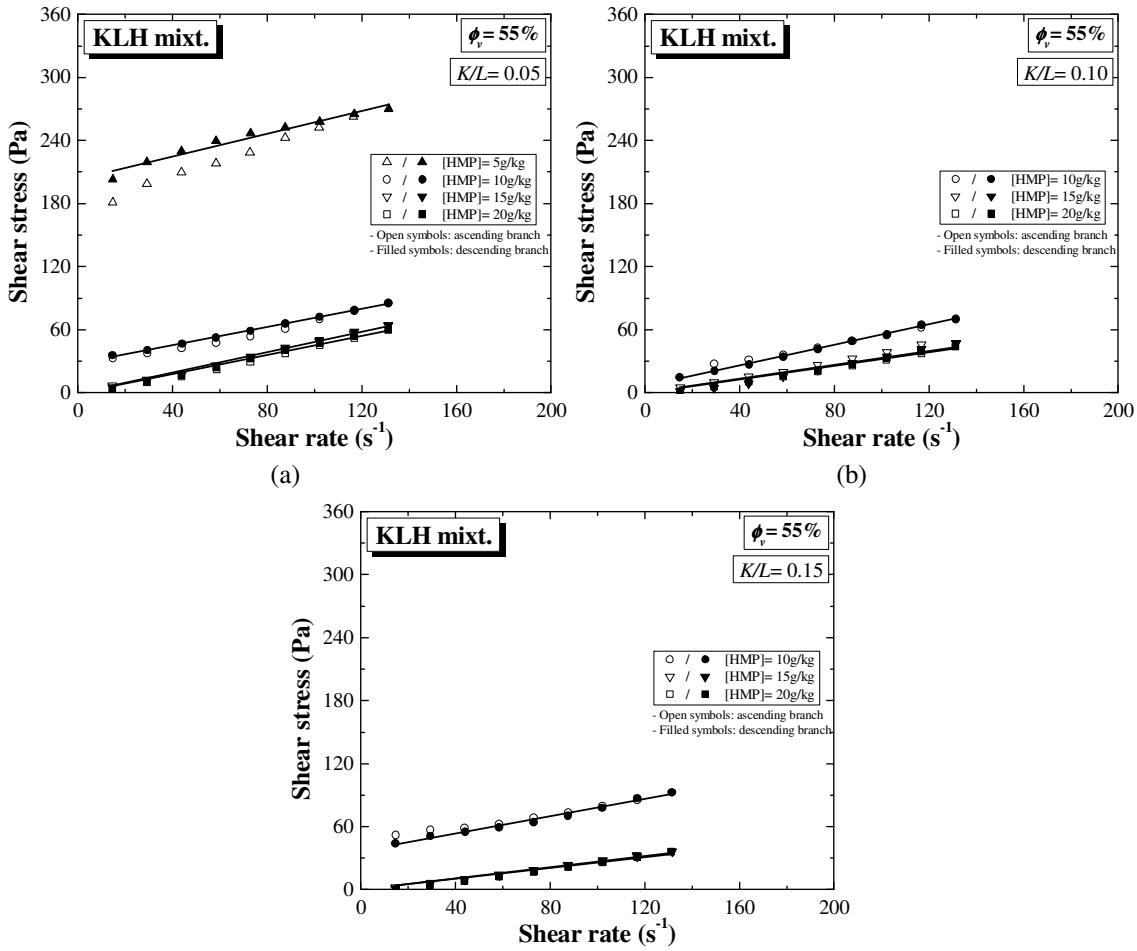

Figure A.9 – Flow curves of the KLH mixtures with ϕ_v= 55%. (Bingham's model fitted to the descending branch): (a) *K/L*= 0.05 (b) *K/L*= 0.10; (c) *K/L*= 0.15.

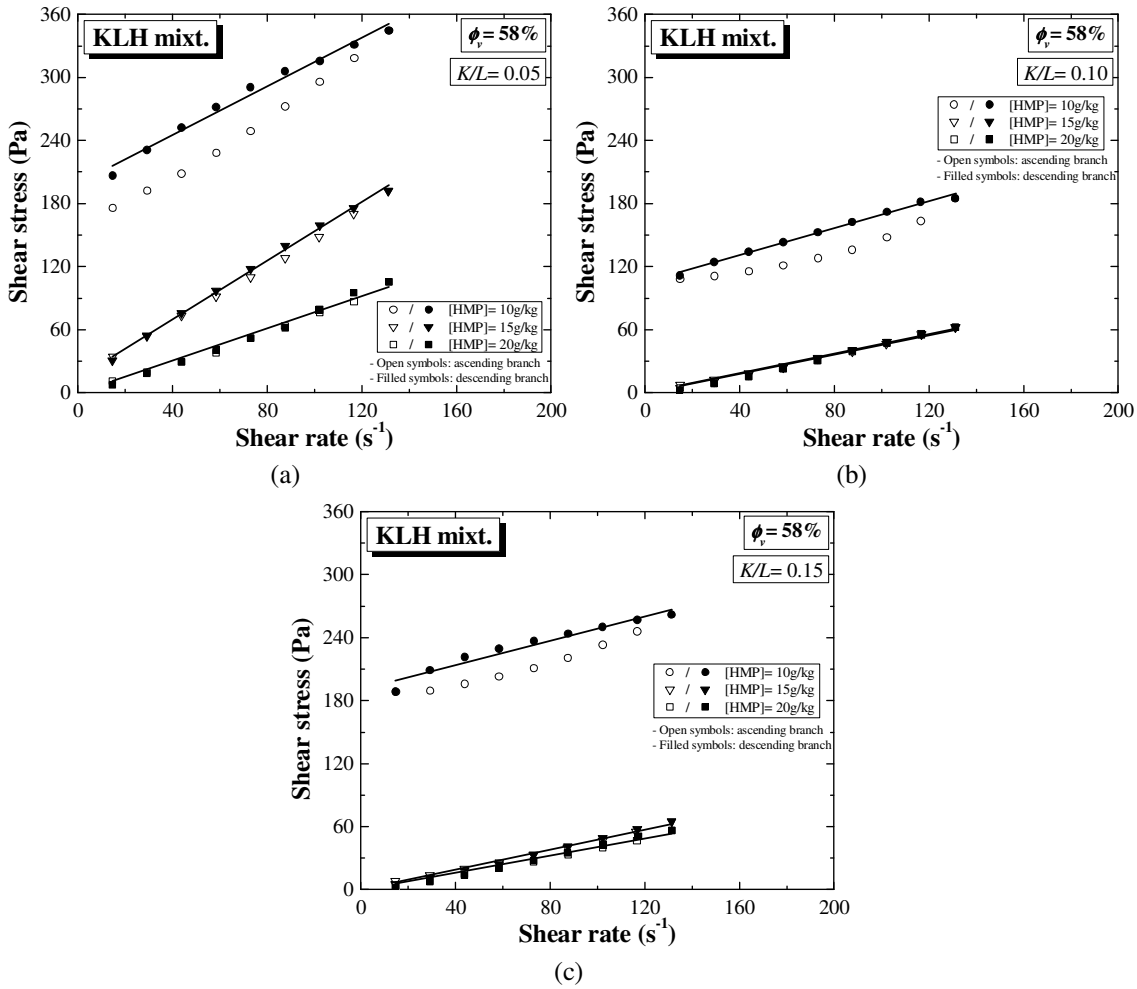

Figure A.10 – Flow curves of the KLH mixtures with ϕ_v= 58%. (Bingham's model fitted to the descending branch): (a) *K/L*= 0.05 (b) *K/L*= 0.10; (c) *K/L*= 0.15.

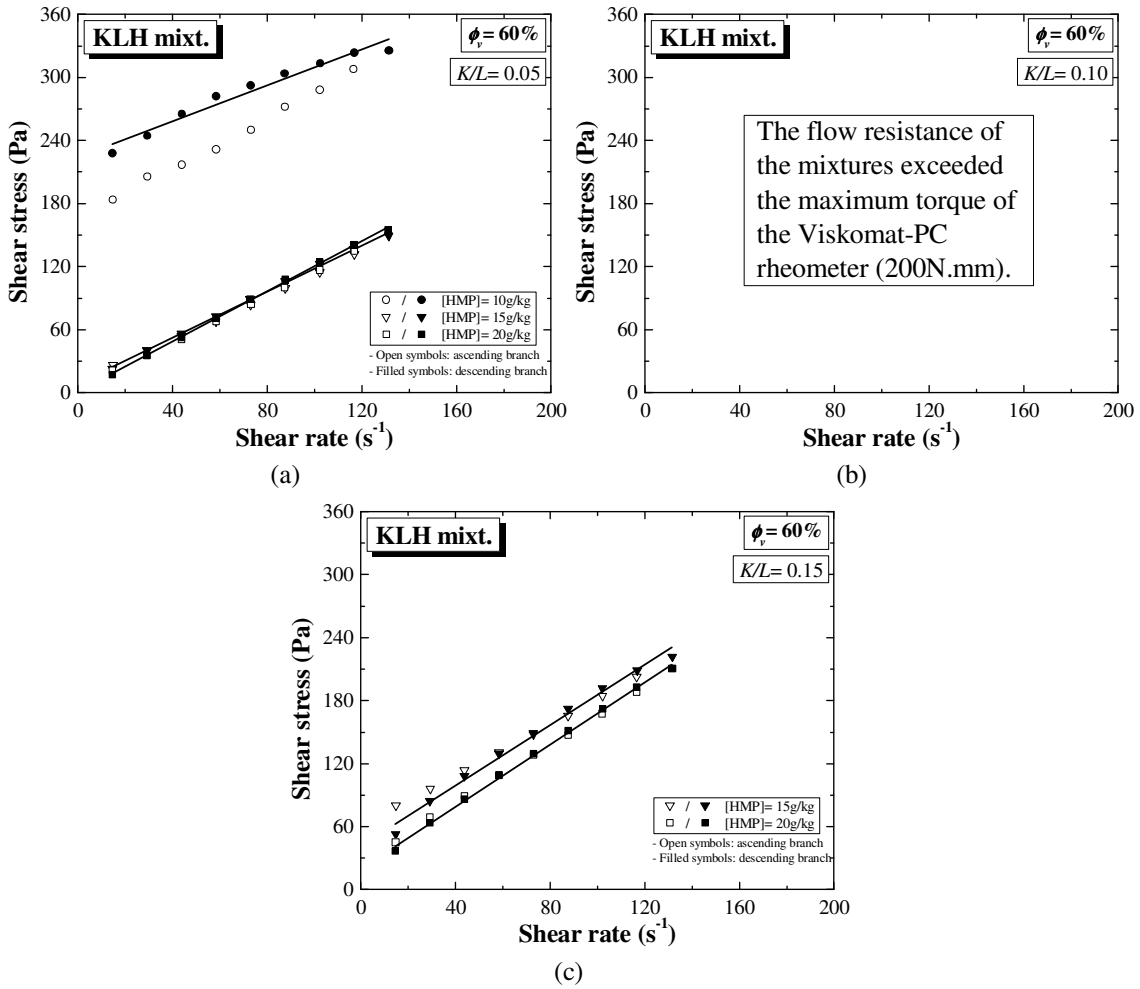

Figure A.11 – Flow curves of the KLH mixtures with ϕ_v= 60%. (Bingham's model fitted to the descending branch): (a) *K/L*= 0.05 (b) *K/L*= 0.10; (c) *K/L*= 0.15.

A.4 Bingham parameters

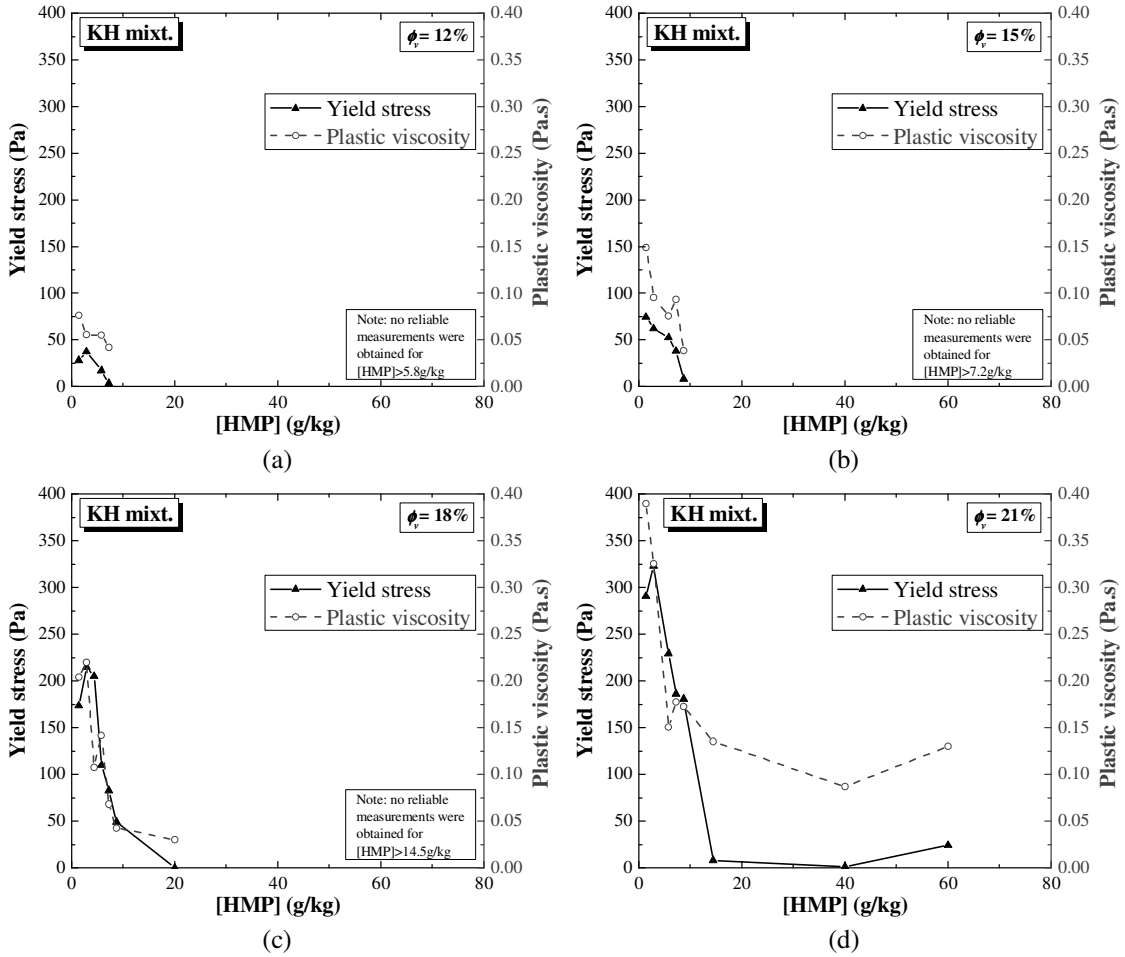

Figure A.12 – Bingham's parameters of the KH mixtures: (a) ϕ_v= 12%; (b) ϕ_v = 15%; (c) ϕ_v = 18%; (d) ϕ_v = 21%.

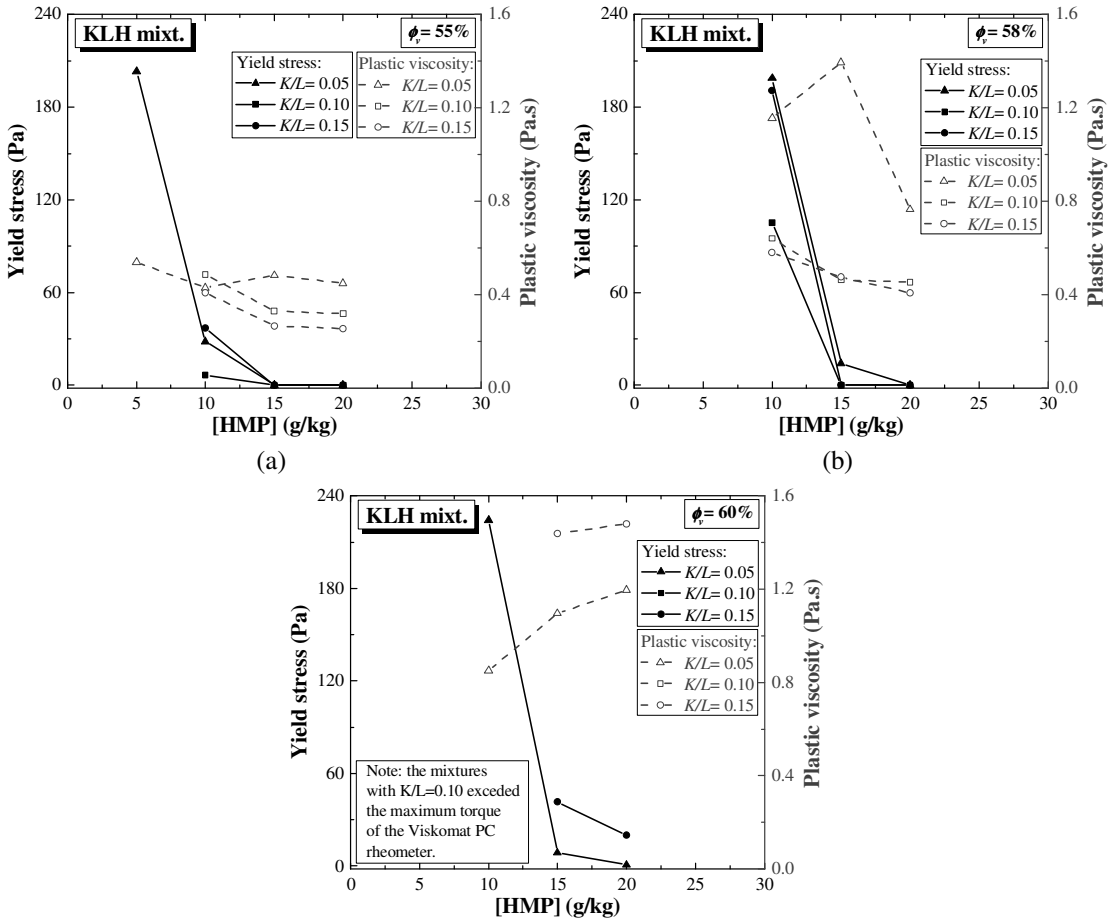

Figure A.13 – Bingham's parameters of the KLH mixtures: (a) ϕ_v= 55%; (b) ϕ_v = 58%; (c) ϕ_v = 60%.

A.5 Strength

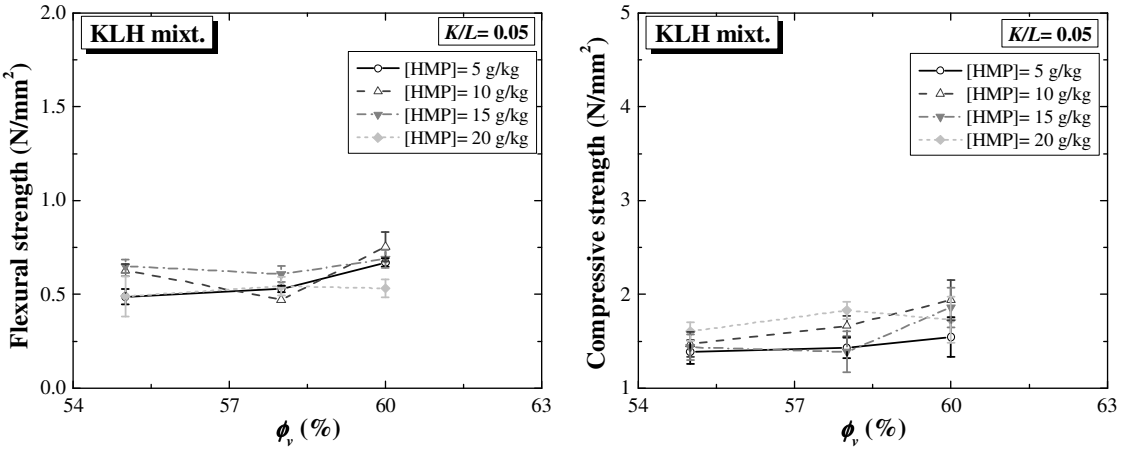

Figure A.14 – Strength of the KLH mixtures with *K/L*=0.05 tested at KULeuven: (a) flexural strength and (b) compressive strength.

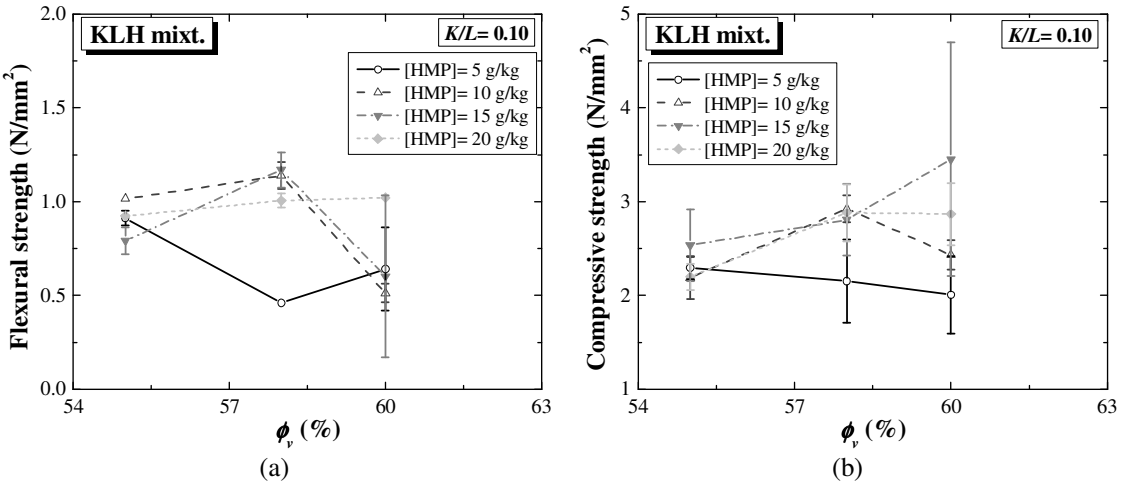

Figure A.15 – Strength of the KLH mixtures with *K/L*=0.10 tested at KULeuven: (a) flexural strength and (b) compressive strength.

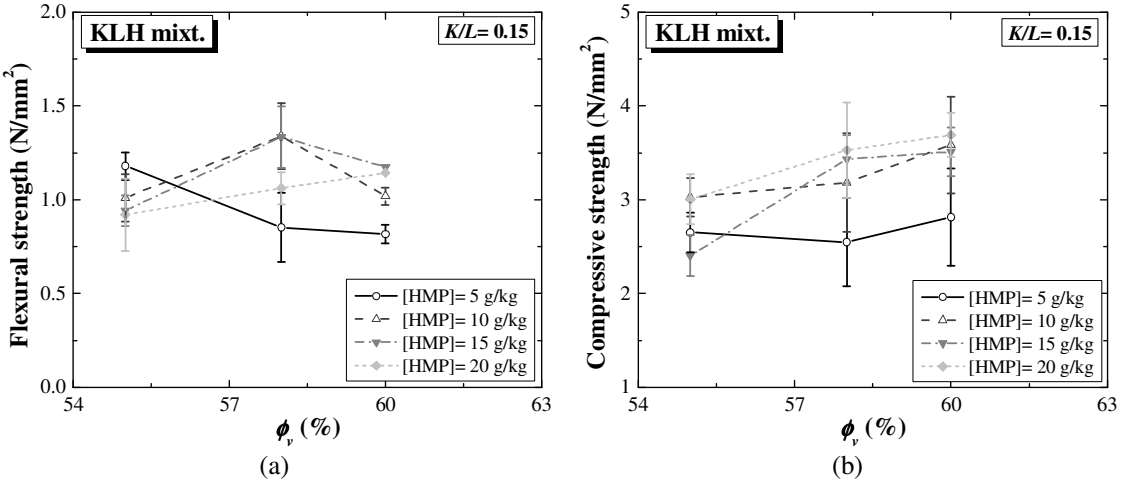

Figure A.16 – Strength of the KLH mixtures with *K/L*=0.10 tested at KULeuven: (a) flexural strength and (b) compressive strength.

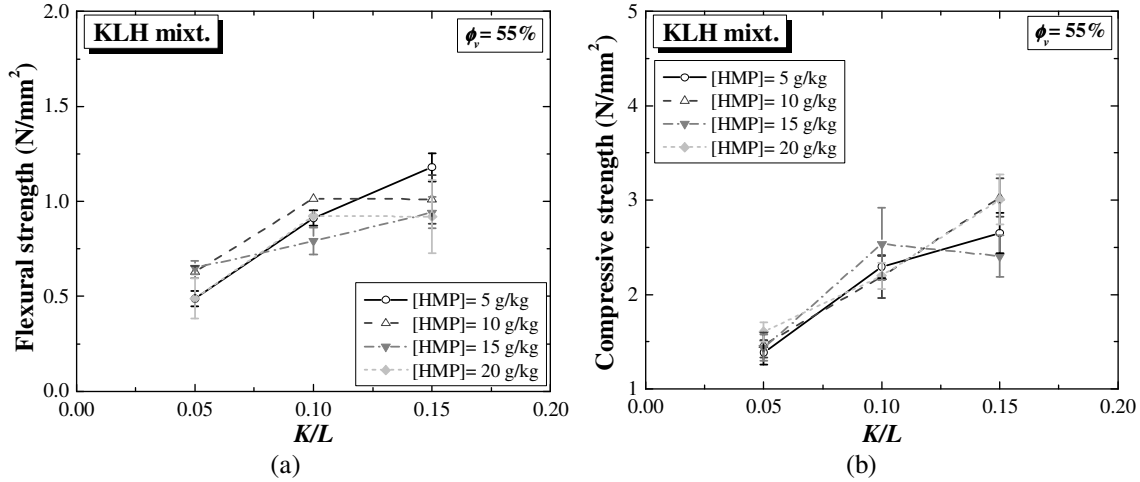

Figure A.17 – Strength of the KLH mixtures with ϕ_v=55% tested at KULeuven: (a) flexural strength and (b) compressive strength.

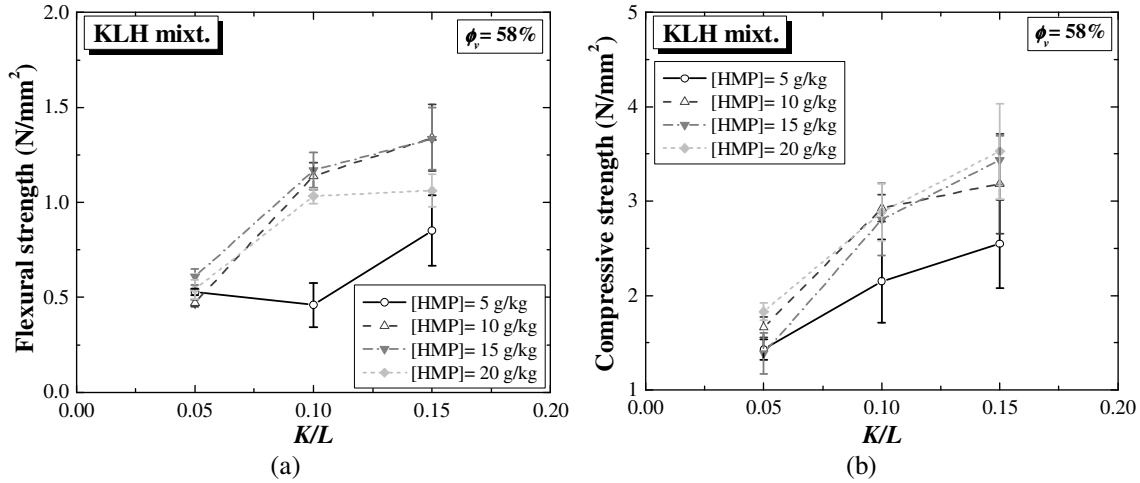

Figure A.18 – Strength of the KLH mixtures with ϕ_v=58% tested at KULeuven: (a) flexural strength and (b) compressive strength.

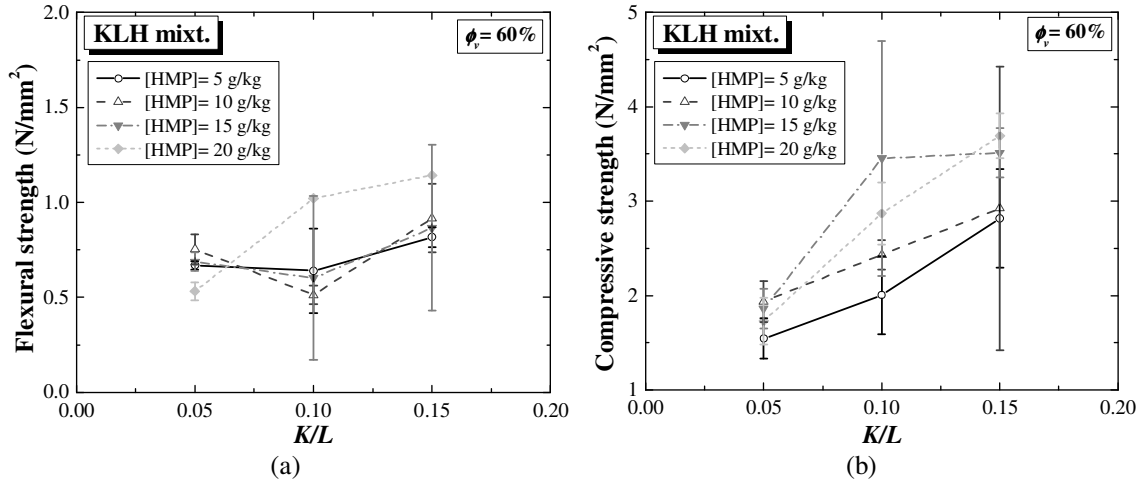

Figure A.19 – Strength of the KLH mixtures with ϕ_v=58% tested at KULeuven: (a) flexural strength and (b) compressive strength.

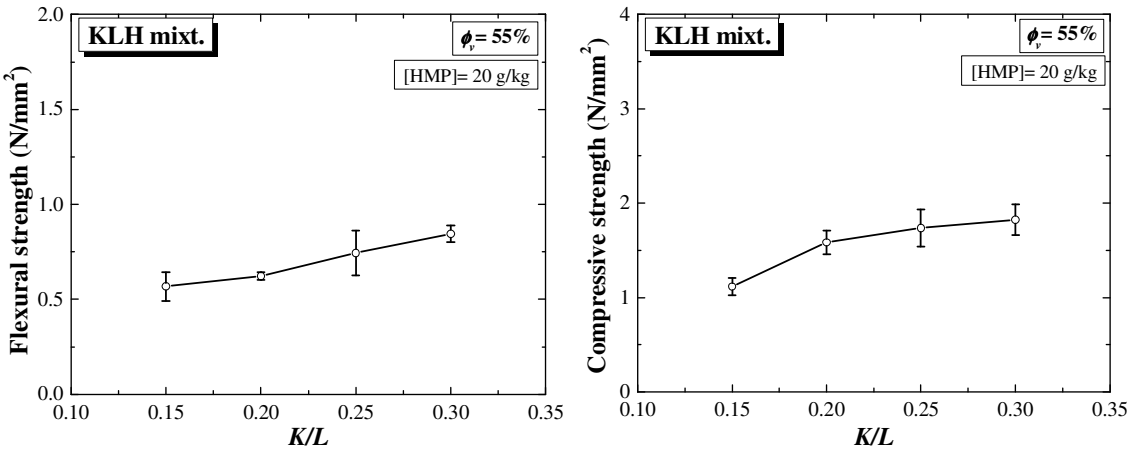

(a) (b)

Figure A.20 – Strength of the KLH mixtures tested at UMinho: (a) flexural strength and (b) compressive strength.

A.6 Volumetric shrinkage

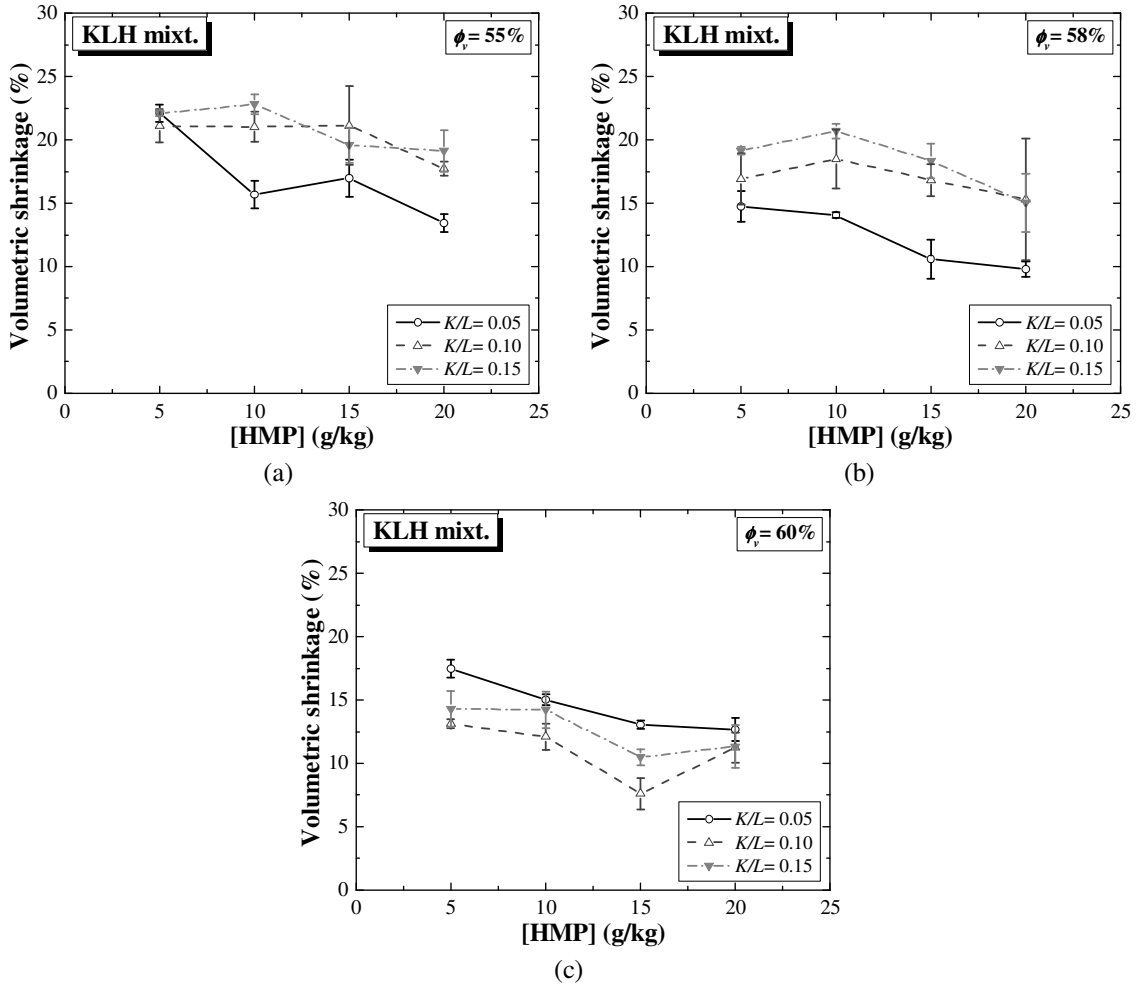

Figure A.21 – Volumetric shrinkage of the KLH mixtures tested at KULeuven: (a) ϕ_v= 55%; (b) ϕ_v = 58%; (c) ϕ_v = 60%.

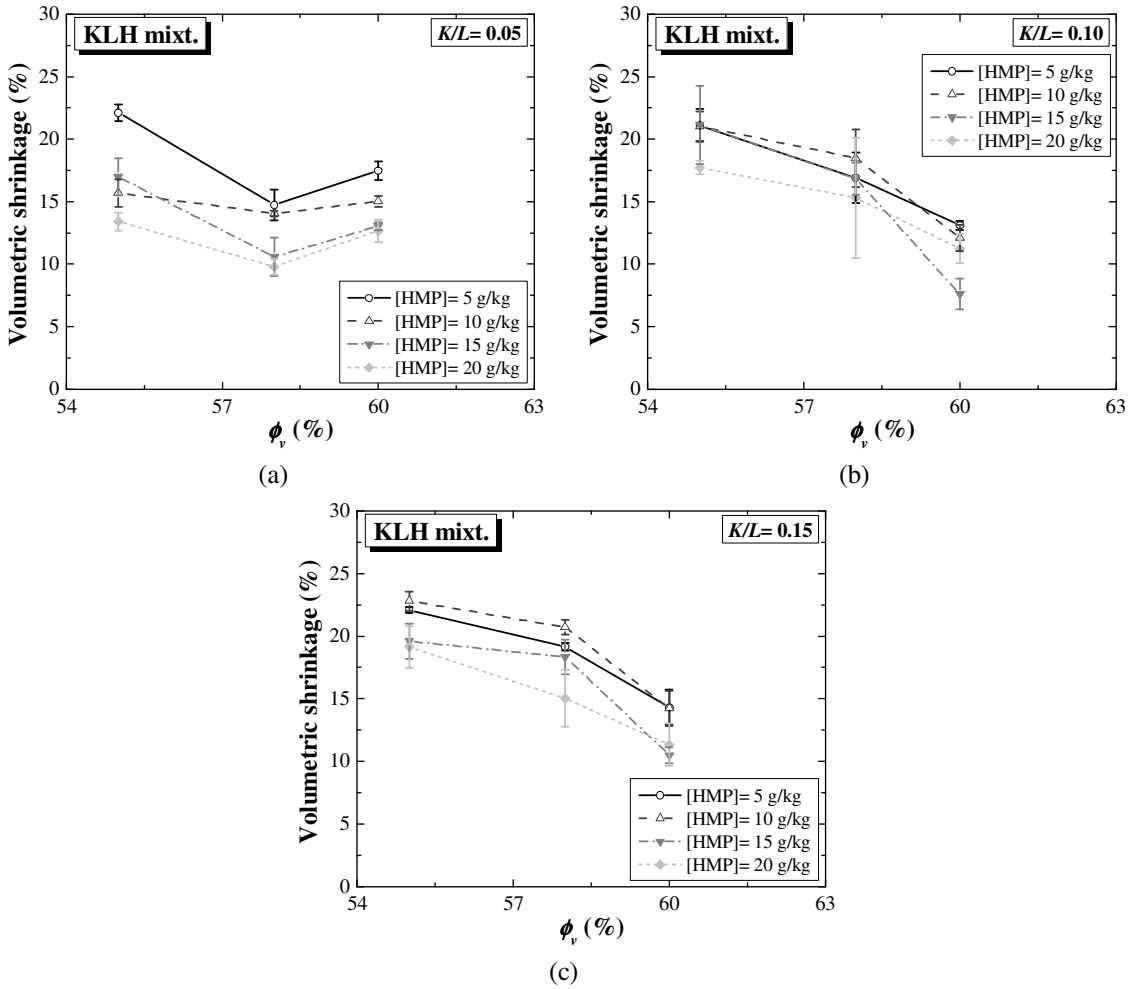

Figure A.22 – Volumetric shrinkage of the KLH mixtures tested at KULeuven: (a) *K/L*= 0.05; (b) *K/L*= 0.10; (c) *K/L*= 0.15.

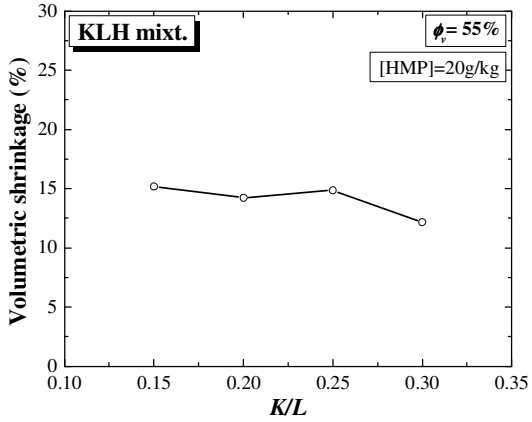

Figure A.23 – Volumetric shrinkage of the KLH mixtures tested at UMinho.

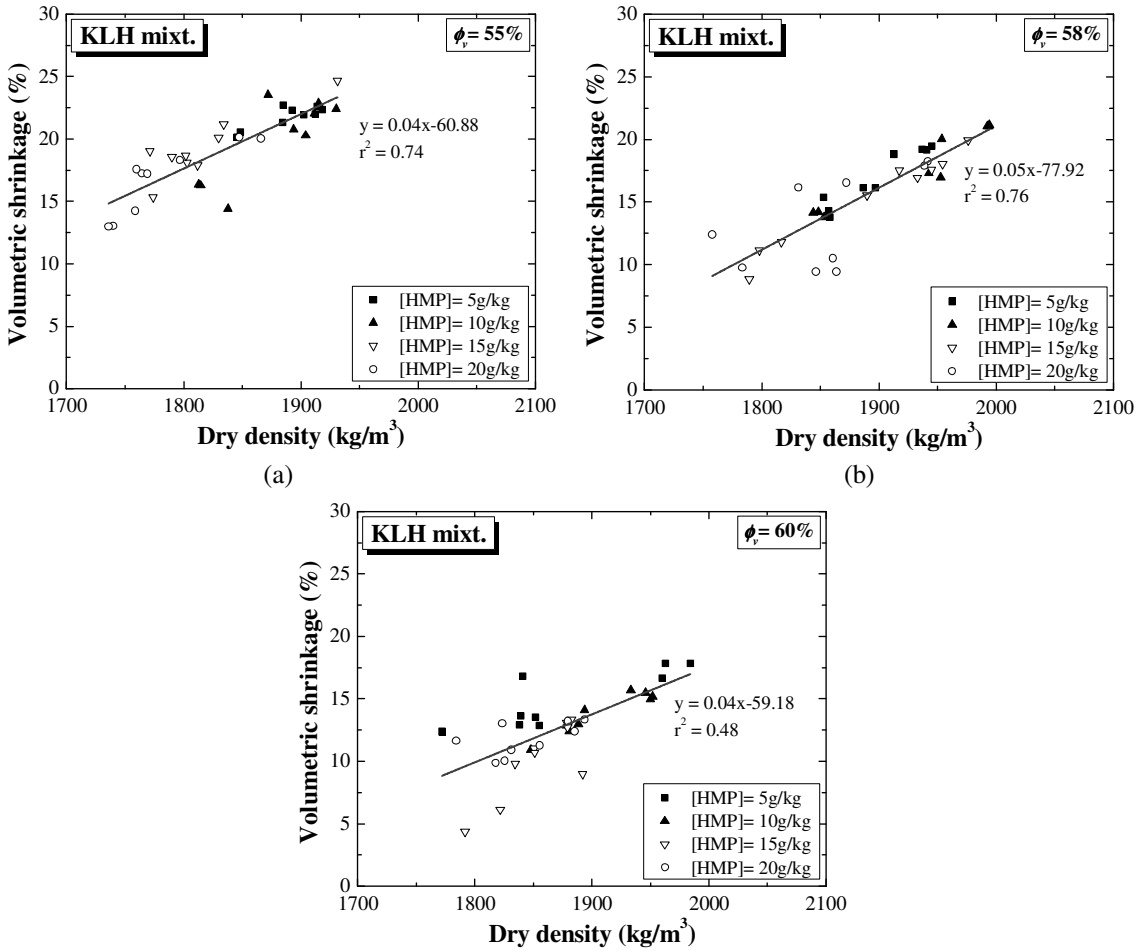

Figure A.24 – Volumetric shrinkage of the KLH mixtures tested at KULeuven as a function of the dry density: (a) ϕ_v= 55%; (b) ϕ_v = 58%; (c) ϕ_v = 60%.

Annex B

Soil Assessment

B.1 Compaction curves

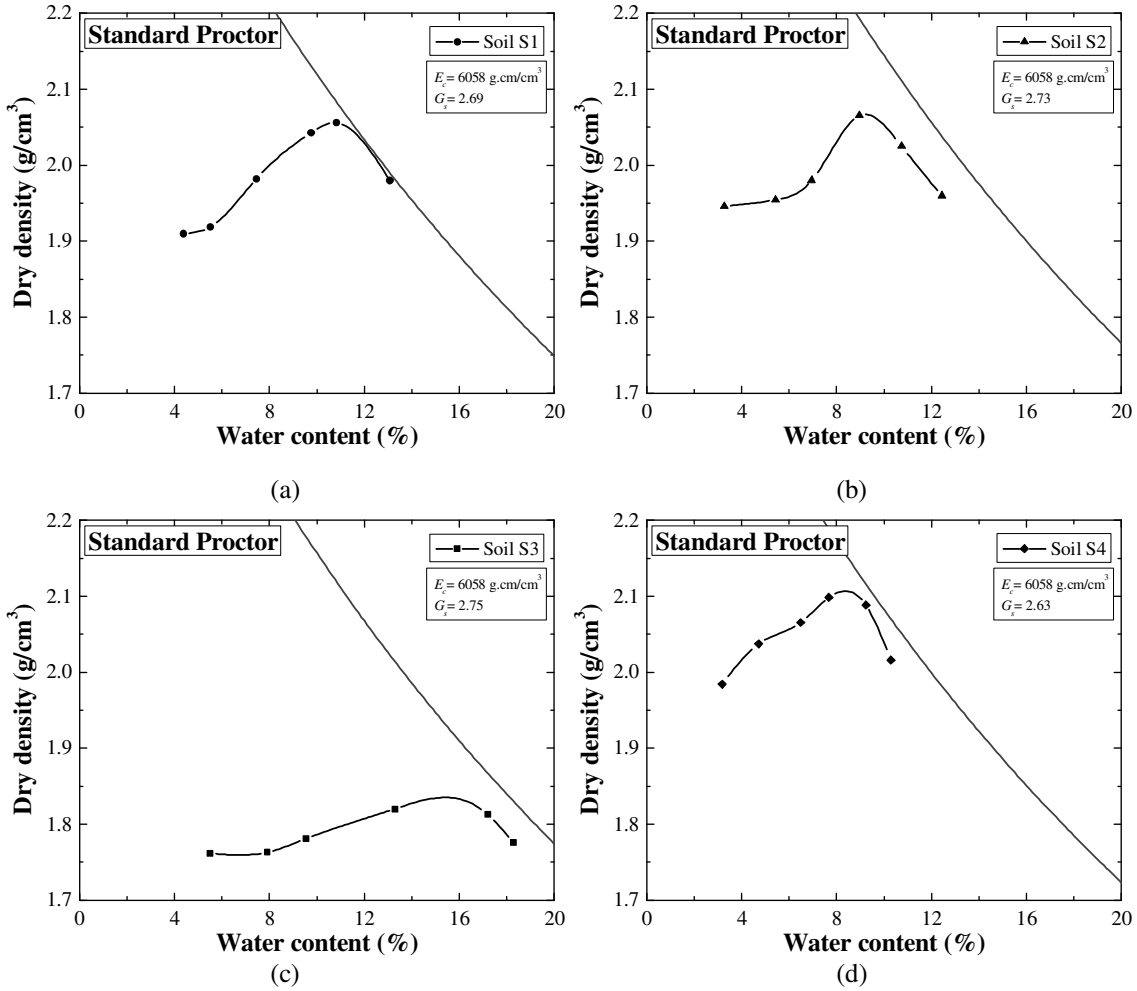

Figure A.25 – Compaction curves of the soils collected from Alentejo: (a) S1; (b) S2; (c) S3 and (d) S4.

B.2 Results of the compression tests

Table B.1 – Results of the rammed earth cylindrical specimens tested under compression.

Specimen	Soil	W (%)	ρ_d (g/cm^3)	f_c (N/mm^2)	E_0 (N/mm^2)	W_{eq} (%)
CURES1_1	S1	3.7	1.91		disaggregated	
CURES1_2	S1	5.6	1.91		disaggregated	
CURES1_3	S1	6.6	1.99	0.36	136	0.9
CURES1_4	S1	9.2	2.05	0.87	317	1.3
CURES1_5	S1	10.1	2.05	0.70	198	1.3
CURES1_6	S1	13.3	1.98	0.71	268	1.5
CURES2_1	S2	3.1	1.94		disaggregated	
CURES2_2	S2	5.2	1.94	0.24	137	0.4
CURES2_3	S2	7.4	1.96	0.36	273	0.3
CURES2_4	S2	9.2	2.05	0.49	348	0.3
CURES2_5	S2	11.0	2.01	0.42	303	0.3
CURES2_6	S2	12.3	1.95	0.29	321	0.4
CURES3_1	S3	4.7	1.76		disaggregated	
CURES3_2	S3	7.7	1.76		disaggregated	
CURES3_3	S3	9.5	1.77	0.18	173	0.6
CURES3_4	S3	12.7	1.82	0.35	442	0.6
CURES3_5	S3	15.9	1.82	0.38	447	0.7
CURES3_6	S3	17.9	1.77	0.43	757	0.7
CURES4_1	S4	2.9	1.98		disaggregated	
CURES4_2	S4	4.2	2.04		disaggregated	
CURES4_3	S4	6.5	2.06	1.02	1331	0.5
CURES4_4	S4	6.9	2.10	0.98	1506	0.5
CURES4_5	S4	8.5	2.09	0.83	2863	0.8
CURES4_6	S4	Unable to auto-sustain after demoulding due to excessively high W				

Annex C

Repair Effectiveness

C.1 Three-point bending tests on medium scale specimens

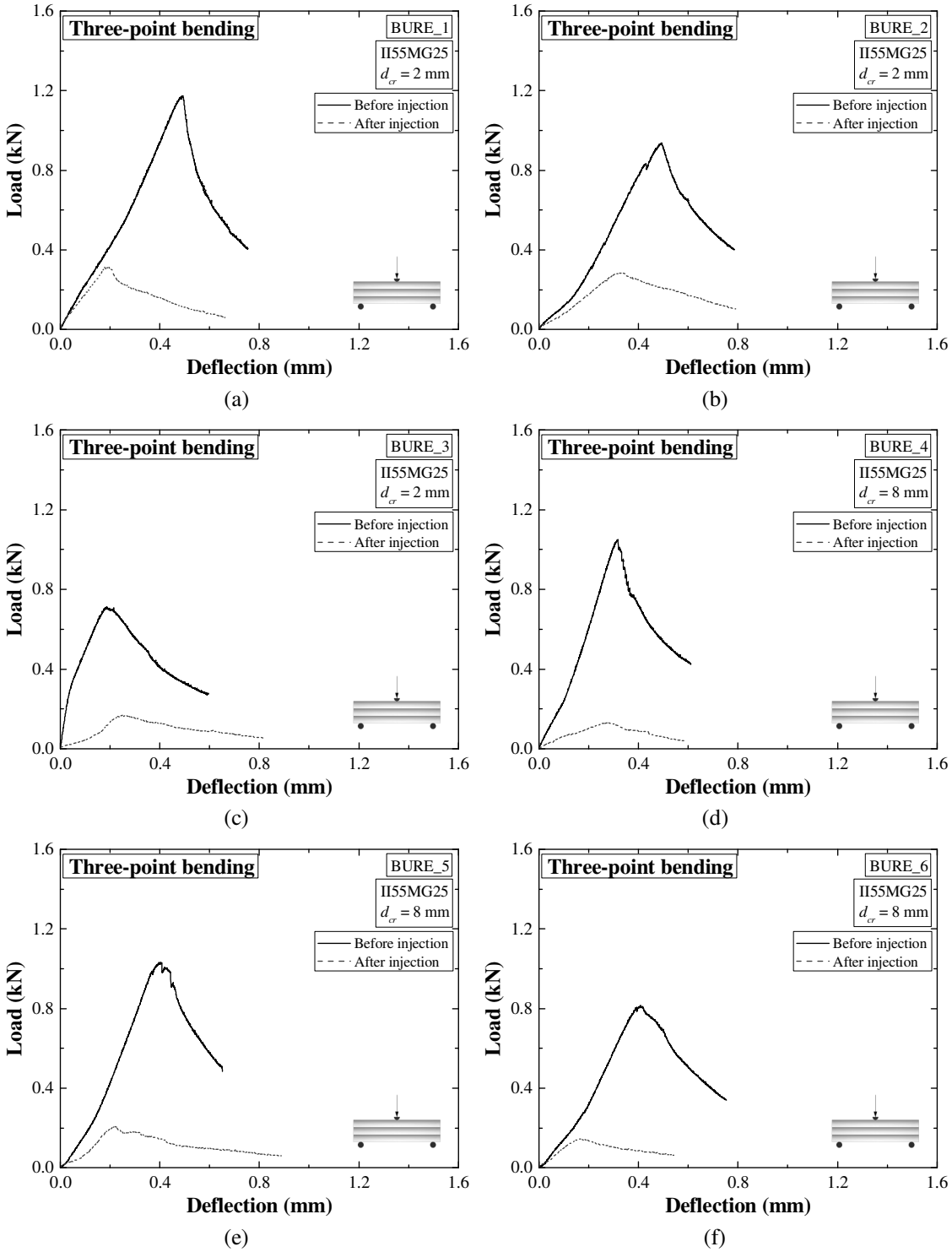

Figure C.1 – Load–deflection curves of the medium-scale specimens repaired with the mud grout II55MG25: (a) BURE_1; (b) BURE_2; (c) BURE_3; (d) BURE_4; (e) BURE_5; (f) BURE_6.

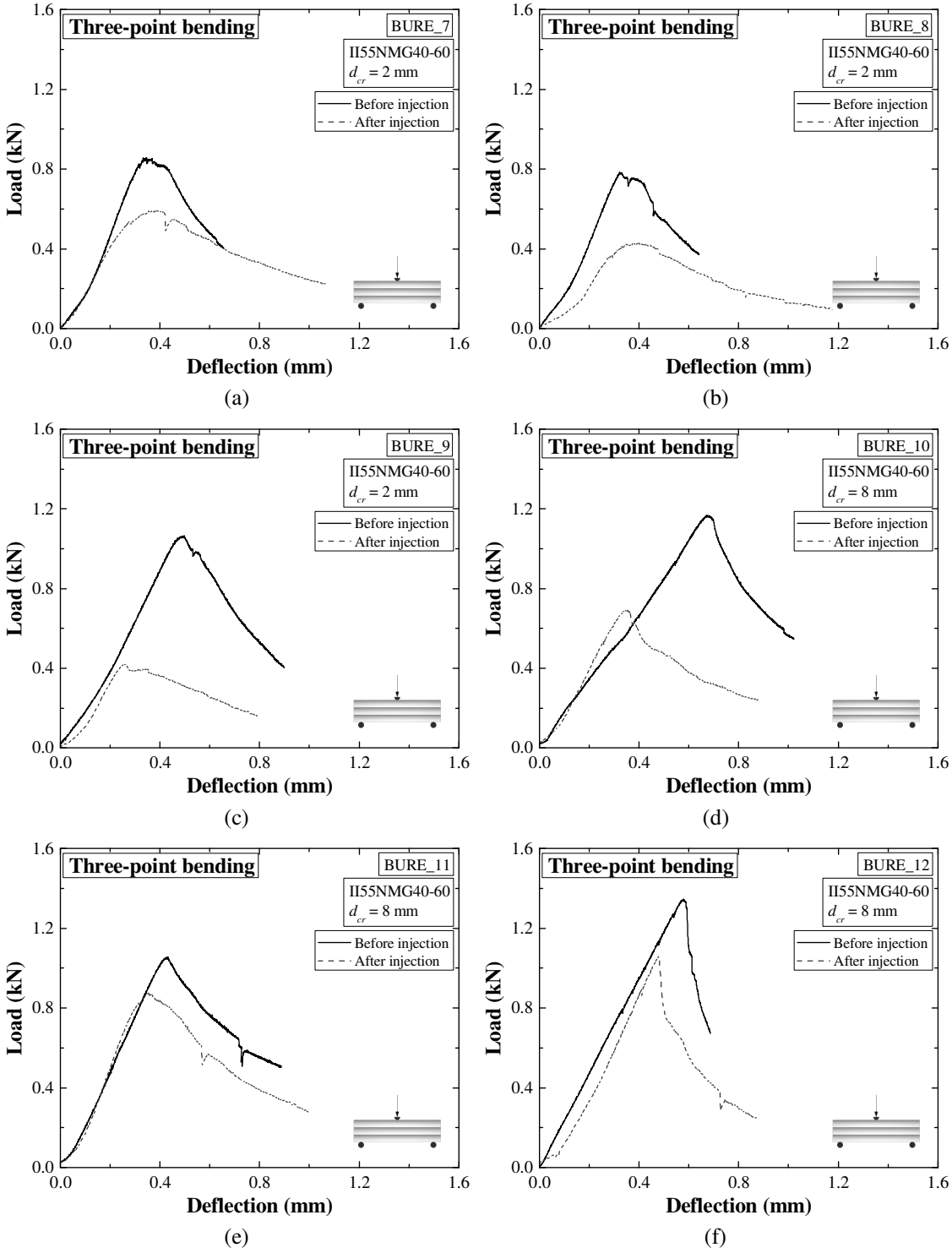

Figure C.2 – Load–deflection curves of the medium-scale specimens repaired with the mud grout II55NMG40-60: (a) BURE_7; (b) BURE_8; (c) BURE_9; (d) BURE_10; (e) BURE_11; (f) BURE_12.

C.2 Diagonal-compression tests on medium scale specimens

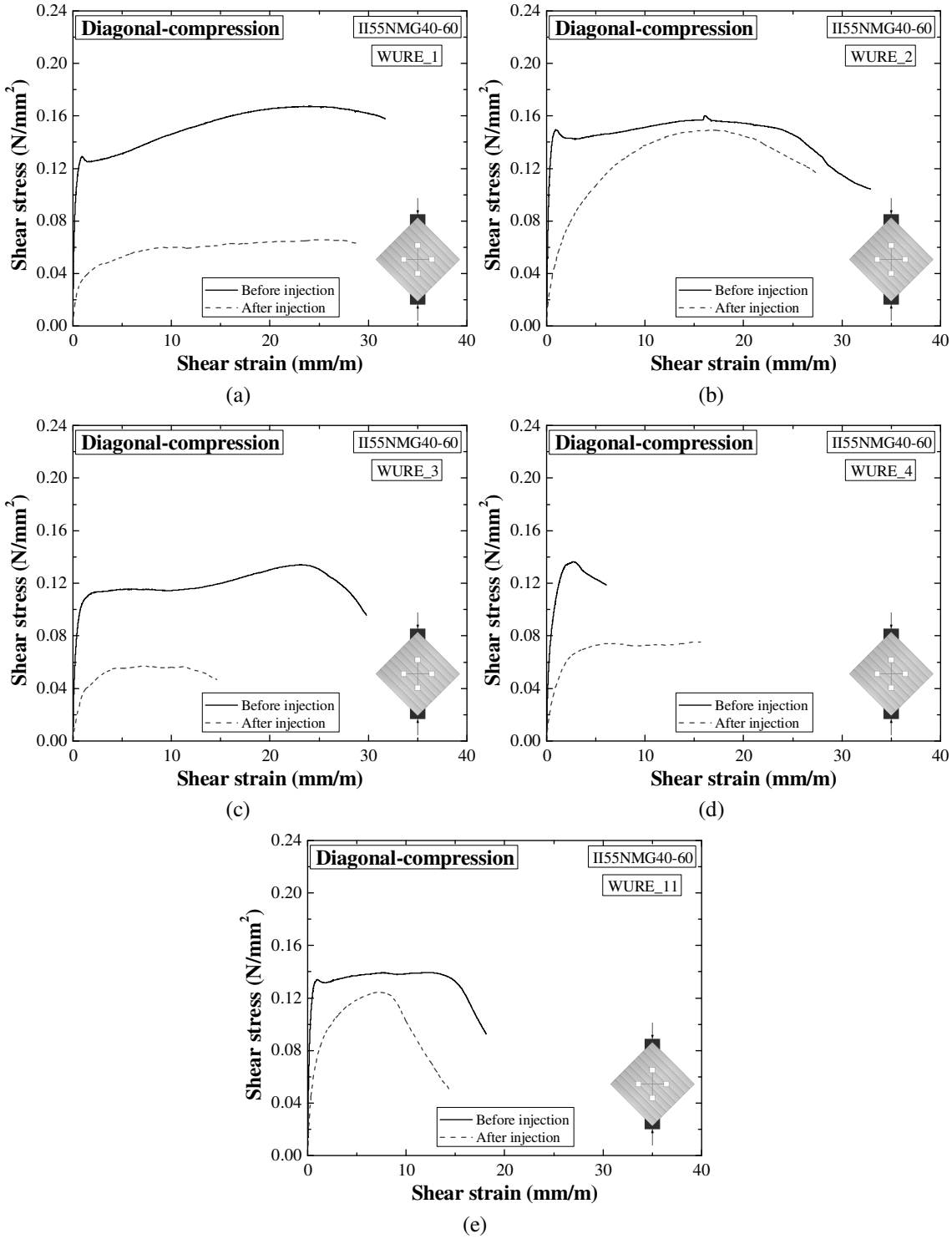

Figure C.3 – Shear stress–shear strain curves of the large-scale specimens repaired with the mud grout II55NMG40-60: (a) WURE_1; (b) WURE_2; (c) WURE_3; (d) WURE_4; (e) WURE_11.

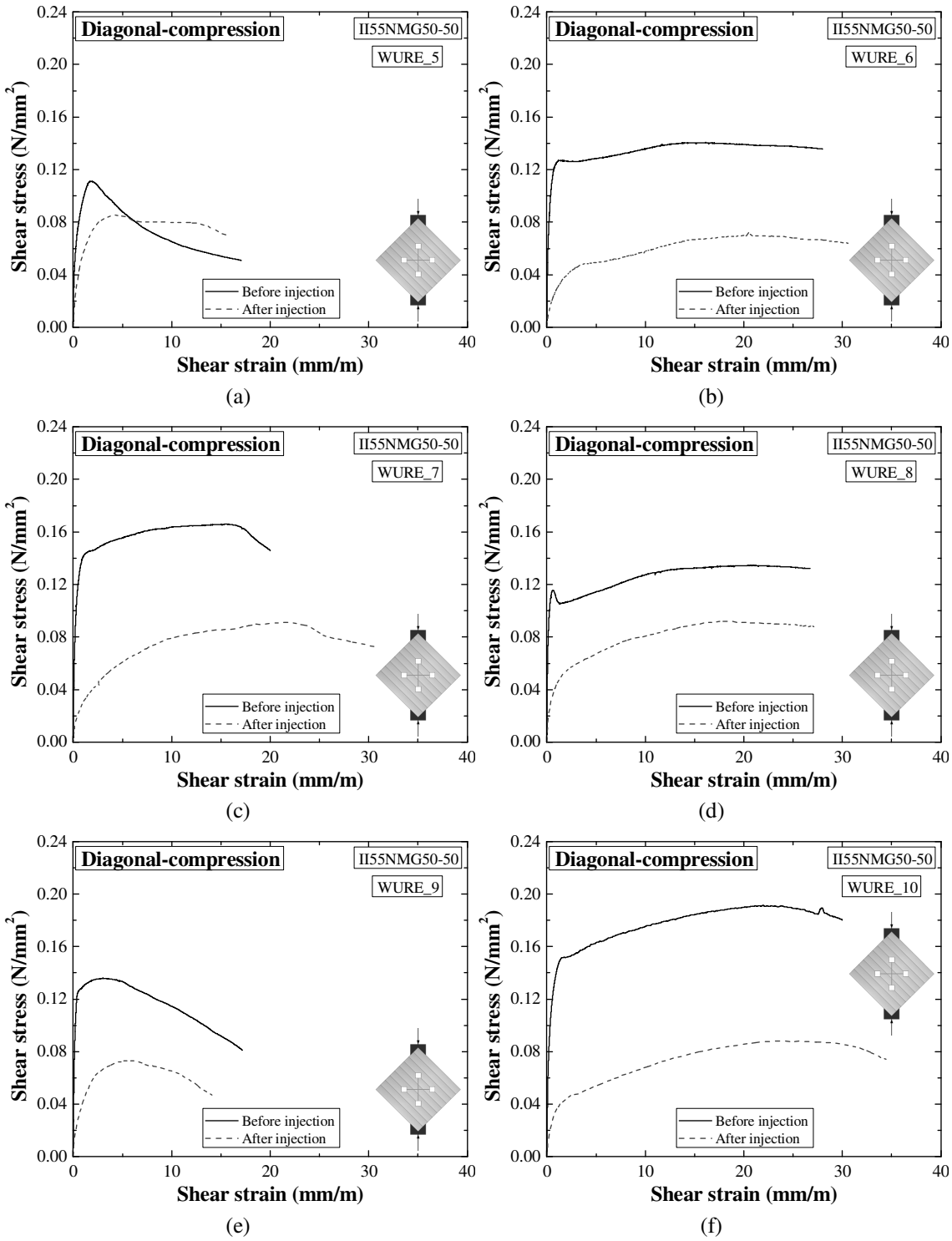

Figure C.4 – Shear stress–shear strain curves of the large-scale specimens repaired with the mud grout II55NMG50-50: (a) WURE_5; (b) WURE_6; (c) WURE_7; (d) WURE_8; (e) WURE_9; (f) WURE_10.